50 năm

XÂY DỰNG VÀ PHÁT TRIỂN
TẠI KHÁNH HÒA
(1976 - 2026)

TUYỂN TẬP CÁC CÔNG TRÌNH KHOA HỌC THUỘC SỐ ĐẶC BIỆT
CỦA TẠP CHÍ REGINOAL STUDIES IN MARINE SCIENCE

NHÂN KỶ NIỆM 50 NĂM TRƯỜNG ĐẠI HỌC NHA TRANG TỌA LẠC TẠI TỈNH KHÁNH HÒA

04/10/1976 – 04/10/2026

TUYỂN TẬP CÁC CÔNG TRÌNH KHOA HỌC THUỘC SỐ ĐẶC BIỆT

CỦA TẠP CHÍ REGINOAL STUDIES IN MARINE SCIENCE

NHÂN KỶ NIỆM 50 NĂM
TRƯỜNG ĐẠI HỌC NHA TRANG
TỌA LẠC TẠI TỈNH KHÁNH HÒA

04/10/1976 - 04/10/2026

MỤC LỤC

1 Effects of temperature, irradiance, and culture medium on carpospore release and germination of the antimethanogenic seaweed *Asparagopsis taxiformis* from Nha Trang, Vietnam", Regional Studies in Marine Science, 102 (2026). https://doi.org/10.1016/j.rsma.2026.105429

2 Hua Thai An, Cao Van Nguyen, Tran Mai Duc, Le Trong Nghia, Vu Thi Mo, Tran Van Huynh, Vu Trong Dai, Huynh Minh Sang, "Reproductive biology of Chinese thorny oyster, *Spondylus sinensis* Schreibers, 1793 in Khanh Hoa seawater, Vietnam", Regional Studies in Marine Science, 101 (2026). https://doi.org/10.1016/j.rsma.2026.105291

3 Ho Son Lam, Do-Huu Hoang, Dang-Tran Tu Tram, Nguyen-Thi Nguyet Hue, Le Thi Bich Nguyen, Hoang-Xuan Ben, Dao-Viet Ha, Tran Van Phuoc, "Effects of Food Type and Feeding Regime on Selected Physiological Characteristics of the Soft Coral, *Sarcophyton serenei* (Tixier-Durivault, 1958)", Regional Studies in Marine Science, 102 (2026). https://doi.org/10.1016/j.rsma.2026.105485

4 Hai-Thanh Thi Nguyen, Viet Do Hung Dang, Dien Duc Tran, Anze Abram, Fabian Gösser, James Davis Reimer, "Coral reef degradation is associated with gut microbiome shifts in the tomato anemonefish *Amphiprion frenatus*", Regional Studies in Marine Science, 102 (2026). https://doi.org/10.1016/j.rsma.2026.105336

5 Anh Thi Pham, Manh Van Ngo, Ha Kim Thi Nguyen, Hung Duc Pham, "Enriching *Artemia* with n-3HUFA modulated growth, survival, digestive enzymes, body composition and stress resistance in giant trevally (*Caranx ignobilis*) larvae", Regional Studies in Marine Science, 100 (2026). https://doi.org/10.1016/j.rsma.2026.105194

6 Thai Truong Quoc, Dat Nguyen Khac, Hong Truong Thi Bich, Sorgeloos Patrick, De Schryver Peter, "Dynamics of carbon and nitrogen profiles in the hatching medium of decapsulated *Artemia franciscana* cysts", Regional Studies in Marine Science, 102 (2026). https://doi.org/10.1016/j.rsma.2026.105430

7 Dung Van Tran, Trang Le Thi Tran, Dang Duyen Thi Thach, Dai Quang Tran, Manh Van Ngo, Dai Trong Vu, Hung Quoc Pham, Thanh Trung Dang, "Optimization of dietary marigold (*Tagetes erecta*) carotenoid levels on growth performance, feed utilization, skin pigmentation, and digestive enzyme activities of juvenile golden trevally (*Gnathanodon speciosus*)", Regional Studies in Marine Science, 102 (2026). https://doi.org/10.1016/j.rsma.2026.105436

8 Tran Vi Hich, Khuong V. Dinh, Nguyen Thi Kim Cuc, Nguyen Thi Thuy Giang, Pham Thi Dan Phuong, Nguyen Cong Minh, Trang Si Trung, Chitosan nanoparticles derived from molted shrimp shells as biodegradable adjuvants for *Vibrio harveyi* vaccination in Asian sea bass (*Lates calcarifer*), Regional Studies in Marine Science, 102 (2026). https://doi.org/10.1016/j.rsma.2026.105385

9 Kim Minh Anh, Vu Duc Manh, Ngo Van Manh, Truong Dinh Hoai, Nguyen Manh Hung, Kim Van Van, "Antiparasitic effects of silver nanoparticles on *Cryptocaryon irritans* and toxicity in juvenile *Trachinotus* spp.", Regional Studies in Marine Science, 101 (2026). https://doi.org/10.1016/j.rsma.2026.105314

10 Hoa Khanh Tran Kiem, Trung Hieu Pham, Phuong Chung Le, Hung Vu-Khac, "First Molecular Detection and Characterization of Red Sea Bream Iridovirus (RSIV) in Cultured Asian Seabass (*Lates calcarifer*) in Vietnam", Regional Studies in Marine Science, 102 (2026).
https://doi.org/10.1016

11 Nguyen Thi Nhu Ha, Nguyen Cong Minh, Vuong Thanh Tung, "Development of chitosan-red onion peel extract coatings for enhancing the quality and shelf life of houndfish (*Tylosurus crocodilus*) during ice storage", Regional Studies in Marine Science, 99 (2026).
https://doi.org/10.1016/j.rsma.2026.105108

12 Van Thi Nguyen, Emiko Okazaki, "Changes in electrical conductivity and physical properties of croaker surimi gels fortified with fish oil under ohmic heating", Regional Studies in Marine Science, 102 (2026).
https://doi.org/10.1016

13 Thi Hong Tuoi Do, Thanh Tra Do, Huong-Giang Le, Thi Kim Anh Le, Van Minh Nguyen, The Han Nguyen, Anh Duy Do, Thi Van Anh Tran, "LC-MS-based chemical profiling and *in vivo* anti-inflammatory effects of the Vietnamese red alga *Tricleocarpa cylindrica*", Regional Studies in Marine Science, 102 (2026).
https://doi.org/10.1016/j.rsma.2026.105427

14 T.V.A. Tran, Thi Dieu Hien Nguyen, Duy Hien Tran, Thi Kim Anh Le, Thi Hong Tuoi Do, V.M. Nguyen, The Han Nguyen, "Bioactive triterpenoid sulfates and carbohydrate derivatives from the Vietnamese red alga *Tricleocarpa cylindrica*", Regional Studies in Marine Science, 102 (2026).
https://doi.org/10.1016/j.rsma.2026.105462

15 Nguyen Thi Kim Chi, Nguyen Van Tai, Nguyen Dac Kien, Nguyen Van Hoa, "Mechanical and Morphological Characterization of Agricultural Waste-Reinforced Recycled HDPE Composites for Offshore Cage Frames", Regional Studies in Marine Science, 101 (2026).
https://doi.org/10.1016/j.rsma.2026.105312

16 Nguyen Thanh Tam, Luu Thi Giao Chau, Nguyen Ngoc Ha, Ong Moc Quya, Nguyen Ngoc Loi, Trong Dai Vu , and Nguyen Phuc Cam Tu, "Microplastic accumulation in oysters and water in farming areas of Can Gio mangroves, Vietnam", Regional Studies in Marine Science, 102 (2026).
https://doi.org/10.1016

17 Nguyen Van Nhi Tran, Quang Nguyen Pham, Duc Dat Duc Nguyen, Tan Phong Nguyen, "Determinants of discarded fishing gear generation and its economic implications in coastal fisheries of Khanh Hoa Province, Vietnam", Regional Studies in Marine Science, 102 (2026).
https://doi.org/10.1016

18 Khanh Q. Nguyen, Minh-Hoang Tran, Phuong Viet Le, Luong T. Nguyen, "Vietnamese fishing labour in global perspective: A critical review of social, economic, behavioural, and governance structures", Regional Studies in Marine Science, 102 (2026).
https://doi.org/10.1016/j.rsma.2026.105461

Regional Studies in Marine Science 102 (2026) 105429

Contents lists available at ScienceDirect

Regional Studies in Marine Science

journal homepage: www.elsevier.com/locate/rsma

Effects of temperature, irradiance, and culture medium on carpospore release and germination of the antimethanogenic seaweed *Asparagopsis taxiformis* from Nha Trang, Vietnam

Pham-Thi Minh-Thu [a], Ngo Dang Nghia [b], Khuc Thi An [a], Nguyen Thi Nhu Thuong [a], Nguyen Thi Kim Cuc [a], Vo Van Trong [c], Tran Ngoc Khanh [c,d], Ngo Thi Hoai Duong [b,*]

[a] *Department of Biotechnology, School of Fisheries and Life Sciences, Nha Trang University, 2 Nguyen Dinh Chieu, North Nha Trang ward, Khanh Hoa province, Vietnam*
[b] *Department of Chemical and Environmental Engineering, School of Fisheries and Life Sciences, Nha Trang University, 2 Nguyen Dinh Chieu, North Nha Trang ward, Khanh Hoa province, Vietnam*
[c] *Australasia Agriculture Company Limited, 10th Floor, Ladeco Building, Ngoc Ha ward, Hanoi, Vietnam*
[d] *Australasia Agriculture and Commodity Consulting, Level 26, 44 Market Street, Sydney, NSW 2000, Australia*

ARTICLE INFO

Dataset link: Dataset for carpospore survival, germination, and early development of Asparagopsis taxiformis under various conditions

Keywords:
Asparagopsis taxiformis
Carpospore
Temperature
Irradiance
Culture medium
Vietnam

ABSTRACT

Asparagopsis taxiformis has emerged as a promising biological candidate for a strategy to mitigate enteric methane emissions in ruminants. However, establishing scalable biomass production systems for local lineages remains a major challenge. This study investigated the reproductive phenology and improved early-stage hatchery protocols for a local lineage collected from Nha Trang Bay in Central Vietnam. The wild populations exhibited high reproductive capacity, characterized by a cystocarp density of 12.3 ± 4.8 cystocarp cm^{-1} . Thermal tolerance experiments identified a narrow optimal temperature range of 24–28°C, at which carpospore survival and germination both reached 100%. In contrast, exposure to 32°C resulted in complete mortality, whereas 20°C significantly inhibited tetrasporophyte development. Among the spore-release methods evaluated, natural induction was quantitatively superior, producing 5–10-fold higher spore yields than forcible release. However, forcible release generated cultures with higher cleanliness (95.8–100%). Light was identified as an essential factor for germination, confirming the positively photoblastic nature of the carpospores. A significant three-way interaction among liberation method, irradiance, and culture medium was observed, indicating that the combination of natural induction, f/2 medium, and 21 μmol photons m^{-2} s^{-1} irradiance yielded the highest performance, including higher spore yield, longest germling length (0.39 ± 0.04 mm) and 100% morphological branching within seven days. Collectively, these findings establish the first hatchery baseline for Vietnamese *A. taxiformis* and provide critical baseline culture conditions for overcoming the developmental lag phase. This study therefore lays an important foundation for the development of a domestic seaweed cultivation industry capable of contributing to both national and global methane mitigation strategies.

1. Introduction

Global climate change, driven mainly by excessive greenhouse gas (GHG) emissions, has intensified, contributing to increasingly severe climate-related events worldwide. Among greenhouse gases, methane (CH_4) is considered particularly important because its global warming potential is approximately 27–30 times greater than that of carbon dioxide (CO_2) over a 100-year period (IPCC, 2021). Recent studies indicate that methane possesses a substantially stronger warming effect than CO_2, making methane mitigation an urgent global priority (Wasson et al., 2022; de Vos et al., 2025). In addition to the fossil fuel sector, agricultural activities have become a major source of methane emissions, largely through enteric fermentation in ruminants. Livestock contributes approximately 14–15% of total anthropogenic greenhouse gas emissions globally (FAO, 2013; Glasson et al., 2022), while livestock-derived methane accounts for nearly 32% of global anthropogenic methane emissions, with cattle representing the dominant source (FAO, 2023). Consequently, reducing enteric methane emissions has become an important objective for improving environmental sustainability and mitigating climate change.

* Corresponding author.
E-mail address: hoaiduong@ntu.edu.vn (N.T.H. Duong).

https://doi.org/10.1016/j.rsma.2026.105429
Received 30 May 2026; Received in revised form 31 July 2026; Accepted 3 September 2026
Available online 7 September 2026

Among the various natural methane mitigation strategies, the red macroalgal genus *Asparagopsis* (Bonnemaisoniaceae) has emerged as one of the most promising biological solutions for reducing methane emissions from ruminant livestock (Kinley et al., 2016). Multiple studies have demonstrated that dietary supplementation with *Asparagopsis* can reduce enteric methane emissions by 50–98%, depending on supplementation level and feeding conditions (Machado et al., 2016; Kinley et al., 2020; Roque et al., 2021a, 2021b). These antimethanogenic effects are primarily attributed to halogenated secondary metabolites, particularly bromoform ($CHBr_3$), which inhibits methyl-coenzyme M reductase, a key enzyme involved in methanogenesis by ruminal archaea (Paul et al., 2006; Mata et al., 2012). Due to its strong methane-reducing capacity, *Asparagopsis* has attracted considerable international attention as a sustainable feed additive with significant environmental and economic potential.

Despite its biotechnological potential, the large-scale commercial application of *Asparagopsis* remains constrained by the lack of reliable and scalable biomass production systems (Zhu et al., 2021; Statton, 2024). Species within this genus, including the pan-tropical *A. taxiformis* (Delile) Trevisan and the temperate *A. armata* Harvey, possess a complex heteromorphic triphasic life cycle (Bonin and Hawkes, 1987; Zanolla et al., 2014). This life cycle alternates among a macroscopic haploid gametophyte, a microscopic diploid carposporophyte, and a filamentous diploid tetrasporophyte stage conventionally referred to as the *Falkenbergia* phase (Chihara, 1961; Bonin and Hawkes, 1987; Zanolla et al., 2022; Rule et al., 2025).

While the macroscopic gametophyte is the preferred target for eventual ocean-based cultivation, the filamentous tetrasporophyte serves as the primary industrial foundation for large-scale production due to its capacity for rapid vegetative propagation and its ease of year-round maintenance in land-based systems (Mata et al., 2012; Zhu et al., 2021; Statton, 2024). However, establishing reliable tetrasporophyte cultures from wild-collected filaments is often compromised by heavy epiphytic contamination and the relative rarity of this stage in natural reef environments (Zhu et al., 2021; Rule et al., 2025). Consequently, the most viable pathway to secure unialgal and genetically consistent founder lines is the collection of mature, wild gametophytes bearing fertile cystocarps to facilitate the controlled release and germination of carpospores (Statton, 2024; Rule et al., 2025). This transition – from carpospore liberation to the establishment of a robust tetrasporophyte biomass – represents the critical starting point for any commercial hatchery pipeline. Despite its importance, the specific abiotic factors required to optimize carpospore performance remain poorly defined for many geographic isolates, particularly tropical lineages distributed throughout Southeast Asia (Mihaila et al., 2023; Theobald et al., 2024; Torres et al., 2024).

In Vietnam, *A. taxiformis* (locally known in Vietnamese as “Rong măng leo” or “Rong hải tùng”) has been documented for more than five decades, with a distribution extending approximately 2500 km along the coastline from Quang Tri to Kien Giang provinces (Pham, 1969; Do and Do, 2013). Field surveys have identified this species as a common component of reef-associated marine flora in Central Vietnam (Nguyen et al., 2013). Located along the south-central coast of Vietnam, Nha Trang is characterized by tropical marine conditions, including seawater temperatures ranging from approximately 24.4–29.1°C throughout the year (Chung et al., 2024) and relatively high annual irradiance (Le et al., 2023), which together provide favorable conditions for the distribution of *A. taxiformis*. The presence of *A. taxiformis* has also been reported in Nha Trang in recent years (Nghia and Minh-Thu, 2025). Despite the relatively well-documented distribution of the species, fundamental biological information remains scarce regarding the reproductive phenology, life cycle transitions, and hatchery requirements of Vietnamese populations. Such information is essential for developing a domestic *Asparagopsis*-based aquaculture industry capable of contributing to global methane mitigation efforts.

Therefore, this study aimed to evaluate the reproductive potential and identify favorable conditions for the early development of the *A. taxiformis* lineage collected from Nha Trang, Vietnam. Specifically, the study investigated: (1) the density and maturation of reproductive structures in wild populations; (2) the trade-off between carpospore yield and culture purity under different spore liberation methods; and (3) the interactive effects of temperature, irradiance, and nutrient media on carpospore germination and the subsequent transition to the tetrasporophyte phase. The findings of this study provide an essential baseline for establishing sustainable hatchery systems in Central Vietnam while contributing to broader understanding of local adaptation and cultivation biology in this ecologically and economically important seaweed species.

2. Materials and methods

2.1. Algae collection

Based on field observations by experienced phycologists, the reproductive season of *A. taxiformis* in Khanh Hoa Province typically occurs from spring to early summer. Accordingly, preliminary surveys were conducted at two-week intervals from February onward until mature cystocarps were observed. Mature carposporophytes of *A. taxiformis* were subsequently collected from Hon Chong, Khanh Hoa Province, Vietnam (12.274154° N, 109.193231° E; Fig. 1 in Nghia and Minh-Thu, 2025) during March 2025 and April 2026. Mature gametophytes bearing visible mature cystocarps were hand-collected from natural populations by snorkeling at depths of less than 2 m.

Following collection, the algal samples were maintained in fresh seawater under continuous aeration using a portable air pump. During transportation, seawater temperature was maintained close to *in situ* conditions by adding seawater ice cubes. Samples were transported to the laboratory within 4 h of collection.

2.2. Environmental parameters collection

Environmental parameters including salinity, irradiance, and air and seawater temperature were measured on site during each sampling event. Salinity was measured by a refractometer (Master-S28M, Atago, Japan), whereas illuminance and air and seawater temperature were recorded using a data logger (MX2202, Hobo, USA). These measurements represented the *in situ* environmental conditions within the algal habitat.

To characterize environmental conditions throughout the bloom periods (March 2025 and April 2026), additional datasets were retrieved from multiple databases integrating satellite remote sensing and meteorological modeling. Sea surface temperature (SST) data were extracted from the National Oceanic and Atmospheric Administration (NOAA) database via virtual monitoring stations corresponding to the study site coordinates (Ventusky, 2026; SeaTemperature.info, 2026). Hourly shortwave solar radiation data (W/m^2) were retrieved from the Global Forecast System (GFS) model integrated into the Ventusky (InMeteo) platform (Ventusky, 2026; Time and Date, 2026). Salinity data was obtained from periodic marine environmental monitoring reports published by the Vietnam Ministry of Natural Resources and Environment (MONRE) and relevant regional oceanographic studies (World Bank, 2016).

To standardize irradiance measurements across the dataset, solar radiation ($W\ m^{-2}$) obtained from the GFS model and illuminance recorded by the MX2202 data logger were converted to photosynthetic photon flux density (PPFD; μmol photons $m^{-2}\ s^{-1}$) using standard daylight spectral conversion factors ($1\ W\ m^{-2} = 1.96$ μmol photons $m^{-2}\ s^{-1}$; Lopez and Runkle, 2021; and $1\ lux = 0.0185$ μmol photons $m^{-2}\ s^{-1}$; Sager and McFarlane, 1997; respectively).

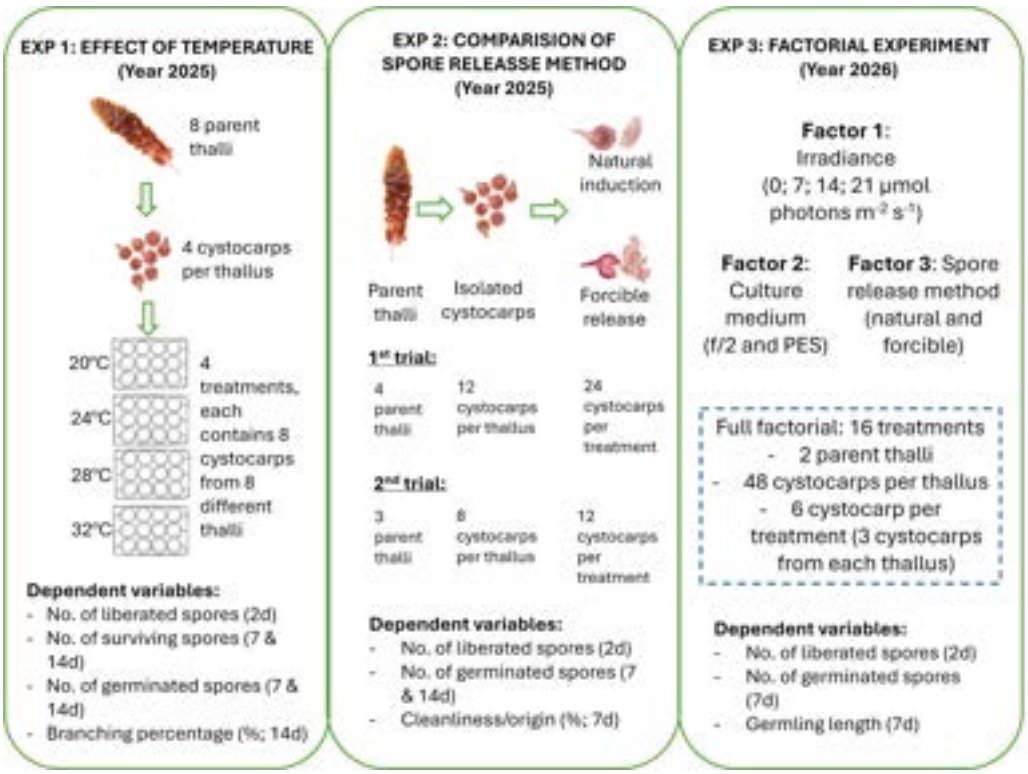

Fig. 1. Schematic diagram illustrating the overall experiment.

2.3. Sample preparation and primary cleaning

In the laboratory, algal samples were thoroughly rinsed with seawater to remove sand, debris, and loosely attached epiphytes. Seawater was pretreated with 20 ppm chloramine-B and neutralized with sodium thiosulfate at least 2 days before use. To preserve the integrity of the delicate gametophytic fronds, no stress treatments (e.g., freshwater or disinfectants) were applied at this stage, as *A. taxiformis* has demonstrated high sensitivity and potential pigment loss when exposed to such stressors.

Twenty algal clumps were used to measure frond length, and cystocarp numbers were quantified from ten mature fronds. Mature cystocarps, indicated by their pink to red colour and a visible apical ostiole (Fig. 1d), were carefully excised from the female gametophytes using sterile fine-tipped forceps under a stereomicroscope and transferred to sterile 60-mm Petri dishes containing autoclaved seawater prior to subsequent experimental procedures.

2.4. Carpospore release and germination

The induction step was performed immediately after cystocarp isolation using two methods: forcible release, involving the mechanical extraction of carpospores from cystocarps (Rule et al., 2025), and natural induction, which promotes spontaneous carpospore release under controlled conditions (Statton, 2024; Rule et al., 2025), with minor modifications as described below.

Forcible release: All excised cystocarps were immersed in 0.5% iodine solution for 30 s, then rinsed four to five times with autoclaved seawater. Each clean cystocarp was transferred onto a sterile glass microscope slide, after which a second slide was gently placed on top to sandwich the cystocarp. The slides were then gently pressed and rubbed to induce carpospore release. Following release, the slides were carefully separated, and the released carpospore clumps were transferred into culture wells by pipetting sterile seawater across the glass surface.

Natural induction: Isolated cystocarps were washed three times with sterile seawater, after which each cystocarp was gently dragged across the surface of an agar plate at least five times. Each cystocarp was subsequently transferred into a sterile dish and rinsed three additional times with sterile seawater to remove residual agar and potential contaminants.

For forcible release, each clump of released carpospores was transferred individually into a culture well, whereas for natural induction, individual cystocarps were cultured directly. All treatments were maintained in clear 12-well culture plates (Biologix, USA), each containing 6 mL of the appropriate nutrient medium. The culture medium was supplemented with germanium dioxide (GeO_2; Sigma-Aldrich, Germany) at a concentration of 0.1 mg L^{-1} to inhibit the proliferation of epiphytic diatoms. Culture plates were maintained under experimental conditions according to the respective treatments.

2.5. Experimental designs

The experiments were conducted over two consecutive years due to the seasonal availability of mature gametophytes (Fig. 1). Although the experiments were performed in different years, broodstock was collected from the same location during the peak reproductive season under comparable environmental conditions (Table 1), thereby minimizing potential physiological variation among experiments.

This study comprised three experimental designs (Fig. 1). The first experiment evaluated the effect of temperature on the early development of the seaweed. The second compared different spore-release methods to identify the more effective approach. The third investigated the combined effects of three factors – irradiance, nutrient medium, and spore-release method – on spore liberation, spore germination and early germling growth under laboratory conditions.

Healthy fertile female thalli bearing mature cystocarps were randomly collected from the natural population. Each parent thallus was considered an independent biological replicate, whereas multiple cystocarps obtained from the same parent thallus were treated as subsamples of that biological replicate.

Table 1
Environmental parameters recorded at the collection site (Hon Chong, Nha Trang) during study periods in 2025 and 2026.

Parameters	*In-situ* data		Retrieved data		
	March 14th, 2025	April 2nd, 2026	March 2025	April 2026	Source
Sea surface temperature (°C)	26.2	27.0	26.5 – 27.2	27.5 – 28.5	Ventusky, (2026); SeaTemperature.info, (2026)
Seawater salinity (‰)	32.0	32.0	32.5 – 33.2	33.0 – 33.8	World Bank, (2016)
Surface irradiance (μmol photons m^{-2} s^{-1})	1400*	1710*	710 – 800	830 – 960	Ventusky, (2026); Time and Date, (2026)
Photoperiod (L:D)	12:12	12.25:11.75	12: 12	12.5:11.5	Time and Date, (2026)

* Measured at peak intensity (midday).

2.5.1. *The first experimental design (conducted in 2025)*

Four temperature treatments were established using a chiller (20 ± 1°C), an air conditioner (24 ± 1°C), and heaters (28 ± 1 and 32 ± 1°C) to evaluate their effects on spore liberation, survival, germination, and contamination. Four cystocarps were collected from each of eight parent thalli, and one cystocarp from each parent thallus was randomly assigned to each temperature treatment. This balanced design minimized variation among parent thalli while ensuring that all temperature treatments were represented within each biological replicate.

2.5.2. *The second experimental design (conducted in 2025)*

Two spore-release methods, forcible release and natural induction (Statton, 2024; Rule et al., 2025), were compared to determine the more effective method based on spore liberation, germination, and culture contamination.

The experiment consisted of two independent trials. In each trial, cystocarps from every parent thallus were equally divided between the two spore-release methods, allowing direct within-thallus comparisons while controlling for variation in physiological condition and microbial load among parent thalli, both of which may substantially influence culture establishment and decontamination success.

In the first trial, 12 cystocarps were collected from each of four parent thalli (48 cystocarps in total), with six cystocarps from each parent thallus assigned to each release method. In the second trial, eight cystocarps were collected from each of three parent thalli (24 cystocarps in total), with four cystocarps from each parent thallus assigned to each release method.

2.5.3. *The third experimental design (conducted in 2026)*

A full-factorial experimental design was employed to evaluate the effects of three factors – irradiance, nutrient formulation and spore-release method – on spore liberation, spore germination, and germling growth. Irradiance was tested at four levels (0, 500, 1000, and 1500 lux) using cool-white LED lamps under a 10 L:14D photoperiod. Light intensity was converted to photosynthetic photon flux density (PPFD) using a conversion factor of 0.014 (Sager and McFarlane, 1997), corresponding to 0, 7, 14, and 21 μmol photons m^{-2} s^{-1} , respectively. Two nutrient media commonly used for seaweed culture were evaluated: f/2 medium (Guillard and Ryther, 1962) and Provasoli's Enriched Seawater (PES) medium (Provasoli, 1966). The two spore-release methods were the same as those described in the second experiment.

In this experiment, two fertile parent thalli bearing abundant mature cystocarps were selected because the factorial design required a large number of cystocarps (48 healthy, mature cystocarps per thallus) to accommodate all 16 treatment combinations (2 spore-release methods × 4 irradiance levels × 2 culture media). Cystocarps collected from each parent thallus were randomly and equally distributed among all treatment combinations, with three cystocarps from each thallus assigned to each treatment. This balanced allocation minimized potential confounding effects associated with differences among source individuals while ensuring sufficient replication within each treatment.

2.6. *Data collection*

Spore release, survival, germination, branching, and contamination were monitored daily. The number of spores was manually counted using a stereomicroscope (Optika SLX-2, Italy) or analyzed from digital images using ImageJ software (version 1.54 g, National Institutes of Health, NIH, USA; Schneider et al., 2012). The length of early filamentous tetrasporophytes was monitored and documented through digital imaging and ImageJ-based analysis.

Germination was defined as the first visible cell division or germ tube emergence. Surviving spores included both germinated spores and ungerminated spores that retained their original red pigmentation. A well was classified as "branching" when the first secondary cell division originating from the main stem of any germling was observed.

2.7. *Quantification criteria*

Number of liberated spores was counted only for freely released spores, distinguished by their spherical morphology. Spores remaining attached to the gonimoblast filament in the forcible release treatment were typically pyriform in shape and were therefore excluded from quantification. However, germinated spores were counted regardless of attachment, provided they exhibited clear features of germination.

2.8. *Calculated parameters*

Germination percentage (%) was calculated as the ratio of germinated spores to the total number of released spores per cystocarp, expressed as a percentage.

Spore survival (%) was defined as the proportion of red-pigmented or germinated spores relative to the total number of released spores per cystocarp.

Contamination (%) was the proportion of culture wells (or cystocarps) that showed visible symptoms of microbial growth relative to the total number of wells originating from the same parent thallus in each treatment.

Cleanliness (%) was calculated as 100 – contamination (%)

Branching percentage (%) was calculated as the proportion of wells exhibiting branching relative to the total number of wells within each treatment.

2.9. *Statistical analysis*

All data were expressed as means or estimated marginal means ± standard deviations (SD) or standard errors (SE). Statistical analyses were performed using the R statistical environment (RStudio 2026.04.0, build 526; Posit Team, 2026), with supplementary data processing conducted in Microsoft Excel.

For the first experiment, the effects of temperature on spore release, spore survival (7 and 14 days), and spore germination (7 and 14 days) were analyzed using generalized linear mixed models (GLMMs). Because multiple cystocarps originated from the same parent thallus, parent thallus was treated as the experimental unit and included as a random effect to account for variation among source individuals. Count data were initially fitted using a Poisson distribution and subsequently evaluated for overdispersion using the DHARMa package. When overdispersion was detected, models were refitted using a negative binomial distribution. Because no spores survived or germinated at 32°C, this

treatment was excluded from the analyses of survival and germination, and comparisons were performed only among 20, 24, and 28°C. Fixed effects were assessed using likelihood ratio tests (LRTs), and pairwise comparisons were conducted using estimated marginal means with Bonferroni adjustment.

For the second experiment, the effects of spore-release method on spore liberation and germination were analyzed using GLMMs with parent thallus included as a random effect. Model selection and validation followed the same procedure as described above, with Poisson models fitted initially and replaced by negative binomial models when overdispersion was detected. Differences between models with and without the fixed effect were evaluated using likelihood ratio tests, and estimated marginal means were compared using Bonferroni-adjusted pairwise comparisons. The proportion of clean cultures was analyzed using a generalized linear model with a binomial error distribution and logit link.

For the third experiment, the effects of spore-release method, irradiance, culture medium, and their interactions on spore liberation and development were analyzed using generalized linear models (GLMs). Parent thallus was not included as a random effect because two levels are insufficient for reliable estimation of its variation. Count data, including numbers of liberated and germinated spores were initially fitted using a Poisson distribution and evaluated for overdispersion using the DHARMa package. When overdispersion was detected, models were refitted using a negative binomial distribution. Seedling length was analyzed using a generalized linear model with a Gamma error distribution and log link after confirming that the response variable was continuous and strictly positive. Model assumptions were assessed using diagnostic residual plots generated by the DHARMa package. The significance of main effects and interactions was evaluated using likelihood ratio tests, and pairwise comparisons among treatment means were performed using estimated marginal means with Bonferroni adjustment. Because the factorial design required a large number of cystocarps, cystocarps from two fertile parent thalli were randomly and equally allocated across all treatment combinations. Therefore, potential variation associated with source individuals was controlled through the balanced experimental design rather than explicitly included in the statistical model.

Differences were considered statistically significant at $P < 0.05$.

3. Results and discussion

3.1. Environmental context and sample characteristics

The environmental parameters recorded at Hon Chong, Nha Trang, during the primary collection periods (March 2025 and April 2026) characterized the habitat as a stable, high-energy tropical marine ecosystem.

Sea surface temperatures (SSTs) at the collection site ranged from 26.2 to 27.2°C in March 2025–27.0–28.5°C in April 2026 (Table 1). This thermal regime is typical of the south-central coast of Vietnam during the spring-to-summer transition. The observed SSTs closely align with the reported peak growth conditions of other tropical *A. taxiformis* populations, such as those in Indian waters (24 ± 2°C; Mairh, 1977). In contrast, populations from temperate regions such as southern California and the Azores experience substantially cooler and more variable thermal regimes (15–22°C), where the gametophyte stage is typically restricted to cooler periods of the year (Batista, 2020; Resetarits et al., 2024). These differences suggest geographic variation in thermal adaptation among tropical and temperate populations of *A. taxiformis*.

Seawater salinity at Hon Chong remained consistent at 32.0‰ and 33.8‰ (Table 1). This stability is biologically important because *A. taxiformis* typically thrives at salinities around 35‰ but maintains healthy growth within a window of 30–40‰ (Mairh, 1977; Hurd et al., 2014; Statton, 2024). The optimal osmotic environment at Hon Chong may support the high reproductive potential observed in the local population, which exhibited a mean cystocarp density of 12.3 ± 4.8 cystocarps cm^{-1} . Such high reproductive output suggests substantial propagule pressure, which may represent an adaptation for survival and dominance in high-energy reef environments (Zanolla et al., 2017).

The light environment featured high surface irradiance, with midday peaks of 1400–1710 μmol photons m^{-2} s^{-1} (Table 1). Furthermore, the photoperiod shifted from 12 L:12D in March to a longer day-length of 12.5 L:11.5D in April. This increasing day length, coinciding with the peak abundance of fertile gametophytes, may serve as a primary phenological trigger for reproductive synchrony and the onset of carposporogenesis in the Nha Trang lineage (Guiry and Dawes, 1992; Statton, 2024; Rule et al., 2025).

3.2. Morphological traits and reproductive potential of seed stock

The harvested gametophytes of *A. taxiformis* from Nha Trang were typically medium to dark reddish-brown in color, gradually fading to greyish-red with age (Figs. 2a, 2b). Gametophytes were attached to rocky or coral substrates (Fig. 2a) through a well-developed network of basal stolons and rhizoids (Fig. 2b). The average frond length within collected clusters, including both juvenile and mature branches, was 6.04 ± 2.27 cm, whereas mature reproductive fronds bearing visible cystocarps (Fig. 2c) reached an average length of 9.7 ± 2.1 cm (Table 2). Although these fronds were shorter than the 20–40 cm lengths commonly reported for Australian populations (Rule et al., 2025; Statton, 2024), they exceeded the average thallus lengths reported for three Indonesian strains, which ranged from 3.6 and 4.4 cm (Jayanti et al., 2026). The broad size distribution observed among Vietnamese specimens (2.0–13.2 cm) suggests continuous recruitment and development of fronds within individual clusters (Table 2).

The Vietnamese specimens also exhibited a remarkably high density of reproductive structures (Fig. 2b). An average of 120.0 ± 59.3 cystocarps per frond was recorded, equating to a density of 12.3 ± 4.8 cystocarps cm^{-1} (Table 2). With an average of 276–362 spores per cystocarp (Table 3), the total number of carpospores could reach approximately 36,000 per frond. This high reproductive allocation is a critical indicator of the population's suitability as a seed stock source. The mechanism behind such dense cystocarp formation in the Nha Trang lineage may reflect the favorable thermal and nutrient conditions of the collection site, which may allow the alga to invest heavily in sexual reproduction in addition to vegetative growth. In many *Asparagopsis* lineages, high propagule pressure has been proposed as an adaptive strategy for survival and dominance in high-energy reef environments (Zanolla et al., 2017). Statton (2024) and Rule et al. (2025) emphasized that the number of fecund thalli is a major determinant of hatchery success. Therefore, the high density of mature pink-to-red cystocarps observed even in relatively small Vietnamese specimens supports the potential of this population for large-scale carpospore production and hatchery-based seedling propagation.

3.3. Thermal constraints and local adaptation in carpospore development

The experimental results demonstrated that although temperature did not significantly influence the initial quantity of carpospores liberated ($P > 0.05$), it acted as a decisive regulatory factor governing all subsequent developmental processes, including survival, germination, and morphological branching (Table 3).

The Nha Trang lineage exhibited optimal performance between 24°C and 28°C. At these temperatures, spore survival and germination reached 100% within the first 7 days (Table 3). This range closely matched the ambient seawater temperatures of 26.5–27.2°C recorded during the collection periods (Table 1), suggesting local thermal adaptation. Similar thermal preferences have been reported for other tropical *A. taxiformis* populations, including Australian isolates from Magnetic Island (Queensland), where approximately 25°C was identified as the optimal germination temperature (Rule et al., 2025; Statton, 2024). This

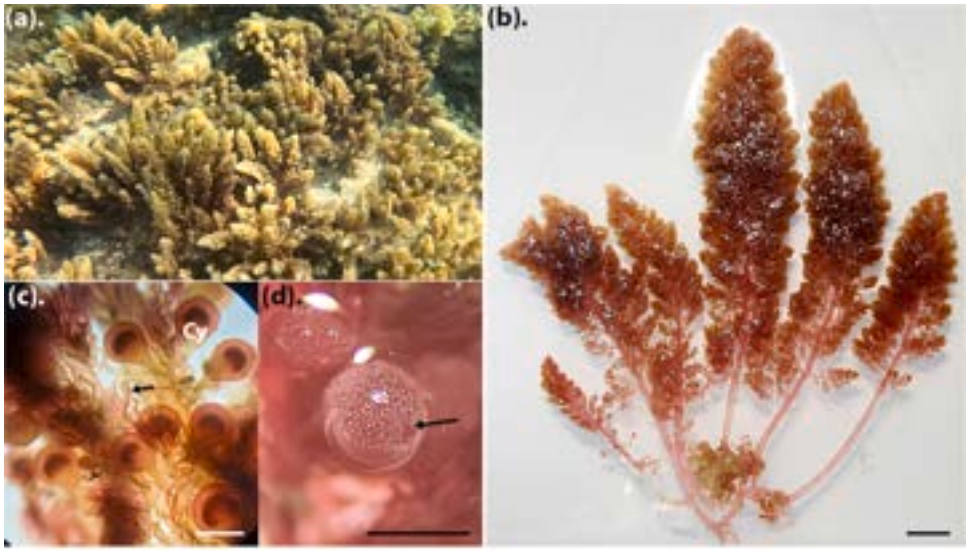

Fig. 2. Morphological and reproductive features of wild-collected *Asparagopsis taxiformis* from Nha Trang, Vietnam. (a). Gametophytes in natural habitat. (b). A cluster of seaweed whose fronds connect to each other by the basal stolon and rhizoids. (c). Densely distributed cystocarps (Cy) and spermatangia (arrow) on the frond. (d). A mature cystocarp with a visible apical ostiole (arrow). Bar (in b): 1 cm, (in c and d): 1 mm.

Table 2
Morphological characteristics and cystocarp density of collected A. taxiformis specimens.

Morphological parameters	Value (Mean ± SD, standard deviation)	Sample size (n)
Average frond length (cm)	6.04 ± 2.27	285
Range of frond length (cm)	2.0 – 13.2	285
Mature frond length (cm)	9.7 ± 2.1	10
No of cystocarps/frond	120.0 ± 59.3	10
No of cystocarp cm^{-1}	12.3 ± 4.8	10

pattern likely reflects reproductive synchrony, whereby seaweeds coordinate life-cycle transitions with stable environmental conditions in their native habitats to maximize recruitment success (Rule et al., 2013).

Conversely, exposure to 32°C resulted in total mortality within 2 days (Fig. 3), indicating that this temperature likely approaches the upper lethal threshold for the carpospore stage of the Nha Trang lineage. According to the National Hatchery Network data, *A. taxiformis* tetrasporophytes generally experience mortality above 33°C (Rule et al., 2025). The rapid collapse at 32 ± 1°C in our study suggests that the carpospore stage may be as sensitive to heat stress as the established tetrasporophyte. Exposure to elevated temperatures is known to induce the accumulation of reactive oxygen species (ROS) and cause irreversible damage to photosystem II and cellular membranes, ultimately leading to bleaching and cell death (Allakhverdiev et al., 2008; Eggert, 2012).

Values are EMMs (estimated marginal means) ± SE (standard error) obtained from the negative binomial generalized linear mixed model. Sample sizes were n = 7 for 20°C; n = 8 for 24°C, 28°C, and 32°C. Different letters within a column indicate significant differences based on Bonferroni-adjusted pairwise comparisons ($P < 0.05$). The 32°C treatment was excluded from the statistical analyses of surviving and germinated spores because all observations were zero. N.D: not detected due to complete sample mortality.

Branching was observed exclusively in the 24°C and 28°C treatments, where the branching percentage reached 100% at day 7 (Table 3). In contrast, the 20°C treatment produced only minimal germination and no observable branching even after 14 days (Table 3). In the practical framework of *Asparagopsis* hatcheries, the emergence of the first branch represents a critical developmental milestone for scaling up production. Statton (2024) noted that this morphological transition indicates that germlings are sufficiently robust for transfer from static multi-well plates to large aerated culture systems (tumble culture). The present results suggest that maintaining temperatures between 24°C and 28°C is essential for inducing branching within the first week of development. By accelerating early morphological maturation, hatchery systems in Central Vietnam may substantially reduce the developmental lag phase and achieve harvestable biomass within the economically viable production window of approximately 4–6 weeks proposed for industrial cultivation (Statton, 2024).

3.4. Trade-offs between spore yield and culture cleanliness associated with two spore-release methods

Statistical analysis revealed a significant effect of the spore-release method on both spore yield and culture quality ($P < 0.01$). Data from the first trial showed that the natural induction method yielded a mean of 217.3 ± 56.2 carpospores per cystocarp, which was more than tenfold higher than the 20.4 ± 5.4 spores obtained via the forcible release method (Table 4). A similar trend was observed in the second trial, in

Table 3
Effects of temperature on the survival, germination, and branching of Asparagopsis taxiformis carpospores over 14 days of cultivation.

		20°C	24°C	28°C	32°C
No of liberated spores	2d	366.7^{a}±68.1	263.1^{a}± 45.9	294.1^{a}±50.2	302.0^{a}±52.2
No of surviving spores	7d	260.7^{b}±56.6	266.3^{b}±54.1	294.8^{b}±59.8	0.0^{a} ± 0.0
	14d	134.9^{b}±38.6	266.3^{c}± 71.0	294.8^{c}±78.6	0.0^{a} ± 0.0
No of germinated spores	7d	2.0^{a} ± 0.7	266.3^{b}±62.1	294.8^{b}±68.7	0.0^{a} ± 0.0
	14d	2.9^{a} ± 0.9	266.3^{b}±55.5	294.8^{b}±61.4	0.0^{a} ± 0.0
Branching percentage (%)	7d	0	100.0	100.0	N.D
	14d	0	100.0	100.0	N.D

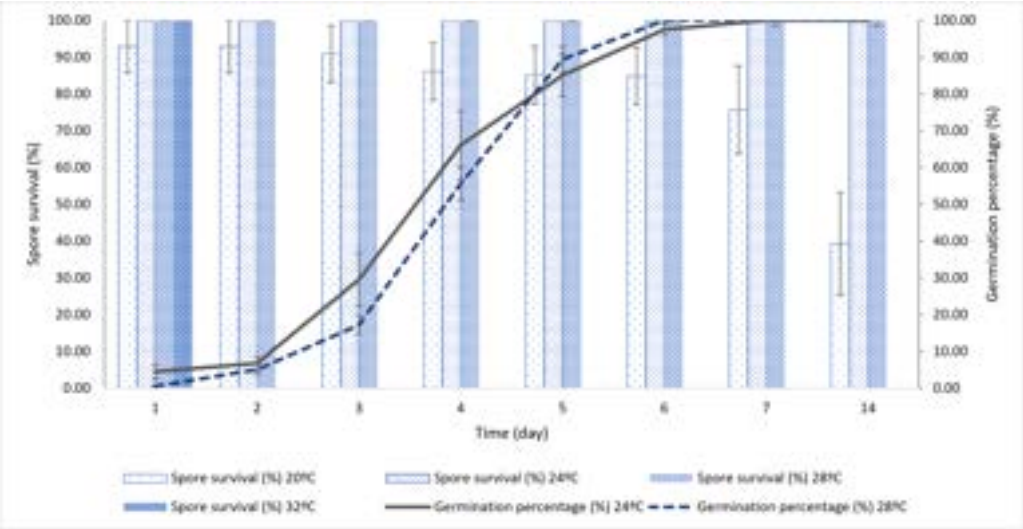

Fig. 3. Temporal variations in carpospore survival and germination percentage under different temperature regimes over 14 days. Error bars represent SE (n = 7 for 20°C; n = 8 for 24°C, 28°C, and 32°C). Data for the 32°C treatment (spore survival and germination percentage) and the 20°C treatment (germination percentage) were omitted from the graphs due to their zero and near-zero values, respectively.

which natural induction again generated significantly higher spore yields (118.7 ± 34.5) than forcible release (10.7 ± 3.3).

Values are EMMs (estimated marginal means) ± SE (standard error) obtained from the negative binomial generalized linear mixed model. In the first trial, n = 24 cystocarps per method; four parent thalli included as a random effect. Corresponding numbers for the second trial were n = 12 and three thalli. *P* values were derived from likelihood ratio tests, and pairwise comparisons were performed using estimated marginal means with Bonferroni adjustment. $*P < 0.05$, $** P < 0.01$.

The quantitative superiority of the natural induction method suggests that carpospore liberation in the Nha Trang lineage may represent an active biological process rather than a purely mechanical event. In many red algae, synchronized spore-release is triggered by specific physiological or osmotic signals that require the structural integrity of the cystocarp to remain intact (Rule et al., 2025). Similar patterns have been reported for tropical *A. taxiformis* populations from Magnetic Island, Australia, where natural induction generated approximately sixfold higher carpospore yields than forcible release under optimal conditions (Rule et al., 2025).

This discrepancy may be explained by differences in cystocarp physiology and the mechanics of spore liberation. Natural induction allows carpospores to mature fully, detach from the gonimoblast filaments, and exit through the apical ostiole according to their endogenous developmental rhythm. In contrast, the lower yield obtained from the forcible release method may be due to potential damage occurred during the sandwiching process, together with spore loss during transfer from the glass surface. Furthermore, many forcibly extruded spores remained attached to the gonimoblast filament and occasionally retained this connection after germination. These pyriform gonimoblast-associated spores were therefore excluded from liberated spore counts. However, they were fully accounted for in the germinated spore and subsequent germling counts as they successfully initiated cultivation.

Despite the substantially lower spore yield, the forcible release method proved superior in establishing clean founder cultures. In the first trial, the forcible method achieved 95.8% cleanliness, which improved to 100% cleanliness in the second trial (Table 4). In contrast, cleanliness in the natural induction treatment declined from 66.7% in the first trial to complete contamination (0% cleanliness) in the second trial. This deterioration may have been associated with poorer physiological condition and heavier epiphytic contamination of the broodstock collected during the second sampling period (data not shown).

The inverse relationship between spore yield and culture cleanliness represents a major technical challenge in *Asparagopsis* hatchery systems. Contamination during natural induction is likely associated with the prolonged immersion (typically 12–72 h) of wild-collected maternal tissues in nutrient-enriched culture media (Statton, 2024; Rule et al., 2025). This duration provides sufficient time for epiphytic diatoms, bacteria, and microscopic algae – which are ubiquitous on wild gametophytes – to migrate from the parental tissue and colonize the nutrient-rich environment of the culture wells (Mickelson, 2013; Rule et al., 2025). The forcible method mitigates this risk by utilizing a brief 30-second iodine sterilization and immediate mechanical isolation of spores, thereby reducing contact time between wild tissues and the culture medium (Rule et al., 2025).

Interestingly, natural induction in the first trial was estimated to produce approximately 148.3 clean germlings (estimated from EMM × cleanliness) despite lower overall cleanliness, suggesting that high initial spore densities may partially compensate for moderate contamination levels. However, the complete contamination observed in the second trial highlights the limited reliability of this method when relying on wild-sourced broodstock. Wild *A. taxiformis* specimens collected from shallow nearshore habitats in Nha Trang were frequently associated with dense epiphytic communities, including bacteria, invertebrates, microalgae, and macroalgae. Moreover, coastal habitats near urbanized regions are likely to be subjected to greater anthropogenic disturbance, potentially increasing microbial and epiphytic loads on collected thalli. Although the agar-dragging procedure reduced surface contamination to some extent, it appeared insufficient for removing

Table 4
Comparison of carpospore yield and culture cleanliness between forcible release and natural induction methods.

	No. of liberated spore/carp at day 2		No of germinated spores/carp at day 7		Cleanliness (%)/origin at day 7		No. of clean germlings at day 7	
Trial	Forcible	Natural	Forcible	Natural	Forcible	Natural	Forcible	Natural
1st	20.4 ± 5.4	217.3**±56.2	54.3 ± 11.6	222.4**±47.4	95.8*±1.7	66.7 ± 2.8	52.0	148.3
2nd	10.7 ± 3.3	118.7**±34.5	26.2 ± 5.9	116.4**± 25.4	100.0**±0.0	0.0 ± 0.0	26.2	0

firmly attached epiphytes, particularly filamentous algae associated with cystocarp surfaces.

Consequently, for industrial-scale hatchery development in Central Vietnam, a hybrid production strategy is recommended, similar to those proposed for the Australian industry (Rule et al., 2025). The forcible release method should be prioritized for establishing and maintaining clean founder cultures and genetically stable seed stocks, whereas natural induction may be more suitable for large-scale biomass expansion when combined with advanced decontamination procedures, such as repeated agar-dragging or antibiotic-assisted cleaning protocols, to maintain the long-term viability of the tetrasporophyte phase.

Overall, tetrasporophyte germlings could be obtained by two pathways illustrated in Fig. 4. Carpospore liberation occurred either through natural release via the cystocarp ostiole or through forcible extrusion by mechanical compression between glass slides. Spore liberation was generally completed within 3 days, followed by germination after approximately 1–2 additional days. Initial branching was consistently observed within 7 days after spore liberation.

3.5. Promotion of carpospore liberation and germination

Generalized linear model (GLM) analysis identified that the spore-release method was the most influential factor affecting both carpospore liberation ($\chi^2 = 80.182$, $P < 0.01$) and subsequent germination ($\chi^2 = 34.069$, $P < 0.01$). Although irradiance did not significantly affect the initial quantity of liberated spores ($P > 0.05$), it strongly influenced germination ($P < 0.01$). Interestingly, culture medium (f/2 versus PES) showed no significant independent or interactive effects on either parameter ($P > 0.05$), suggesting limited dependence on external nutrients during the earliest stages of development (Table 5).

3.5.1. Superiority of natural induction over forcible release

The experimental data demonstrated a clear superiority of natural induction for maximizing spore yield. Under this method, the number of liberated spores reached a peak of 63.78 ± 17.92 spores per cystocarp at 7 μmol photons m^{-2} s^{-1}, which was approximately five to six times higher than the yield obtained through forcible release under identical conditions (9.00 ± 2.09 spores/cystocarp) (Table 6). This finding was consistent with the previous experiment (Section 3.4).

3.5.2. Interactive effects of light and release method on germination

Although light was not required for the mechanical process of spore liberation, it functioned as an essential trigger for germination. The GLM identified a significant Method × Light interaction for both liberation ($P = 0.021$) and germination ($P = 0.032$) (Table 5). Under both spore-release methods, germination was initiated as early as day 2 and reached a plateau by day 7 (data not shown). In the natural induction treatments, all spores germinated into germlings under illuminated conditions (Fig. 5). In the forcible release treatment, the number of germlings observed on day 7 was higher than the number of liberated spores recorded on day 2 because the germling counts included germinated spores derived from both freely liberated carpospores and spores that remained attached to the gonimoblast filaments, which were not included in the initial spore counts on day 2.

The near-complete suppression of germination under total darkness (0 μmol photons m^{-2} s^{-1}), which yielded only minimal counts (4.67 and 10.33 germlings in forcible release and natural induction treatments, respectively), confirmed that *A. taxiformis* carpospores are positively photoblastic. These results are consistent with the hatchery protocols established by Statton (2024) and Rule et al. (2025), which recommend low-light environments (5–20 μmol photons m^{-2} s^{-1}) to trigger germination. Total darkness or excessively high irradiance both resulted in a poor germination performance.

These findings suggest that carpospore germination in the Nha Trang lineage is a photomorphogenic process in which light acts not only as a photosynthetic energy source but also as an essential developmental signal (Theobald et al., 2024; Mihaila et al., 2023). The observation that germination reached a plateau at 7 μmol photons m^{-2} s^{-1} suggests that the metabolic requirements for initial cell division are largely satisfied at very low irradiance. This low-light adaptation may reflect an ecological adaptation of tropical *Asparagopsis* strains to ensure recruitment in shaded reef habitats or during low-light settlement windows such as dawn (Rule et al., 2025). Furthermore, the consistency of this light response across both f/2 and PES media indicates that the initial stages of germination rely primarily on the spore's internal metabolic reserves and are independent of external inorganic nutrient concentrations (Mihaila et al., 2023).

The absence of significant medium effects (f/2 versus PES) during the first 7 days suggests that early germination is primarily fueled by endogenous energy reserves. Floridean starch is the primary storage polysaccharide in red algae (Rhodophyceae), including the genus *Asparagopsis* (Sheath et al., 1981). These stored reserves likely provide sufficient energy to support the initial mitotic divisions and early rhizoid and filament formation before the developing germlings become fully dependent on exogenous nutrient uptake.

3.5.3. Evaluation of nutrient media for germling growth and morphological branching

The growth of *Asparagopsis taxiformis* germlings during the first seven days was primarily driven by light intensity and culture medium

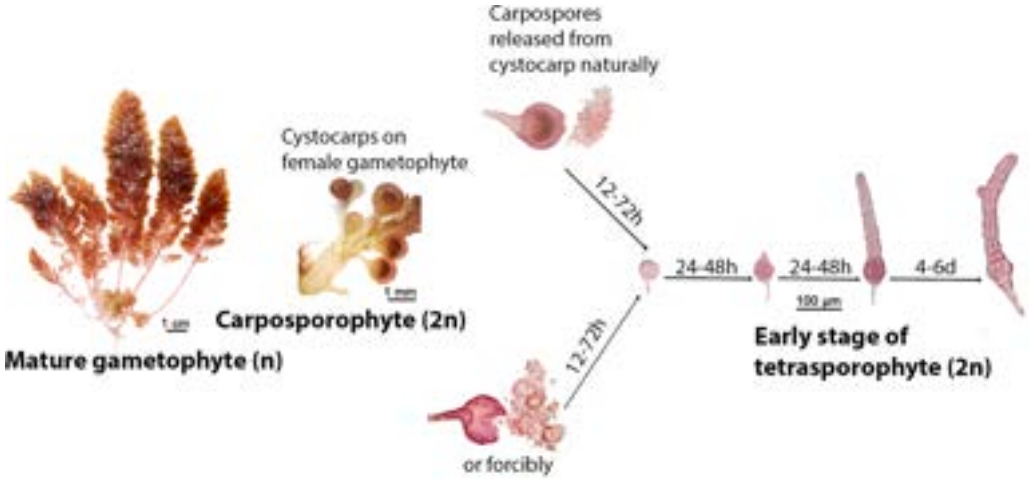

Fig. 4. Microscopic developmental sequence of Asparagopsis taxiformis from released carpospores to branched filamentous germlings (tetrasporophyte).

Table 5
Summary of generalized linear model analysis for number of liberated spores, germinated spores, and germling length.

	No. of liberated spores at day 2			No. of germinated spores at day 7			Germling length (mm) at day 7		
	χ^2	Df	p	χ^2	df	p	χ^2	df*	P
Method	80.182	1	**< 2e-16**	34.069	1	**5.320e-09**	0.088	1	0.7663365
Light	3.324	3	0.34435	62.247	3	**1.945e-13**	22.004	2	**1.667e-05**
Medium	0.044	1	0.83312	0.097	1	0.75573	59.151	1	**1.461e-14**
Method × Light	9.712	3	**0.02118**	8.784	3	**0.03231**	4.249	2	0.1194802
Method × Medium	0.049	1	0.82507	2.926	1	0.08714	0.267	1	0.6051217
Light × Medium	4.578	3	0.20544	3.033	3	0.38656	10.733	2	**0.0046695**
Method × Light × Medium	2.343	3	0.50430	1.855	3	0.60306	14.636	2	**0.0006636**

* Because no spores in dark conditions showed symptoms of germination, the treatment of 0 μmol photons m^{-2} s^{-1} was omitted from the analysis of germling length at day 7.

Table 6
Interactive effects of spore-release method, light intensity, and culture medium on germling length after 7 days. Values are presented as estimated marginal means ± SE (n = 18) derived from the generalized linear model. Different letters indicate significant differences based on Bonferroni-adjusted pairwise comparisons (P < 0.05).

Method	Light (μmol photons m^{-2} s^{-1})	Medium	Germling length (mm)
Forcible release	7	f/2	0.20 ± 0.01^{bcd}
	7	PES	0.09 ± 0.01^{a}
	14	f/2	**0.26 ± 0.03^{cde}**
	14	PES	0.17 ± 0.01^{bcd}
	21	f/2	**0.30 ± 0.02^{de}**
	21	PES	0.18 ± 0.02^{bcd}
Natural induction	7	f/2	0.19 ± 0.01^{bcd}
	7	PES	0.15 ± 0.01^{abc}
	14	f/2	0.20 ± 0.02^{bcd}
	14	PES	0.18 ± 0.05^{bcd}
	21	f/2	**0.39 ± 0.04^{e}**
	21	PES	0.12 ± 0.01^{ab}

(both $P < 0.001$), while the spore-release method showed significant effects only through its interactions with these abiotic factors ($P < 0.001$) (Table 5). The interaction plots demonstrated distinct response patterns of germling length across light intensities depending on both release method and culture medium (Fig. 6). Pairwise differences among treatment combinations are presented in Table 6.

In the f/2 medium, germling length generally increased with increasing light intensity under both spore-release methods. Germlings derived from forcible release exhibited a gradual increase in length from 0.20 mm at 7 μmol photons m^{-2} s^{-1} to 0.30 mm at 21 μmol photons m^{-2} s^{-1} . In contrast, natural induction showed only a slight increase between 7 and 14 μmol photons m^{-2} s^{-1} , followed by a marked increase at 21 μmol photons m^{-2} s^{-1} , reaching the highest recorded value (0.39 ± 0.04 mm) (Fig. 6, Table 6).

In the PES medium, the response pattern differed substantially. Germling length under forcible release increased from 0.09 ± 0.01 mm at 7 μmol photons m^{-2} s^{-1} to 0.18 ± 0.02 mm at 21 μmol photons m^{-2} s^{-1} . However, under natural induction, germling length increased slightly at the intermediate light intensity but declined at the highest light level, decreasing to 0.12 ± 0.01 mm at 21 μmol photons m^{-2} s^{-1} (Fig. 6, Table 6). These contrasting response patterns between the two media supported the significant three-way interaction among Method, Light, and Medium.

The greatest germling elongation was observed in naturally induced spores cultured in f/2 medium at 21 μmol photons m^{-2} s^{-1}, reaching a length of 0.39 ± 0.04 mm. Comparable results were also obtained in forcibly released spores cultured in f/2 medium at 14–21 μmol photons m^{-2} s^{-1} (Table 6). Additional evidence supporting the superiority of the f/2 medium was observed in branching development. In all f/2 treatments, 100% of wells contained at least one branched germling by day 7, whereas branching in PES cultures occurred approximately 1–2 days later. Within the f/2 treatments, neither irradiance nor spore-release

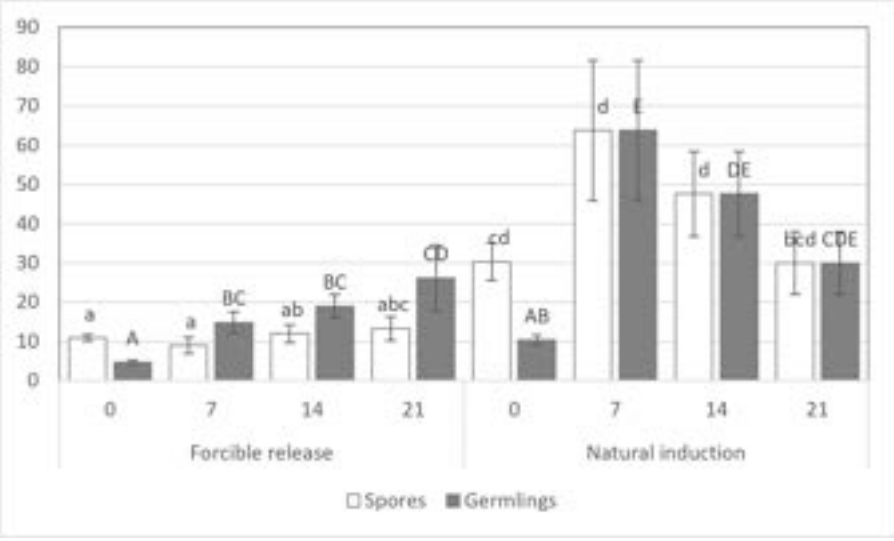

Fig. 5. Number of liberated and germinated carpospores per cystocarp under different spore-release methods (forcible release and natural induction) and light intensities (0, 7, 14, 21 μmol photons m^{-2} s^{-1}). Liberated and germinated spores were quantified on days 2 and 7, respectively. Values are presented as estimated marginal means ± SE (n = 12) derived from the generalized linear model. Data were pooled across culture media for presentation because the medium effect was not statistically significant. Different lowercase or uppercase letters in one set indicate significant differences based on Bonferroni-adjusted pairwise comparisons (P < 0.05).

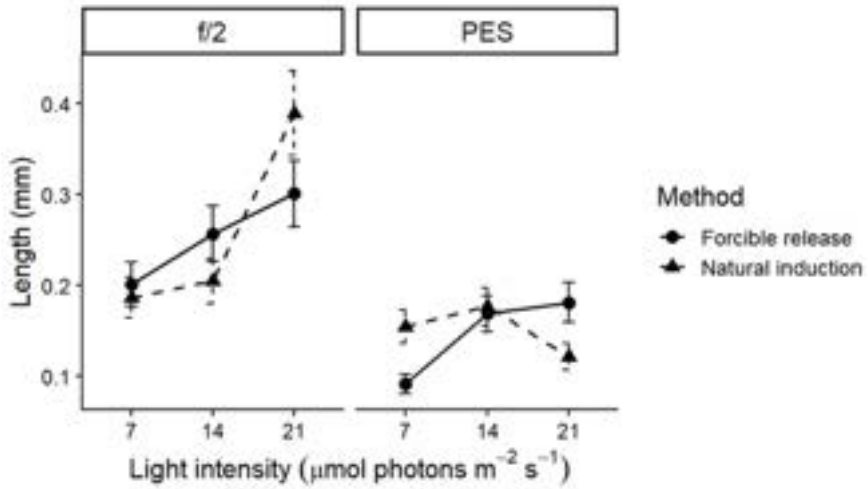

Fig. 6. Interaction effects of release method, light intensity, and culture medium on germling length of A. taxiformis. Values are presented as EMMs, estimated marginal means ± SE, standard error (n = 18) derived from the Gamma generalized linear model.

method exerted significant effects on branching frequency (data not shown).

The better performance of the f/2 medium relative to PES in promoting germling growth suggests that, although initial germination is supported by endogenous carbohydrate reserves such as floridean starch (Sheath et al., 1981), the subsequent transition to rapid filament elongation may become increasingly dependent on the availability of external inorganic nutrients (Hurd et al., 2014; Rule et al., 2025). Differences in germling growth between the two media may therefore reflect differences in nutrient composition, particularly the availability of inorganic macronutrients required to sustain continued cell division and filament development. Although PES medium provides essential trace elements and vitamins that support initial spore stabilization, the comparatively better performance observed in f/2 suggests that its nutrient composition may be more favorable for rapid biomass expansion and branching during the early tetrasporophyte phase (Guillard, 1975; Rule et al., 2025).

Within industrial hatchery systems, early branching represents the transition to the robust tetrasporophyte stage, which can then be further propagated through fragmentation (Statton, 2024). The present findings suggest that although carpospore germination can be initiated successfully in multiple nutrient media, transferring cultures to f/2 medium within the first week of development is likely essential for overcoming the developmental lag observed under less nutrient-enriched conditions and for ensuring that germlings reach harvestable biomass within the economically viable 4–6 week production window proposed for commercial cultivation (Statton, 2024; Mihaila et al., 2023).

Although germling lengths obtained under the forcible release treatment in f/2 medium at irradiances of 7–14 μmol photons m^{-2} s^{-1} were comparable to those observed under natural induction in f/2 medium at 21 μmol photons m^{-2} s^{-1} , the substantially higher spore yield achieved through natural induction made the latter treatment the more practical option for hatchery production. Therefore, from an industrial perspective, the combination of natural induction, f/2 medium, and an irradiance of 21 μmol photons m^{-2} s^{-1} appears particularly effective for maximizing spore production and accelerating the establishment of dense tetrasporophyte biomass, thereby potentially reducing the duration of the early developmental lag phase.

It is important to acknowledge that the experiments were conducted over two consecutive years (2025 and 2026) due to the seasonal availability of mature gametophytes. Although the environmental conditions at the collection site remained comparable between the two periods (Table 1), year-to-year physiological variation in wild broodstock could potentially influence carpospore responses. The consistency of the results regarding the spore-release methods across both years suggests that these temporal variations did not substantially alter the observed developmental trends. However, this year-to-year separation remains a limitation of the study, and future research utilizing long-term cultivated lines would further validate the robustness of these abiotic thresholds.

4. Conclusion

This study establishes the first baseline dataset for the reproductive cultivation of Vietnamese *Asparagopsis taxiformis*. Wild populations from Nha Trang exhibited strong potential as a seed-stock source, characterized by a high reproductive density of 12.3 ± 4.8 cystocarps cm^{-1} . The results further demonstrated that a relatively narrow thermal range of 24–28°C supported 100% carpospore survival and germination. Among the tested culture conditions, the combination of natural induction, f/2 medium, and an irradiance of 21 μmol photons m^{-2} s^{-1} consistently produced the most favorable overall performance, resulting in higher spore release, survival, germination, early germling growth, and morphological branching. This combination is expected to facilitate the rapid establishment of dense tetrasporophyte biomass while reducing the developmental lag phase during hatchery production. In contrast, forcible release produced cleaner cultures under some conditions and may therefore be preferred for establishing clean founder cultures. Overall, the present findings provide an important technical foundation for the development of hatchery systems for Vietnamese *A. taxiformis* and contribute to the advancement of sustainable *Asparagopsis*-based aquaculture to support methane mitigation strategies.

CRediT authorship contribution statement

Khuc Thi An: Investigation. **Nguyen Thi Nhu Thuong:** Investigation. **Nguyen Thi Kim Cuc:** Investigation. **Vo Van Trong:** Investigation. **Tran Ngoc Khanh:** Resources. **Ngo Thi Hoai Duong:** Writing – review & editing, Supervision, Conceptualization. **Pham-Thi Minh-Thu:** Writing – original draft, Validation, Methodology, Investigation, Formal analysis, Data curation, Conceptualization. **Ngo Dang Nghia:** Writing – original draft, Methodology, Formal analysis, Conceptualization.

Declaration of Competing Interest

The authors declare that they have no known competing financial interests or personal relationships that could have appeared to influence the work reported in this paper.

Acknowledgements

This study was financially supported by the Ministry of Education and Training (MOET), Vietnam under project number: B2026-TSN-25. It was also supported by Australasia Agriculture Company Limited, Vietnam.

This work contributes to the celebration of the 50th anniversary of Nha Trang University, located in Khanh Hoa Province, Vietnam.

Data availability

Data will be made available on request.

Dataset for carpospore survival, germination, and early development of Asparagopsis taxiformis under various conditions (Zenodo)

References

Allakhverdiev, S.I., Kreslavski, V.D., Klimov, V.V., Los, D.A., Mimuro, M., Murata, N., 2008. Heat stress: an overview of molecular responses in photosynthesis. Photosynth. Res. 98, 541–550. https://doi.org/10.1007/s11120-008-9331-0.

Batista, M.M., 2020. Reproduction and cultivation of Asparagopsis taxiformis (Delile) Trevisan (Master's thesis). University of Algarve.

Bonin, D.R., Hawkes, M.W., 1987. Systematics and life histories of New Zealand Bonnemaisoniaceae (Bonnemaisoniales, Rhodophyta): I. The genus *Asparagopsis*. N. Z. J. Bot. 25 (4), 577–590. https://doi.org/10.1080/0028825X.1987.10410088.

Chihara, M., 1961. Life cycle of Bonnemaisoniaceous algae in Japan (1). Sci. Repub. Tokyo Kyoiku Daigaku Sect. B 10, 121–154.

Chung, T.V., Tien, N.M., Khang, N.H.T., Tuan, L.C., Minh-Thu, P., 2024. Sea Surface Temperature Variability in Nha Trang Bay, Vietnam: Patterns and Mechanisms. Asian J. Fish. Aquat. Res. 26 (7), 1–11. https://doi.org/10.9734/ajfar/2024/v26i7775.

de Vos, B., Payet, S., Rose, M., Adonis, D., Morin, Z., Monthy, D., Grant, L., Lerata, M., Beukes, D., Lesperance, A., 2025. Assessing the potential for red seaweed *Asparagopsis taxiformis* aquaculture in Seychelles. West. Indian. Ocean. J. Mar. Sci. 24 (1), 11–18.

Do, A.D., Do, V.K., 2013. Current status of seaweed species diversity in investigated islands of Vietnam. J. Mar. Sci. Technol. 13 (2), 105–115.

Eggert, A., 2012. Seaweed responses to temperature. In: Wiencke, C., Bischof, K. (Eds.), Seaweed biology: Novel insights into ecophysiology, ecology and utilization. Springer, pp. 47–66.

FAO, 2013. Tackling climate change through livestock: A global assessment of emissions and mitigation opportunities. Food and Agriculture Organization of the United Nations.

FAO. (2023). *Pathways towards lower emissions: A global assessment of greenhouse gas emissions and mitigation options from livestock agrifood systems*. Rome.

Glasson, C.R.K., Kinley, R.D., de Nys, R., King, N., Adams, S.L., Packer, M.A., Svenson, J., Eason, C.T., Magnusson, M., 2022. Benefits and risks of using seaweed containing bromoform in feed for the reduction of methane production from ruminants. Algal Res. 64, 102673. https://doi.org/10.1016/j.algal.2022.102673.

Guillard, R.R.L., 1975. Culture of phytoplankton for feeding marine invertebrates. In: Smith, W.L., Chanley, M.H. (Eds.), Culture of Marine Invertebrate Animals. Plenum Press, pp. 29–60.

Guillard, R.R.L., Ryther, J.H., 1962. Studies of marine planktonic diatoms. I. *Cyclotella nana* Hustedt, and *Detonula confervacea* (Cleve) Gran. Can. J. Microbiol. 8, 229–239. https://doi.org/10.1139/m62-029.

Guiry, M.D., Dawes, C.J., 1992. Daylength, temperature and nutrient control of tetrasporogenesis in *Asparagopsis armata* (Rhodophyta). J. Exp. Mar. Biol. Ecol. 158 (2), 197–217. https://doi.org/10.1016/0022-0981(92)90226-F.

Hurd, C.L., Harrison, P.J., Bischof, K., Lobban, C.S., 2014. Seaweed ecology and physiology. Cambridge University Press.

IPCC, 2021. Climate Change 2021: The Physical Science Basis. Cambridge University Press.

Jayanti, S.L.L., Tuwo, A., Yasir, I., Tresnati, J., Melanie, H., Yanti, A., 2026. Bioecological analysis of *Asparagopsis taxiformis* (Delile) Trevisan de Saint-Léon, 1845: relationship between morphology, habitat characteristics, and water quality. AACL Bioflux 19 (2), 568–577.

Kinley, R.D., de Nys, R., Vucko, M.J., Machado, L., Tomkins, N.W., 2016. The red macroalgae *Asparagopsis taxiformis* is a potent natural antimethanogenic that reduces methane production during in vitro fermentation with rumen fluid. Anim. Prod. Sci. 56 (3), 282–289. https://doi.org/10.1071/AN15576.

Kinley, R.D., Martinez-Fernandez, G., Matthews, M.K., de Nys, R., Tomkins, N.W., Magnusson, M., 2020. Mitigating the carbon footprint and improving productivity of ruminant livestock using a red seaweed. J. Clean. Prod. 259, 120836. https://doi.org/10.1016/j.jclepro.2020.120836.

Le, V.D., Le, T.T., Rangaraju, S., Vo, P.L., Nguyen, K.V., 2023. The potential for solar energy in Vietnam. Int. J. Manag. Technol. Res. Stud. 05 (02), 20235.

Lopez, R.G., Runkle, E.S. (Eds.), 2021. Light Management in Controlled Environments. Meister Media Worldwide, Willoughby, OH.

Machado, L., Magnusson, M., Paul, N.A., de Nys, R., Tomkins, N., 2016. Effects of marine and freshwater macroalgae on in vitro total gas and methane production. PLoS. ONE 11 (1), e0165892. https://doi.org/10.1371/journal.pone.0165892.

Mairh, O.P., 1977. Studies on *Asparagopsis taxiformis* (Delile) Collins and Harvey from Indian waters. J. Mar. Biol. Assoc. India 19, 97–106.

Mata, L., Gaspar, H., Santos, R., 2012. Carbon/nutrient balance in relation to biomass production and halogenated compound content in the red alga *Asparagopsis taxiformis*. J. Phycol. 48 (1), 248–253. https://doi.org/10.1111/j.1529-8817.2011.01104.x.

Mickelson, A., 2013. Defining culture requirements for reproduction and growth of Asparagopsis taxiformis, a Hawaiian native red alga (MSc Thesis). University of Hawai'i.

Mihaila, A.A., Lawton, R.J., Glasson, C.R.K., Magnusson, M., 2023. Early hatchery protocols for tetrasporogenesis of the antimethanogenic seaweed *Asparagopsis armata*. J. Appl. Phycol. 35, 2323–2335. https://doi.org/10.1007/s10811-023-02985-6.

Nghia, N.D., Minh-Thu, P.T., 2025. *Asparagopsis taxiformis*: potential and perspective for Vietnam seaweed industry to reduce CH4 emission in animal husbandry. Vietnam. J. Mar. Sci. Technol. 25 (3), 369–370. https://doi.org/10.15625/1859-3097/21111.

Nguyen, T.V., Le, N.H., Lin, S.M., Steen, F., De Clerck, O., 2013. Checklist of the marine macroalgae of Vietnam. Bot. Mar. 56 (3), 207–227. https://doi.org/10.1515/bot-2013-0010.

Paul, N.A., de Nys, R., Steinberg, P.D., 2006. Chemical defence against bacteria in the red alga *Asparagopsis armata*: linking structure with function. Mar. Ecol. Progress. Ser. 306, 87–101. https://doi.org/10.3354/meps306087.

Pham, H.H., 1969. *Seaweeds of Vietnam*. Ministry of Education and Youth. Saigon Center for Learning Materials.

Posit Team. *(2026)*. RStudio: Integrated Development Environment for R (Version 2024.12.1+563) [Computer software]. Posit Software, PBC. https://posit.co/products/open-source/rstudio/.

Provasoli, L., 1966. Media and prospects for the cultivation of marine algae. Proc. US-Jpn. Conf. Sept. 1966.

Resetarits, H.M., Dishon, G., Agarwal, V., Smith, J.E., 2024. The effects of temperature and CO2 enrichment on the red seaweed *Asparagopsis taxiformis* from Southern California with implications for aquaculture. J. Phycol. 60 (6), 1567–1584. https://doi.org/10.1111/jpy.13481.

Roque, B.M., Salwen, J.K., Kinley, R., Kebreab, E., 2021a. Inclusion of *Asparagopsis armata* in lactating dairy cows' diet reduces enteric methane emissions by over 50 %. J. Clean. Prod. 284, 124386. https://doi.org/10.1016/j.jclepro.2020.124386.

Roque, B.M., Venegas, M., Kinley, R.D., de Nys, R., Duarte, T.L., Yang, X., Kebreab, E., 2021b. Red seaweed (*Asparagopsis taxiformis*) supplementation reduces enteric methane by over 80 % in beef steers. PLoS. ONE 16 (3), e0247820. https://doi.org/10.1371/journal.pone.0247820.

Rule, M.B., Wernberg, T., Kendrick, G.A., Rule, M.J., 2013. Reproductive synchrony in a habitat-forming kelp and its relationship with environmental conditions. Mar. Biol. 160, 119–126. https://doi.org/10.1007/s00227-012-2069-0.

Rule, M.B., Lane, J., Martins, A.P., Cyrus, M.D., Nayar, S., Hoang, T., Knauer, J., 2025. Hatchery and cultivation manual for the red seaweed Asparagopsis spp. Fisheries Research and Development Corporation.

Sager, J.C., Mc Farlane, J.C., 1997. Radiation. In: Langhans, R.W., Tibbitts, T.W. (Eds.), Plant Growth Chamber Handbook. Iowa Agriculture and Home Economics Experiment Station Special Report, pp. 1–30.

Schneider, C.A., Rasband, W.S., Eliceiri, K.W., 2012. NIH Image to ImageJ: 25 years of image analysis. Nat. Methods 9 (7), 671–675. https://doi.org/10.1038/nmeth.2089.

SeaTemperature.info. (2026). Average water temperature in Nha Trang, Khanh Hoa [Online]. Available: https://seatemperature.info. Accessed on May 15, 2026.

Sheath, R., Hellebust, J., Sawa, T., 1981. Ultrastructure of the floridean starch granule. Phycologia 20, 292–297. https://doi.org/10.2216/i0031-8884-20-3-292.1.

Statton, J., 2024. Asparagopsis taxiformis hatchery and cultivation manual: Developing Asparagopsis cultivation at scale for rapid industry growth. AgriFutures Australia. Publication, pp. 24–083 (no).

Theobald, E.J., Rule, M.B., Jackson, T.L., Rula, N.A., Diaz-Pulido, G., Jackson, E.L., 2024. Abiotic triggers for maximising germling numbers in *Asparagopsis taxiformis* (Rhodophyta, Bonnemaisoniales) via tetrasporogenesis. J. Appl. Phycol. https://doi.org/10.1007/s10811-024-03264-w.

Torres, R., Campos, A.M., Goldman, J., 2024. Effects of light quality and intensity on growth and bromoform content of the red seaweed *Asparagopsis taxiformis*. J. Appl. Phycol. 36, 627–637. https://doi.org/10.1007/s10811-023-03126-9.

Time and Date. **(2026).** Sun graph and day duration for Nha Trang [Online]. Available: https://www.timeanddate.com. Accessed on May 15, 2026.

Ventusky (2026). Sea temperature and Solar radiation data for Hon Chong, Nha Trang (March 2025, April 2026). InMeteo [Online]. Available at https://www.ventusky.com/nha-trang. Accessed on May 15, 2026.

Wasson, D., Yarish, C., Hristov, A.N., 2022. Enteric methane mitigation through *Asparagopsis taxiformis* supplementation and potential algal alternatives. Front. Anim. Sci. 3, 999338. https://doi.org/10.3389/fanim.2022.999338.

World Bank, 2016. Vietnam - Coastal Cities Sustainable Environment Project: environmental and social impacts assessment for NhaTrang city sub-project (Report No. SFG2540). World Bank Group, Washington, D.C.

Zanolla, M., Carmona, R., De la Rosa, J., Salvador, N., Sherwood, A.R., Andreakis, N., Altamirano, M., 2014. Morphological differentiation of cryptic lineages within the invasive genus *Asparagopsis*. Phycologia 53, 233–242. https://doi.org/10.2216/13-202.1.

Zanolla, M., Carmona, R., Altamirano, M., 2017. Reproductive ecology of an invasive lineage 2 population of *Asparagopsis taxiformis* (Bonnemaisoniales, Rhodophyta) in

the Alboran Sea (western Mediterranean Sea). Bot. Mar. 60 (6), 627–638. https://doi.org/10.1515/bot-2017-0030.

Zanolla, M., Carmona, R., Mata, L., De la Rosa, J., Sherwood, A., Barranco, C.N., Munos, A.R., Jeschke, M.A., 2022. Concise review of the genus *Asparagopsis* Montagne, 1840. J. Appl. Phycol. 34, 1–10. https://doi.org/10.1007/s10811-021-02665-z.

Zhu, P., Li, D., Yang, Q., Su, P., Wang, H., Heimann, K., Zhang, W., 2021. Commercial cultivation, industrial application, and potential halocarbon biosynthesis pathway of *Asparagopsis* sp. Algal Res. 56, 102319. https://doi.org/10.1016/j.algal.2021.102319.

Regional Studies in Marine Science 101 (2026) 105291

Contents lists available at ScienceDirect

Regional Studies in Marine Science

journal homepage: www.elsevier.com/locate/rsma

Reproductive biology of Chinese thorny oyster, *Spondylus sinensis* Schreibers, 1793 in Khanh Hoa seawater, Vietnam

Hua Thai An [a], Cao Van Nguyen [a], Tran Mai Duc [a], Le Trong Nghia [a], Vu Thi Mo [a], Tran Van Huynh [a], Vu Trong Dai [b], Huynh Minh Sang [a,c,*]

[a] *Institute of Oceanography - Vietnam Academy of Science and Technology, Viet Nam*
[b] *Nha Trang University, Viet Nam*
[c] *Graduate University of Sciences and Technology – Vietnam Academy of Science and Technology, Viet Nam*

ARTICLE INFO

Keywords:
Spondylus sinensis
Reproductive biology
Fecundity
Spawning season
Sexual maturity
Vietnam

ABSTRACT

This study investigates the reproductive biology of the Chinese thorny oyster *Spondylus sinensis* in the nearshore waters of Khanh Hoa Province, Vietnam, to provide baseline information for stock management and aquaculture development. A total of 30 individuals were collected monthly from November 2024 to October 2025 and examined for reproductive characteristics. Five gonadal maturity stages were identified, consistent with reproductive patterns typical of tropical bivalves. The population exhibited a significantly male-biased sex structure, with 55.5% males, 30.0% females, 10.3% hermaphrodites, and 4.1% indeterminate individuals, resulting in a sex ratio of 1.9:1. The gonadosomatic index showed clear seasonality, with peak spawning activity occurring from March to May and a secondary spawning period from July to October. The size at first sexual maturity (L50) was estimated at 50.9 mm shell height, and individuals began reproducing at approximately 46 mm. Absolute fecundity increased with size, averaging 854,540 ± 322,468 eggs per individual, while relative fecundity averaged 8540 ± 2358 eggs per gram of body weight. These findings indicate that *S. sinensis* exhibits an extended spawning season, high fecundity, and size-dependent reproductive characteristics. Establishing harvest size limits above 56 mm and regulating wild collection are recommended to ensure population sustainability. Overall, the study provides foundational reproductive data essential for effective resource management and for supporting future hatchery development of *S. sinensis* in Vietnam.

1. Introduction

Species of the genus *Spondylus* are economically, culturally, and ecologically important marine bivalves distributed throughout tropical and subtropical seas. In Vietnam, they are valued as a high-quality seafood resource and are also widely utilized as raw materials for shell handicrafts, jewelry, and decorative products, contributing to the livelihoods of coastal communities (Lodeiros et al., 2016). Ecologically, *Spondylus* species are reef-associated bivalves that permanently attach to hard substrates such as rocks and coral reefs, where they function as ecosystem engineers by increasing habitat complexity and providing settlement surfaces and refuges for numerous associated organisms (Logan, 1974; Mackensen et al., 2012). Their shells support diverse epibiont and endobiont communities, thereby enhancing local biodiversity and contributing to the structure of benthic ecosystems (Mackensen et al., 2012). Given their ecological importance and commercial value, understanding the biological characteristics and population dynamics of *Spondylus* species is essential for the sustainable management and conservation of these resources.

The thorny oyster (*Spondylus* spp.) is a group of sessile bivalve mollusks characterized by strong attachment to substrates and a wide distribution across tropical and subtropical marine regions worldwide (Stone, 1998; Waller, 2006). In many regions, such as South America and Mediterranean countries, *Spondylus* species are commonly used as food resources (Windler, 2019; Roterman et al., 2015). The Chinese thorny oyster (*Spondylus sinensis*), a member of the broadly distributed genus Spondylus, inhabits tropical and subtropical marine waters (Stone, 1998; Waller, 2006). Species of this genus occur in reef ecosystems ranging from the Caribbean and Atlantic regions to the tropical Indo-Pacific (Lodeiros et al., 2016). As filter feeders, *Spondylus* oysters typically inhabit rocky reef habitats from the intertidal zone to depths of up to 55 m. Individuals attach to rocks, coral reefs, or other solid

* Corresponding author at: Institute of Oceanography - Vietnam Academy of Science and Technology, Viet Nam.
E-mail address: hmsang2000@yahoo.com (H.M. Sang).

https://doi.org/10.1016/j.rsma.2026.105291
Received 13 May 2026; Received in revised form 23 June 2026; Accepted 19 July 2026
Available online 23 July 2026

substrates using byssal threads and often form small clusters of 5–10 individuals per substrate (Lodeiros et al., 2016).

In Khanh Hoa Province, *Spondylus* spp. are economically valuable bivalves due to their high market demand and favorable meat quality. According to our preliminary survey, their commercial price ranges from 200,000 to 400,000 VND/kg (after shell removal). However, the current supply relies entirely on wild harvest because artificial seed production technology has not yet been developed. Unregulated exploitation may increase the risk of resource depletion, highlighting the need for biological studies to support sustainable management and future aquaculture development.

Research on the reproductive biology of the Chinese thorny oyster in the nearshore waters of Khanh Hoa is therefore essential. Such studies provide crucial information on gonadal development stages, sex ratios, spawning seasons, size at first sexual maturity, and fecundity. These data serve as a scientific foundation for proposing management strategies aimed at sustaining, protecting, and responsibly exploiting thorny oyster resources in Khanh Hoa in particularly and in Vietnam's coastal regions in general.

2. Materials and methods

2.1. Sample collection and processing

The study was conducted from November 2024 to October 2025 in the nearshore waters of Khanh Hoa Province, Vietnam (Fig. 1). Each month, thirty S. sinensis individuals of varying sizes were randomly collected yielding a total of 360 specimens. Oyster specimens were collected from natural populations in Nha Trang Bay, Khanh Hoa Province, Vietnam (coordinates: 12°07′03"N–12°18′58"N, 109°11′45"E - 109°22′20"E). Sampling was conducted by SCUBA diving from reef-associated habitats where oysters were attached to rocky substrates, coral rubble, and dead coral colonies. The sampling depth ranged from 10 to 20 m. During the study period, salinity at the collection sites ranged from 33 to 35 ppt. Water temperature was monitored during sampling and ranged from 23 to 26°C. All samples were transported on ice to the Institute of Oceanography, Vietnam, for laboratory analysis (Fig. 2).

2.2. Morphometric measurements

In the laboratory, oysters were sacrificed, and morphometric parameters were recorded. Shell height was measured as the linear distance from the umbo to the ventral shell margin. Total body weight (Wtt) and soft tissue weight (Wtm) were determined using a Pocket Scale Mini AND HL202 electronic balance (capacity: 200 g; accuracy: 0.01 g).

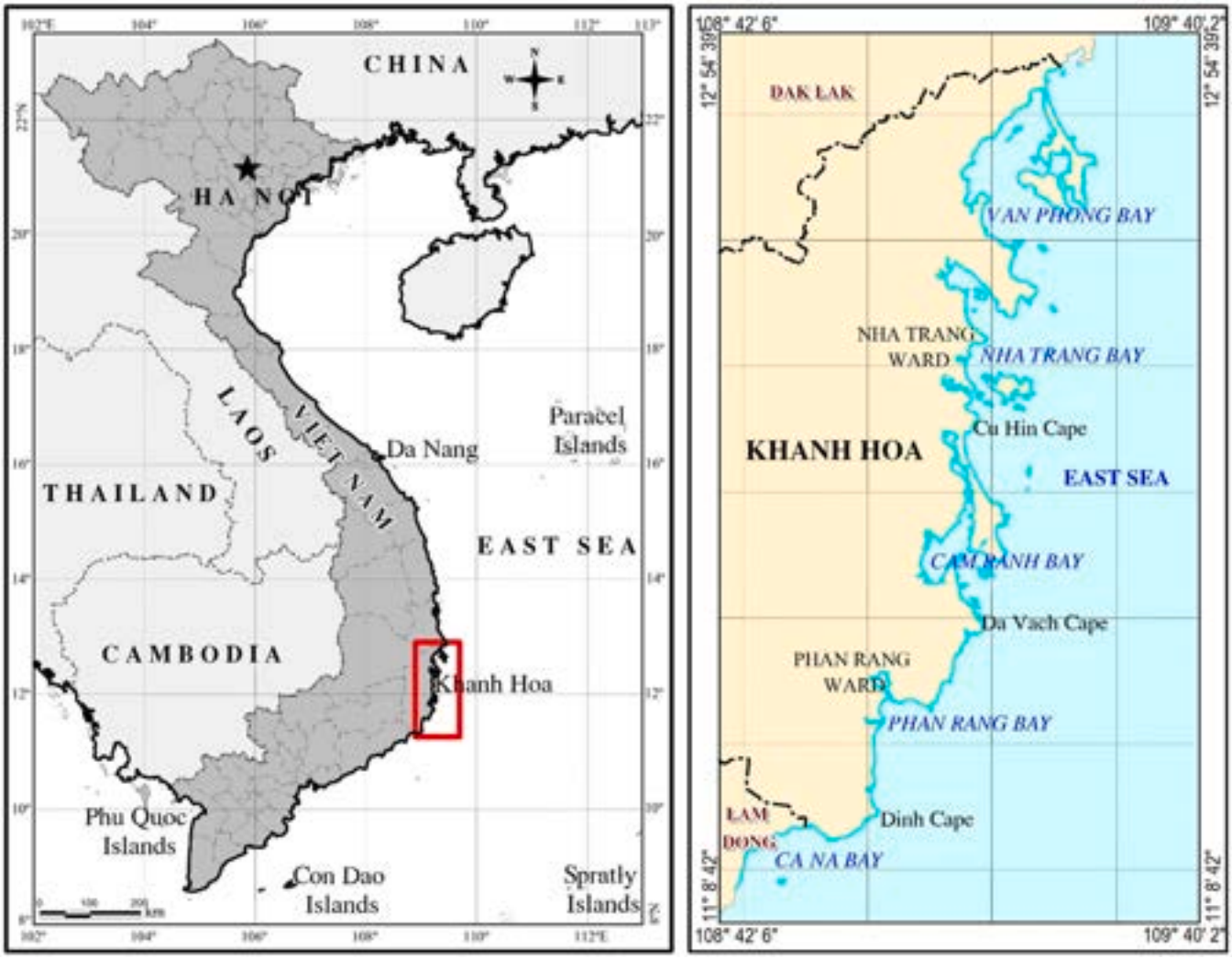

Fig. 1. Sample collection site.

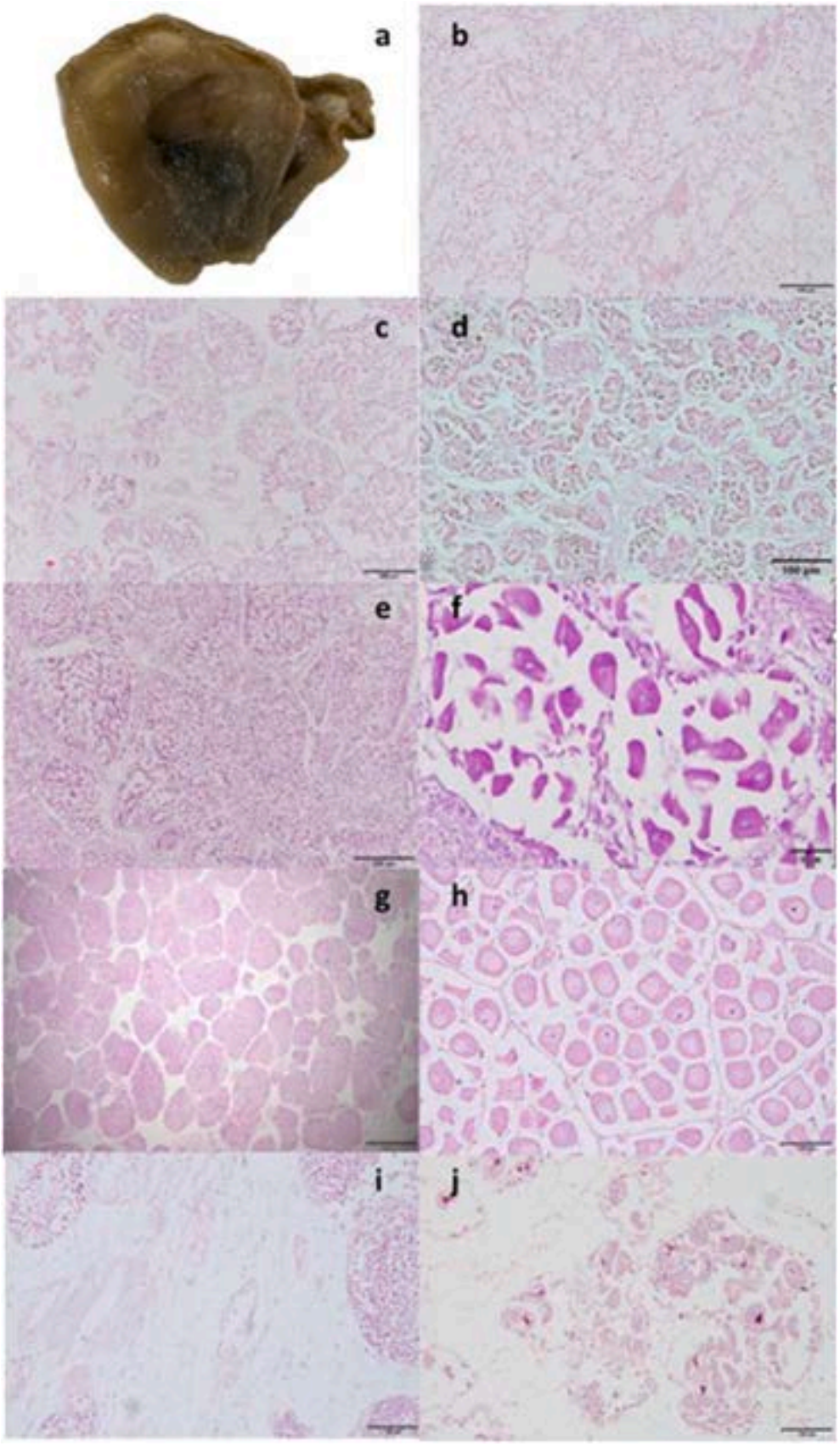

Fig. 2. Histological sections of the ovaries and testes of the *S. sinensis* in Khanh Hoa seawater. (a, b: gonads at stage I; c, e, g, j: testes at stage II, III, IV and V, respectively; d, f, h, j: ovaries at stage II, III, IV and V, respectively).

2.3. Gonad extraction and histological preparation

Histological analysis was performed according to Genc et al. (2007). Reproductive tissues (ovaries or testes) were carefully dissected from each individual and fixed in 5% phosphate-buffered formalin (pH 7.0–7.2) for 24 h prior to dehydration. Gonadal tissues representing each developmental stage were dehydrated through a graded ethanol series (70%, 85%, and 98%) and embedded in paraffin under vacuum. Sections of 4–5 μm were stained with hematoxylin and eosin (H&E).

2.4. Sample analysis and data collection

Gonadal development stages: In females, gonadal development was evaluated based on both the macroscopic appearance of the ovaries and the microscopic characteristics of oocytes. In males, assessment was conducted primarily through the external morphology of the testes. Gonadal developmental stages were classified according to Vaitilingon et al. (2005), using an Olympus BX50 microscope at 10 × and 20 × magnification. Histological sections were photographed and documented at 20 × magnification using the same microscope.

Sex determination and sex ratio: Sex in *S. sinensis* cannot be determined externally; therefore, individuals were dissected and their gonads were examined macroscopically based on morphology and coloration. Monthly and size-specific sex ratios were determined by counting males, females, hermaphrodites, and indeterminate individuals. Individuals exhibiting distinct male- and female-like gonadal tissues within the same gonad were classified as hermaphrodites, whereas specimens with undeveloped or unclear gonadal characteristics were classified as indeterminate.

Sex ratios were calculated as follows:

- Female (%) = (number of females / total individuals) × 100
- Male (%) = (number of males / total individuals) × 100
- Male to Female ratio = a:b (a = number of males; b = number of females)

.

Deviation from the expected 1:1 sex ratio was evaluated using the Chi-square test (χ^2), following Hayslett (1991).

Spawning Season: The spawning season was determined based on the presence of mature and spent individuals in monthly commercial landings and the monthly gonadosomatic index (GSI). The GSI was calculated as:

$$GSI = 100 \times \frac{GW}{BW}$$

where GW is gonad weight and BW is total body weight(gr).

Size at first sexual maturity: Shell height (SH) was measured as the straight-line distance from the umbo to the ventral shell margin, perpendicular to the hinge line, using a digital caliper (±0.01 mm). Shell height was used as the size proxy for all analyses because it is the standard morphometric measurement commonly applied in oyster reproductive studies and is considered a reliable indicator of individual size. To estimate the size at first maturity (H_m), female oysters were grouped into six shell-height classes, and individuals at gonadal stage III or above were considered mature. Size at first sexual maturity was defined as the shell height at which 50% of females possessed ovaries in advanced stages of development (King, 1995). For each size class, the proportion of mature females (P) was adjusted using a correction factor so that the largest size class represented 100% maturity. A linear relationship between shell-height class and ln[(1 − P)/P] was established, and H_m was calculated at P = 0.5.

Fecundity: Absolute and relative fecundity were estimated from 30 mature ovaries (stages III–IV), with each ovary obtained from a different randomly selected mature female, ensuring that each individual contributed only one sample to the analysis. From each ovary, three tissue subsamples (≤ 0.01 g) were taken from the anterior, middle, and posterior regions. Each subsample was diluted in 10 ml of water and homogenized. A 1 ml aliquot was placed in a counting chamber, and stage III–IV oocytes were counted three times, with the mean value calculated.

Absolute fecundity (F) was calculated following Crim and Glebe (1990):

$$F = \frac{G}{g} \times n$$

where G is ovary weight, g is subsample weight, and n is the mean number of oocytes in the subsample.

Relative fecundity was calculated following Bagenal and Tesch (1978).

$$\text{Relative fecundity} = \frac{F}{\text{total body weight}}$$

2.5. Data analysis

Data were analyzed using descriptive and inferential statistical methods. Sex ratio was calculated monthly and for the entire sampling period, and deviations from the expected 1:1 ratio were tested using the chi-square (χ^2) test. The gonadosomatic index (GSI) was expressed as mean ± standard deviation (SD). Gonadal developmental stages were determined histologically, and the relative frequency of each stage was calculated by month to describe the reproductive cycle. Size at first sexual maturity (L_{50}) was estimated by fitting a logistic regression model to the proportion of mature individuals in each shell height class. Absolute and relative fecundity were expressed as mean ± SD. All statistical analyses were performed using Microsoft Excel program.

3. Results

3.1. Gonadal development stages

The Gonadal development stages of *S. sinensis* in Khanh Hoa was described in Table 1

3.2. Sex and sex ratio

Of the 360 samples, 108 (30.0%) were females, 200 (55.6%) were males, 15 (4.2%) were indeterminate, and 37 (10.3%) were hermaphroditic. The overall male to female ratio was 1.9:1, which differed significantly from the expected 1:1 ratio ($\chi^2 = 27.48$, df = 1, $p < 0.001$) (Table 2).

Sex ratios varied by month, with significant deviations observed in November 2024, April 2025, August 2025, and October 2025. These fluctuations may reflect reproductive cycles, environmental influences, or size-dependent sex differentiation (Table 2).

3.3. Spawning season

Gonadosomatic index (GSI) values varied significantly throughout the year. The lowest GSI was observed in January 2025 (3.36%), corresponding to the resting/recovery period. GSI increased from February onward, reaching its annual peak in May (14.12%), indicating peak gonadal maturity and major spawning activity. After the peak, GSI declined but remained relatively high from June to October (10.56–11.41%), suggesting prolonged or intermittent spawning (Fig. 3).

Mature and spawning stages (III–IV) occurred nearly year-round, confirming that *S. sinensis* exhibits an extended spawning period. The primary reproductive peak occurred from March to May, with a secondary spawning period from July to October. Minimal reproductive

Table 1
Maturity stages of the S. sinensis oyster in Khanh Hoa seawater.

Maturity stages	Particular of the gonads
Stage I, Resting/Early redevelopment	*Macroscopic appearance*: Gonads appear as empty, transparent, sac-like structures. Sex cannot be distinguished. *Histology*: Gonads occupy a small area; connective tissue predominates. Residual late-stage gametes (oocytes or spermatocytes) may be present in individuals that recently spawned. Considered a resting or early redevelopment phase (Fig. 2).
Stage II, Initial differentiation	*Macroscopic appearance*: Gonads appear as faint white streaks around the visceral mass. *Histology*: Sparse clusters of small germ cells are visible. Females exhibit small primary oocytes without yolk accumulation, while males show early spermatogenic follicles containing spermatogonia and primary spermatocytes. Connective tissue remains abundant (Fig. 2).
Stage III, Developing/Maturing gonads	*Macroscopic appearance:* Gonads enlarge, swollen, occupying a major portion of the visceral cavity. *Histology:* Well-defined follicles with surrounding somatic layers. Female oocytes increase in size (13–30 μm), stain strongly, and display peripheral nutrient cells. Male follicles contain abundant spermatocytes and active spermatozoa (Fig. 2).
Stage IV: Fully mature/ Spawning-ready	*Macroscopic appearance:* Gonads reach maximum size, thick, filling the visceral cavity. Female gonads range from orange-yellow to deep orange; male gonads are milky white and dense. Free mature gametes are abundant in the gonadal lumen. *Histology:* Mature oocytes (30–70 μm) exhibit eccentric nuclei and thin membranes. Male follicles are distended and densely packed with mature spermatozoa (Fig. 2).
Stage V: Spent / Post-Spawning	*Macroscopic appearance:* Gonads shrink, soften, and regress toward Stage I–II morphology. *Histology:* Follicles collapse; oocytes degenerate; phagocytic cells are present; connective tissue redevelops. Male follicles contain few residual spermatozoa. Marks the end of the reproductive cycle (Fig. 2).

activity was observed in November–December and February (Fig. 4).

3.4. Size at first sexual maturity

The proportion of mature individuals increased with shell height. Individuals began reproducing at approximately 46–50 mm, whereas the 50% maturation threshold (Hm was reached at a shell height of 50.9 mm (Fig. 5).

3.5. Fecundity

The absolute fecundity of *Spondylus sinensis* increased with shell height, with an overall mean of 854,540 ± 322,468 eggs per individual. In the 50–60 mm shell-height group, absolute fecundity ranged from 164,340 to 1176,480 eggs, with a mean of 538,618 ± 302,925 eggs per individual. Individuals in the 61–71 mm size group exhibited markedly higher fecundity, averaging 673,069 ± 196,808 eggs per individual (range: 466,667–954,196 eggs). The largest size group (>71 mm) displayed the highest fecundity values, with a mean of 1174,703 ± 627,762 eggs per individual (range: 317,017–2345,250 eggs). A strong positive relationship was observed between shell height and absolute fecundity, described by the regression equation F = 31,804 H – 1E + 06 (R^2 = 0.90), indicating that larger individuals contributed disproportionately to reproductive output. (Table 3).

4. Discussion

Understanding the reproductive biology of marine bivalves is essential for effective fishery management and aquaculture development. This study provides the first comprehensive assessment of key reproductive parameters of the Chinese thorny oyster *S. sinensis* in the coastal waters of Khanh Hoa. Five gonadal maturity stages were identified, a pattern commonly observed among tropical bivalves that exhibit year-round reproductive activity. Furthermore, the presence of primary growth oocytes alongside vitellogenic oocytes in mature stages suggests continuous gametogenesis, supporting the species' capacity for prolonged spawning under stable tropical conditions.

Beyond taxonomic comparison, the observed reproductive pattern of *S. sinensis* reflects species-specific responses to local environmental conditions. Compared with other tropical oysters such as *Crassostrea (Magallana) bilineata* and *Saccostrea cucullata* from Southeast Asia, which show more synchronized spawning peaks linked closely to monsoonal temperature and salinity fluctuations, *S. sinensis* exhibited a more extended spawning window (Doinsing et al., 2024). This difference likely reflects its reef-associated habitat, where environmental parameters such as temperature and food availability remain relatively stable throughout the year, reducing the need for tightly synchronized spawning events. Recent studies on tropical oysters have demonstrated that prolonged gametogenic activity is often associated with stable thermal regimes and continuous phytoplankton availability (Ezgeta-Balic et al., 2020; Doinsing et al., 2024). In this context, the extended spawning period of *S. sinensis* appears to represent an adaptive reproductive strategy that maximizes reproductive output under relatively predictable environmental conditions.

The increasing proportion of hermaphroditic individuals in larger size classes observed in this study supports the hypothesis that *S. sinensis* exhibits flexible sexual strategies, potentially enhancing reproductive success under fluctuating demographic conditions. Such sexual plasticity has been widely reported in tropical bivalves and is considered advantageous in low-density or heavily exploited populations (Gosling, 2015; Pafras et al., 2024).

Table 2
Monthly variation in sex ratio of the S. sinensis in Khanh Hoa seawater.

Month	Male (No)	Female (No)	Unidentified sex (No)	Hermaphroditic	Total	Male: Female
11/24	16	6	2	6	30	2.7:1
12/24	11	11	4	4	30	1:1
1/25	15	8	6	1	30	1.9:1
2/25	15	13	2	0	30	1.2:1
3/25	15	13	1	1	30	1.2:1
4/25	25	4	0	1	30	6.3:1
5/25	19	9	0	2	30	2.1:1
6/25	16	8	0	6	30	2.0:1
7/25	18	11	0	1	30	1.6:1
8/25	20	8	0	2	30	2.5:1
9/25	15	11	0	4	30	1.4:1
10/25	15	6	0	9	30	2.5:1
Total	200	108	15	37	360	1.9:1
%	**55.6**	**30.0**	**4.2**	**10.3**	**100**	

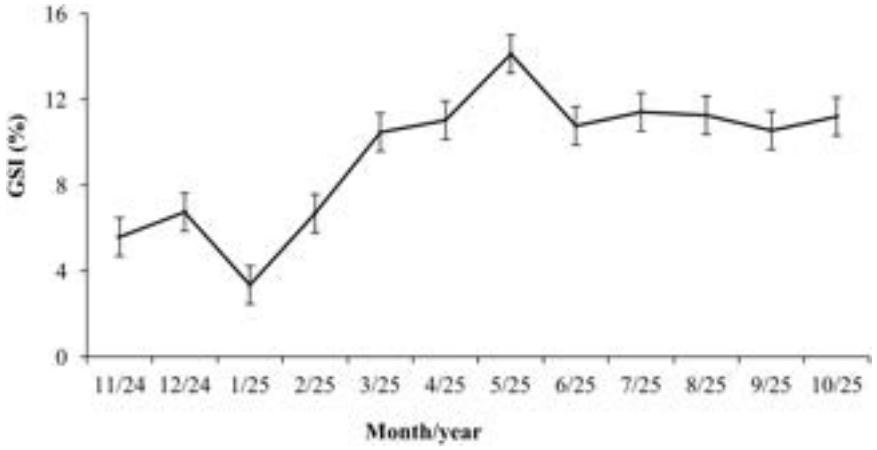

Fig. 3. Monthly Distribution of Gonadosomatic index of the female the *S. sinensis* in Khanh Hoa seawater.

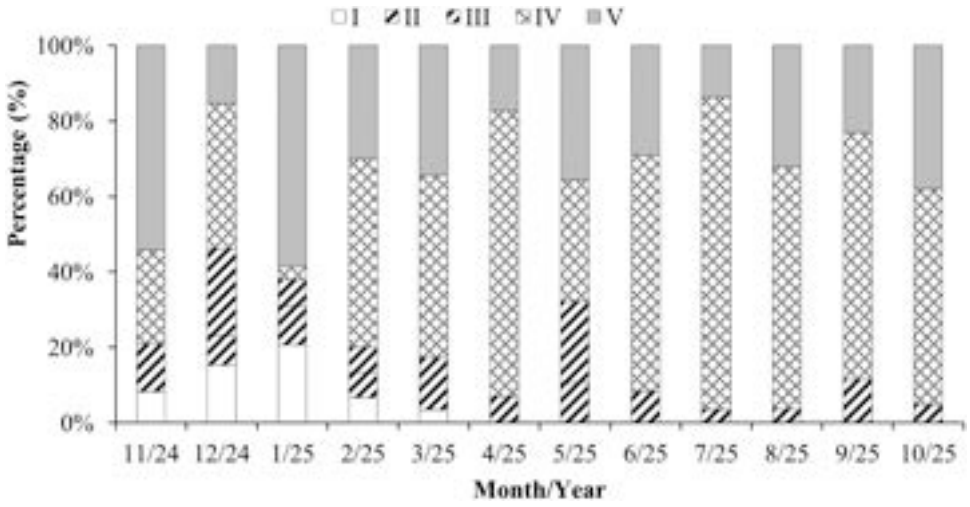

Fig. 4. Monthly distribution of gonadal stage of the *S. sinensis* in Khanh Hoa seawater.

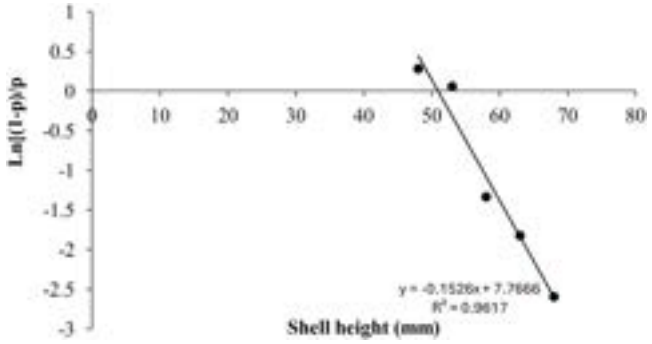

Fig. 5. Relationship between size group and Ln[(1-p)]/p of the *S. sinensis* in Khanh Hoa seawater (P is the proportion of the female oyster at maturation stage).

The sex ratio of *S. sinensis* differed notably from those reported for other *Spondylus* species, which exhibit considerable geographic and species-specific variability. In this study, males dominated the population (1.9:1), similar to male-biased populations reported for *S. leucacanthus* (Villalejo-Fuerte, Garcia-Dominguez, 1998) but contrasting with female-biased or balanced sex ratios observed in *S. gaederopus* (Galinou-Mitsoudi et al., 2019) and *S. varius* (Ruaza and Ilano, 2023). Such discrepancies among studies are unlikely to be taxonomic alone and may be driven by differences in population structure, size composition, and environmental stressors. Recent research on oyster reproductive dynamics indicates that sex ratios can be strongly influenced by growth rate, energy allocation, and habitat quality, particularly in species capable of sex reversal or functional hermaphroditism (Pafras et al., 2024; Barman et al., 2024). A limitation of the present study is that sex determination was based solely on macroscopic examination of gonadal characteristics without histological verification. Consequently, individuals classified as hermaphrodites were identified according to external gonadal appearance, and the simultaneous presence of male and female germ cells within the same gonad could not be confirmed. Further studies combining histological analyses are therefore needed to verify hermaphroditism and to investigate potential sex-changing patterns in this species.

Table 3
Size – dependent of absolute fecundity and relative fecundity of the S. sinensis in Khanh Hoa seawater.

Shell height (mm)	Absolute fecundity (eggs/Ind.)	Relative fecundity (egg/gram body)
50–60	538.618 ± 302.925	9.651 ± 7.108
61–71	673.069 ± 196.808	8.270 ± 3.023
> 71	1.174.703 ± 627.762	8.431 ± 4.517
Mean	**968.708 ± 322.468**	**8.540 ± 2.358**

Monthly gonadal development and gonadosomatic index (GSI)

dynamics revealed an extended spawning season from March to October, with a primary peak in April–May and a secondary peak from July to October (Quayle and Newkirk, 1989). Minimal reproductive activity occurred in November–December and February, corresponding to the resting phase, during which the GSI dropped to a minimum of 3.36%. These observations indicate a cyclical but prolonged reproductive pattern, consistent with other tropical and subtropical *Spondylus* species, including *S. leucacanthus* (June–October; Villalejo-Fuerte and Garcia-Dominguez, 1998), *S. calcifer* (August–September; Villalejo-Fuerte et al., 2002), *S. princeps* (March–July; Villalejo-Fuerte et al., 2005), and *S. spinosus* (June–August; Shabtay et al., 2015). Differences among species are likely influenced by local environmental drivers such as temperature stability, food availability, and hydrodynamics, which affect both gametogenesis and spawning cues. Similar bimodal or prolonged spawning patterns have been reported in tropical oysters such as *Crassostrea gigas* and *C. gasar*, where reproductive activity is closely linked to seasonal increases in temperature and primary productivity (Ezgeta-Balic et al., 2020). However, the presence of mature gonads throughout the year suggests that *S. sinensis* is capable of opportunistic spawning outside the main reproductive peaks, which may enhance population resilience and facilitate rapid recovery following disturbances. The primary (March–May) and secondary (July–October) spawning peaks observed in this study may reflect seasonal variations in environmental conditions, as reproductive activity in marine bivalves is often influenced by factors such as temperature, food availability, salinity, and other environmental cues. Nevertheless, because environmental variables were not monitored during the study period, the factors responsible for triggering these spawning events could not be identified. Future studies integrating reproductive and environmental monitoring are needed to better understand the mechanisms regulating reproduction in *S. sinensis*.

The estimated maturity size of *S. sinensis* (Hm = 50.9 mm) is comparatively smaller than that reported for several congeners Previous studies have reported first maturity or spawning sizes of approximately 65–100 mm in *S. varius* (Ruaza and Ilano, 2023), 86–113 mm in *S. calcifer* (Soria, et al., 2009), and 107.9 mm in *S. limbatus* (Villalejo-Fuerte et al., 2023). These interspecific differences likely reflect variations in growth rates, environmental conditions, and life-history strategies among populations. Compared with larger-bodied species that mature at greater shell heights, the relatively early maturity of *S. sinensis* may represent a trade-off between rapid reproduction and vulnerability to size-selective harvesting. Similar trends have been reported for tropical oysters inhabiting nearshore reef systems, where early maturation is advantageous but increases susceptibility to overexploitation (Doinsing et al., 2024; Pafras et al., 2024).

Fecundity patterns revealed that absolute fecundity increased with shell height, ranging from 164,340–1176,480 eggs in the 50–60 mm size group to 1174,703 ± 627,762 eggs in individuals > 71 mm. Relative fecundity showed less variation, indicating that reproductive investment primarily scales with somatic growth. Compared with conspecifics, fecundity of *S. sinensis* is moderate—lower than highly fecund species such as *S. princeps* (2.2–8.3 million eggs per female) and *S. calcifer* (2.9–35 million eggs per female) but higher than *S. gaederopus* (67,054–1343,303 eggs) Galinou-Mitsoudi et al., (2019)). These variations may be associated with differences in life-history traits, reproductive strategies, and environmental conditions among species. In tropical environments, where favorable conditions often persist throughout the year, reproductive output may be spread across multiple spawning events rather than concentrated into a single, highly fecund spawning episode.

Overall, *S. sinensis* exhibits biological traits characteristic of tropical bivalves: prolonged gametogenic activity, extended spawning season, moderate-to-high fecundity, and early maturity. These features support its potential for aquaculture but also highlight the importance of regulating exploitation, as early-maturing species are particularly susceptible to overharvesting. Protecting individuals below the maturity threshold, restricting fishing during peak spawning months, and monitoring population sex structure are recommended to ensure long-term sustainability. The reproductive baseline established in this study provides a critical foundation for developing hatchery techniques, enhancing restocking programs, and guiding conservation planning for *S. sinensis* in coastal ecosystems.

CRediT authorship contribution statement

Tran Van Huynh: Investigation. **Vu Trong Dai:** Writing – review & editing. **Huynh Minh Sang:** Writing – original draft, Methodology, Investigation, Data curation, Conceptualization. **Tran Mai Duc:** Investigation. **Le Trong Nghia:** Investigation. **Vu Thi Mo:** Investigation. **Hua Thai An:** Project administration, Funding acquisition, Conceptualization. **Cao Van Nguyen:** Investigation.

Ethical statement

This study was conducted in accordance with internationally accepted guidelines for the ethical use of aquatic organisms in research. The oyster species used in this study are invertebrates and are not subject to specific ethical approval requirements under the relevant national and institutional regulations. No endangered or protected species were involved. All experimental and farming procedures were designed to minimize stress and ensure animal welfare throughout the study.

Funding

The authors gratefully acknowledge the financial and logistical support provided by the research project CSCL17.02/25–26.

Declaration of Competing Interest

The authors declare that they have no known competing financial interests or personal relationships that could have appeared to influence the work reported in this paper.

Acknowledgment

The authors gratefully acknowledge the financial and logistical support provided by the research project CSCL17.02/25–26. We also extend our sincere appreciation to Mrs. Le Thi Thu Thao for her dedicated technical assistance during field sampling and laboratory analyses. The authors would like to thank the Institute of Oceanography for providing essential facilities and support throughout the implementation of this study. This work contributes to the celebration of the 50th anniversary of Nha Trang University, located in Nha Trang City, Khanh Hoa Province, Viet Nam.

Data availability

Data will be made available on request.

References

Bagenal, T.B., Tesch, F.W., 1978. Age and Growth. In: Bagenal, T.B. (Ed.), Methods for assessment of fish production in fresh waters, 3rd ed. Blackwell Scientific Publications, pp. 101–136.

Barman, A.C., Wong, N.L.W.S., Abd Karim, M.M., 2024. Reproductive cycle of the oyster *Crassostrea* (Magallana) *saidii* (Wong and Sigwart, 2021) from Southeast Asia. Aquac. Fish. 9 (4), 653–662. https://doi.org/10.1016/j.aaf.2022.05.007.

Crim, L.W., Glebe, B.D., 1990. Reproduction. In: Schreck, C.B., Moyle, P.B. (Eds.), Method for Fish Biology. American Fisheries Society, pp. 529–553.

Doinsing, J., Azad, S., Ransangan, J., 2024. Reproductive biology and spawning pattern of the oyster *Magallana bilineata* in Mengkabong Bay, Sabah, Malaysia. Croat. J. Fish. 82 (1), 19–32. https://doi.org/10.2478/cjf-2024-0003.

Ezgeta-Balic, D., Radonic, I., Bojanic-Varezic, D., Zorica, B., Arapov, J., Staglicic, N., Jozic, S., Peharda, M., Briski, E., Lin, Y., Segvic-Bubic, T., 2020. Reproductive cycle

of a non-native oyster, *Crassostrea gigas*, in the Adriatic Sea. Mediterr. Mar. Sci. 21 (1), 146–156. https://doi.org/10.12681/mms.21304.
Galinou-Mitsoudi, S., Imsiridou, A., Koutra, A., Samaras, D., Samara, E., 2019. Ecology, life cycle and genetic approach of *Spondylus gaederopus* Linnaeus, 1758 (Bivalvia). J. Environ. Prot. Ecol. 20 (2), 713–722.
Genc, M.A., Aktas, M., Genc, E., Yilmaz, E., 2007. Effects of dietary mannan oligosaccharide on growth, body composition and hepatopancreas histology of *Penaeus semisulcatus* (de Haan 1844). Aquac. Nutr. 13, 156–161. https://doi.org/10.1111/j.1365-2095.2007.00469.x.
Gosling, E., 2015. Marine Bivalve Molluscs, 2nd ed. Wiley-Blackwell, 544 pp. https://doi.org/10.1002/9781119045212.
Hayslett, H.T., 1991. Stat. Made Simple Books. 246.
King, M., 1995. Fisheries biology, assessment and management. Fish. N. Books. 341.
Lodeiros, C., Soria, G., Valentich-Scott, P., 2016. Spondylids of Eastern Pacific Ocean. J. Shellfish. Res. 35 (2), 279–293. https://doi.org/10.2983/035.035.0203.
Logan, A., 1974. Morphology and Life Habits of the Recent Cementing Bivalve Spondylus americanus Hermann from the Bermuda Platform. Bull. Mar. Sci. 24 (3), 568–594.
Mackensen, A.K., Brey, T., Bock, C., Luna, S., 2012. Spondylus crassisquama Lamarck, 1819 as a microecosystem and the effects of associated macrofauna on its shell integrity: Isles of biodiversity or sleeping with the enemy? Mar. Biodivers. 42, 449–458.
Pafras, D., Katsanevakis, S., Galinou-Mitsoudi, S., 2024. Reproductive traits and sexual plasticity of the pearl oyster *Pinctada radiata* in the eastern Mediterranean. J. Mar. Sci. Eng. 12 (8), 1259. https://doi.org/10.3390/jmse12081259.
Quayle, D.B., Newkirk, G.F., 1989. Farming Bivalve Molluscs Methods Study and Development. Advances in World Aquaculture. The World Aquaculture Society, p. 294.
Roterman, Y.R., Benayahu, Y., Reshef, L., Gophna, U., 2015. The gill microbiota of invasive and indigenous *Spondylus* oysters from the Mediterranean Sea and northern Red Sea. Environ. Microbiol. Rep. 7 (6), 860–867. https://doi.org/10.1111/1758-2229.12315.
Ruaza Jr, F.C., Ilano, A.P., 2023. Reproductive Cycle of *Spondylus varius* (Sowerby, 1827) in Lianga Bay, Surigao Del Sur, Eastern Mindanao, Philippines. Int. J. Aquat. Biol. 11 (5), 374–382. https://doi.org/10.22034/ijab.v11i5.1705.
Shabtay, A., Rilov, G., Benayahu, Y., 2015. The Indo-Pacific oyster *Spondylus spinosus* Schreibers, 1793 in the eastern Mediterranean sea: Reproductive features. Mollusca Res. 35 (3), 206–212. https://doi.org/10.1080/13235818.2015.1007534.
Soria, G., Cisneros-Mata, M.A., Arreola-Lizárraga, J.A., Cudney-Bueno, R., 2009. Spawning induction, fecundity estimation, and larval culture of Spondylus calcifer (Carpenter, 1857) (Bivalvia: Spondylidae). J. Shellfish. Res. 28 (4), 871–880.
Stone, H.M.I., 1998. On predator deterrence by pronounced shell ornament in epifaunal bivalves. Palaeontology 41 (5), 1051–1068.
Vaitilingon, D., Rasolofonirina, R., Jangoux, M., 2005. Reproductive cycle of edible echinoderms from the southwestern Indian ocean I. *Tripneustes gratilla* L.(Echinoidea, Echinodermatata). West. Indian. Ocean. J. Mar. Sci. 4 (1), 47-60. https://doi.org/10.4314/wiojms.v4i1.28473.
Villalejo-Fuerte, M., Garcia-Dominguez, F., 1998. Reproductive cycle of *Spondylus leucacanthus* at Danzante Island, Gulf of California. J. Shellfish. Res. 17 (4–5), 1037–1042.
Villalejo-Fuerte, M., Arellano-Martinez, M., Ceballos-Vazquez, B., Garcia-Dominguez, F., 2002. Reproductive cycle of *Spondylus calcifer* in Bahia de Loreto National Park, Mexico. J. Shellfish. Res. 21 (1), 103–108.
Villalejo-Fuerte, M., Tripp-Quezaday, A., Garcia-Dominguez, F., 2005. Variations in gonadal, muscle and digestive gland indices of *Spondylus princeps*. Rev. Biol. Mar. Oceanogr. 40 (1), 87–90.
Villalejo-Fuerte, M., Ruiz-Domínguez, M., Cota-Hernández, G.G., Melo-Barrera, F.N., Tripp-Quezada, A., 2023. Parameters of the Spondylus limbatus G.B. Sowerby II, 1847 population in the central-west Gulf of California, Mexico. Invertebr. Reprod. & Dev. 67 (1), 1–13.
Waller, T.R., 2006. Phylogeny of families in the Pectinoidea: Importance of the fossil record. Zool. J. Linn. Soc. 148 (3), 313–342.
Windler, A., 2019. The Use of *Spondylus gaederopus* during the Neolithic of Europe. J. Open. Archaeol. Data 7 (2), 7. https://doi.org/10.5334/joad.59.

Regional Studies in Marine Science 102 (2026) 105336

Contents lists available at ScienceDirect

Regional Studies in Marine Science

journal homepage: www.elsevier.com/locate/rsma

Coral reef degradation is associated with gut microbiome shifts in the tomato anemonefish *Amphiprion frenatus*

Hai-Thanh Thi Nguyen [a,*], Viet Do Hung Dang [b], Dien Duc Tran [b], Anze Abram [c,d], Fabian Gösser [d], James Davis Reimer [d,e]

[a] Department of Biotechnology, School of Fisheries and Life Sciences, Nha Trang University, Khanh Hoa, Viet Nam
[b] Coastal Branch of Joint Vietnam-Russia Tropical Science and Technology Research Center, Khanh Hoa, Viet Nam
[c] Jožef Stefan Institute, Ljubljana, Slovenia
[d] Molecular Invertebrate Systematics & Ecology Lab, Faculty of Science, University of the Ryukyus, Nishihara, Okinawa, Japan
[e] Tropical Biosphere Research Center, University of the Ryukyus, Nishihara, Okinawa, Japan

ARTICLE INFO

Keywords:
Microbiome
16S amplicon
Coral reef
Anemonefish
Nha Trang Bay

ABSTRACT

Anemonefish in association with anemones are iconic images of tropical coral reefs and essential to maintaining the structure and function of coral reefs. Coral reef degradation may influence host-associated microbiomes, yet its effects on anemonefish gut microbial communities remain poorly understood. This study compared the gut microbiomes of the tomato anemonefish, *Amphiprion frenatus,* in symbiosis with the bubble anemone host *Entacmaea quadricolor*, inhabiting two contrasting reef ecosystems: a degraded reef system (Nha Trang Bay - NTB) and a relatively pristine reef system (Van Phong Bay - VPB), Vietnam. Gut microbiomes from 30 fish (n = 15 per bay) were analyzed using 16S rRNA amplicon sequencing. Although Shannon diversity and Evenness did not differ significantly between bays (Shannon: 7.22 ± 0.71 in VPB vs. 6.86 ± 0.70 in NTB; Evenness: 0.84 ± 0.04 vs. 0.85 ± 0.05), fish from VPB harbored significantly richer gut microbiomes, with higher observed ASV richness (407.9 ± 144.7 vs. 282.6 ± 95.3) and Chao1 diversity estimates (626.5 ± 300.9 vs. 367.5 ± 142.8). Beta-diversity analyses showed statistically significant differences in microbial composition and density between sample groups in NTB and VPB (PERMANOVA, R^2=0.094 p = 0.006). Proteobacteria and Firmicutes were dominant phyla in both communities with Firmicutes accounted for 41.59% of sequences in VPB compared with 38.04% in NTB, whereas Proteobacteria represented 35.88% and 42.59%, respectively. In contrast, NTB fish showed a greater relative abundance of Proteobacteria and Planctomycetota. PICRUSt2-based functional predictions suggested enrichment of fermentation and energy acquisition pathways in VPB fish, whereas microbiomes from NTB were associated with predicted functions related to a variety of biosynthetic and metabolic processes. These findings suggest that habitat conditions may be associated with the carbon and nitrogen cycles mediated by the microbial communities within the anemonefish-anemone symbiotic relationship.

1. Introduction

Microbial associations are important for animal biology by providing nutritional supplements and vitamins (Kau et al., 2011), defending hosts against pathogenic invasion (Buffie and Pamer, 2013), and shaping host behaviour (Ezenwa et al., 2012; Gilbert et al., 2016). Although internal microbiomes involve microbes from multiple animal compartments or organs, most of these appear to associate with the digestive and respiratory systems (Woodhams et al., 2020). The significance of gastrointestinal microbes in sustaining host health is well established across mammals and various other taxa (Ley and Hamady, et al., 2008; Ley and Lozupone, et al., 2008), with substantial research in aquaculture fish species and some coral reef fish (Tarnecki et al., 2017; Egerton et al., 2018; Wang et al., 2018; Clever et al., 2022). In coral reef fish, the internal microbiome can affect essential physiological functions related to nutrient absorption, metabolic homeostasis, and immune response of the host (Ngugi et al., 2017; Chausson et al, 2018).

The microbial communities of intestinal tracts of aquatic animals are shaped by a range of intrinsic and extrinsic factors. Intrinsic factors include host genetics, developmental stage, physiological status, and

* Corresponding author.
E-mail address: thanhnth@ntu.edu.vn (H.-T.T. Nguyen).

https://doi.org/10.1016/j.rsma.2026.105336
Received 19 March 2026; Received in revised form 24 June 2026; Accepted 5 August 2026
Available online 9 August 2026

nutritional condition. Extrinsic factors mainly involve dietary and environmental conditions (Chen et al., 2022). Environmental degradation caused by anthropogenic activities has been considered one of the major threats to the maintenance of mutualistic relationships that lead to ecosystem stability (Kiers et al., 2010). Habitat degradation, solely or in combination with other environmental stressors can affect the structure, function, and fitness of their inhabitants at different levels, including disruption of host microbiomes. For example, fish gut microbiomes of the butterflyfish *Chaetodon capistratus* have been seen to have considerably greater variability at degraded reefs, a trend primarily influenced by shifts in the relative abundance of the most prevalent taxa, which may be linked to environmental stress (Clever et al., 2022). Fish living on severely degraded coral reefs were observed to harbor lower abundances of *Endozoicomonas* and a higher diversity of anaerobic fermentative bacteria in their gut microbacterial communities. Nutrients also increase bacterial opportunism and mortality in corals bitten by parrotfish, turning normal trophic interactions deadly for corals (Zaneveld et al., 2016).

The anemonefish-anemone symbiosis is an iconic image of tropical coral reefs and an important model system for understanding potential adaptation mechanisms. In this mutualistic relationship, thirty species of anemonefish have adapted to coexist with 10 species of anemones on coral reefs of the Indian and Pacific Oceans, with various host preferences among the fish species. These anemonefish and anemone associations encompass a broad range of reef environments and involve a variety of anemonefish– anemone combinations, ranging from specialist fish species that are found only on one anemone host species, to generalists that may live with any one of a number of anemone host species (Fautin and Allen, 1992). Among anemonefish, the tomato anemonefish *A. frenatus* can be considered an extreme specialist, found at depths from 2 to 10 m in symbiosis only with the anemone *Entacmaea quadricolor*, both at sites with extensive coral cover and at other sites where the host species is present (Fautin and Allen, 1997). *Amphiprion frenatus*'s strict association with a single host anemone species minimizes host-related variation and allows clearer evaluation of habitat-associated microbiome changes.

Despite their fundamental ecological roles in coral reef symbioses, in many areas anemonefish and anemones populations are losing their natural habitat, due to anthropogenic activities in combination with environmental stressors, thereby reducing species diversity and altering coral reef community structure. Many different coral reef areas are facing urban degradation (Heery et al., 2018), and among these areas, the conditions of coral reefs are particularly concerning in Nha Trang Bay (NTB), Vietnam, as the coral reefs in this region have declined by more than 90% in abundance and coverage compared to earlier levels in a very short time (Tkachenko et al., 2021). The reefs of NTB can currently be considered as both highly degraded and threatened. Indeed, a recent study has also indicated the loss of diversity in anemonefish and their host anemones in this region when compared to both past data and nearby more pristine Van Phong Bay (Nguyen et al., 2026). Van Phong Bay, the largest bay in Khanh Hoa Province, boasts substantial coral reefs, and is generally considered as an area with good water exchange and environmental quality (Phu et al., 2022), in contrast to NTB. Coral reef degradation may be associated with changes in habitat quality, dietary resources, environmental microbial communities, and host physiological stress, which may in turn be linked to shifts in the gut microbiome.

The microbiome composition of hosting clownfish has been shown to be significantly different from those that are non-hosting, and more diverse in both the anemone and the hosting fish. Upon separation of anemonefish from anemones, the microbiomes of these anemonefishes converge to resemble those of non-hosted fish, suggesting that in anemonefish with anemones that there is some kind of transfer from or enrichment by the anemone (Pratte et al., 2018). The convergence of epithelial bacterial communities in both anemonefish and anemones likely plays a key role in their mutual acceptance before first contact (Émie et al., 2021). Furthermore, this anemonefish-anemone specialization is a key factor influencing the taxonomic diversity of the symbiotic anemonefish microbiome, and there is convergence among host anemone microbiomes (Titus et al., 2020).

Although microbial communities play essential roles in host recognition and immunity, the impact of habitat degradation on these communities associated with anemonefish remains largely unknown. Symbioses could help enhance organismal resilience to environmental stressors (Apprill, 2020), such as the facilitation of anemonefish aiding in bleaching recovery of host anemones (Pryor et al., 2020). However, depleted populations of anemones and anemonefish caused by environmental disturbances have been seen to have very slow rates of recovery, implying this dependence may become an obstacle for the recovery of anemonefish and/or anemone populations (Frisch et al., 2019). Therefore, the impacts of ongoing threats caused by direct/indirect anthropogenic activities on the symbioses are unpredictable. The investigation of anemonefish gut microbiomes living on degraded reefs is one essential way to understanding possible adaptation mechanisms of coral reef fish under habitat degradation.

In this study, we examined the variability and composition of the gut microbiome of the anemonefish, *A. frenatus*, occupying the host anemone *E. quadricolor* on a set of reefs in two bays in Viet Nam where the degrees of human impacts are different. We hypothesized that *A. frenatus* inhabiting degraded reefs would exhibit reduced microbial richness, altered community composition, and shifts in predicted metabolic functions relative to conspecific fish from less disturbed reefs.

2. Methods

2.1. Study design

Fish guts for microbiome analyses were collected at two contrasting bays with different levels of reef degradation: 1) from a comparatively disturbed reef area, Nha Trang Bay (NTB), and 2) at comparatively pristine area nearby Van Phong Bay (VPB). The designation of NTB and VPB as environmentally contrasting systems is based on a combination of previously published studies and supporting environmental observations. Specifically, NTB has been described as a highly impacted reef system affected by eutrophication, riverine and urban inputs, coastal development, and severe coral decline (Ben et al., 2025; Hieu et al., 2025, Tkachenko, 2023), whereas VPB has been reported to have better water exchange and several reefs that remain in relatively good condition (Phu et al., 2022).

Two sites in NTB (site 2 and site 6) and one site in VPB (site 9), were targeted for fish collection. Study area and focal species are shown in Fig. 1, geographic coordinates of all sites are provided in Table S1. Sampling sites followed the station nomenclature established in a previous study (Nguyen et al., 2026). At each site, three to four divers searched for anemonefish and anemones within an approximate radius of maximum 200–500 m from the specified coordinates. Visual surveys of anemonefish, their host anemones, and their communities were conducted to evaluate the biodiversity of each study site (Table S1). From each colony of *E. quadricolor*, one to three individuals of *A. frenatus* were collected for fish gut microbiome analyses. At NTB, 10 individual fish were collected from 6 anemone colonies (Ane1- Ane6, Table S2) at site 2; and 5 individual fish were collected from 2 anemone colonies at site 6 (Ane7- Ane8, Table S2). At VPB, 15 individual fish were collected from 10 anemone colonies at site 9 (Ane9- Ane18, Table S2). A total of 15 fish per bay were collected, and the gut dissected for microbiome analyses. For each bay, three surface sea water samples were also collected for microbiome analyses.

2.2. Sample collection

Captured fish, after anesthetization with clove oil, were placed on ice in an individual and labeled sterile Whirl-Pak bag. Total length of each

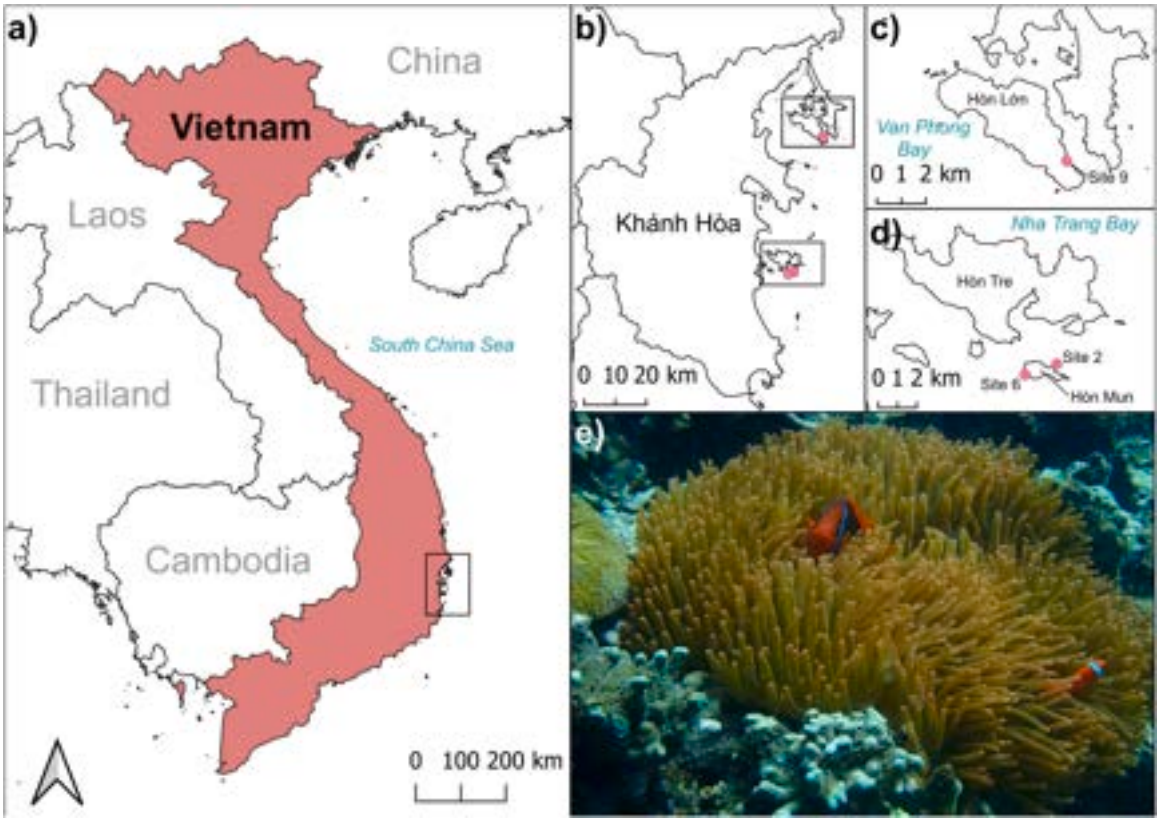

Fig. 1. Study area and focal species. (a) Map of Vietnam with the location of Khánh Hòa Province indicated by the rectangular box. (b) Regional overview of the Khánh Hòa coastline, with inset boxes highlighting the two study areas. (c) Van Phong Bay, showing the sampling location (Site 9). (d) Nha Trang Bay, showing sampling locations around Hòn Mun and adjacent reefs (Sites 2 and 6). Scale bars indicate distance. (e) Tomato clownfish (*Amphiprion frenatus*) inhabiting a bubble-tip anemone (*Entacmaea quadricolor*), representative of the host association observed in the study area.

fish (cm TL) was measured with a digital caliper (Table S2). Afterward, fish were preserved in absolute ethanol and transported on ice to the laboratory as quickly as possible. Upon return to the laboratory, the whole gut of each fish was dissected and then preserved in falcon tubes and stored at −80°C until DNA extraction. Water samples, which were contained in sterile bags, were stored on ice until arrival at the laboratory within 24 h, where the samples were filtered through Sterivex filter (0.22um, Milipore-Merck) using a pump. We transferred bacterial biomass in the filters to falcon tubes using ATL buffer and Proteinase K, and the tubes were then stored at −80°C. In total, 30 fish guts samples and six seawater samples were collected for further analyses.

2.3. DNA extraction and 16S amplification

The microbial DNA of each gut sample was extracted using Qiagen Powersoil DNA isolation kit (Qiagen - USA) following the manufacturer's protocol, in which tissues of all potential preys and fish were homogenized at once. DNA concentration was determined by fluorescence measurement (Qubit - ThermoFisher Scientific, USA). Samples were considered of sufficient quality for further experimental steps when concentrations were ≥ 0.20 ng/μL, amount ≥ 15.00 ng and OD260/OD280 ≥ 1.50.

2.4. Sequencing library and DNA sequencing

The library was prepared by KTest (KTest Science Co. Ltd., Ho Chi Minh, Vietnam) using the xGen™ 16S Amplicon Panel v2 kit (IDT, USA) following the manufacturer's instructions. This assay uses a proprietary multiplex primer pool to generate multiple overlapping amplicons targeting the V1–V9 variable regions of the 16S rRNA gene, the panel produces amplicons with an average size of approximately 425 bp. Final libraries were sequenced on an MGI DNBSEQ-G99 platform using paired-end 150 bp chemistry. Adapter sequences, primers, and low-quality bases were removed using Trimmomatic v0.39 and Cutadapt v2.10 (Martin, 2011). Reads were clustered and dereplicated into amplicon sequence variants (ASVs) using the q2 - DADA2 plugin and denoise single method within the QIIME2 pipeline (Callahan et al., 2016). Unless otherwise specified, default parameters were used for all bioinformatic analyses. ASV subspecies analyses were performed with QIIME2 on the SILVA version 138 SSURef Nr99 database (Quast et al., 2013). Rarefaction depth for diversity analyses was determined based on the sequencing depth distribution and rarefaction curves.

2.5. Analyses of sequence data

Analyses were performed using statistical software R (v1.5.57 R Core Team 2024). Illumina adapter and primer sequences were excised from both forward and reverse reads using Trimmomatic v0.33 (Bolger et al., 2014) together with the barcodes and low-quality bases (Q-score=30). The *mergePairs* function in DADA2 (Callahan et al., 2016) was used to combine denoised paired end reads. Afterward, chimeric sequences were detected and eliminated with the *removeBimeraDenovo* function, yielding high-quality sequences. Amplicon Sequence Variants (ASVs) were assigned to seven taxonomic levels in QIIME2 (Bolyen et al., 2019) using the q2-feature-classifier plugin with the classify consensus blast method against the SILVA SSURef NR99 database (release 138) (Quast et al., 2013) with Blastn sequence similarity ranging from 80% to 97%, to reference sequences.

2.6. Diversity analyses

The relative abundance (%) of Amplicon Sequence Variants (ASVs)

was determined by calculating the ratio of the number of clusters to that of high-quality sequences. Taxonomic composition among samples was visualized using QIIME2 taxa barplots at three hierarchical levels (Phylum, Genus, and Species), focusing on the 20 most abundant taxa. Unidentified species were grouped under "Others". Rarefaction curves were constructed for comparing the number of observed ASVs/features across sequencing depths (see Fig. S1). To evaluate gut microbiome diversity across fish samples and sea water, alpha diversity including Observed taxa, Shannon, Chao1, and Evenness were calculated and visualized by using boxplots. As Shapiro–Wilk tests indicated non-normal distribution of the data, non-parametric Kruskal–Wallis tests were utilized to compare alpha diversity across reefs within the two reef zones (NTB and VPB) ($n = 15$). A distance matrix for ASVs in each sample was calculated using Bray–Curtis dissimilarity to analyze beta diversity across sample categories. Post hoc comparisons with PERMANOVA assessed differences and clustering of fish gut microbiomes among sites. To test for multivariate dispersion (homogeneity of spread) affecting PERMANOVA, Distance-based Test for Homogeneity (DTH), was used with *vegan* package (version 2.7–1) in R (R Core Team 2024), which compares distances from group centroids, revealing if group spreads differ (Anderson, 2006). If significant, then Tukey's HSD would perform pairwise mean comparisons, to find which specific groups have significantly different mean dispersions (Anderson, 2006). nMDS ordination plots are used to interpret beta diversity analyses.

Linear discriminant analysis effect size (LEfSe) analysis was performed using default parameters, with significance assessed using a Kruskal–Wallis test ($\alpha = 0.05$) and an LDA score threshold of 2.0 (Segata et al., 2011). LEfSe analysis was conducted to identify the taxonomic groups of bacteria that are more abundant in the gut of *A. frenatus* symbiotic with anemones at NTB versus VPB. MetaStat was employed to compare species abundance between groups and highlight significant differences (White et al., 2009). To assess gut microbiome metabolism in different groups, PICRUSt was used to infer pathways from the KEGG database (Langille et al., 2013). We then tested whether functional changes in fish gut microbiomes correlated to the habitat the fish inhabited by using Kruskal–Wallis tests. Functional analyses were performed at KEGG levels 2 and 3. Statistical analyses of the collected data were carried out using R Studio software (R Core Team 2024).

3. Results

3.1. Fish length

Fish total length ranged from 1.82 cm to 13.87 cm. The mean total length was 7.63 ± 3.83 cm for NTB and 6.48 ± 2.87 cm for VPB (Table 1). Statistical analysis showed no significant differences in fish total length between the two bays (*t*-test, $t = 0.806$, $p = 0.377$)

3.2. Composition of the fish gut microbiome and biodiversity indexes in the two bays

Quality filtering, followed by bioinformatic processing, a total of 48,666,070 high-quality reads were retained for analyses. The number of reads on each sample ranged from 3783 to 500,358 (Table S3). The total number of different ASVs for the fish gut dataset was 10,357, of which 345 ± 137 (a mean $\pm$ SD) of ASVs per sample, these for the seawater dataset was and 10,323, of which 1720 ± 139 (a mean $\pm$ SD) of ASVs per sample.

Alpha diversity: In both VPB and NTB, the microbial diversity of seawater was significantly higher than the microbial diversity of fish gut when considering ASV frequency with the number of observed features, Shannon index, Everness index and Chao.1 index (Fig. 2; Kruskal-Wallis, $p < 0.01$, File S1). In contrast, seawater microbiomes did not significantly differ between NTB and VPB (Figs. 2B, 2C and 2D; ASVs, $p = 0.97$; Shannon, $p = 0.96$; Chao.1, $p = 0.97$, File S1). There was no significant difference observed in the Shannon index regarding the gut microbiome of fish inhabiting the two bays (Fig. 2A; Kruskal-Wallis, $p = 0.25$, Shannon, $p = 0.61$, File S1). However, both the OTUs and Chao.1 index were found to be significantly higher in VPB compared to NTB (Kruskal-Wallis, OTUs, $p < 0.05$; Chao.1, $p < 0.01$, File S1). The Evenness index was not different between seawater or fish guts in both bays (Kruskal-Wallis, $p = 0.25$, File S1)

Table 1
Total length (cm) of *Amphiprion frenatus* from Nha Trang Bay (NTB) and Van Phong Bay (VPB).

Bay	N	Total length (cm) Mean ± SD	Range (cm)	*t*-test (NTB vs VBP) p-value
Nha Trang Bay (NTB)	15	7.63 ± 3.83	1.82 – 13.87	0.377
Van Phong Bay (VPB)	15	6.48 ± 2.87	2.34 – 11.94	

3.3. Beta diversity

An nMDS plot revealed three main clusters of microbiomes: NTB, VPB, and the sea water groups (Fig. 3). The taxonomic composition of the gut microbiome of *A. frenatus* living in NTB was significantly different from that in VPB, although there was some overlap between fish microbiomes of NTB and VPB (PERMANOVA, $R^2 = 0.094$, $p = 0.006$, Table 2). No significant differences were observed in the microbial composition of the seawater from the two bays (PERMANOVA, $R^2 = 0.608$ $p > 0.05$ Table 2), nor between the microbiomes of fish inhabiting VPB and VPB seawater (PERMANOVA, $R^2 = 0.503$ $p > 0.05$, Table 2**)**. However, significant differences were found between the intestinal microbiome of fish in NTB and sea water in both bays (NTB - SWNTB $R^2 = 0.245$ $p < 0.001$; NTB - SWVPB $R^2 = 0.234$ $p = 0.001$, PERMANOVA, Table 2). A similar grouping pattern was observed in the hierarchical clustering analysis based on ASV-level composition (Fig. S2).

Approximately 99% of all bacteria was grouped into 45 phyla and 948 genera and 1539 species. The dominant taxa in the fish gut microbiome of *A. frenatus* differed between NTB and VPB at multiple taxonomic levels (Figs. 4–6).

At the phylum level, Proteobacteria was the predominant group in NTB (accounting for 42.59%, followed by Firmicutes at 38.04%, Cyanobacteria at 10.58%, and Actinobacteria at 2.87%. In contrast, he dominant phylum in the fish guts from VPB was Firmicutes (41.59%), succeeded by Proteobacteria (35.88%), Cyanobacteria (11.9%), and Actinobacteria (4.23%) (Fig. 5). LEfSe analysis identified significant differences among four gut microbiota phyla between the two bays (LEfSe analysis, Table S4), with two of these phyla-Firmicutes and Planctomycetota-being among the five most abundant phyla ($p < 0.05$, Table S4).

At the genus level, 45 genera were found to have significant differences in abundance between the two bays (LEfSe analysis, Table S4), but no significant differences were observed in top five dominant genera (Table S5).

At the species level, 46 species were observed to have significant differences in abundance between the two bays (LEfSe analysis, Table S4). Of the five most dominant fish gut microbiome species in VPB, *Romboutsia ilealis* was significantly less abundant compared to NTB (Fig. 6, LEfSe analysis, Table S5), while *Paraclostridium benzoelyticum* was more abundant (Fig. 6, LEfSe analysis, Table S5).

3.4. Predicted gut microbiome function using PICRUSt

PICRUSt analyses indicated that *A. frenatus* in symbiosis with anemones in different habitats exhibited similar gene functions at KEGG levels 2 and 3 (Fig. 7, File S2). At level 3, the relative abundance of 57/415 genes for superpathways, generation of precursor metabolite and

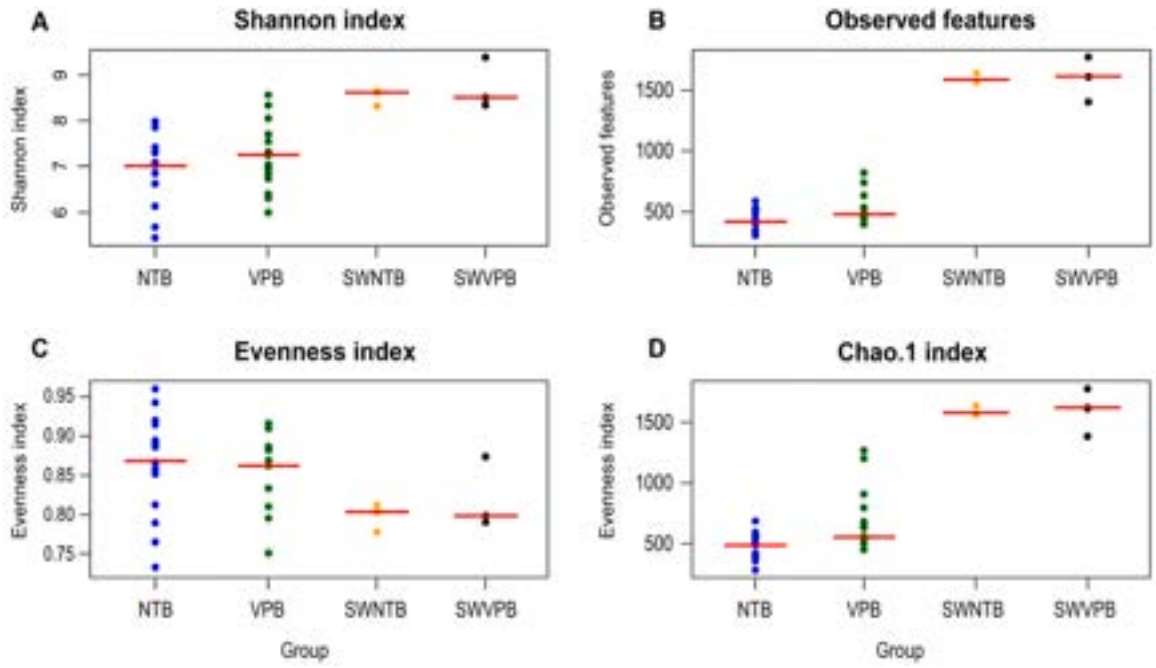

Fig. 2. Differences in alpha diversity (medians shown by red lines) of ASVs between the gut microbiome of *Amphiprion frenatus* and sea waters across two bays.

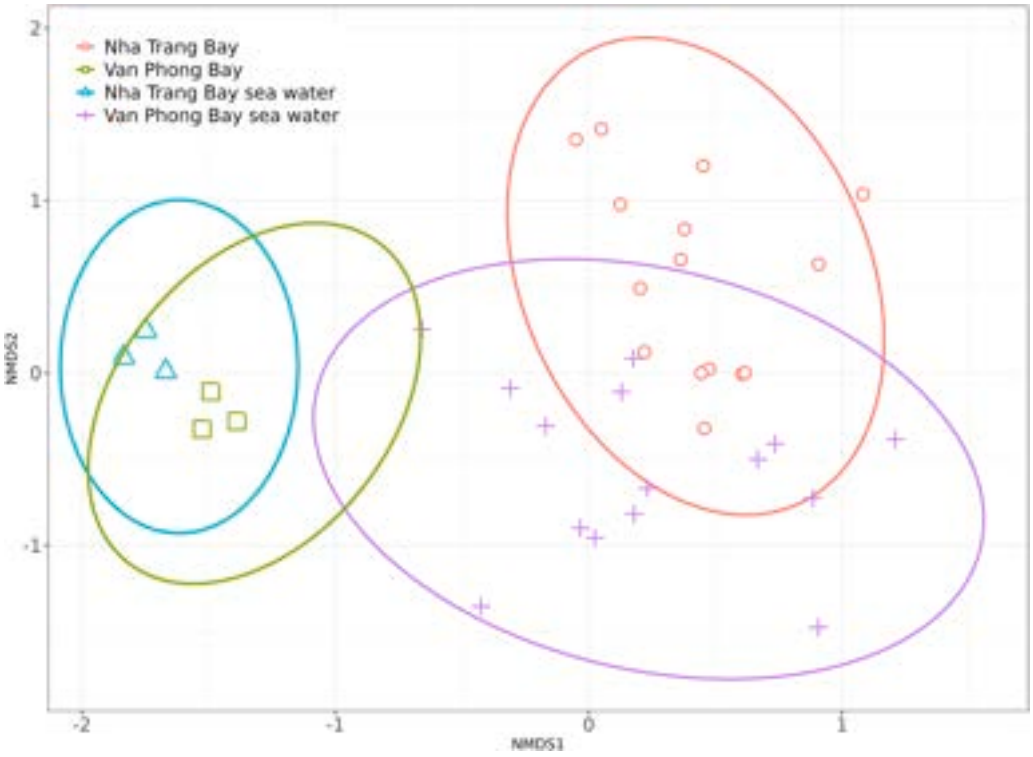

Fig. 3. nMDS plot of Bray–Curtis dissimilarities of microbiome in the gut of fish living in NTB (n = 15) and VPB (n = 15) and surrounding waters (n = 3 for each bay) with 95% confidence ellipses.

energy, degradation/utilization/assimilation and biosynthesis showed statistically significant differences (Kruskal-Wallis test, $p < 0.05$, File S2) between NTB and VPB populations. At level 2, the relative abundance of 15/24 gene groups were significantly different in the two bays (Fig. 7). The relative abundances for six gene groups, including secondary metabolite biosynthesis, inorganic nutrient metabolism; cofactor, prosthetic group, electron carrier degradation; amine and polyamine degradation, fermentation, 1,5-anhydrofructose degradation and other degradation/utilization/assimilation) in VPB were higher than in the NTB population (File S2). Nevertheless, the relative abundances for nine other gene groups, including nucleoside and nucleotide biosynthesis; amino acid biosynthesis amino acid degradation; glycolysis; superpathway of histidine, purine, and pyrimidine biosynthesis; superpathway of glycolysis and the Entner-Doudoroff pathway; aspartate superpathway adenosylcobalamin biosynthesis II (aerobic); adenosylcobalamin biosynthesis I (anaerobic) of the VPB population were

Table 2
One-way PERMANOVA with Bonferroni corrected p values testing significant differences between groups.

	NTB	SWNTB	VPB	SWVPB
NTB	1	0.0066	0.006	0.0078
SWNTB	**0.0066***	1		0.5976
VPB	**0.006***		1	0.1194
SWVPB	**0.0078***	0.5976	0.1194	1

Asterisk (*) indicates statistical difference ($p < 0.05$).

lower than those in the NTB population.

4. Discussion

The present study provides the first comparative assessments of the gut microbiomes of *Amphiprion frenatus* across two ecologically distinct bays in central Vietnam; Nha Trang Bay (NTB) and Van Phong Bay (VPB). By integrating ecological surveys of host anemones and fish communities with high-resolution ASV-based microbial analyses, our findings highlight how differences in habitat condition and environmental context may shape both microbial diversity and taxonomic composition in this anemonefish species.

Ecological patterns observed from the two bays also show that reef degradation and human impacts, especially in NTB, may have influenced the host anemones and associated fish species distributions (Nguyen et al., 2026). Anemones and anemonefish were generally found in deeper areas of NTB, whereas in VPB, anemones were more often encountered in shallower depths, with these being larger in size. It is important to highlight these ecological differences when analysing the gut microbiome patterns found in *A. frenatus*.

Host developmental stage and associated size-related changes can influence gut microbiome composition in fish (Dehler et al., 2017; Bledsoe et al., 2016). To account for this potential confounding factor, we measured the total length of all individuals. The results showed no significant differences in fish total length between NTB and VPB. Therefore, we consider that body size is unlikely to be a major factor of the microbiome differences observed between bays in this study, and thus this factor was not included as a covariate in the microbiome.

4.1. Alpha diversity

The gut microbiome has significant effects on fitness and adaptive plasticity of hosts. Therefore, changes in the composition of the gut microbiome within and among hosts, particularly in relation to environmental variables, provide useful insights into the mechanisms underlying the response of hosts to environmental changes (Miyake et al., 2015; Jones et al., 2018; Clever et al., 2022). Consistent with previous research showing that host-associated microbiomes can vary across environmental gradients, our results revealed notable differences in microbial diversity between the two populations. While Shannon and Evenness indices did not differ significantly between bays, the gut microbiomes of *A. frenatus* were more diverse (higher Observed number of Species - Table 1) and richer (higher Chao.1 index - Table 1) in VPB than those in NTB. These findings indicate that fish residing in VPB may possess a more diverse gut microbiome when rare taxa are considered, could be linked to variations in diet availability, habitat quality or environmental microbial sources.

The structure of intestinal microbial communities is strongly influenced by the host's phylogeny, diet and digestion mechanisms (Miyake et al., 2015; Hayes et al., 2025). Diet was shown to significantly affect the gut microbiome of nine species of surgeonfishs and three other coral reef fish species (Miyake et al., 2015). A more varied diet of piscivorous fish compared to omnivorous fish has been shown to increase the diversity of the gut microbiome (Bledsoe et al., 2016). Anemonefish are carnivorous omnivores, primarily prey up zooplankton, bottom-dwelling invertebrates and algae. The most common prey found in their stomach are copepods and larval tunicates. They also consume dead or diseased tentacles of their host anemones (Fautin and Allen, 1992). Members of a dominant anemonefish pair may range widely to feed, with fish of larger species, including *A. clarkii* and *A. frenatus*, swimming up to many meters from their host anemones to forage. VPB is not located near any major urban center, and is considerably less developed than NTB. As well, VPB sites were further from the coast of mainland Viet Nam, and thus overall less impacted by human activities such as tourism and fishing compared to our NTB sites. Anemonefishes residing within anemones in VPB exhibited increased boldness and a broader range of movement in foraging behavior (Hai Thanh T. Nguyen, personal observation). Consequently, the diet of anemonefish individuals in VPB may support a broader dietary niche, which could in turn contribute to gut microbiome divergence between bays. Furthermore, the shallower coral reefs in VPB may also provide a different prey field and feeding environment, potentially influencing the composition of the gut microbiome. Previously, NTB has been reported as a disturbed ecosystem due to reef degradation (Hieu *et al.* 2025, Tkachenko, 2023) whereas VPB is generally considered as an area with good water exchange and comparatively better marine environment quality (Phu et al., 2022). These differences may be an associated ecological basis to possibly help explain the gut microbiome dissimilarity between bays.

Studies on other reef fishes suggest that habitat degradation and environmental change can influence host-associated microbiomes through multiple ecological pathways, including altered food availability, shifts in foraging behavior, and physiological stress. For example, the facultative coral-feeding butterflyfish *Chaetodon capistratus* living in a degraded coral inner bay zone contained a higher microbial diversity than fish residing in areas of higher levels of coral cover in an outer bay zone (Clever et al., 2022). *C. capistratus* exhibits the capacity to utilize a wide variety of dietary resources, and it has been theorized that that when preferred food sources in degraded coral reefs are scarce, their foraging behavior may diversify. This diversification could result in heightened individual specialization on alternative food items, which in turn may lead to greater variability in gut microbiome composition (Clever et al., 2022). Conversely, under ocean warming, the sergeant major damselfish *Abudefduf vaigiensis* experiences a simplification (reduced diversity) of their stomach microbiome, which restricts their current rate of range extensions and establishment in temperate ecosystems (Hayes et al., 2025).

4.2. Beta diversity

As predicted, *A. frenatus'* gut microbiome composition was distinct from the microbiome in seawater and from each other in the two bays (Fig. 3, Table 1). nMDS and PERMANOVA results showed clear separations between fish microbiomes from the two bays, despite some overlap. Interestingly, seawater microbiota was not significantly different among bays, and the microbiota of VPB fish was not significantly different from VPB seawater. However, NTB fish microbiota showed significant differences from seawater microbiota in both NTB and VPB. This indicates that the gut microbiota of fish in NTB is more influenced by host-intrinsic properties and diet rather than by the surrounding seawater.

NTB and VPB are in the same coastal area in central Vietnam. In this region, the potential for oceanographic mixing exists, which could lead to the homogenization of waterborne microbial communities. Thus, although the two bays differ ecologically, the pelagic microbiome remains relatively uniform. The similarity between VPB fish and VPB seawater might be explained by the fact that our results indicate that VPB fish acquire more microbes directly from the environment compared to NTB fish. Furthermore, larger and healthier host anemones in VPB could potentially assist in providing support to a more diverse environmental microbial life. Also, the reduced levels of pollution and disturbances in VPB result in a more stable microbial community in the

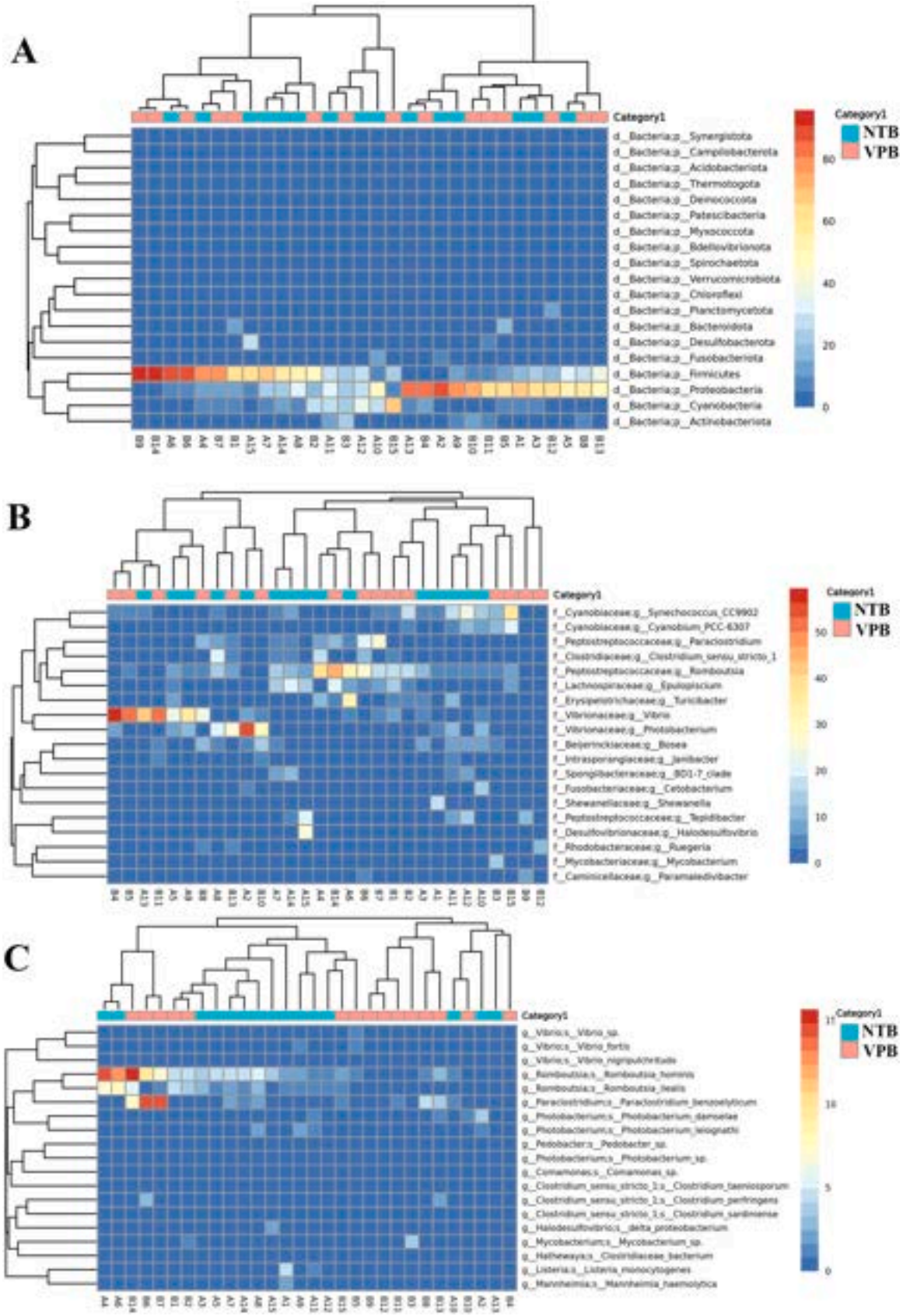

Fig. 4. Heatmap revealing the top 20 most abundant phyla (%), genera (%) and species (%) of internal microbiomes of the anemonefish *Amphiprion frenatus* from NTB and VPB. (A) Phylum, and (B) Genus; (C) Species.

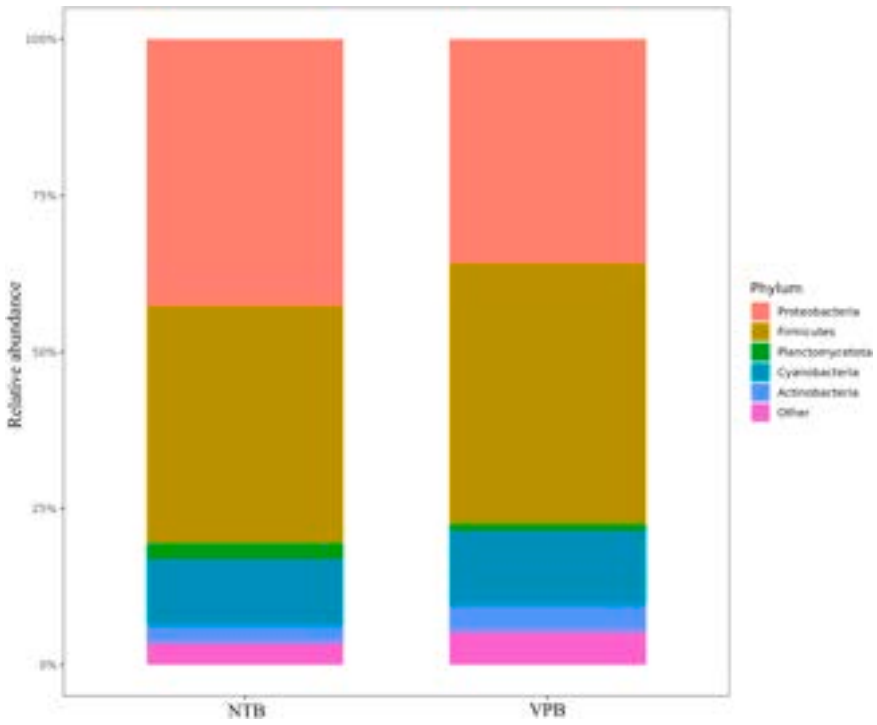

Fig. 5. Relative abundance of the top 5 phylum of the gut microbiota between two bays NTB: Nha Trang Bay; VPB: Van Phong Bay.

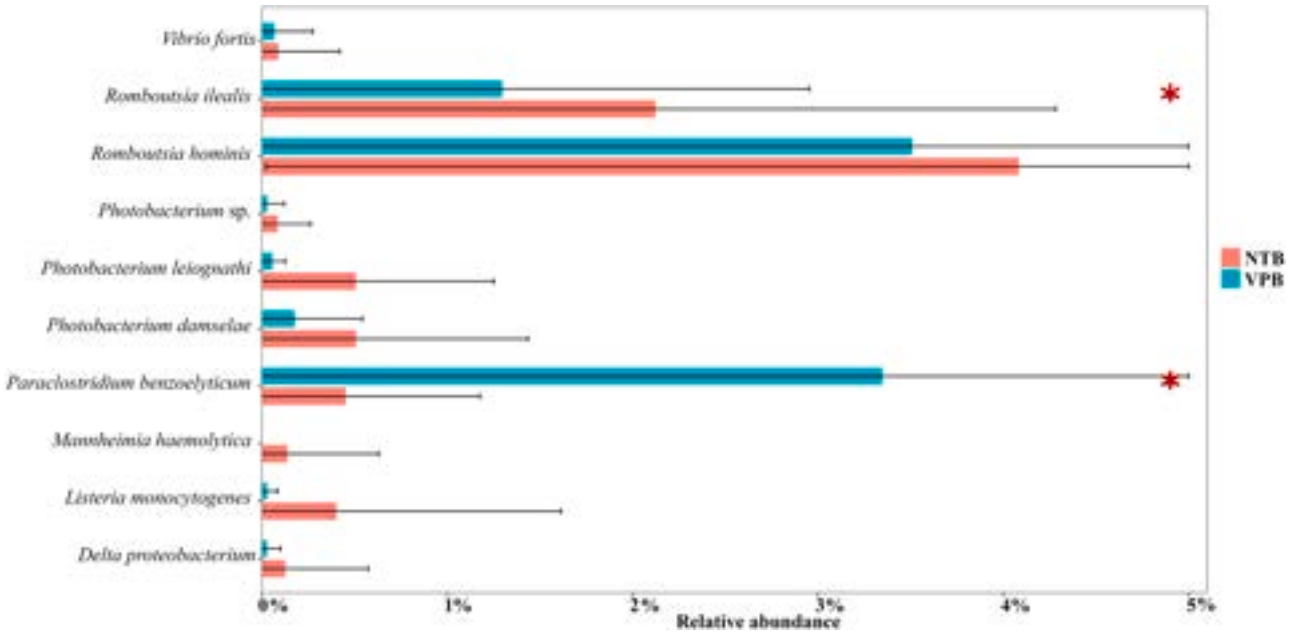

Fig. 6. Relative abundance of the top 10 species of the fish gut microbiota in the two bays. Asterisk (*) indicates statistical difference ($p < 0.05$).

water, which is conductive microbial colonization. Therefore, it appears that the microbiome in VPB fish gut is primarily governed by environmental factors, leading to its similarity with the seawater microbiome.

However, it must also be noted that the significant differences between the fish gut microbiomes and sea water microbiomes in both bays should be interpreted with caution due to considerable disparities in multivariate dispersion among groups. Distance-based Test for Homogeneity (DTH) analysis revealed that when compared to seawater communities, fish gut microbiomes (NTB and VPB) shown substantially higher distances to group centriods, indicating higher within-group variability (Fig. S3), whereas seawater microbiomes were comparatively homogeneous. As PERMANOVA results can be influenced by differences in centroid location and overdispersion, the significant separation between fish and seawater microbiomes seen in the nMDS may also reflect heterogeneity in variance rather than true compositional differences alone. However, the permutation test for homogeneity of multivariate dispersions did not show any significant difference between NTB and VPB fish microbiomes (Figure S3), and the consistent taxonomic and functional divergence suggests that the observed pattern represents biologically meaningful differences. The observed separation in nMDS space and significant results obtained in PERMANOVA indicate actual compositional differences that allow robust biological inferences.

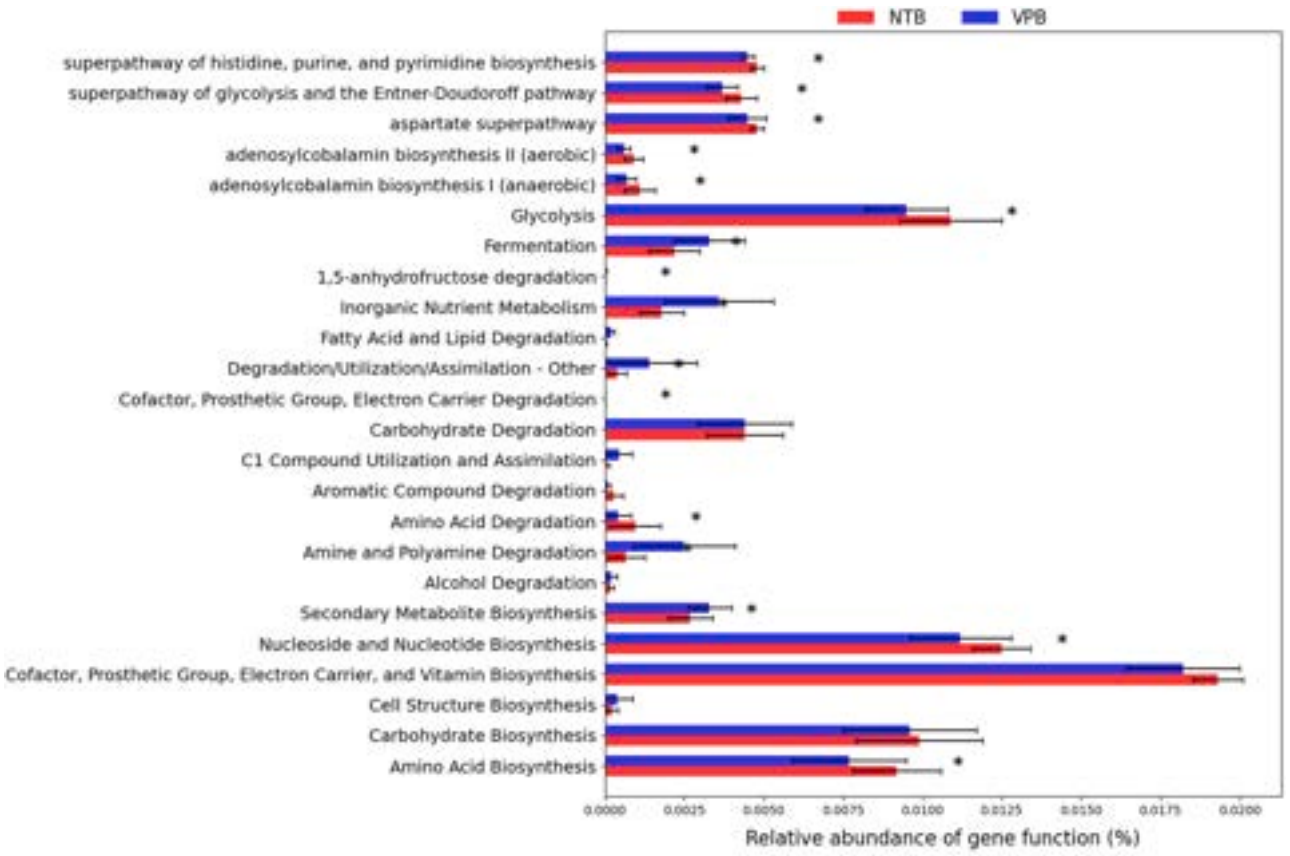

Fig. 7. Comparison of the relative abundance of PICRUSt functional analysis of between fish gut of *Amphiprion frenatus* inhabiting NTB and VPB. Significant differences indicated by asterisk in gene categories at level 2 (t test, $p < 0.05$).

In NTB, coral reefs have experienced significant degradation over the past several decades, especially in shallow waters (1–2 m depths) (Astakhow, 2002; Tkachenko, 2023). Under conditions of environmental disturbance or nutritional limitation, fish undergo increased physiological stress, which in turn increases the selective pressure exerted by the host on its inner microbiome. Thus, their gut microbial assemblages tend to become dominated by more host-filtered, specialized, or even stress-tolerant taxa. Furthermore, dietary shifts linked with to habitat degradation also impact the composition of these microbial assemblages. This leads to a gut microbiome that is less affected by seawater microbial communities and more strongly shaped by intrinsic host factors (Logares et al., 2020), which accounts for the significant differences observed between NTB fish and seawater microbiomes in both bays.

Our findings align with previous research showing that fish harbor microbiomes distinct from those found in their environment (Rawls et al., 2006; Legrand et al., 2020). The microbial gut communities of butterflyfish *C. capistratus* showed a significant difference from that of associated seawater microbiome as well as from potential prey organisms, including sessile invertebrate (Clever et al., 2022). Bledsoe at al. (2016) revealed that food-associated microbiota had a considerable influence on the composition of gut microflora among mummichogs (*F. heteroclitus*). Water is essential for the survival of aquatic animals, and for accessing potential microbes. Nevertheless, it is worth noting that the surrounding water microbiome does not always indicate the host's microbiome aquatic animals as the it is subjected to a variety of unpredicted environmental factors, including host and environmental factors (Chen et al., 2022). Similarly, anemonefish, including *A. frenatus*, live in symbiotic with the host anemone, and these symbioses could help enhance organismal resilience to environmental stressors (Apprill, 2020), while the identity of the hosts and the association of anemonefish depict the majority in the taxonomic diversities of the fish microbiome (Titus et al., 2020).

4.3. Divergence in microbial community structure and functional pathways between two bays

Indeed, in this study, the gut microbiota of *A. frenatus* in symbiosis with *E. quadricolor* living in two bays differed significantly in microbiota composition at all levels, including the phylum, genus and species levels. Taxonomic differences at multiple levels further support the divergence between bays. Difference in multi-level taxonomic composition further supports the divergence between bays. Proteobacteria and Firmucutes were the most dominant communities within the two regions, although their relative proportions differed significantly. LEfSe analysis demonstrated several phyla, including Firmicutes and Planctomycetota, that had significantly different abundances between bays. At lower taxonomic levels, 45 genera and 46 species were noted to have significant, therefore indicating substantial reconstruction of the microbial communities across populations. Specifically, *Romboutsia ilealis* was found more frequently in NTB, and *Paraclostridium benzoelyticum* was more common in VPB, suggesting these shifts may relate to changes in nutrient processing or gut function.

At the phylum level, differences in relative abundance of Proteobacteria and Firmicutes between two bays may indicate variation in environmental stress, water quality, and habitat degradation. Firmicutes and Proteobacteria are found to be the most two abundant phyla in farm-raised fishes when compared to wild-caught fish (Kanika et al., 2025). Proteobacteria are found to thrive in disturbed environments (Shin et al., 2015). In contrast, Firmicutes are Gram-positive bacteria that are known to be essential for host metabolism by fermenting complex carbohydrates and synthesis short-chain fatty acids (SCFAs), which

helps in nutrient absorption and stabilising intestinal pH (Moya and Ferrer, 2016; Blaak et al., 2020). The higher Firmicutes in VPB and higher Proteobacteria in NTB therefore may be associated with better conditions and habitat quality, coupled with lesser physiological stress in VPB.

Under conditions of stress or environmental alteration, hosts frequently impose intensified selective pressure on their gut microbiomes, favouring taxa better adapted to to the modified internal milieu (Clever et al., 2022; Yu et al., 2024). Shallower and healthier VPB habitats likely provide more diverse array of food resources, including zooplankton, mucus-associated microbes, particulate organic matter, whereas degraded NTB reefs may provide an alternative prey spectrum or diets of lower nutritional quality. On severely degraded reefs, fish gut microbiomes show decreased Endozoicomonas, an indicator of healthy hosts, and increased anaerobic fermentative bacteria, suggesting a shift away from coral-based diets (Clever et al., 2022). Heat stress altered the large intestine bacterial communities of calves, characterizing by increased genus Butyrivibrio_3, a known butyrate-producing organism, and changes in bacteria metabolism of energy and amino acid (Yu et al., 2024). A strong positive correlation between the rectal temperature and pro-inflammatory *Eggerthii* spp. was detected in heat stress calves (Yu et al., 2024). The NTB environment has been reported to be more degraded and heavily impacted by tourism and overfishing (Nguyen et al., 2026). Host organisms that are exposed to environmental or physiological stress tend to show a higher relative abundance of Proteobacteria, indicative of the growth of opportunistic heterotrophic microorganisms in conditions of dysbiosis (Shin et al., 2015; Zaneveld et al., 2017).

Variation in diets related to depth, prey, or habitat also significantly influences gut composition in fishes (Nayak, 2010; Sullam et al., 2012). Planctomycetota are common in aquatic environments, which are characterized by an abundance of organic matter, such as biofilms, aggregates, and detritus. Planctomycetota are recognized for their contribution to the degradation of polysaccharide and organic polymers (Fuerst and Sagulenko, 2011). An increased abundance of Planctomycetota in NTB suggests efficient decomposition of complex organic matter, as they are known for having carbohydrate-degrading enzymes (Klimek et al., 2024).

The function of microorganisms can help the host adapt to the specific conditions of each bay. Taxa such as *Romboutsia* and *Paraclostridium* are not only indicators of taxonomic divergence and but also represent different ecological strategies. *Romboutsia* species are flexible anaerobes adapted to nutrient-rich environments with abundance in carbohydrates, exogenous sources of amino acids and vitamins (Gerritsen et al., 2017), a function that may be favored in more stressful and nutrient-variable environments of NTB. In contrast, *P. benzoelyticum*, a member of the Clostridiaceae family, is recognized for its ability to degrade benzoate and other aromatic compounds. This species is typically found in anaerobic environments, including the gastrointestinal tracts of animals, in soil, and other organic-rich substrates. The presence of *P. benzoelyticum* is often linked to the degradation of aromatic compounds, its potential applications in bioremediation, and its interactions within microbial communities (Karakaş et al., 2024). The enrichment of *P. benzoelyticum* in VPB may suggest that this bay is not environmentally uniform at local scales. Although VPB is generally considered less impacted than NTB, aquaculture and other coastal activities in parts of the bay may locally increase organic and nutrient inputs (Phu et al., 2022). Under this interpretation, the higher abundance of *P. benzoelyticum* may reflect the availability of aromatic or other complex organic substrates associated with localized enrichment rather than contradiction of the broader environmental contrast between bays. Furthermore, natural sources of aromatic carbon, including colored dissolved organic matter from algae and seaweed, along with secondary compounds from sponges, corals, and microalgae, may also support the abundance of these bacteria. However, as we did not measure organic pollutants in the water, sediments, or fish tissue, the precise mechanism remains hypothetical and necessitates future verification.

Taxonomic differences at multiple levels reflect the separation between bays and correspond to unique functional profiles. Verde et al. (2015) proposed that the exchange of nutrients between anemone and anemonefish is mediated by microbes. Therefore, shifts in microbial communities may affect carbon and nitrogen cycles (Pratte et al., 2018). Although Proteobacteria and Firmicutes were dominant in gut microbiomes for both regions, a significantly higher proportion of Firmicutes was observed in VPB fish, whereas Proteobacteria, in association with Planctomycetota, were significantly higher in NTB fish. In the same context, the pathways for relative abundance of fermentation, secondary metabolite biosynthesis, and degradation were higher in VPB. This may be due to the well-known fermenting and energy-harvesting capabilities of Firmicutes. On the other hand, glycolysis, amino acid and nucleotide biosynthesis, and super pathways were higher in NTB compared with VPB. This may be due to the common link with the presence of Proteobacteria. The greater presence of Planctomycetota in NTB may suggest efficient degradation of complex organic matter due to altered environmental conditions or dietary influences specific to this bay.

The present study provides evidence for bay-specific variation in the gut microbiome of anemonefish *A. frenatus*, but several limitations should be considered when interpreting the ecological drivers of these patterns. Firstly, our sampling was conducted at a limited number of reef sites, and hence site-specific environmental factors could have influenced the microbiome differences between NTB and VPB. Secondly, although dietary differences represent a biologically plausible explanation for microbiome divergence, their role could not be assessed directly because no dietary samples were collected during the survey. Finally, environmental parameters were also not measured concurrently with microbiome sampling, and therefore reef condition should be viewed cautiously as one of several possible contributors to microbiome variation rather than as a direct explanatory factor. Future studies combining broader spatial sampling with dietary and environmental measurements will be needed to resolve the relative roles of habitat condition, trophic ecology, and local environmental variation in shaping the gut microbiome of *A. frenatus*.

5. Conclusions

These findings revealed that the environmental conditions and ecological context of the host population appear to have a significant influence on both the composition and function of the gut microbiome in *A. frenatus*, an anemonefish that live in association with bubble tip anemone *E. quadricolor*. The anemonefish living in VPB harbor higher microbial diversity with unique function that could be indicate off a less – disturbed or stable ecosystem as compared to NTB, where severe coral reef degradation and anthropogenic impacts has been reported. Further studies, including diet analyses, experimental studies, and long-term environmental monitoring, are needed to fully understand the mechanisms underlying microbiome diversity and their consequences for fish health and ecological resilience.

CRediT authorship contribution statement

Hai-Thanh Thi Nguyen: Writing – original draft, Visualization, Project administration, Methodology, Investigation, Funding acquisition, Formal analysis, Conceptualization. **Anze Abram:** Writing – review & editing, Investigation. **Fabian Gösser:** Writing – review & editing, Writing – original draft, Validation. **James Davis Reimer:** Writing – review & editing, Supervision, Investigation, Funding acquisition, Conceptualization. **Viet Do Hung Dang:** Writing – review & editing, Investigation. **Dien Duc Tran:** Writing – review & editing, Investigation.

Declaration of Generative AI and AI-assisted technologies in the writing process

The author (HTTN) used ChatGPT to check cohesiveness and clarity in some paragraphs of the manuscript's discussion during the preparation. The authors reviewed the sections, taking full responsibility for the content of the published article.

Declaration of Competing Interest

The authors declare that they have no known competing financial interests or personal relationships that could have appeared to influence the work reported in this paper.

Acknowledgements

We are grateful to Huynh Trung Thao for his assistance with field work, and paperwork for NTB. This study was supported by funding from the Nagao Natural Environment Foundation to HTTN and JDR; Ktest company [contract number 02/HĐ/KT-GRANT 2023]; the Joint Vietnam-Russia Tropical Science and Technology Research Center [grant number: VB.Đ1.08/23]. This work contributes to the celebration of the 50th anniversary of Nha Trang University, located in Khanh Hoa Province, Viet Nam. We thank two anonymous reviewers for their comments that greatly improved an earlier version of the manuscript.

Appendix A. Supporting information

Supplementary data associated with this article can be found in the online version at doi:10.1016/j.rsma.2026.105336.

Data availability

Data will be made available on request.

References

Anderson, M.J., 2006. Distance-based tests for homogeneity of multivariate dispersions (Available at:). Biometrics 62 (1), 245–253. https://doi.org/10.1111/j.1541-0420.2005.00440.x.

Apprill, A., 2020. The role of symbioses in the adaptation and stress responses of marine organisms (Available at:). Annu. Rev. Mar. Sci. 12 (1), 291–314. https://doi.org/10.1146/annurev-marine-010419-010641.

Astakhow, D., 2002. "Species composition of anemone-fishes (Perciformes, Pomacentridae) and Their Symbiotic Sea Anemones (Cnidaria, Actiniaria) in the Khanhhoa (South Vietnam),". Vopr. Ikhtiologii 42 (1), 41–55 (In Russian; English translation: *Journal of Ichthyology*, **42**: 37–50).

Ben, H.X., Thinh, T.C., Minh-Thu, P., 2025. A dataset of environmental toxins for water monitoring in coastal waters of southern centre, Vietnam: Case of Nha Trang Bay (Available at:). Data 10 (10), 155. https://doi.org/10.3390/data10100155.

Blaak, E.E., et al., 2020. Short chain fatty acids in human gut and metabolic health (Available at:). Benef. Microbes 11 (5), 411–455. https://doi.org/10.3920/BM2020.0057.

Bledsoe, J.W., et al., 2016. Ontogenetic characterization of the intestinal microbiota of channel catfish through 16S rRNA gene sequencing reveals insights on temporal shifts and the influence of environmental microbes (Available at:). PLoS. ONE 11 (11). https://doi.org/10.1371/journal.pone.0166379.

Bolger, A.M., et al., 2014. Trimmomatic: a flexible trimmer for Illumina sequence data (Available at:). Bioinformatics 30 (15), 2114–2120. https://doi.org/10.1093/bioinformatics/btu170.

Bolyen, E., et al., 2019. Reproducible, interactive, scalable and extensible microbiome data science using QIIME 2 (Available at:). Nat. Biotechnol. 37 (8), 852–857. https://doi.org/10.1038/s41587-019-0209-9.

Buffie, C.G., Pamer, E.G., 2013. Microbiota-mediated colonization resistance against intestinal pathogens (Available at:). Nat. Rev. Immunol. 13 (11), 790–801. https://doi.org/10.1038/nri3535.

Callahan, B.J., et al., 2016. DADA2: High-resolution sample inference from Illumina amplicon data (Available at:). Nat. Methods 13 (7), 581–583. https://doi.org/10.1038/nmeth.3869.

Chausson, J., Srinivasan, M., Jones, G.P., 2018. Host anemone size as a determinant of social group size and structure in the orange clownfish (*Amphiprion percula*) (Available at:). PeerJ 6 (11), e5841. https://doi.org/10.7717/peerj.5841.

Chen, C.-Z., et al., 2022. Exploring the interactions between the gut microbiome and the shifting surrounding aquatic environment in fisheries and aquaculture: A review (Available at:). Environ. Res. 214 (P4), 114202. https://doi.org/10.1016/j.envres.2022.114202.

Clever, F., et al., 2022. The gut microbiome variability of a butterflyfish increases on severely degraded Caribbean reefs (Available at:). Commun. Biol. 5 (1), 770. https://doi.org/10.1038/s42003-022-03679-0.

Dehler, C.E., et al., 2017. Environmental and physiological factors shape the gut microbiota of Atlantic salmon parr (*Salmo salar* L.) (Available at:). Aquaculture 467, 149–157. https://doi.org/10.1016/j.aquaculture.2016.07.017.

Egerton, S., et al., 2018. The Gut Microbiota of Marine Fish (Available at:). Front. Microbiol. 9 (MAY), 1–17. https://doi.org/10.3389/fmicb.2018.00873.

Émie, A.-G., et al., 2021. Microbiomes of clownfish and their symbiotic host anemone converge before their first physical contact (Available at:). Microbiome 9 (1), 109. https://doi.org/10.1186/s40168-021-01058-1.

Ezenwa, V.O., et al., 2012. Animal Behavior and the Microbiome (Available at:). Science 338 (6104), 198–199. https://doi.org/10.1126/science.1227412.

Fautin, D.G., Allen, G.R., 1992. Field guide to anemone fishes and their host sea anemones. Western Australian Museum, Perth, WA (Available at: http://www.nhm.ku.edu/inverts/ebooks/intro.html).

Fautin, D.G., Allen, G.R., 1997. Anemone fishes and their host sea anemones: a guide for aquarists and divers, Revised edition. Western Australian Museum, Perth, WA.

Frisch, A.J., et al., 2019. Recovery potential of mutualistic anemone and anemonefish populations (Available at:). Fish. Res. 218, 1–9. https://doi.org/10.1016/j.fishres.2019.04.018.

Fuerst, J.A., Sagulenko, E., 2011. Beyond the bacterium: planctomycetes challenge our concepts of microbial structure and function (Available at:). Nat. Rev. Microbiol. 9 (6), 403–413. https://doi.org/10.1038/nrmicro2578.

Gerritsen, J., et al., 2017. Genomic and functional analysis of *Romboutsia ilealis* CRIB T reveals adaptation to the small intestine (Available at:). PeerJ 5, e3698. https://doi.org/10.7717/peerj.3698.

Gilbert, J.A., et al., 2016. Microbiome-wide association studies link dynamic microbial consortia to disease (Available at:). Nature 535 (7610), 94–103. https://doi.org/10.1038/nature18850.

Hayes, C., et al., 2025. Stomach Microbiome Simplification of a Coral Reef Fish at Its Novel Cold-Range Edge Under Climate Change (Available at:). Mol. Ecol., e17704. https://doi.org/10.1111/mec.17704.

Heery, E.C., et al., 2018. Urban coral reefs: Degradation and resilience of hard coral assemblages in coastal cities of East and Southeast Asia. Mar. Pollut. Bull. 135, 654–681. https://doi.org/10.1016/j.marpolbul.2018.07.041.

Jones, J., et al., 2018. The Microbiome of the Gastrointestinal Tract of a Range-Shifting Marine Herbivorous Fish (Available at:). Front. Microbiol. 9, 2000. https://doi.org/10.3389/fmicb.2018.02000.

Kanika, N.H., et al., 2025. Fish gut microbiome and its application in aquaculture and biological conservation (Available at:). Front. Microbiol. 15. https://doi.org/10.3389/fmicb.2024.1521048.

Karakaş, İ., et al., 2024. The first record of *Paraclostridium benzoelyticum* and *Enterococcus thailandicus* bacteria isolated from the *Eryx jaculus* (Linnaeus, 1758) snake species distributed in Türkiye (Available at:). GSC Biol. Pharm. Sci. 28 (2), 297–304. https://doi.org/10.30574/gscbps.2024.28.2.0287.

Kau, A.L., et al., 2011. Human nutrition, the gut microbiome and the immune system (Available at:). Nature 474 (7351), 327–336. https://doi.org/10.1038/nature10213.

Kiers, T.E., et al., 2010. Mutualisms in a changing world: an evolutionary perspective (Available at:). Ecol. Lett. 13 (12), 1459–1474. https://doi.org/10.1111/j.1461-0248.2010.01538.x.

Klimek, D., et al., 2024. Comparative genomic analysis of Planctomycetota potential for polysaccharide degradation identifies biotechnologically relevant microbes (Available at:). BMC Genom. 25 (1), 523. https://doi.org/10.1186/s12864-024-10413-z.

Langille, M.G.I., et al., 2013. Predictive functional profiling of microbial communities using 16S rRNA marker gene sequences (Available at:). Nat. Biotechnol. 31 (9), 814–821. https://doi.org/10.1038/nbt.2676.

Legrand, T.P.R.A., et al., 2020. A microbial sea of possibilities: current knowledge and prospects for an improved understanding of the fish microbiome (Available at:). Rev. Aquac. 12 (2), 1101–1134. https://doi.org/10.1111/raq.12375.

Ley, R.E., Hamady, M., et al., 2008. Evolution of Mammals and Their Gut Microbes (Available at:). Science 320 (5883), 1647–1651. https://doi.org/10.1126/science.1155725.

Ley, R.E., Lozupone, C.A., et al., 2008. Worlds within worlds: evolution of the vertebrate gut microbiota (Available at:). Nat. Rev. Microbiol. 6 (10), 776–788. https://doi.org/10.1038/nrmicro1978.

Logares, R., et al., 2020. Disentangling the mechanisms shaping the surface ocean microbiota (Available at:). Microbiome 8 (1), 55. https://doi.org/10.1186/s40168-020-00827-8.

Martin, M., 2011. Cutadapt removes adapter sequences from high-throughput sequencing reads. EMBnet. J. 17 (1), 10–12. https://doi.org/10.14806/ej.17.1.200.

Miyake, S., et al., 2015. Diet strongly influences the gut microbiota of surgeonfishes (Available at:). Mol. Ecol. 24 (3), 656–672. https://doi.org/10.1111/mec.13050.

Moya, A., Ferrer, M., 2016. Functional Redundancy-Induced Stability of Gut Microbiota Subjected to Disturbance (Available at:). Trends Microbiol. 24 (5), 402–413. https://doi.org/10.1016/j.tim.2016.02.002.

Nayak, S.K., 2010. Role of gastrointestinal microbiota in fish (Available at:). Aquac. Res. 41 (11), 1553–1573. https://doi.org/10.1111/j.1365-2109.2010.02546.x.

Ngugi, D.K., et al., 2017. Genomic diversification of giant enteric symbionts reflects host dietary lifestyles (Available at:). Proc. Natl. Acad. Sci. 114 (36), E7592–E7601. https://doi.org/10.1073/pnas.1703070114.

Nguyen, H.-T.T., et al., 2026. Differences in communities of anemones, anemonefish, and other associated species between two bays under different levels of anthropogenic

impacts in Viet Nam (Available at:). Discov. Oceans 3 (1), 39. https://doi.org/10.1007/s44289-026-00153-1.
Phu, L.H., et al., 2022. Environmental Concerns for Sustainable Mariculture in Coastal Waters of South-Central Vietnam (Available at:). Sustainability 14 (13), 8126. https://doi.org/10.3390/su14138126.
Pratte, Z.A., et al., 2018. Association with a sea anemone alters the skin microbiome of clownfish (Available at:). Coral Reefs 37 (4), 1119–1125. https://doi.org/10.1007/s00338-018-01750-z.
Pryor, S.H., et al., 2020. Anemonefish facilitate bleaching recovery in a host sea anemone (Available at:). Sci. Rep. 10 (1), 1–9. https://doi.org/10.1038/s41598-020-75585-6.
Quast, C., et al., 2013. The SILVA ribosomal RNA gene database project: improved data processing and web-based tools (Available at:). Nucleic Acids Res. 41 (D1), D590–D596. https://doi.org/10.1093/nar/gks1219.
Rawls, J.F., et al., 2006. Reciprocal Gut Microbiota Transplants from Zebrafish and Mice to Germ-free Recipients Reveal Host Habitat Selection (Available at:). Cell 127 (2), 423–433. https://doi.org/10.1016/j.cell.2006.08.043.
Segata, N., et al., 2011. Metagenomic biomarker discovery and explanation (Available at:). Genome Biol. 12 (6), R60. https://doi.org/10.1186/gb-2011-12-6-r60.
Shin, N.-R., et al., 2015. Proteobacteria: microbial signature of dysbiosis in gut microbiota (Available at:). Trends Biotechnol. 33 (9), 496–503. https://doi.org/10.1016/j.tibtech.2015.06.011.
Sullam, K.E., et al., 2012. Environmental and ecological factors that shape the gut bacterial communities of fish: a meta-analysis (Available at:). Mol. Ecol. 21 (13), 3363–3378. https://doi.org/10.1111/j.1365-294X.2012.05552.x.
Tarnecki, A.M., et al., 2017. Fish intestinal microbiome: diversity and symbiosis unravelled by metagenomics (Available at:). J. Appl. Microbiol. 123 (1), 2–17. https://doi.org/10.1111/jam.13415.
Titus, B.M., et al., 2020. Host identity and symbiotic association affects the taxonomic and functional diversity of the clownfish-hosting sea anemone microbiome (Available at:). Biol. Lett. 16 (2), 20190738. https://doi.org/10.1098/rsbl.2019.0738.
Tkachenko, K.S., et al., 2021. Extensive coral reef decline in Nha Trang Bay, Vietnam: *Acanthaster planci* outbreak: the final event in a sequence of chronic disturbances (Available at:). Mar. Freshw. Res. 72 (2), 186. https://doi.org/10.1071/MF20005.
Tkachenko, K.S., 2023. Degradation of Coral Reefs under Complex Impact of Natural and Anthropogenic Factors with Nha Trang Bay (Vietnam) as an Example (Available at:), 13 (5), 442–459. https://doi.org/10.1134/S2079086423050079.
Verde, E.A., Cleveland, A., Lee, R.W., 2015. Nutritional exchange in a tropical tripartite symbiosis II: direct evidence for the transfer of nutrients from host anemone and zooxanthellae to anemonefish. Mar. Biol. 162 (12). https://doi.org/10.1007/s00227-015-2768-8.
Wang, A.R., et al., 2018. Progress in fish gastrointestinal microbiota research (Available at:). Rev. Aquac. 10 (3), 626–640. https://doi.org/10.1111/raq.12191.
White, J.R., Nagarajan, N., Pop, M., 2009. Statistical methods for detecting differentially abundant features in clinical metagenomic samples. PLoS comput. biol. 5 (4), e1000352. https://doi.org/10.1371/journal.pcbi.1000352.
Woodhams, D.C., et al., 2020. Host-associated microbiomes are predicted by immune system complexity and climate (Available at:). Genome Biol. 21 (1), 23. https://doi.org/10.1186/s13059-019-1908-8.
Yu, Z., et al., 2024. Heat stress–associated changes in the intestinal barrier, inflammatory signals, and microbiome communities in dairy calves (Available at:). J. Dairy. Sci. 107 (2), 1175–1196. https://doi.org/10.3168/jds.2023-23873.
Zaneveld, J.R., et al., 2016. Overfishing and nutrient pollution interact with temperature to disrupt coral reefs down to microbial scales (Available at:). Nat. Commun. 7 (1), 11833. https://doi.org/10.1038/ncomms11833.
Zaneveld, J.R., et al., 2017. Stress and stability: applying the Anna Karenina principle to animal microbiomes (Available at:). Nat. Microbiol. 2 (9), 17121. https://doi.org/10.1038/nmicrobiol.2017.121.

Regional Studies in Marine Science 100 (2026) 105194

Contents lists available at ScienceDirect

Regional Studies in Marine Science

journal homepage: www.elsevier.com/locate/rsma

Enriching *Artemia* with n-3HUFA modulated growth, survival, digestive enzymes, body composition and stress resistance in giant trevally (*Caranx ignobilis*) larvae

Anh Thi Pham [a], Manh Van Ngo [a], Ha Kim Thi Nguyen [b], Hung Duc Pham [a,*,1]

[a] School of Fisheries and Life Sciences, Nha Trang University, Khanh Hoa, Vietnam
[b] College of Aquaculture and Fisheries, Can Tho University, Can Tho, Vietnam

ARTICLE INFO

Keywords:
Caranx ignobilis
Enrichment
N-3 HUFA
Digestive enzyme
Stress resistance

ABSTRACT

High mortality of marine fish larvae during live-prey feeding and metamorphosis is a bottleneck in commercial hatchery production. This study investigated the effects of dietary highly unsaturated fatty acids (HUFA) used to enrich *Artemia* on the growth, survival, digestive enzyme activity, proximate composition and stress resistance of giant trevally (*Caranx ignobilis*) larvae. The 13 days after hatching larvae were fed *Artemia* enriched with a rich HUFA emulsion at five levels (0, 150, 300, 450 and 600 mg/L) for 28 days. The results indicated that enriched HUFA *Artemia* significantly increased the survival of giant trevally larvae. Larval growth tended to increase in fish fed enriched *Artemia*, with the highest weight and length obtained in a dietary n-3HUFA of 19.03% total fatty acids (TFA). There were no differences in protein and moisture of the larvae fed experimental diets, while lipid content was significantly increased in fish fed n-3HUFA enrichment at 150, 300 and 450 mg/L. The activities of pepsin and trypsin remained unchanged in larvae fed enriched HUFA diets, but significantly increased compared to the unenriched *Artemia* group ($P < 0.05$). Activity of chymotrypsin increased to a peak at 300 mg/L enrichment and was significantly reduced in the 450 and 600 mg/L groups. The mortalities of the larvae after the salinity test were significantly reduced in the 300, 450 and 600 mg/L groups. Overall, dietary n-3HUFA requirements to maximize final body weight and survival for giant trevally during *Artemia* feeding were estimated at 15.63% and 22.67% TFA, respectively based on polynomial regression analysis.

1. Introduction

Giant trevally *Caranx ignobilis* has become an importantly commercial marine fish in Vietnam and Philippines due to its high growth rate, high market price and their high adaptations to brackish and seawater culture (Mutia et al., 2017; Nguyen et al., 2022). Although, preliminary achievements have been reported in broodstock culture, induced spawning and larval rearing, low survival rate (4 – 6%), high deformity and susceptibility to stress during rotifers and *Artemia* feeding and metamorphosis remain challenges to larval rearing (Mutia et al., 2020; Pham, 2023). In the practical rearing, 15 days after hatching (dah) larvae often exhibit abnormal behaviors such as floating on the water surface, forming dense clusters of larvae in tank walls and corners, which limit their capturing and feeding of live-prey, resulting in high mortality during 18 – 22dah (Mutia et al., 2024; Pham, 2023). High mortality of marine larvae has been associated with suboptimal rearing conditions, and poor quality live feed with a deficiency in highly unsaturated fatty acids (HUFA), which do not meet the nutritional requirements of the larvae (Cavrois-Rogacki et al., 2020; Dhont et al., 2013; Monroig et al., 2003; Pham et al., 2022, 2023). HUFA deficiency may result in impaired growth, survival, and susceptibility to stresses in the larvae because it plays crucial roles in the development of nervous and visual systems as well as maintaining cell membrane integrity (Izquierdo et al., 2010; Roo et al., 2019; Thépot et al., 2016; Villeneuve et al., 2007). Mutia et al. (2024) investigated the effects of combinations of different live prey such as copepods, rotifer and *Artemia* in giant trevally larvae rearing for 40 days, in which rotifer and *Artemia* were enriched with commercial emulsion. The results indicated that survival of the larvae fed a combination of rotifers and *Artemia* was 11.67% and significantly lower than those fed both rotifer and copepods (23.47%).

* Corresponding author.
E-mail address: hungpd@ntu.edu.vn (H.D. Pham).
[1] ORCID ID: 0000-0002-7533-3593

https://doi.org/10.1016/j.rsma.2026.105194
Received 10 May 2026; Received in revised form 22 June 2026; Accepted 23 June 2026
Available online 3 July 2026

This suggested that giant trevally larvae might require higher HUFA concentrations than most marine fish species (Mutia et al., 2024), consequently *Artemia* enrichment protocols of other marine fish may not be sufficient for this species and need to be clarified. Besides, in the aforementioned study by Mutia et al. (2024), *Artemia* was enriched with a commercial emulsion for only 4 h before feeding. Previous results have showed that enrichment duration significantly impacts nutritional values of enriched *Artemia*, in which prolonged enrichment increases the enriched nutrient incorporation into *Artemia*, and enrichment period in 24 h can be sufficient to maximize HUFA contents and reducing potential oxidative stress (Ramena et al., 2025), thus, insufficient enrichment period might reduce incorporation of n−3HUFA into *Artemia*, resulting in low survival rate in giant trevally larvae fed enriched *Artemia* than copepods feeding groups.

Nowadays, *Artemia* has become a major live feed in marine larviculture because of its stable supply, eases of storage and use and reasonable price (Dhont et al., 2013). A primary constraint in the usage of *Artemia* as a major live-feed is the negligible levels of HUFA, especially DHA in *Artemia* (Hamre et al., 2013; Mozanzadeh et al., 2021), which are essential nutrients for maintaining normal physiological, immune functions and growth in marine larvae due to their inability to synthesize these HUFA (Ramena et al., 2025). Consequently, unenriched *Artemia* cannot provide adequate essential fatty acids for larvae during critical developmental stages (Jamali et al., 2024). *Artemia* enrichment protocols have been developed and become a standard practice to boost its essential nutrients that meet nutritional demands in marine larvae (Joshua et al., 2022; Ramena et al., 2025), resulting in improved survival, growth response and resistance to stressful factors as well as reduced abnormal development in greater amberjack *Seriola dumerili* (Roo et al., 2019), barramundi *Lates calcarifer* (Pham et al., 2023; Thépot et al., 2016), seabream *Sparus aurata* (Izquierdo et al., 2012), Japanese flounder *Paralichthys olivaceus* (Izquierdo et al., 1992). Moreover, oil emulsion enrichment also enhances the physiological and biochemical responses in aquaculture species (Ramena et al., 2025). For example, enriched Artemia alleviated osmotic stress and facilitated swim bladder inflation in yellow perch *Perca flavescens* (Grayson and Dabrowski, 2022), improved concentrations of polyunsaturated fatty acids in the larvae tissues (Lundova et al., 2018), and modulated immune-related factors (González et al., 2017), thereby promoting overall production outcomes in reared larvae.

Nevertheless, excessive dietary HUFA also produces deleterious effects in fish larvae. Results described in European sea bass *Dicentrarchus labrax* larvae indicated that dietary DHA and EPA of above 2% could increase skeletal anomalies (Villeneuve et al., 2007), whereas tissue oxidative stress and poor growth were reported in the larvae fed high dietary HUFA levels (Betancor et al., 2012). Barramundi larvae fed high n−3HUFA diets reduced stress resistance compared to those fed an adequate amount of EFA (Pham et al., 2022). These negative impacts can be attributed to the formation of reactive oxygen species (ROS) and free radicals as dietary n−3HUFA levels surpass the larvae's physiological threshold (Izquierdo et al., 2010). Therefore, optimizing dietary n−3HUFA would be necessary to enhance growth, physiological and immune responses in marine fish larvae. To date, there is limited knowledge on essential fatty acid requirements in giant trevally during the larval stage, thus, the study aimed to determine the effects of enriched HUFA *Artemia* on growth, biochemical responses and enzyme activity, as well as stress resistance in this species.

2. Material and methods

2.1. Ethic statement

The giant trevally *Caranx ignobilis* is not designated as protected, endangered, or rare under current Vietnamese legislation, including the 2018 Law on Livestock and Government Decree No. 06/2019/ND-CP. Fish husbandry was fully compliant with the Vietnamese Code of practice for the care of animals for scientific purposes.

2.2. Artemia enrichment

Artemia cysts (Vinh Chau strain, Vietnam) were incubated in a 300-L composite tank for 24 h. Water quality parameters during incubation were kept at a temperature of 28–29°C, dissolved oxygen > 5 mg/L, pH of 8.0–8.5, and salinity of 33–34ppt. Continuous vigorous aeration was provided to keep the cysts in suspension and prevent clumping. After hatching, the harvested nauplii were rinsed with clean seawater before being transferred to enrichment tanks.

Artemia enrichment was conducted in 5-liters white plastic buckets, with each bucket dedicated to a specific experimental treatment. *Artemia* nauplii were enriched with a commercial emulsion (A1 DHA Selco, INVE, Thailand) at five levels: 0, 150, 300, 450, and 600 mg/L in 18 h, following the manufacturer's protocols to produce five dietary treatments, namely HF0, HF150, HF300, HF450 and HF600, respectively. Strong aeration was applied to ensure dissolved oxygen levels above 5 mg/L. Prior to feeding, enriched *Artemia* were rinsed with clean seawater. Enriched *Artemia* from the five different treatment levels (100 g per treatment) were sampled and stored at −80°C for fatty acid analysis. The fatty acid composition of enriched *Artemia* is presented in Table 1.

2.3. Larval preparation and rearing

The larvae used for the experiment was obtained from artificial reproduction. The broodstock (8–10 kg/fish) were cultured in a 64 m^3 sea-cage and fed fresh trash fish once daily. Matured females and males were induced to spawn using a combination of 40 µg/kg of luteinizing hormone-releasing hormone analog (LHRH-A) and 1.200UI of human chorionic gonadotropin (HCG). After hatching, newly hatched larvae were reared in a gray-cement tank (2 m x 2 m x 1.3 m per tank) at a

Table 1
Fatty acid composition (% of total fatty acid, TFA) of enriched *Artemia* with different emulsion levels.

Fatty acid	HF0	HF150	HF300	HF450	HF600
C14:0	1.51	1.24	1.14	1.50	1.77
C15:0	-	0.53	0.41	0.35	0.29
C16:0	16.94^{b}	14.11^{ab}	12.21^{ab}	11.83^{a}	14.73^{ab}
C17:0	0.78	0.78	0.69	0.67	0.64
C18:0	11.61^{b}	6.85^{a}	5.73^{a}	5.34^{a}	5.51^{a}
C20:0	-	0.57	0.57	0.53	0.51
SFA	30.89^{b}	24.06^{a}	20.74^{a}	20.21^{a}	23.46^{a}
C16:1	7.17^{b}	5.70^{a}	4.68^{a}	6.01^{ab}	5.82^{a}
C18:1n−9	24.62	23.93	24.06	25.26	26.65
C20:1	0.67	1.17	1.10	1.05	0.99
C22:1n−9	-	0.11	0.09	0.08	0.07
MUFA	32.46	30.91	30.97	32.45	33.57
C18:2n−6	7.58	7.12	7.84	9.17	9.43
C18:3n−3	18.09^{b}	12.02^{a}	11.46^{a}	11.52^{a}	10.93^{a}
C18:3n−6	0.55^{b}	0.34^{a}	0.35^{a}	0.35^{a}	0.39^{a}
C20:2	-	0.34	0.34	0.33	0.31
C20:3n−3	-	0.22	0.31	0.31	0.29
C20:3n−6	-	-	0.16	0.16	0.16
C20:4n−6	2.75	2.68	2.61	2.37	2.38
C20:5n−3	7.27^{a}	10.05^{b}	10.03^{b}	9.49^{b}	9.09^{b}
C22:6n−3	0.42^{a}	12.27^{b}	12.13^{b}	10.72^{b}	10.04^{b}
PUFA	36.65^{a}	45.03^{b}	45.22^{b}	44.42^{b}	42.97^{ab}
n−3HUFA	7.69^{a}	22.31^{b}	22.16^{b}	20.21^{b}	19.13^{b}
DHA/EPA	0.06^{a}	1.22^{b}	1.21^{b}	1.13^{b}	1.10^{b}
EPA/ARA	0.16^{a}	4.57^{b}	4.65^{b}	4.56^{b}	4.21^{b}

Data are mean of triplicates; SFA: saturated fatty acids; MUFA: monounsaturated fatty acids; PUFA: polyunsaturated fatty acids; HUFA: highly unsaturated fatty acids; DHA: docosahexaenoic acid; EPA: eicosapentaenoic acid; ARA: arachidonic acid. HF0, HF150, HF300, HF450 and HF600; Artemia enriched with 0, 150, 300, 450 and 600 mg/L of HUFA emulsion, respectively. Means with different lowercase superscripts within a row indicate the significant differences among the treatments.

density of 15 larvae/L in green water using Nano 3600 paste (Reed Mariculture, USA) at a density of 170.000 cells/ml. The larvae were fed enriched rotifers at 1 – 3 rotifers/ml from 2 dah to 4 dah and 4 – 10 rotifers/ml from 5 dah until 12 dah before being transferred into experimental tanks.

Before larval stocking, microalgae were added to the experimental tanks to minimize stress for the larvae. The 13 days old larvae (0.34 cm and 0.002 g) were gently collected using 500 μm soft net and distributed into 15 composite tanks (100 L/tank) at a stocking density of six larvae/liter. Each tank was equipped with an air-stone. The larvae were fed enriched *Artemia* at a density of 1–5 individuals/ml, depending on larval size, with 4 times a day at 7:30, 11:00, 14:30, and 17:30 for 28 days. Uneaten *Artemia* was completely removed using a PVC pipe covered with a 500 μm net. Water quality was managed through siphoning and water exchange and maintained within suitable ranges for fish growth: temperature at 28–30°C, salinity at 33–35 ppt, pH at 8.0–8.5, DO > 4.5 mg/L, and total ammonia nitrogen (TAN) < 0.2 mg/L. Photoperiod was maintained at 16 L:8D during feeding period.

2.4. Sample collection and analysis

At the termination of the feeding period, the larvae were starved for 12 h after the last feeding. The larvae were weighed using a digital scale (50 ×0.0001 g) and length measured with a plastic ruler. 10 g larvae from each tank at the end of the feeding period were collected (5 g in the HF0 tank), pooled and stored at −80°C for digestive enzyme and chemical analyses.

2.5. Enzyme activity analyses

The samples were thawed and ground in a pH 6.9 buffer solution (KH2PO4 20 mM and NaCl 6 mM). Then, the mixture was centrifuged at 4200 rpm, 4°C for 30 min, and the supernatant was transferred to 0.5 ml Eppendorf tubes for analysis of digestive enzyme activity. Trypsin activity was analyzed following Tseng et al. (1982), 15 μL of the supernatant was reacted with 10 μL of 0.1 M BAPNA (10.87 mg Na-Benzoyl-DL-Arginine P-nitroanilide in 250 μL DMSO) and phosphate buffer pH 8.2. Trypsin activity was measured at 407 nm for 5 min using a spectrophotometer (UV-Vis Cary 50, Varian, Inc USA). Activities of pepsin and chymotrypsin were determined following Worthington (1982). For chymotrypsin, 50 μL of the sample was reacted with BTEE and buffer solution pH 7.8, then measured at 256 nm for 5 min. Pepsin activity was measured by reacting 100 μL of the sample with 500 μL of hemoglobin as a buffer (2% w/v hemoglobin in 0.06 HCl) and measured at 280 nm. Amylase was determined by reacting 100 μL of the sample with 100 μL of 1% starch solution at 25°C, adding 200 μL of substrate solution, and incubating at 100°C for 5 min before measuring at 540 nm (Bernfeld, 1951).

2.6. Body composition analysis

Protein and lipid determinations were performed according to standard methods of the Association of Official Analytical Chemists (AOAC). Protein content was measured by determining total nitrogen using the Kjeldahl method, while lipid content was determined by dissolving lipids in petroleum ether, and quantifying by Soxhlet extraction. Moisture content was measured after drying the samples at 105 ^{0}C in an oven; ash was determined by combustion at 550 ^{0}C for 24 h in an electric muffle furnace.

2.7. Salinity stress test

After four weeks of the feeding period, twenty larvae were randomly collected from each tank and transferred into buckets containing 20 liters of freshwater (0 ppt) with continuous aeration. After 30 min, the tested larvae were retransferred into the respective experimental tank for recovery. The number of fish exhibiting shock symptoms was recorded after 10 and 30 min. Mortality was recorded 10 min after restocking into the recovery tank.

2.8. Calculation and statistical analysis

Growth parameters of giant trevally larvae were calculated using the following equations.

$$\text{Specific growth rate(SGR, \%/day)} = \left[\frac{\ln(\text{final body weight or lenght}) - \ln(\text{pooled initial body weight or length})}{\text{days}}\right] \times 100$$

$$\text{Survival(\%)} = \left[\frac{\text{number of final fish}}{\text{number of initial fish}}\right] \times 100$$

$$\text{Cofficient of variation(CV, \%)} = \left[\frac{\text{standard of deviation}}{\text{mean}}\right] \times 100$$

.

2.9. Statistical analysis

All data were presented as mean ± standard error. The dataset's distributional properties were evaluated before data analysis using the Shapiro-Wilk test. The survival data was arcsine-transformed before analyzing. All parameters were subjected to One-way ANOVA using SPSS Version 25 unless otherwise specified. Tukey's HSD multiple comparison test was applied to examine differences among groups. The statistical significance was evaluated at $P < 0.05$. Polynomial regression was applied to express relationship between dietary n−3HUFA and growth and survival of giant trevally. The principal component analysis (PCA) was used on the dataset collected from the five dietary treatments and various measured parameters: growth, survival, body composition, and enzyme activity of giant trevally at the termination of the feeding period to evaluate the covariation of their respective variables. The PCA and Pearson correlation matrix were performed in Origin 2026 (OriginLab, Northampton, USA).

3. Results

3.1. Growth performance

The growth performance of giant trevally larvae fed *Artemia* enriched n−3HUFA is displayed in Table 2. After four weeks of feeding, there were no differences in body length, body height, weight, and SGR of the larvae fed HF0, HF150 and HF300 diets, but significantly increased in those fed HF450 and HF600 diets compared to the unenriched *Artemia*

Table 2
Growth performance of giant trevally larvae fed enriched *Artemia*.

Parameters	Enriched *Artemia*				
	HF0	HF150	HF300	HF450	HF600
IBL (cm)	0.34 ± 0.01	0.34 ± 0.01	0.34 ± 0.01	0.34 ± 0.01	0.34 ± 0.01
IBW (g)	0.002	0.002	0.002	0.002	0.002
FBL (cm)	1.38 ± 0.04^{a}	1.54 ± 0.1^{ab}	1.52 ± 0.58^{ab}	1.64 ± 0.05^{b}	1.73 ± 0.08^{b}
FBW (g)	0.11 ± 0.01^{a}	0.14 ± 0.02^{ab}	0.14 ± 0.01^{ab}	0.17 ± 0.01^{bc}	0.20 ± 0.01^{c}
FBH (cm)	0.80 ± 0.02^{a}	0.86 ± 0.03^{ab}	0.86 ± 0.02^{ab}	0.92 ± 0.02^{b}	0.94 ± 0.03^{b}
SGR_L (%/day)	5.71 ± 0.08^{a}	6.05 ± 0.20^{ab}	5.97 ± 0.11^{ab}	6.20 ± 0.10^{b}	6.40 ± 0.14^{b}
SGR_W (%/day)	13.81 ± 0.18^{a}	14.61 ± 0.40^{ab}	14.54 ± 0.30^{ab}	15.37 ± 0.25^{bc}	15.87 ± 0.20^{c}
Biomass (g)	5.58 ± 0.85^{a}	17.57 ± 2.70^{b}	18.90 ± 2.68^{b}	24.31 ± 2.54^{b}	24.23 ± 1.84^{b}

Data are displayed as mean ± standard error (n = 3). IBL, initial body length; FBL, final body length; IBW, initial body weight; FBW, final body weight; FBH, final body height; SGR, specific growth rate. HF0, HF150, HF300, HF450 and HF600; Artemia enriched with 0, 150, 300, 450 and 600 mg/L of HUFA emulsion, respectively. Means with different lowercase superscripts within a row indicate the significant differences among the treatments.

group ($P < 0.05$). The biomass in the HF0 was significantly lower than that of the enriched HUFA *Artemia* groups, however, there were no differences in the biomass of the larvae as increasing dietary enrichment levels increased from 150 to 600 mg/L. The coefficient variations for length and weight showed reduced trends as increasing dietary enrichment levels, but no differences were detected. Enriched HUFA *Artemia* significantly increased larval survival (Fig. 1). The dietary n−3HUFA requirements to maximize final body weight and survival in giant trevally during *Artemia* feeding were estimated at 15.63% and 22.67% TFA, respectively based on polynomial regression analysis (Fig. 2).

3.2. Enzyme activity

The effects of dietary HUFA in *Artemia* enrichment on the enzyme activity of giant trevally are presented in Fig. 3. The activities of pepsin and trypsin were lowest in HF0 and significantly different from enriched *Artemia* groups ($P < 0.05$). However, pepsin and trypsin activity did not change with increasing dietary HUFA enrichment levels from 150 to 600 mg/L ($P > 0.05$). Activity of chymotrypsin increased and reached a peak on the HF300 diet, and was significantly reduced on the HF450 and HF600 diets. There was no difference in amylase activity among dietary treatments.

3.3. Proximate composition

The effects of dietary HUFA on the proximate composition of the larvae were presented in Table 3. There were no differences in protein and moisture contents of the larvae fed different HUFA levels after four weeks of feeding. The larvae fed HF0 and HF600 had significantly lower lipid concentrations than those fed HF150, HF300 and HF450 diets ($P < 0.05$). The ash content in the larvae fed HF300 and HF450 were significantly higher than that in HF150 and HF600 groups.

3.4. Salinity stress test

There were effects of dietary HUFA enrichment on the percentage of stressed larvae and mortality after the salinity challenge test (Fig. 4). After 30 min, the most stressed fish were observed in the HF0, followed by HF150 and HF300, and were significantly higher than those in the HF450 group ($P < 0.05$). The larvae fed HF300, HF450 and HF600 diets had significantly lower mortality rates than the control ($P < 0.05$). There was no difference in the mortality among the larvae fed HF300, HF450 and HF600 diets ($P > 0.05$).

3.5. PCA and correlation analysis

Principal component analysis (PCA) was applied to evaluate the effects of dietary groups on growth, survival, enzyme activity and body composition in giant trevally larvae. The first two principal component axes (PC1 and PC2) interpreted more than 78% of the variation in the evaluated data. Larvae fed HF0 was grouped in the PCA biplot negative zone, while HF450 and HF600 were grouped in the biplot positive areas (Fig. 5). The HF450 and HF600 were classed together in the PC1 positive site, in which survival, biomass, pepsin, trypsin and lipid were strongly positive correlated (Fig. 5).

The Pearson correlation analysis indicated that survival was significantly correlated with fish growth, pepsin, trypsin and lipid, but not connected with protein. Pepsin and trypsin activities showed positive correlations with biomass and survival but had no correlation with fish growth (Fig. 6).

4. Discussion

This study provides the appropriate enrichment levels to be used for giant trevally larvae. The results indicated that enriched HUFA *Artemia* significantly increased the survival of the larvae. This is consistent with those reported in barramundi (Pham et al., 2023; Rimmer et al., 1994), greater amberjack (Roo et al., 2019), yellowfin seabream *Acanthopagrus latus* and Japanese flounder (Izquierdo et al., 1992). The relatively lower survival of the larvae fed unenriched *Artemia* in comparison to those fed enriched *Artemia* suggests that relying on the nutritional profile of

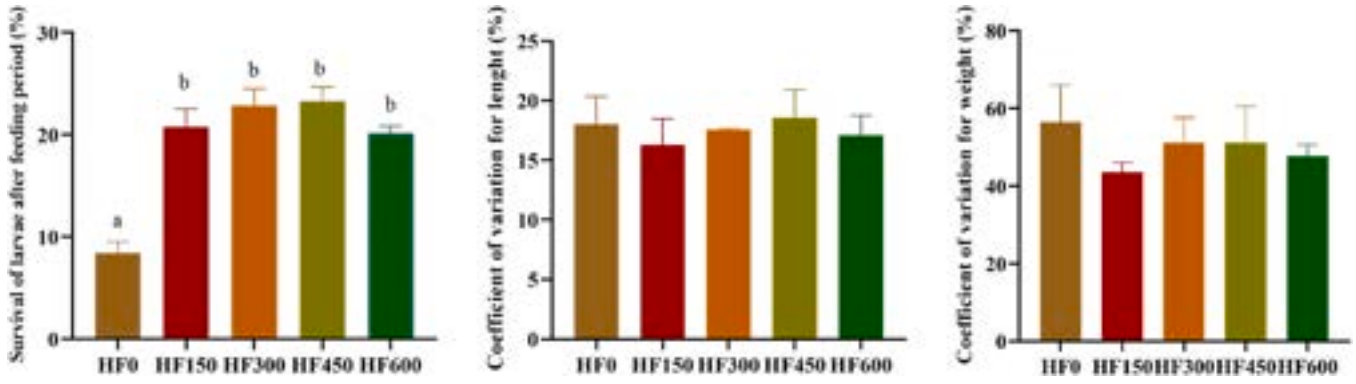

Fig. 1. Survival rate, coefficient of variation for length and weight of giant trevally larvae after four weeks of feeding period. HF0, HF150, HF300, HF450 and HF600; Artemia enriched with 0, 150, 300, 450 and 600 mg/L of HUFA emulsion, respectively. Different letters are significant differences($P < 0.05$).

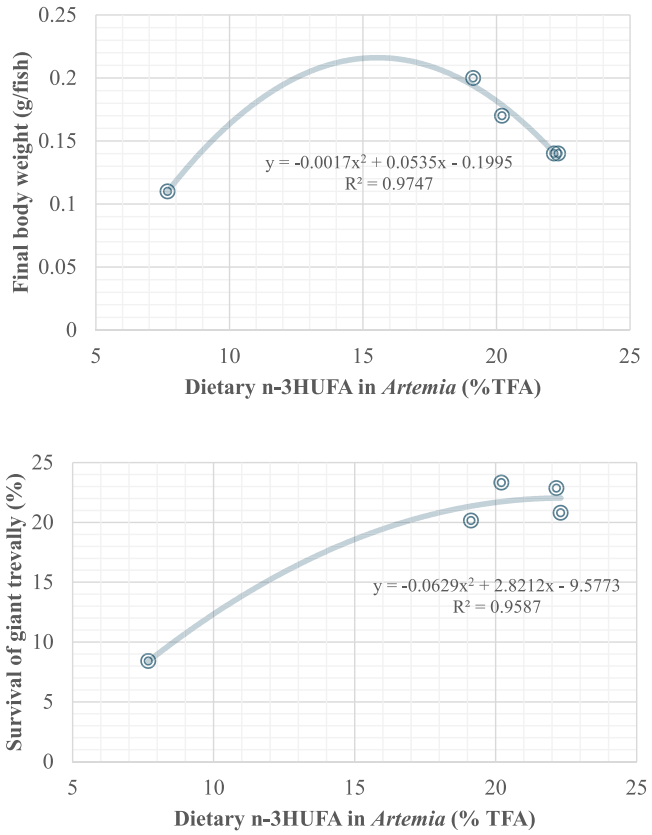

Fig. 2. The relationship between dietary n−3 HUFA in *Artemia* and final body weight and survival of giant trevally larvae. TFA; total fatty acids.

non-enriched *Artemia* may not provide adequate EFA for marine fish during larval rearing. At this stage, DHA is preferentially assimilated into nervous and retinal tissues (Villalta et al., 2008), and inadequate DHA can lead to high mortality (Tocher, 2010) as seen in the current study. However, increasing dietary emulsion levels from 150 to 600 mg/L did not improve the survival of giant trevally larvae. Roo et al. (2019) also found that there were no differences in survival of greater amberjack fed different n−3HUFA levels. Similarly, there was no difference in the survival of barramundi larvae fed *Artemia* enriched with different n−3HUFA levels (Pham et al., 2022). Currently, there is very little information on n−3HUFA demands in giant trevally larvae. Mutia et al. (2024) reported that the survival rates of giant trevally larvae fed combinations of rotifer + *Artemia*; rotifer + copepods and rotifer + copepods + *Artemia* for 40 days were 11.67, 23.47 and 14.37%, respectively, in which rotifer and *Artemia* were enriched with commercial emulsions for 4 h before feeding. However, the fatty acid profile

Table 3
Body composition (%, wet weight) of giant trevally larvae fed enriched *Artemia*.

Parameters	Enriched *Artemia*				
	HF0	HF150	HF300	HF450	HF600
Protein	16.60 ± 0.26	16.70 ± 0.20	16.10 ± 0.25	16.90 ± 0.40	17.10 ± 0.41
Lipid	1.54 ± 0.02^{a}	1.78 ± 0.01^{b}	1.75 ± 0.0^{b}	1.72 ± 0.06^{b}	1.51 ± 0.02^{a}
Ash	4.50 ± 0.04^{ab}	4.15 ± 0.10^{a}	4.89 ± 0.58^{b}	4.77 ± 0.05^{b}	4.17 ± 0.08^{a}
Moisture	77.80 ± 0.20	76.81 ± 0.35	77.86 ± 0.54	78.15 ± 0.50	77.69 ± 0.46

Data are displayed as mean ± SE (n = 3). HF0, HF150, HF300, HF450 and HF600; Artemia enriched with 0, 150, 300, 450 and 600 mg/L of HUFA emulsion, respectively. Means with different lowercase superscripts within a row indicate the significant differences among the treatments.

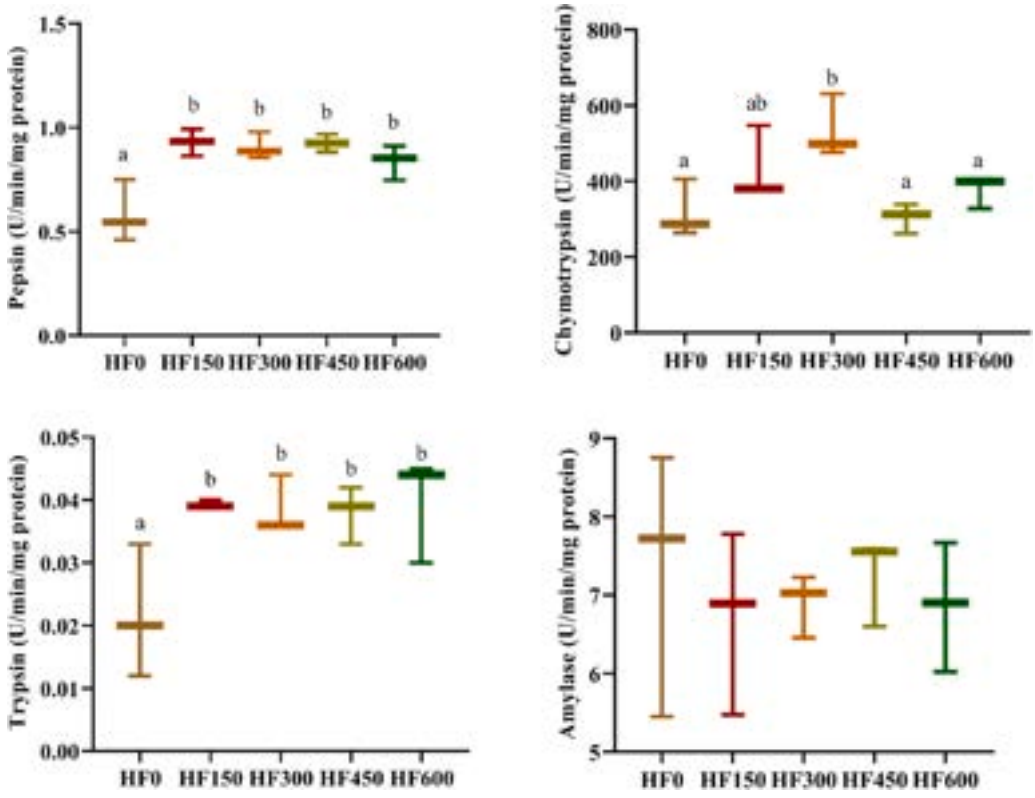

Fig. 3. Enzyme activity of giant trevally larvae fed enriched *Artemia* for four weeks. HF0, HF150, HF300, HF450 and HF600; Artemia enriched with 0, 150, 300, 450 and 600 mg/L of HUFA emulsion, respectively. Different letters are significant differences ($P < 0.05$).

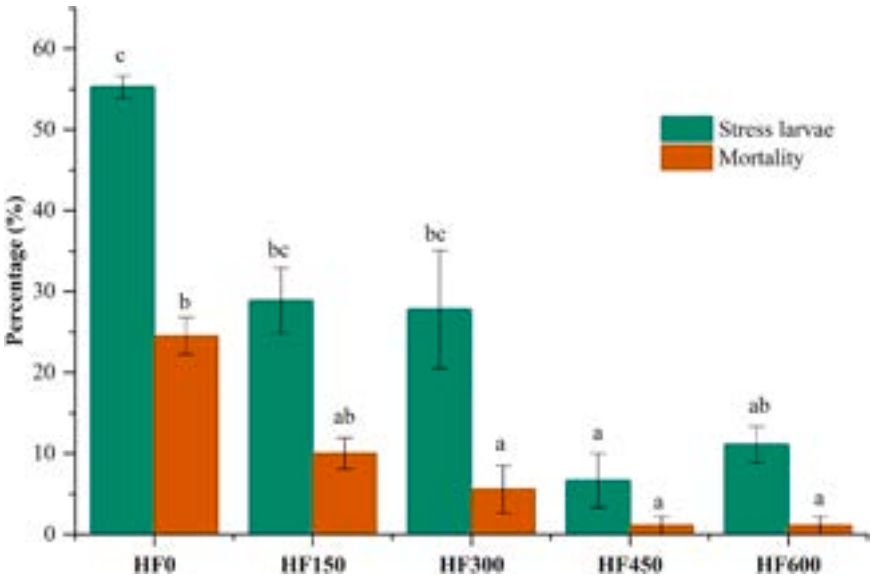

Fig. 4. Percentages of stress larvae and mortality after salinity test. HF0, HF150, HF300, HF450 and HF600; Artemia enriched with 0, 150, 300, 450 and 600 mg/L of HUFA emulsion, respectively. Values in similar patterns with different letters are significant differences ($P < 0.05$).

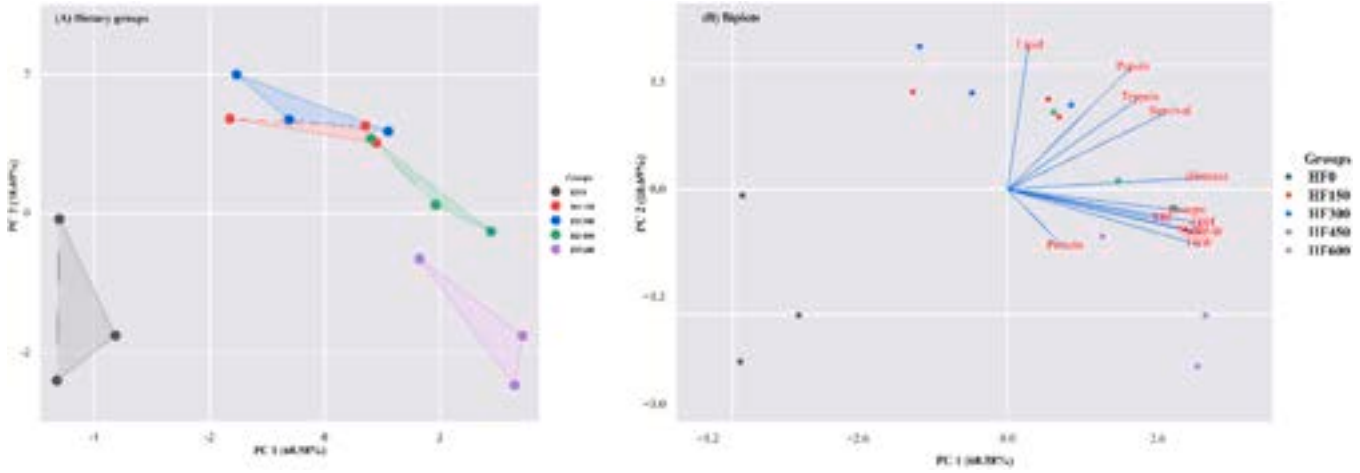

Fig. 5. PCA score and biplot with various dietary groups and measured variables after four weeks. The graph shows positive and negative association between various dietary groups (A) and variables loading (B). Different markers with convex hull display means from various dietary treatments performed in the investigation, and loadings show the contribution of the variable to the development of PC1 and PC2.

of live feed was not detailed to investigate dietary HUFA requirements. Thus, in the current study, it seems that the dietary DHA and EPA should be at least 10.04 and 9.09% of TFA, respectively to support the survival of giant trevally larvae.

Regarding growth performance, FBL, FBH, FBW, SGR in giant trevally showed positive trends with increasing dietary HUFA enrichment levels. The larvae fed HF150 and HF300 tended to increase in FBL, FBH and FBW compared to HF0, although no difference was recorded. In this study, nonenriched *Artemia* contains 7.27 and 0.42% of EPA and DHA (% of TFA), which may provide a portion of EFA to support larval growth. This is similar to observations in greater amberjack fed unenriched *Artemia* and *Artemia* enriched with low HUFA level (Roo et al., 2019). To date, there are scarce specific studies quantifying the quantitative EFA requirements for marine fish larvae. Based on model analysis in Florida pompano *Trachinotus carolinus*, a tropical marine fish, Mejri et al. (2021) found that early larvae required at least 16% DHA and 7% EPA of TFA, respectively to satisfy growth. Roo et al. (2019) also suggested that dietary n−3HUFA in the range of 12 – 17% of TFA was sufficient for greater amberjack larvae, while the dietary n−3HUFA requirements for optimum growth in red seabream *Pagrus major* was 15% TFA (Izquierdo, 1989). These results were in range with those found in the current study, in which the giant trevally larvae required dietary n−3HUFA at 19.13% TFA with DHA and EPA contents 10.04 and 9.09% TFA, respectively to optimize growth rate. This is relatively higher than the required n−3HUFA for barramundi and Japanese flounder larvae during *Artemia* feeding (Izquierdo et al., 1992; Pham et al., 2023). Along with EFA requirements, ratio of DHA/EPA also plays important role in larval development and ratio of 2:1 has been recommended as sufficient for larval nutrition (Hamre et al., 2013). Previous results also demonstrated that ratio of DHA/EPA > 3 is adequate for longfin yellowtail *Seriola rivoliana* (Mesa-Rodriguez et al., 2018), Florida pompano (Mejri et al., 2021). However, in this study, giant trevally larvae achieved highest growth rate at DHA/EPA ratios of 1.1 – 1.3. This is consistent with findings reported in greater amberjack (Roo et al., 2019) and barramundi (Pham et al., 2023). In contrast, dietary DHA/EPA ratios had no effect on the growth of red drum *Sciaenops ocellatus* larvae (Brinkmeyer and Holt, 1998). These incompatible results can be due to the different species, experimental conditions among

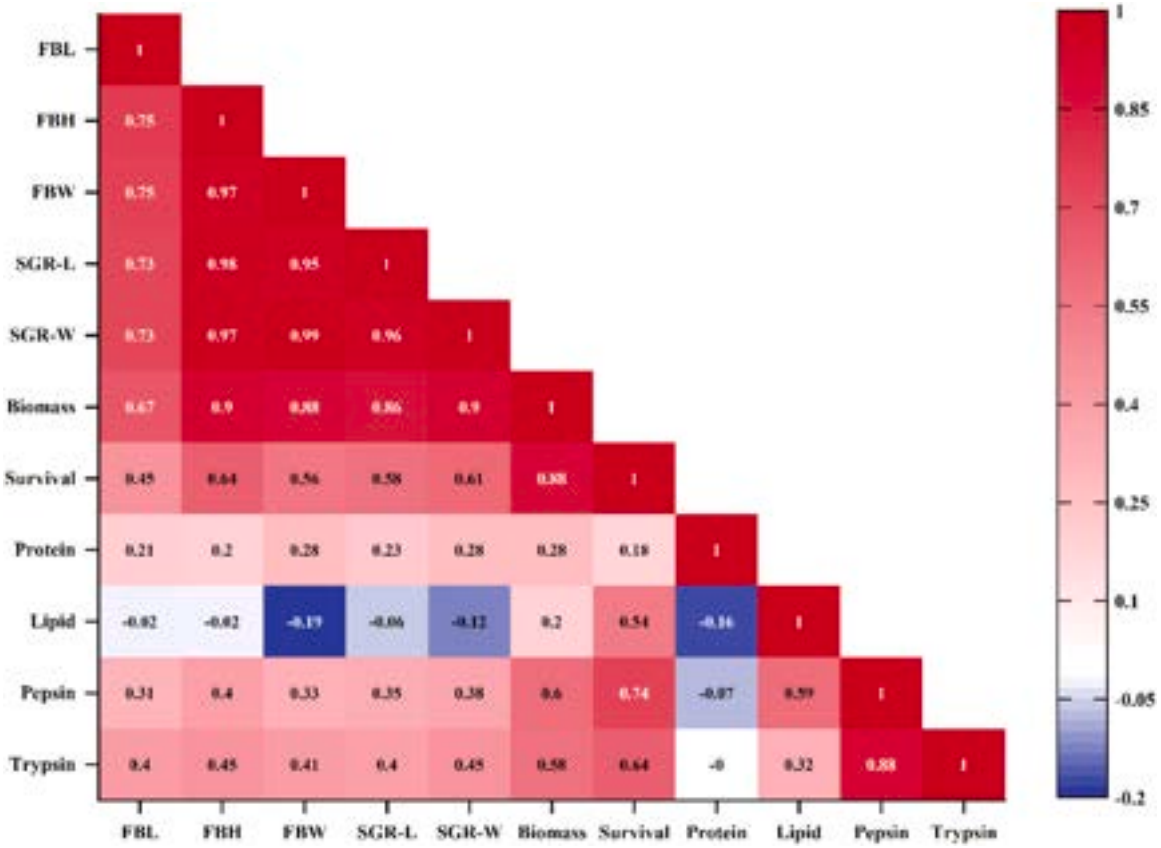

Fig. 6. Pearson correlation matrix of growth characteristics, coefficient of variation and survival rate in giant trevally larvae.

studies and need further investigation.

Nutrient digestion in fish is strongly influenced by digestive enzyme activity (Santigosa et al., 2008), which significantly changed during the transition of feeding behaviors and structural and functional changes in the digestive tract from a straight tube to differentiated parts as stomach, foregut and hindgut during larval development (Arenas-Pardo et al., 2024). Therefore, knowledge of enzymatic activities during the live-prey feeding and metamorphosis can support useful information to optimize feeding and rearing protocols for the larvae (Infante and Cahu, 2007). In this study, giant trevally fed enriched HUFA *Artemia* showed significantly higher activities of pepsin and trypsin than those fed unenriched *Artemia*. These enzymes have crucial roles in protein digestion and can be used as useful indicators in evaluating nutritional health in the larvae (Arenas-Pardo et al., 2024), in which trypsin has been link to favorable conditions that enhance growth performance (Rungruangsak-Torrissen et al., 2006). While a good nutritional status can enhance stomach development, resulting in increased pepsin activity in fish larvae (Sheng et al., 2022). The increased pepsin and trypsin activities in giant trevally larvae fed enriched *Artemia*, thus indicating beneficial roles of dietary HUFA in modulating protease enzymes in the larvae. The increased chymotrypsin-specific activity in marine fish larvae has been linked to diminished or depressed growth due to food limitation (Cara et al., 2007; Rungruangsak-Torrissen et al., 2006). In the current study, chymotrypsin activity significantly increased in the larvae fed HF300 compared to those fed HF0, HF450 and HF600 diets. To date, the effects of dietary EFA on dynamic and role of chymotrypsin remain unknown and need to be investigated. In contrast, amylase activity was not different between dietary treatments. This is consistent with observations reported in European seabass *Dicentrarchus labrax* larvae, in which amylase secretion was not affected by dietary HUFA after pancreatic maturation (Vagner et al., 2007).

In the current study, there were no differences in protein and moisture contents in the larvae among treatments, whereas increased lipid concentrations were recorded in fish fed HF150, HF300 and HF450 diets. This is consistent with observations in barramundi larvae, in which increasing dietary HUFA increased lipid contents (Pham et al., 2022). In contrast, greater amberjack larvae fed different n−3HUFA levels did not show any difference in larval lipid (Roo et al., 2019). The PCA analysis have been used to investigate effect of HUFA levels in enriching *Artemia* on growth, immunity and health parameters in barramundi, in which HUFA emulsification of 300 mg/L showed favorable influence on fish performance, and unenriched *Artemia* or 100 mg/L HUFA enriched *Artemia* had negatively correlated to fish growth and survival (Pham et al., 2023). In this study, the position of growth, enzymatic activity, proximate composition and dietary treatments in the plot indicated that HF0 diet had a negative association with fish growth and survival, whereas enriched *Artemia* groups showed a favorable impact on growth performance. Based on the PCA analysis, HUFA enrichment levels up to 600 mg/L can be recommended to improve growth, survival and digestive enzyme activity.

The important roles of dietary n−3HUFA in handling stress resistance have been documented in marine larvae, wherein the improvement of larval resistance to stressors can be achieved by increasing dietary DHA in fast-growing fish (Roo et al., 2019). Reduced mortality rates after stress testing have been reported in the larvae of barramundi (Pham et al., 2023; Thépot et al., 2016), greater amberjack (Roo et al., 2019), and longfin yellowtail (Roo et al., 2014) fed sufficient n−3HUFA diets. These results suggested that increases in dietary HUFA improved oxygen transport efficiency and fluidity in the gill membrane, thereby restoring normal oxygen concentrations after the air exposure test. In this study, giant trevally larvae fed enriched HUFA *Artemia* showed significantly higher survival after a salinity challenge test. This is consistent with observations in white-leg shrimp *Litopenaeus vannamei*, in which postlarvae fed medium HUFA levels showed increased gill

area and EFA levels in the gill, which could improve osmoregulatory mechanisms, resulting in higher survival in response to low salinity (Palacios et al., 2004).

5. Conclusion

Based on overall findings and under experimental conditions applied, dietary n−3HUFA within the range of 15.63–22.67% TFA was recommended to enhance growth, survival and stress resistance of giant trevally during *Artemia* feeding. Besides, quantifying the requirements for DHA, EPA, ARA and DHA/EPA ratio is needed in further research to better understand the specific role of each fatty acid, their interaction and DHA/EPA ratio affecting growth performance and development of giant trevally larvae.

CRediT authorship contribution statement

Anh Thi Pham: Writing – original draft, Visualization, Methodology, Investigation, Data curation, Conceptualization. **Manh Van Ngo:** Writing – original draft, Supervision, Resources, Methodology, Conceptualization. **Ha Kim Thi Nguyen:** Writing – original draft, Validation, Formal analysis, Data curation. **Hung Duc Pham:** Writing – review & editing, Supervision, Project administration, Methodology, Formal analysis, Conceptualization.

Funding

This research is supported by Vietnam National Foundation for Science and Technology Development (NAFOSTED) under grant number 106.05–2024.28.

Declaration of Competing Interest

The authors declare that they have no known competing financial interests or personal relationships that could have appeared to influence the work reported in this paper.

Acknowledgment

This work contributes to the celebration of the 50th Anniversary of Nha Trang University, located in Khanh Hoa Province, Vietnam.

Data availability

Data will be made available on request.

References

Arenas-Pardo, M.A., Gaxiola-Cortés, M.G., Barreto-Altamirano, A.F., Paredes-Medina, Ad.C., Palomino-Albarrán, I.G., Balam-Uc, P.M., Maldonado-Flores, J.C., Álvarez-González, C.A., 2024. Changes in digestive enzyme activities during larval development of spotted seatrout (Cynoscion nebulosus). Aquac. Nutr. 2024 (1), 1309390. https://doi.org/10.1155/2024/1309390.

Bernfeld, P., 1951. Enzymes of Starch degradation and synthesis. Adv. Enzymol. Relat. Areas Mol. Biol. 379–428.

Betancor, M.B., Caballero, M., Terova, G., Saleh, R., Atalah, E., Benítez-Santana, T., Bell, J.G., Izquierdo, M., 2012. Selenium inclusion decreases oxidative stress indicators and muscle injuries in sea bass larvae fed high-DHA microdiets. Br. J. Nutr. 108 (12), 2115–2128. https://doi.org/10.1017/S0007114512000311.

Brinkmeyer, R.L., Holt, G.J., 1998. Highly unsaturated fatty acids in diets for red drum (Sciaenops ocellatus) larvae. Aquaculture 161 (1), 253–268. https://doi.org/10.1016/S0044-8486(97)00274-3.

Cara, B., Moyano, F.J., Zambonino, J.L., Fauvel, C., 2007. Trypsin and chymotrypsin as indicators of nutritional status of post-weaned sea bass larvae. J. Fish. Biol. 70 (6), 1798–1808. https://doi.org/10.1111/j.1095-8649.2007.01457.x.

Cavrois-Rogacki, T., Rolland, A., Migaud, H., Davie, A., Monroig, O., 2020. Enriching Artemia nauplii with selenium from different sources and interactions with essential fatty acid incorporation. Aquaculture 520, 734677. https://doi.org/10.1016/j.aquaculture.2019.734677.

Dhont, J., Dierckens, K., Støttrup, J., Van Stappen, G., Wille, M., Sorgeloos, P., 2013. Rotifers, Artemia and copepods as live feeds for fish larvae in aquaculture. In: Allan, G., Burnell, G. (Eds.), Advances in Aquaculture Hatchery Technology, 5. Woodhead Publishing, pp. 157–202.

González, A., Silva, A., Gajardo, G., Martínez, C., 2017. Survival and growth improvement of palm ruff, Seriolella violacea, larvae fed Artemia nauplii enriched with an experimental emulsion. J. World Aquac. Soc. 48 (2), 268–279.

Grayson, J.D., Dabrowski, K., 2022. Utilization of live-food enrichment with polyunsaturated fatty acids (PUFA) for the Intensive culture of yellow perch larvae. North. Am. J. Aquac. 84 (2), 131–148.

Hamre, K., Yúfera, M., Rønnestad, I., Boglione, C., Conceição, L.E., Izquierdo, M., 2013. Fish larval nutrition and feed formulation: knowledge gaps and bottlenecks for advances in larval rearing. Rev. Aquac. 5, S26–S58.

Infante, J.Z., Cahu, C., 2007. Dietary modulation of some digestive enzymes and metabolic processes in developing marine fish: applications to diet formulation. Aquaculture 268 (1-4), 98–105.

Izquierdo, M.S., 1989Requirement of larval red seabream Pagrus major for essential fatty acids. 日本水産学会誌 55(5), 859-867..

Izquierdo, M.S., Arakawa, T., Takeuchi, T., Haroun, R., Watanabe, T., 1992. Effect of n-3 HUFA levels in Artemia on growth of larval Japanese flounder (Paralichthys olivaceus). Aquaculture 105 (1), 73–82. https://doi.org/10.1016/0044-8486(92)90163-F.

Izquierdo, M.S., Socorro, J., Roo, J., 2010. Studies on the appearance of skeletal anomalies in red porgy: effect of culture intensiveness, feeding habits and nutritional quality of live preys. J. Appl. Ichthyol. 26 (2), 320–326. https://doi.org/10.1111/j.1439-0426.2010.01429.x.

Izquierdo, M.S., Scolamacchia, M., Betancor, M., Roo, J., Caballero, M.J., Terova, G., Witten, P.E., 2012. Effects of dietary DHA and α-tocopherol on bone development, early mineralisation and oxidative stress in Sparus aurata (Linnaeus, 1758) larvae. Br. J. Nutr. 109 (10), 1796–1805. https://doi.org/10.1017/S0007114512003935.

Jamali, H., Ahmadifard, N., Noori, F., Agh, N., Gisbert, E., 2024. Enrichment of Artemia franciscana with soybean-lecithin and its beneficial effect on biochemical composition of broodstocks and fatty acids composition of eggs in Cichlid Green Terror (Aequidens rivulatus).

Joshua, W.J., Kamarudin, M.S., Ikhsan, N., Yusoff, F.M., Zulperi, Z., 2022. Development of enriched Artemia and Moina in larviculture of fish and crustaceans: a review. Lat. Am. J. Aquat. Res. 50 (2), 144–157.

Lundova, K., Kouril, J., Sampels, S., Matousek, J., Stejskal, V., 2018. Growth, survival rate and fatty acid composition of sterlet (Acipenser ruthenus) larvae fed fatty acid-enriched Artemia nauplii. Aquac. Res. 49 (10), 3309–3318.

Mejri, S.C., Tremblay, R., Audet, C., Wills, P.S., Riche, M., 2021. Essential fatty acid requirements in tropical and cold-water marine fish larvae and juveniles. Front. Mar. Sci. 8, 2021. https://doi.org/10.3389/fmars.2021.680003.

Mesa-Rodriguez, A., Hernández-Cruz, C.M., Betancor, M.B., Fernández-Palacios, H., Izquierdo, M.S., Roo, J., 2018. Effect of increasing docosahexaenoic acid content in weaning diets on survival, growth and skeletal anomalies of longfin yellowtail (Seriola rivoliana, Valenciennes 1833). Aquac. Res. 49 (3), 1200–1209. https://doi.org/10.1111/are.13573.

Monroig, Ó., Navarro, J.C., Amat, I., González, P., Amat, F., Hontoria, F., 2003. Enrichment of Artemia nauplii in PUFA, phospholipids, and water-soluble nutrients using liposomes. Aquac. Int. 11 (1), 151–161.

Mozanzadeh, M.T., Bahabadi, M.N., Morshedi, V., Azodi, M., Agh, N., Gisbert, E., 2021. Weaning strategies affect larval performance in yellowfin seabream (Acanthopagrus latus). Aquaculture 539, 736673. https://doi.org/10.1016/j.aquaculture.2021.736673.

Mutia, M.T.M., Muyot, M.C., Muyot, F.B., Balunan, R.L., 2017. Value chain analysis of maliputo, *Caranx ignobilis* in the Philippines. Philipp. J. Fish. 27, 137–156.

Mutia, M.T.M., Muyot, F.B., Magistrado, M.L., Muyot, M.C., Baral, J.L., 2020. 2020. Induced breeding of giant trevally, maliputo *Caranx ignobilis* (Forsskål, 1775) using human chorionic gonadotropin (HCG) and luteinising hormone-releasing hormone analogue (LHRHa). Asian Fish. Sci. 33, 118–127.

Mutia, M.T.M., Muyot, F.B., Baral, J.L., Garcia, L.C., 2024. Larval rearing of the giant trevally, *Caranx ignobilis* (Forsskål, 1775), fed live food combinations of rotifers, copepods and *Artemia salina*. Asian Fish. Sci. 37 (3). https://doi.org/10.33997/j.afs.2024.37.3.005.

Nguyen, M.C., Fotedar, R., Pham, H.D., 2022. Effects of dietary protein and lipid levels on growth performance, feed utilization and body composition of juvenile giant trevally (Caranx ignobilis Forsskal, 1775). Aquac. Res. 53 (17), 6254–6263. https://doi.org/10.1111/are.16098.

Palacios, E., Bonilla, A., Pérez, A., Racotta, I.S., Civera, R., 2004. Influence of highly unsaturated fatty acids on the responses of white shrimp (Litopenaeus vannamei) postlarvae to low salinity. J. Exp. Mar. Biol. Ecol. 299 (2), 201–215. https://doi.org/10.1016/j.jembe.2003.09.007.

Pham, D.H., 2023. Developing protocols for artificial reproduction and growth-out of giant trevally (Caranx ignobilis) in Khanh Hoa province. Project funded by The People's Committee of Khanh Hoa Province. Nha Trang University.

Pham, H.D., Le, M.-H., Dinh, K.V., Siddik, M.A.B., Hoang, D.-H., Ngo, M.V., 2022. Effects of enrichment Artemia with organic selenium and essential fatty acids on growth performance and fatty acid composition of barramundi (Lates calcarifer) larvae. Reg. Stud. Mar. Sci. 55, 102595. https://doi.org/10.1016/j.rsma.2022.102595.

Pham, H.D., Siddik, M.A.B., Rahman, M.A., Huynh, L.T., Nahar, A., Vatsos, I.N., 2023. Effects of n-3 HUFA-enriched Artemia on growth, biochemical response, skeletal morphology and stress resistance of Asian sea bass (Lates calcarifer) larvae reared at high temperature. Aquaculture 574, 739732. https://doi.org/10.1016/j.aquaculture.2023.739732.

Ramena, Y., Kurapati, R.B., Bosteels, T., Ramena, G., 2025. Artemia enrichment strategies: a comprehensive review of nutritional enhancements with emphasis on

fatty acid profiles in aquatic species. Rev. Aquac. 17 (4), e70080. https://doi.org/10.1111/raq.70080.

Rimmer, M.A., Reed, A.W., Levitt, M.S., Lisle, A.T., 1994. Effects of nutritional enhancement of live food organisms on growth and survival of barramundi, Lates calcarifer (Bloch), larvae. Aquac. Res. 25 (2), 143–156. https://doi.org/10.1111/j.1365-2109.1994.tb00570.x.

Roo, J., Fernández-Palacios, H., Hernández-Cruz, C.M., Mesa-Rodriguez, A., Schuchardt, D., Izquierdo, M., 2014. First results of spawning and larval rearing of longfin yellowtail Seriola rivoliana as a fast-growing candidate for European marine finfish aquaculture diversification. Aquac. Res. 45 (4), 689–700. https://doi.org/10.1111/are.12007.

Roo, J., Hernández-Cruz, C.M., Mesa-Rodriguez, A., Fernández-Palacios, H., Izquierdo, M.S., 2019. Effect of increasing n-3 HUFA content in enriched Artemia on growth, survival and skeleton anomalies occurrence of greater amberjack Seriola dumerili larvae. Aquaculture 500, 651–659. https://doi.org/10.1016/j.aquaculture.2018.09.065.

Rungruangsak-Torrissen, K., Moss, R., Andresen, L.H., Berg, A., Waagbø, R., 2006. Different expressions of trypsin and chymotrypsin in relation to growth in Atlantic salmon (Salmo salar L.). Fish. Physiol. Biochem. 32 (1), 7–23. https://doi.org/10.1007/s10695-005-0630-5.

Santigosa, E., Sánchez, J., Médale, F., Kaushik, S., Pérez-Sánchez, J., Gallardo, M.A., 2008. Modifications of digestive enzymes in trout (Oncorhynchus mykiss) and sea bream (Sparus aurata) in response to dietary fish meal replacement by plant protein sources. Aquaculture 282 (1), 68–74. https://doi.org/10.1016/j.aquaculture.2008.06.007.

Sheng, Z., Turchini, G.M., Xu, J., Fang, Z., Chen, N., Xie, R., Zhang, H., Li, S., 2022. Functional properties of protein hydrolysates on growth, digestive enzyme activities, protein metabolism, and intestinal health of larval largemouth bass (Micropterus salmoides). Front. Immunol. 13, 2022. https://doi.org/10.3389/fimmu.2022.913024.

Thépot, V., Mangott, A., Pirozzi, I., 2016. Rotifers enriched with a mixed algal diet promote survival, growth and development of barramundi larvae, Lates calcarifer (Bloch). Aquac. Rep. 3, 147–158. https://doi.org/10.1016/j.aqrep.2016.02.003.

Tocher, D.R., 2010. Fatty acid requirements in ontogeny of marine and freshwater fish. Aquac. Res. 41 (5), 717–732. https://doi.org/10.1111/j.1365-2109.2008.02150.x.

Tseng, H.C., Grendell, J.H., Rothman, S.S., 1982. Food, duodenal extracts, and enzyme secretion by the pancreas. Am. J. Physiol. 243 (4), G304–G312. https://doi.org/10.1152/ajpgi.1982.243.4.G304.

Vagner, M., Robin, J.H., Zambonino Infante, J.L., Person-Le Ruyet, J., 2007. Combined effects of dietary HUFA level and temperature on sea bass (Dicentrarchus labrax) larvae development. Aquaculture 266 (1), 179–190. https://doi.org/10.1016/j.aquaculture.2007.02.040.

Villalta, M., Estevez, A., Bransden, M.P., Bell, J.G., 2008. Effects of dietary eicosapentaenoic acid on growth, survival, pigmentation and fatty acid composition in Senegal sole (Solea senegalensis) larvae during the Artemia feeding period. Aquac. Nutr. 14 (3), 232–241. https://doi.org/10.1111/j.1365-2095.2007.00522.x.

Villeneuve, L., Gisbert, E., Zambonino-Infante, J.L., Quazuguel, P., Cahu, C.L., 2007. Effect of nature of dietary lipids on European sea bass morphogenesis: implication of retinoid receptors. Br. J. Nutr. 94 (6), 877–884. https://doi.org/10.1079/BJN20051560.

Worthington, 1982. Enzymes and related biochemicals. Biochemical Products Division. Worthington Diagnostic System, Freehold, NJ, USA.

Regional Studies in Marine Science 102 (2026) 105430

Contents lists available at ScienceDirect

Regional Studies in Marine Science

journal homepage: www.elsevier.com/locate/rsma

Dynamics of carbon and nitrogen profiles in the hatching medium of decapsulated *Artemia franciscana* cysts

Thai Truong Quoc [a,c,*], Dat Nguyen Khac [a], Hong Truong Thi Bich [b], Sorgeloos Patrick [c], De Schryver Peter [c]

[a] Central Research Center for Brackish and Marine Aquaculture, Vietnam Academy of Fishery Sciences, Nguyen Tat Thanh avenue, Nam Nha Trang ward, Khanh Hoa province, Viet Nam
[b] Department of Aquaculture, School of Fisheries and Life Sciences, Nha Trang University, 02 Nguyen Dinh Chieu street, Bac Nha Trang ward, Viet Nam
[c] Laboratory of Aquaculture and Artemia Reference Center, Ghent University, Coupure Links 653, Gent B-9000, Belgium

ARTICLE INFO

Keywords:
Artemia
Dormant cysts
Trehalose
Glycerol
Glycogen
Hatching medium

ABSTRACT

During hatching, a carbon metabolism drives the release of nauplii from the cysts of the zooplankton brine shrimp *Artemia*. In this study, the change in carbonaceous compounds (trehalose, glycerol, glycogen and total organic carbon) and total nitrogen in the axenic hatching medium of decapsulated *Artemia franciscana* cysts was determined throughout the hatching process. Three different salinities (5, 12 and 35 g L^{-1}) of the incubation medium were applied. Trehalose appeared in the medium in small quantities (maximally 2.6 mg C g^{-1} incubated dry cysts L^{-1}) as compared to glycerol and glycogen (maximally 28.5 ± 1.2 and 13.8 ± 1.0 mg C g^{-1} incubated dry cysts L^{-1}, respectively). This is consistent with the conversion of trehalose within the cyst into glycogen for energy delivery during respiration and into glycerol for hatching of the nauplius out of the shell. Salinity only seemed to substantially affect glycerol release which was significantly higher at 12 g L^{-1} and 35 g L^{-1} than at 5 g L^{-1} for most of the incubation period. The maximum total organic carbon (TOC) levels were 38.6 ± 9.0, 55.2 ± 6.0 and 58.7 ± 7.7 mg g^{-1} incubated dry cysts L^{-1} and the maximum total nitrogen (TN) levels were 3.0 ± 0.4, 4.6 ± 0.3 and 6.9 ± 0.4 mg g^{-1} incubated dry cysts L^{-1} for the 5 g L^{-1}, 12 g L^{-1} and 35 g L^{-1} treatment, respectively. The resulting C/N ratio was 10 or more throughout most of the cyst incubation period in each treatment and showed adequate to support bacterial growth of the probiotic bacterium *Bacillus* sp. LT12. The observations from this study can form the basis of further studies on the integration of *Artemia* live feed production and bacterial culture to apply in larviculture.

Aim

Artemia nauplii are the most important live feed used in the culture of fish and shrimp larvae. The aim of this study was to investigate the change in total organic carbon (TOC, via glycerol, glycogen and trehalose) and total nitrogen (TN), as well as the hatching success, in a gnotobiotic *Artemia* cysts hatching medium throughout the incubation period. Three different salinities (5, 12 and 35 g L^{-1}) were applied in the incubation medium to determine the variation in the different parameters that were evaluated. The results yielded information on the C/N ratio in the incubation medium throughout hatching which determines the possibility to use the carbon released into hatching medium as a substrate for probiotic bacteria to be applied in aquaculture.

1. Introduction

The brine shrimp *Artemia* is used as a live feed for the larval culture of almost all fish and crustacean species due to its high protein content and ability to produce encysted embryos for long term storage (Léger et al., 1987; Sorgeloos et al., 1998; Interaminense et al., 2014). *Artemia* can also be raised easily to produce nauplii, larvae and adults (Bagshaw, 1989; Hajirostamloo, 2008). According to FAO (2014), *Artemia* can be found globally in hypersaline habitats such as inland salt lakes, coastal salt pans and man-managed saltworks. Over 90 % of the world's cyst market originates from the Great Salt Lake (Utah, USA), with annual harvests in the order of 2.500 – 3.000 tonnes of finished product. The activity of shrimp hatcheries consumes about 80–85 % of the total sales

* Corresponding author at: Central Research Center for Brackish and Marine Aquaculture, Vietnam Academy of Fishery Sciences, Nguyen Tat Thanh avenue, Nam Nha Trang ward, Khanh Hoa province, Viet Nam.
E-mail addresses: tqthai@vafis.net, truongqt115@gmail.com (T. Truong Quoc).

https://doi.org/10.1016/j.rsma.2026.105430
Received 21 May 2026; Received in revised form 29 August 2026; Accepted 29 August 2026
Available online 7 September 2026

of *Artemia* cysts, the remainder being used in marine fish culture in Europe and East Asia and for the pet fish market (FAO, 2014).

Artemia can reproduce by two modes depending on the prevailing environmental conditions. When living conditions are favorable, the fertilized eggs in the brood pouch of the female develop into free-swimming nauplii (ovoviviparous reproduction). When embryonic development is held back at the gastrula stage because of unfavorable environmental conditions such as high salinity, low oxygen levels, temperature stress, food depletion, etc (Lavens and Sorgeloos, 1987), cysts are produced inside the uterus (oviparous reproduction). In the processes of cyst production and later hatching of nauplii from the cyst, three carbon compounds - trehalose, glycogen and glycerol - are of primordial importance. During the process of embryos entering into a cryptobiotic state, trehalose accumulates in the dormant cysts at the expense of glycogen (Clegg, 1965). The presence of trehalose prevents the denaturation of proteins and retains cellular integrity in the cysts (Jain and Roy, 2008) as it is particularly effective in stabilizing dry membranes, phospholipid bilayers and proteins (Crowe et al., 1987). It is not maternally derived but is synthesized by the embryo itself (Clegg, 1965) and accumulates up to 15% of the dry weight of a dormant cyst which weighs about 2.5 µg (Clegg, 1962). Glycogen and glycerol are two other forms of carbon present in dormant cysts. Clegg (1962) reported that the glycogen remaining after conversion into trehalose represents about 1% on cyst dry weight. Glycerol is suggested to serve as a cryo-protectant to prevent low temperature damage to the embryos (Cheng et al., 2014). It is mainly produced out of trehalose at the moment the metabolism in the cyst resumes. Nonetheless, it is present in dormant cysts in small quantities of approximately 2–5% on dry weight (Clegg, 1962). Together, trehalose, glycogen and glycerol have been estimated to make up to 98% of the total carbohydrate content in dormant cysts (Dutrieu, 1960; Carpenter and Hand, 1986).

During aerobic incubation of *Artemia* cysts under favorable environmental conditions, the embryonic metabolism resumes and conversion of trehalose into glycogen and glycerol sets in (Dutrieu, 1960; Muramatsu, 1960; Emerson, 1963; Clegg, 1964; Carpenter and Hand, 1986; Lavens and Sorgeloos, 1987). The oxidation of trehalose during the trehalose-glycogen conversion acts as an energy supply for respiration (Clegg, 1965), while the glycerol accumulates between the embryo and the shell as a hygroscopic compound necessary for the embryo to break out of the shell and hatch (Clegg, 1964). The changes in biochemical components in the dormant cyst during embryonic development have been considered in several studies. It was found that by the moment of hatching trehalose within the cyst (at 12 g L^{-1}) had decreased from 163.6 mg g^{-1} to 41.0 mg g^{-1} (~ 67.3 mg g^{-1}) after 14 h incubation (Clegg, 1964), while glycogen and glycerol increased with 67.3 mg g^{-1} cyst dry weight and 22.6 mg g^{-1} cyst dry weight, respectively (Clegg, 1964). It has also been estimated that upon hatching about 8 mg of glycerol is released per gram cyst dry weight into the medium (Clegg, 1964). The above data are valid for non-decapsulated cysts while information for decapsulated cysts is currently not available.

The presence of trehalose and glycogen in the *Artemia* cyst hatching medium has not been determined so far. Likewise, the occurrence of nitrogen compounds inside *Artemia* cysts and their release upon hatching has not yet been considered. The objective of this study was therefore to investigate the changes in carbonaceous compounds (trehalose, glycerol, glycogen and total organic carbon) and total nitrogen in the hatching medium of axenic decapsulated *Artemia* cysts throughout the incubation period up to hatching. As the incubation salinity seems to affect the amount of glycerol that needs to be build up inside the cyst to reach the critical osmotic pressure necessary for hatching (Lavens and Sorgeloos, 1987), three different salinity concentrations (5, 12 and 35 g L^{-1}) were applied in the medium to assess their effect on each of the measured parameters. Based on this knowledge, bacterial growth was quantified in the *Artemia* hatching medium as this may be a very interesting feature for the use of beneficial bacteria in aquaculture.

2. Materials and methods

2.1. Axenic cysts of Artemia franciscana

Experiments were performed with high quality hatching *Artemia franciscana* cysts originating from the Great Salt Lake, Utah, USA (EG® Type, INVE Aquaculture, Belgium). Axenic cysts were obtained using the procedure described by Marques et al. (2004). Briefly, 2 g of cysts were hydrated for 1 h in 90 mL of tap water under continuous aeration. Next, the cysts were decapsulated by the addition of 3.5 mL of NaOH (32%) and 50 mL of NaOCl (14%) under 0.22 µm filtered aeration. After 3 min, 70 mL $Na_2S_2O_3$ (10 g/L) was used to stop the decapsulation reaction. The decapsulated cysts were washed on a sterile 100 µm sieve with 1 L filtered and autoclaved artificial seawater (FAASW) containing 12 g L^{-1} Instant Ocean synthetic sea salt (Aquarium Systems, Sarrebourg, France).

2.2. Bacillus sp. LT12 preparation

Bacillus sp. LT12 is a probiotic Gram-positive and spore-forming rod-shaped bacterium that was previously isolated from a bacterial enrichment culture (EC5) obtained from the digestive tract of *Penaeus vannamei* (Tinh et al., 2007). A ten µl aliquot of the original culture of *Bacillus* sp. LT12 stored in 40% glycerol at −80 °C was inoculated on a Luria-Bertani (LB) agar plate at 12 g L^{-1}. The agar plate was put into an incubator at 28 ^{0}C for 24 h. One colony from the *Bacillus* sp. LT12 agar plate was grown in 25 mL of fresh LB medium (12 g L^{-1}) for 24 h at 28 ^{0}C under constant agitation (120 rpm). The optical cell density of the bacterial culture was determined by a spectrophotometer (BioMerieux, Marcy L'Etoile, France) at 550 nm, washed with FAASW (12 g L^{-1}) and set at a value of 1 (i.e. 1.2 $\times 10^9$ cells mL^{-1}).

Pure cultures of the bacterial strains were grown overnight in marine broth at 28 ^{0}C, transferred to centrifugation tubes, and centrifuged at approximately 8500 x g for 10 min. The supernatant was discarded and the pellet was resuspended in autoclaved nine-salt solution (NSS) (14). The bacterial density was determined spectrophotometrically at 550 nm, assuming that an optical density of 1.000 corresponded to 1.2×10^9 cells mL^{-1} according to the McFarland standard (BioMérieux, Marcy l'Etoile, France) (Verschuere et al., 1999).

2.3. Experimental design

In a first experiment, the changes in carbon and nitrogen patterns during the incubation of axenic and decapsulated *Artemia* cysts were determined. In a second experiment, the growth of *Bacillus* sp. LT12 in the hatching medium of axenic and decapsulated *Artemia franciscana* cysts was assessed.

For experiment 1, glass Schott bottles containing 1 L of FAASW prepared by adding Instant Ocean synthetic sea salt at three different salinities (5, 12 and 35 g L^{-1}) were used to incubate 2 g axenic and decapsulated *Artemia* cysts (n = 3 for each salinity). To maintain axenic conditions during the incubation period, each bottle was supplied of a screw cap with 0.22 µm air filters on the inlet and outlet to provide continuous strong aeration. The cysts were incubated for 22 h at 28 °C under constant illumination of approximately 27 µE m^{-2} sec^{-1}). At 2 h time intervals (from 4 h to 22 h relative to the start of incubation), 100 mL axenic hatching medium of *Artemia* (AHMA) was collected under sterile conditions in a laminar flow after thorough mixing of each bottle for measurement of glycerol, glycogen, trehalose, TOC, TN and cyst hatching success.

In experiment 2, 6 Schott bottles were filled with 1 L FAASW at 12 g L^{-1} and supplemented with 2 g axenic and decapsulated cysts (This medium is called axenic hatching medium of *Artemia* – AHMA). *Bacillus* sp. LT12 was added in three bottles at a concentration of 10^7 cells mL^{-1} (LT12-AHMA). The 3 bottles without addition of *Bacillus* sp. LT12 served as control treatments (Control-AHMA). *Bacillus* sp. LT12 was also added

at 10^7 cells mL^{-1} in 3 Schott bottles containing 250 mL LB broth at 12 ppt (LT12-LB). Each bottle was supplied with a screw cap with 0.22 μm air filters on the inlet and outlet to provide continuous strong aeration and to avoid bacterial contamination. After 26 h of incubation at 28 ^{0}C under constant illumination of approximately 27 μE m^{-2} sec^{-1}, the incubation medium was separated from the *Artemia* cysts, the hatched nauplii and other small particles by filtering over a sterile 30 μm sieve for analysis of the concentration of bacterial cell dry weight (CDW). The samples were stored at −80 ^{0}C until analysis.

2.4. Hatching success of Artemia cysts in experiment 1

The abundances of umbrella and nauplii of *Artemia* in the AHMA samples from experiment 1 were determined in accordance with the method presented by Brendan and Schwarz (2009). One mL of AHMA collected from each well-mixed experimental bottle was diluted 10-folds. A Sedgwick-Rafter slide was used to load 1 mL of the diluted sample and supplemented with one or two drops Lugol's solution to immobilize the *Artemia* nauplii. Using a stereomicroscope (Nikon, Model Alphaphot YS), the number of intact umbrella and nauplii of *Artemia* was counted. This procedure was repeated 3 times for each bottle to determine an average. The averages were multiplied by the dilution factor to obtain the number of umbrella and nauplii of *Artemia* in the experimental bottles.

2.5. Carbon and nitrogen analyses of AHMA samples from experiment 1

The liquid phase in the AHMA samples from each sampling time in experiment 1 was separated from the *Artemia* cysts, already hatched nauplii and other small particles by subsequent filtering over a sterile 30 μm sieve and a sterile 0.22 μm filter (VWR® Syringe Filter, USA). The filtered AHMA samples were stored at −20 ^{0}C until analysis.

2.5.1. Glycerol

A glycerol assay kit (Megazyme International, Bray, Ireland) was used to measure the glycerol concentration in the filtered AHMA samples according to the manufacturer's protocol.

2.5.2. Glycogen

A glycogen colorimetric assay kit (BioVision, Inc., Milpitas, California, USA) was used to measure the glycogen concentration in the filtered AHMA samples according to the manufacturer's protocol.

2.5.3. Trehalose

A trehalose assay kit (Megazyme International, Bray, Ireland) was used to measure the trehalose concentration in the filtered AHMA samples according to the manufacturer's protocol.

2.5.4. Total organic carbon (TOC)

The TOC in the AHMA samples was determined according to the ISO 10694:1995 standard protocol "Determination of organic and total carbon after dry combustion (elementary analysis)" using a Shimadzu TOC-V analyzer with IR detection following thermal oxidation Shimadzu Solid Sample Module (SSM-5000A). In brief, the principle of total organic carbon analysis was as follows: firstly, the AHMA sample was introduced into the combustion tube for total carbon (TC) analysis. Then, it was filled with an oxidation catalyst and heated to 680 ^{0}C. The sample was burned in the combustion tube and as a result the carbon in the sample was converted into carbon dioxide (CO_2). The peak area of the CO_2 is proportional to the TC concentration in the sample. Secondly, the inorganic carbon (IC) was measured as the carbon contained in carbonates and carbon dioxide dissolved in the AHMA sample. By acidifying the sample with a small amount of hydrochloric acid, all the carbonates were converted to carbon dioxide, after which it was volatilized by a sparging process and detected. Finally, the total organic carbon was determined by the formula: TOC = TC – IC.

2.5.5. Total nitrogen (TN)

The TN in the AHMA samples was measured according to the method described by Gross et al. (1999). Briefly, 10 mL of the AHMA sample was pipetted into a 30 mL glass vial. In succession, 5 mL of 0.075 N NaOH and 0.1 g of potassium persulfate were added. All forms of nitrogen compounds were oxidized to nitrate in the persulfate digestion (Ebina et al., 1983; Gross, Boyd, 1998). The vial was autoclaved for 30 min after capping and mixing. The sample was cooled to room temperature, added and mixed with 1 mL of borate buffer (61.8 g boric acid H_3BO_3 and 8 g NaOH in 1 L of distilled water). Turbid samples were centrifuged for 5 min at 4000 rpm to remove the suspended solids. The total nitrate in the digested sample was analysed by UV-absorption using a spectrophotometer (Perkin Elmer Lambda UV/VIS spectrophotometer) at 220 nm.

2.6. OD of Bacillus LT12 in experiment 2

Triplicate 1 mL samples of the medium cultured including control-AHMA, LT12-AHMA and LT12-LB for 26 h were collected as OD samples. OD of *Bacillus* sp. LT12 was determined by spectrophotometer (Thermo Spectronic, USA) at 550 nm set at a value of 1 (i.e. 1.2×10^9 cells mL^{-1}).

2.7. Verification of axenity during hatching in experiment 1 and experiment 2

At the end of experiment 1, 100 μL of non-filtered AHMA from each bottle was plated on marine agar (MA) (Becton Dickinson Benelux N.V., Erembodegem, Belgium) in duplicate. Confirmation of axenicity was established by the absence of visible colonies of bacteria on MA plates after incubation for 5 days at 28 ^{0}C (Gunasekara et al., 2012). The same was done for the control bottles (non-inoculated) from experiment 2. In case contamination was observed, the experiment was completely restarted to maintain consistency across treatments.

2.8. Data analysis

The software SPSS version 22.0 was applied for statistical analyses. Glycerol, glycogen, trehalose, TOC, TN and CDW were analyzed by one-way analysis of variance, followed by a Tukey test for post hoc comparison ($P \leq 0.05$). All the percentage data were normalized by arcsin transformation for statistical analysis, but only non-transformed means are presented.

3. Results

3.1. Hatching success

At each of the three tested salinities, around 40% of the cysts hatched into umbrella-stage *Artemia* between 6 and 8 h of incubation (Fig. 1). The proportion of umbrella stage *Artemia* reached its peak after 10 h of incubation, at approximately 49.2% (5 g L^{-1}), 49.6% (12 g L^{-1}), and 64.5% (35 g L^{-1}), respectively, were observed only in limited quantities of *Artemia* nauplii. Between 10 h and 12 h, *Artemia* nauplii started to appear and made up about half of the total number of cysts that hatched. At about 22 h, the number of hatched cysts reached its maximum with the nauplii stage dominating over the umbrella stage, which representing 71.6% (5 g L^{-1}), 77.6% (12 g L^{-1}) and 81.6% (35 g L^{-1}), respectively. However, no significant differences were observed in the number of *Artemia* nauplii in the hatching medium at different salinities from 14 h up to 22 h.

3.2. Glycerol, glycogen and trehalose content in the AHMA of Artemia

Fig. 2 illustrates the changes in the concentrations of carbonaceous compounds over the 22 h incubation of axenic *Artemia* cysts across

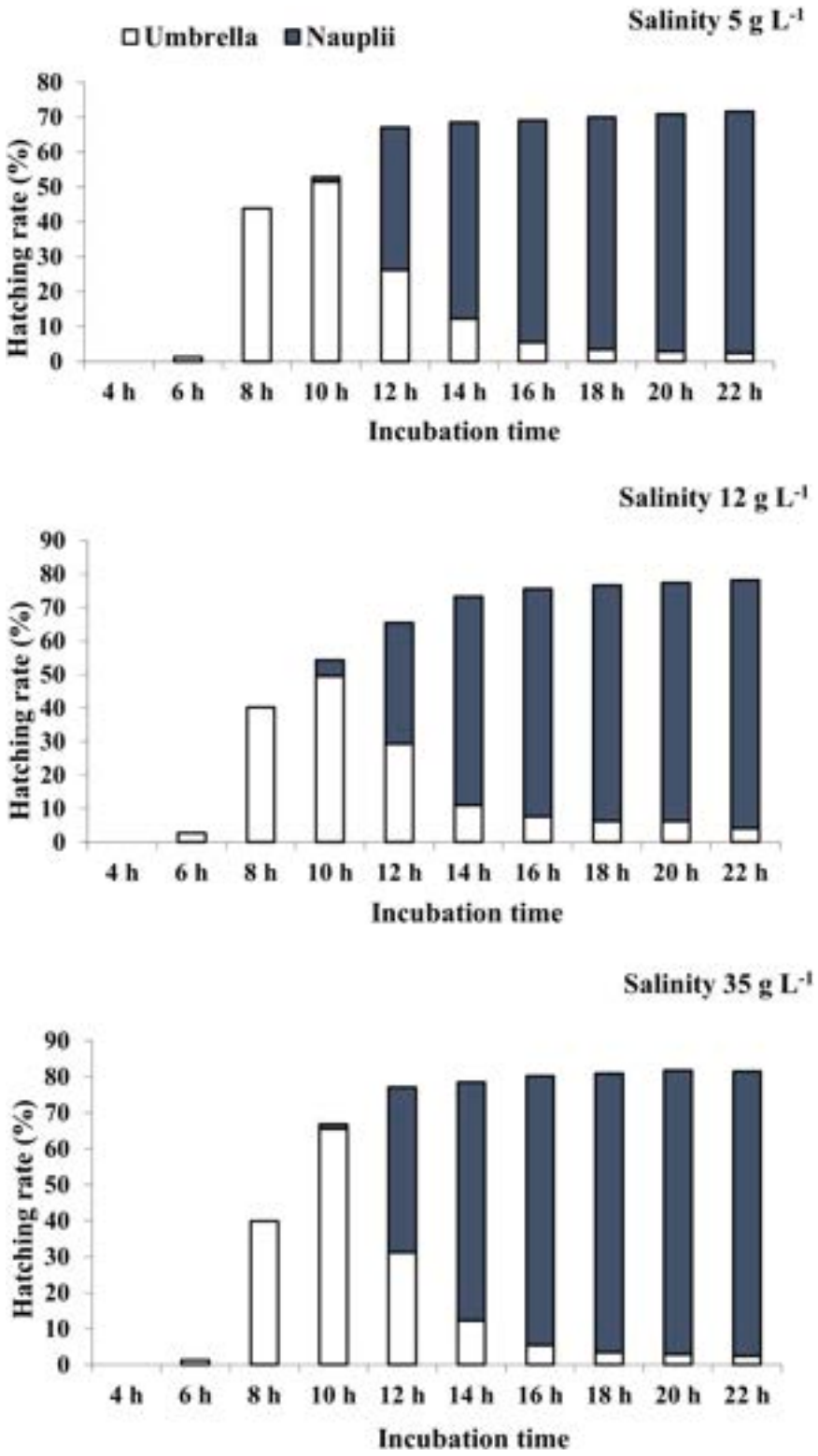

Fig. 1. Hatching percentage of axenic *Artemia* cysts into the umbrella stage and nauplius stage at different incubation salinities.

different salinities (5, 12, and 35 g L^{-1}). The amount of glycerol carbon in the hatching medium increased rapidly during the first 8–10 h of incubation and reached its highest level at about 16 h for each of the three salinities, corresponding to 18.3 ± 0.9 mg g^{-1} cysts L^{-1} (5 g L^{-1}), 25.3 ± 2.0 mg g^{-1} cysts L^{-1} (12 g L^{-1}) and 28.5 ± 1.2 mg g^{-1} cysts L^{-1} (35 g L^{-1}), respectively (Fig. 2A). After 16 h the glycerol carbon level showed a decline in each treatment. From 10 h up to 16 h the glycerol carbon level in the hatching medium was significantly higher at 12 g L^{-1} and 35 g L^{-1} salinity as compared to 5 g L^{-1}. After 16 h, no significant differences were observed through 22 h. By 14 h, the amount of glycogen carbon released into the hatching medium reached 10.2 ± 2.9, 12.3 ± 0.6, and 13.8 ± 1.0 mg g^{-1} cysts L^{-1} at salinities of 5, 12, and 35 g L^{-1}, respectively, after which it showed a slight decrease (Fig. 2B). The concentration of glycogen carbon in the medium was highest at

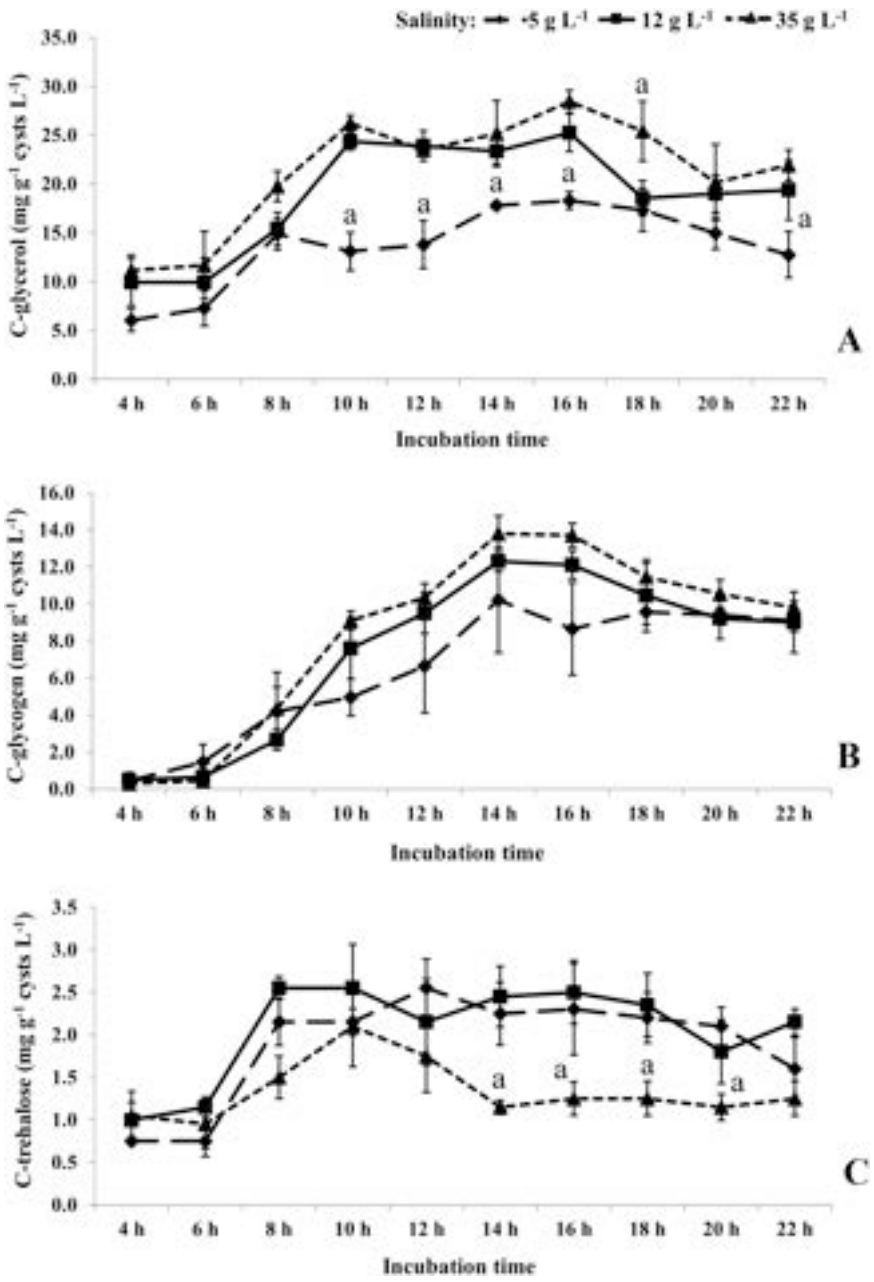

Fig. 2. Glycerol (A), glycogen (B), and trehalose (C) release in the hatching medium of *Artemia* cysts at different incubation salinities. Values indicated with a letter are significantly different from the other values at that specific time point ($p \leq 0.05$).

5 g L^{-1} salinity followed by 12 g L^{-1} and 35 g L^{-1} salinity although there were no significant differences between the different treatments. Trehalose appeared in the hatching medium of each treatment in low amounts (< 2.6 mg g^{-1} cysts L^{-1}) (Fig. 2C). The concentration increased during the first 8–10 h, after which it either remained relatively constant (5 g L^{-1} and 12 g L^{-1}) or decreased again to the original level (35 g L^{-1}). The amount of trehalose released was significantly lower in the 35 g L^{-1} treatment as compared to the other two treatments from 14 h up to 20 h.

3.3. Total organic carbon content in the hatching medium of Artemia

The amount of TOC in the hatching medium during the incubation of the *Artemia* cysts increased progressively for each treatment up to 16 h. At this point, a slight decrease in the TOC concentration set in (Fig. 3). The TOC released was higher in the 35 g L^{-1} than in the 12 g L^{-1} treatment, and higher in the 12 g L^{-1} than in the 5 g L^{-1}. The difference, however, was only significant between the 35 g L^{-1} and the 5 g L^{-1} from 4 h to 22 h (except at time point 18 h). The sum of glycerol, glycogen and trehalose carbon was generally lower than the TOC for the 35 g L^{-1} treatment. The differences were, however, only statistically significant at 6 h. For the 5 g L^{-1} and 12 g L^{-1} treatment, the TOC values showed closely approximated the sum of the different C compounds until 14 h. From 16 h onward, the TOC values were higher in the 35 g L^{-1} treatment. No statistically significant differences were observed between the 5 g L^{-1} and the 12 g L^{-1} across any time points.

3.4. Total nitrogen content in the hatching medium of Artemia

The level of TN in the hatching medium gradually rose in each treatment from the beginning of incubation of the *Artemia* cysts until the end of the experiment (Fig. 4). The influence of salinity on the total

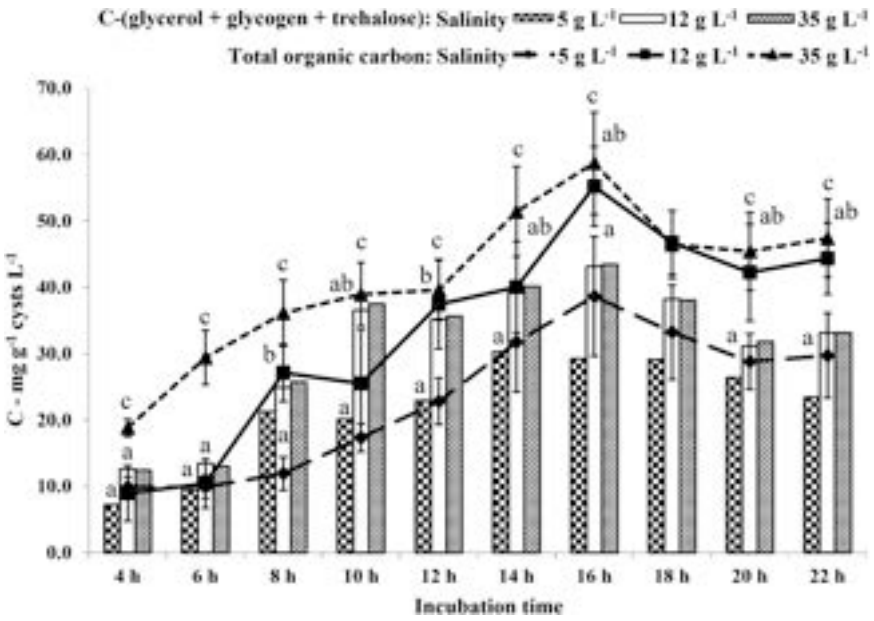

Fig. 3. Total organic carbon release and sum of glycerol-C, glycogen-C and trehalose-C (standard deviation not shown) release in the hatching medium of *Artemia* cysts at different incubation salinities. Values at a specific time point indicated with different letters are significantly different ($p \leq 0.05$).

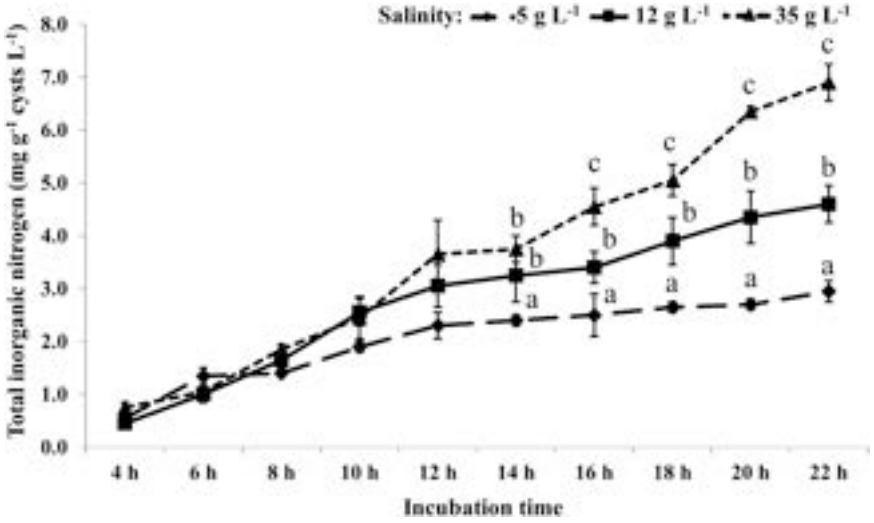

Fig. 4. Total nitrogen release in the hatching medium of axenic *Artemia* cysts at different incubation salinities. Values at a specific time point indicated with a different number of letters are significantly different ($p \leq 0.05$).

nitrogen level in the hatching medium became obvious from 8 to 10 h of incubation onwards. At this point, total nitrogen concentration began to diverge significantly among treatments. However, these differences reached statistical significance only after 14 h. At 22 h, TN release peaked in the 35 g L^{-1} treatment (6.9 ± 0.4 mg g^{-1} cysts L^{-1}), compared to the 12 g L^{-1} (4.6 ± 0.4 mg g^{-1} cysts L^{-1}) and the 5 g L^{-1} (3.0 ± 0.2 mg g^{-1} cysts L^{-1}) treatment.

3.5. Growth of *Bacillus* sp. LT12 in axenic hatching medium of *Artemia*

Bacillus sp. LT12 grew significantly in AHMA and LB medium (12 g L^{-1} salinity) (Fig. 5). The OD of *Bacillus* sp. LT12 was significantly higher when cultured in LB medium (about 3.3) as compared to culturing in AHMA (about 1.5). No bacterial cell was detected in the control treatment without inoculation of *Bacillus* sp. LT12.

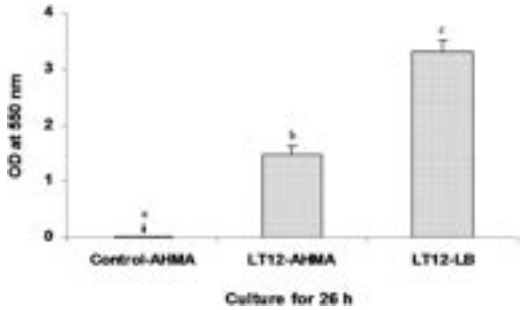

Fig. 5. The OD of *Bacillus* sp. LT12 after 26 h in non-inoculated AHMA (control-AHMA) or in AHMA and LB medium inoculated with 10^7 cells mL^{-1} of *Bacillus* sp. LT12 (LT12-AHMA and LT12-LB, respectively). Bars indicated with different letters are significantly different.

4. Discussion

In dormant embryos of *Artemia*, trehalose is the main carbohydrate (Clegg, 1962; Ewing and Clegg, 1969; Nambu et al., 1997). This compound not only enables dormant embryos to survive stress conditions, it also serves as an energy supply for embryonic development and leads to hatching of the embryo from the cysts under suitable environmental conditions by the formation of glycogen and glycerol, respectively (Clegg, 1964; Cam et al., 2009; Yang et al., 2013). Previous researches on the trehalose metabolism have mainly focused on the biochemical changes within the cyst during different development stages (Muramatsu, 1960; Clegg, 1962; 1964; Boulton and Huggins, 1977). However, very little information is available on the release of metabolic compounds to the cyst hatching medium. In this study, the changes in carbon and nitrogen concentrations in the hatching medium of axenic decapsulated *Artemia* cysts were therefore documented.

According to Clegg (1964), glycerol contained within the cyst is located both in the undeveloped embryo and between the outer membrane and the cyst shell. During embryonic development trehalose is converted into glycerol that accumulates in the extra-embryonic space as a hygroscopic compound. Upon rupture of the cell, this glycerol is released to the medium. In our study, the glycerol carbon concentration in the medium at 5, 12 and 35 g L^{-1} salinity increased rapidly up to 8–10 h and then only slightly increased further to attain its maximum after 16 h of incubation (18.3 ± 0.9, 25.3 ± 2.0 and 28.5 ± 1.2 mg C g^{-1} cysts L^{-1}, respectively). The timepoint of maximal glycerol release corresponded to the timepoint of maximal *Artemia* hatching from the cysts, while the slow increase until 16 h was concomitant with a lower novel appearance of *Artemia* umbrella from the cysts and the increased presence of new nauplii (Supplementary fig. 1). This supports the concept that glycerol is accumulated as a hygroscopic compound required for hatching (Van Stappen, 1996). Clegg (1964) found that 8 mg of glycerol was released into the medium per gram dry cysts upon hatching. Higher values were found for the release of glycerol from the cysts in this study for all salinity treatments (18.3 mg C g^{-1} cyst L^{-1}, 25.3 mg C g^{-1} cyst L^{-1}, 28.5 mg C g^{-1} cyst L^{-1} for the 5 g L^{-1}, 12 g L^{-1} and 35 g L^{-1} treatment, respectively). Normally, one would expect that the difference in pretreatment of the *Artemia* cysts between the experiment of Clegg (1964) and the current experiment may explain for this discrepancy. The former experiment made use of non-decapsulated cysts while for the current experiment decapsulated cysts were incubated. Because the outer layer (chorion) of *Artemia* cysts is removed during the decapsulation process, the breaking of the embryo's outer cuticular membrane requires less osmotic pressure hence a lower production of glycerol (Sorgeloos et al., 1977; Bruggeman et al., 1980; Ribeiro and Jones, 1998). Clegg (1964) and Crowe (2008) stated that at higher external osmotic pressures, more trehalose is converted into glycerol which was confirmed by the results from the current experiment.

The organic carbon released into the incubation medium of the *Artemia* cysts consisted not only of glycerol but also of trehalose and glycogen which have hardly been considered before. The low release of less than 2.6 mg g^{-1} cysts L^{-1} trehalose was indicative for the trehalose-glycerol osmoregulatory system and the trehalose-glycogen conversion during embryonic development prior to hatching (Lavens and Sorgeloos, 1987). This study is the first that describes the occurrence of glycogen in the hatching medium of *Artemia* cysts. So far, glycogen has only been considered within the cysts and various results have been recorded by several authors. Boulton and Huggins (1977) reported that the glycogen content in *Artemia salina* cysts after 12 h of hydration was 5.8 ± 0.0 mg g^{-1} cyst dry weight, while Clegg (1964) reported a value of 83.3 ± 4.2 mg g^{-1} cyst dry weight at 14 h incubation. In this study, the highest amount of glycogen present in the hatching medium was 10.2 ± 2.9 mg C g^{-1} cysts L^{-1} (5 g L^{-1}), 12.3 ± 0.6 mg C g^{-1} cysts L^{-1} (12 g L^{-1}) and 13.8 ± 1.0 mg C g^{-1} cysts L^{-1} (35 g L^{-1}). No significant effect of salinity was detected on the presence of glycogen in the AHMA. The steady increase in glycogen concentration up to 14 h, the moment at which the number of *Artemia* nauplii stabilized, indicates that glycogen in the incubation medium can be explained by its release from the *Artemia* cysts at hatching stage.

The TOC attained maximum values of 38.6 ± 9.0, 55.2 ± 6.0 and 58.7 ± 7.7 mg C g^{-1} cysts L^{-1} at 5, 12 and 35 g L^{-1} salinity, respectively. The sum of carbon from glycerol, glycogen and trehalose reached on average 93.9% (at 5 g L^{-1} salinity), 91.6% (at 12 g L^{-1} salinity) and 75.4% (at 35 g L^{-1} salinity) of these TOC results. It thus appears that other carbon compounds besides glycerol, glycogen and trehalose may be released during cyst hatching. This opinion is supported by the statement of Boulton and Huggins (1977) that glucose can also be present be it in very low amounts.

As for any other organism, nitrogen is one of the most important elements in the *Artemia* tissue with a content that was determined at 7.8% on dry weight in any size of *Artemia* nauplii (Nimura and Miah, 1991). Nitrogen waste is constantly produced by *Artemia* nauplii as an excretion product during morphogenesis. The metabolic activity has been determined before that ammonia nitrogen was excreted by *Artemia* nauplii throughout of different stage of larval development (Hernandorena and Kaushik, 1981). This may explain the substantial increase in TN in the *Artemia* hatching medium from 10 h onwards. However, in this study nitrogen was also observed in the hatching medium before *Artemia* cysts reached the hatching stage (before 10 h). It can be hypothesized that this results from metabolic activity of the embryo inside the cyst that created nitrogenous waste that then diffuses through the membrane into the medium. The concentration of TN released in the hatching medium was positively related to and significantly affected by the salinity used to incubate the *Artemia* cysts, and the highest TN concentrations were reached at 22 h incubation with 3.0 ± 0.2, 4.6 ± 0.4 and 6.9 ± 0.3 mg N g^{-1} cysts L^{-1} at 5, 12 and 35 g L^{-1} salinity, respectively.

As there already is a substantial body of established literature describing the carbon metabolism in (developing) *Artemia* cysts, the novelty in the current research lies in that it considers the combined release of carbon and nitrogen in the hatching medium of *Artemia* for a practical purpose. *Artemia* nauplii are routinely used as live feed for the larvae of fish and shrimp, and on a daily basis several kilograms of cysts can be incubated within a larviculture unit. While the hatching medium of *Artemia* cysts is currently considered as a waste, it may be used as a growth source for the culture of beneficial bacteria to be used in aquaculture. Examples are bacterial probionts with homoserine lactone-degrading or/and poly-β-hydroxybutyrate-accumulating characteristics (Cam et al., 2009). Based on the results of TOC and TN, the evolution of the C/N ratio in the hatching medium could be established (Fig. 6) which is an important criterium when one wants to culture bacteria. For the largest part of the incubation period, the C/N ratio is about 10 or more in the hatching medium of the *Artemia* which is an optimal value for promoting bacterial growth as can be deducted from Avnimelech (1999). The growth of the probiotic bacterium *Bacillus* sp. LT12 in AHMA illustrates the potential to use AHMA as a bacteria culture medium. Although the cell growth of LT12 was not as high as in a traditional nutrient rich medium such as LB, about 1.8×10^{12} CFU could be produced in each liter of hatching medium. This is more than the suggested dose for commercially available probiotic *Artemia* enrichment mixtures such as Sano-Life® MIC-F, INVE Aquaculture (0.5 g L^{-1} for bio-encapsulating of live food). This makes the feature that the beneficial bacteria are cultured in the same medium as the live feed extra interesting. However, the concentration of total organic carbon has determined that is not suitable to support for the cell growth of LT12 in the co-culture with *Artemia*. Thus, it seems that this bacterium uses other carbon sources in the hatching medium for the development such as un-hatched, dead *Artemia*, etc. As *Artemia* nauplii start filter feeding at about 24 h after start incubation (Vanhaecke et al., 1983), they would enrich themselves with these freshly grown beneficial bacteria and make up the perfect delivery medium of these bacteria for the cultured larvae of fish and shrimp. This would make an additional enrichment step

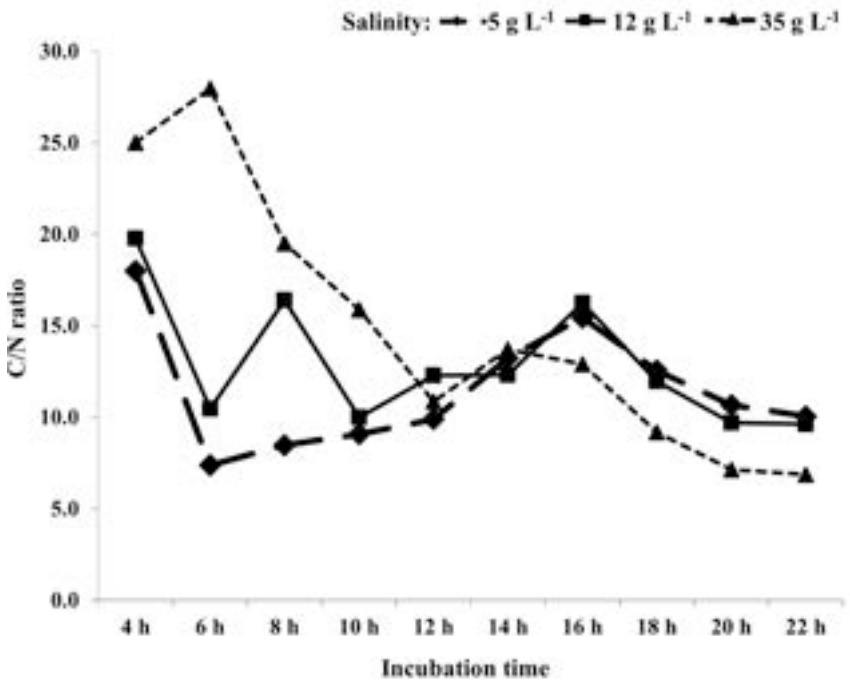

Fig. 6. The C/N ratio in the hatching medium of axenic *Artemia* cysts at different incubation salinities.

unnecessary. However, further research is needed to verify that biosafety can be guaranteed in this way.

5. Conclusion

We reported for the first time the change in total organic carbon and total nitrogen concentrations in the hatching medium of decapsulated *Artemia* cysts during incubation at different salt concentrations. The carbon compounds glycerol and glycogen are released at substantial amounts from the cysts at the moment of shell rupture while nitrogen waste is secreted by *Artemia* continuously set free during incubation. The knowledge that is obtained concerning the C/N ratio in the hatching medium provides useful information for the reuse of the *Artemia* hatching medium as a growth source for beneficial bacteria and will form the basis of future studies on the integration of *Artemia* culture and bacteria culture to apply in larviculture.

CRediT authorship contribution statement

Thai Truong Quoc: Writing – original draft, Visualization, Methodology, Formal analysis, Conceptualization. **Sorgeloos Patrick:** Writing – review & editing, Methodology, Conceptualization. **De Schryver Peter:** Writing – review & editing, Visualization, Supervision. **Dat Nguyen Khac:** Writing – review & editing. **Hong Truong Thi Bich:** Writing – review & editing.

Declaration of Generative AI and AI-assisted technologies in the writing process

During the preparation of this manuscript, the author(s) used ChatGPT, Google Gemini, and Perplexity. These tools were used to improve grammar, phrasing, and overall readability. Following the use of these services, the author(s) reviewed and edited the content as needed and take(s) full responsibility for the scientific integrity and originality of the published article.

Declaration of Competing Interest

The authors declare that they have no known competing financial interests or personal relationships that could have appeared to influence the work reported in this paper.

Acknowledgements

We thank Peter Bossier and Mathieu Wille of the Laboratory of Aquaculture and Artemia Reference Center, Ghent University, Belgium, for their contributions to review and data verification. The financial support by the Vietnamese government project “Main program on development and application of Biological technology in agriculture and development of rural country”. This work contributes to the celebration of the 50th anniversary of Nha Trang University, located in Khanh Hoa Province, Viet Nam.

Appendix A. Supporting information

Supplementary data associated with this article can be found in the online version at doi:10.1016/j.rsma.2026.105430.

Data availability

The data that has been used is confidential.

References

Avnimelech, Y., 1999. Carbon / nitrogen ratio as a control element in aquaculture systems. Aquaculture 176, 227–235.

Bagshaw, J.C., 1989. Adventures and misadventures in the genome of *Artemia*. In: Warner, A.H., Macrae, T.H., Bagshaw, J.C. (Eds.), Cell and molecular biology of Artemia development. Plenum publishing, pp. 277–286.

Boulton, A.P., Huggins, A.K., 1977. Biochemical changes occurring during morphogenesis of the brine shrimp *Artemia salina* and effect of alterations in salinity. Comp. Biochem. Physiol. A 57, 17–22.

Brendan, C.D., Schwarz, M.H.I., 2009. *Artemia* culture for intensive finfish and crustacean larviculture. Virginia Cooperative Extension. Virginia Tech, Virginia State University.

Bruggeman, E., Sorgeloos, P., Vanhaecke, P., 1980. Improvements in the decapsulation technique of *Artemia* cysts. In: Persoone, G., Sorgeloos, P., Roels, O., Jaspers, E. (Eds.), The brine shrimp Artemia. Universa Press, Wetteren, Belgium, pp. 261–269.
Cam, D.T.V., Hao, N.V., Dierckens, K., et al., 2009. Novel approach of using homoserine lactone-degrading and poly-β-hydroxybutyrate-accumulating bacteria to protect *Artemia* from the pathogenic effects of *Vibrio harveyi*. Aquaculture 291, 23–30.
Carpenter, J.F., Hand, S.C., 1986. Arrestment of carbohydrate metabolism during anaerobic dormancy and aerobic acidosis in *Artemia* embryos: determination of pH-sensitive control points. J. Comp. Physiol. B 156, 451–459.
Cheng, C., Yao, F., Chu, B., et al., 2014. Identification of the glycerol kinase gene and its role in diapause embryo restart and early embryo development of *Artemia sinica*. Gene 537, 51–62.
Clegg, J.S., 1962. Free glycerol in dormant cysts of the brine shrimp *Artemia salina*, and its disappearance during development. In: Biol. Bull., 123. Woods Hole, pp. 295–301.
Clegg, J.S., 1964. The control of emergence and metabolism by external osmotic pressure and the role of free glycerol in developing cysts of *Artemia salina*. J. Exp. Biol. 41, 879–892.
Clegg, J.S., 1965. The origin of trehalose and its significance during the formatiom of encysted dormant embryos of *Artemia salina*. Comp. Biochem. Physiol. 14, 135–143.
Crowe, J.H., 2008. Trehalose and anhydrobiosis: the early work of Clegg, J. S. J. Exp. Biol. 211, 2899–2900.
Crowe, J.H., Crowe, L.M., Carpenter, J.F., et al., 1987. Stabilization of dry phospholipid bilayers and proteins by sugars. Biochem. J. 242, 1–10.
Dutrieu, J., 1960. Observations biochimiques et physiologiques sur le developpement d'*Artemia salina* Leach. Archs. Zoo. Exp. G. ėN. 99, 1–133.
Ebina, J., Tsutsui, T., Shirai, T., 1983. Simultaneous determination of total nitrogen and total phosphorus in water using peroxodisulfate oxidation. Water Res. 17, 1721–1726.
Emerson, D.N., 1963. The metabolism of hatching embryos of the brine shrimp *Artemia salina*. Proc. S. Dak. Acad. Sci. 42, 131–135.
Ewing, R.D., Clegg, J.S., 1969. Lactate dehydrogenase activity and anaerobic metabolism during embryonic development in *Artemia salina*. Comp. Biochem. Physiol. 31, 297–307.
FAO, 2014. Culture aquatic species information programme *Artemia spp* (Leach, 1819).
Gross, A., Boyd, C.E., 1998. A digestion procedure for the simultaneous determination of total nitrogen and total phosphorus in pond water. J. World Aqua. Soc. 29, 300–303.
Gross, A., Boyd, C.E., Jinwon, S., 1999. Evaluation of the ultraviolet spectrophotometric method for the measurement of total nitrogen in water. J. World Aquac. Soc. 30, 388–393.
Gunasekara, R.A.Y.S.A., Defoirdt, T., Rekecki, A., Van den Broeck, W., Bossier, P., Sorgeloos, P., et al., 2012. Light and transmission electron microscopy of *Vibrio campbellii* infection in gnotobiotic *Artemia franciscana* and protection offered by a yeast mutant with elevated cell wall glucan. Vet. Microbiol. 158 (3-4), 337–343.
Hajirostamloo, M., 2008. Differences of shell structure in cysts of *Artemia* from various depth of Urmia lake (Iran). Res. J. Biol. Sci. 3, 648–653.
Hernandorena, A., Kaushik, S.J., 1981. Ammonia excretion of *Artemia* sp. (Crustacea: Brachiopoda) under axenic condition. Mar. Biol. 63, 23–27.
Interaminense, J.A., Calazans, N.F., Do Valle, B.C., et al., 2014. *Vibrio* spp. Control at brine shrimp, *Artemia*, hatching and enrichment. J. World Aquac. Soc. 45, 65–74.
Jain, N.K., Roy, I., 2008. Effect of trehalose on protein structure. Prot. Sci. 18, 24–36.
Léger, P., Bengton, D.A., Sorgeloos, P., et al., 1987. The nutritional value of *Artemia*: a review. In: Sorgeloos, P., Bengton, D.A., Decleir, W., Jaspers, E. (Eds.), Artemia research and its applications. Universa Press, Wetteren, Belgium, p. 556.
Lavens, P., Sorgeloos, P., 1987. The cryptobiotic state of *Artemia* cysts, its diapause deactivation and hatching: a review. In: Sorgeloos, P., Bengton, D.A., Decleir, W., Jaspers, E. (Eds.), Artemia research and its applications. Universa Press, Wetteren, Belgium, p. 556.
Marques, A., Dhont, J., Sorgeloos, P., et al., 2004. Evaluation of different yeast cell wall mutants and microalgae strains as feed for gnotobiotically grown brine shrimp *Artemia franciscana*. J. Exp. Mar. Biol. Ecol. 312, 115–136.
Muramatsu, S., 1960. Respiration and its main substrate during the early development of the encysted embryo. Embryol 5, 95–106.
Nambu, Z., Nambu, F., Tanaka, S., 1997. Purification and characterization of trehalose from *Artemia* embryos and larvae. Zoo. Sci. 14, 419–427.
Nimura, Y., Miah, M.I., 1991. Nitrogen excretion by *Artemia franciscana*. Nippon. Suisan Gakk 57, 837–844.
Ribeiro, F.A.L.T., Jones, D.A., 1998. The potential of dried, low-hatch, decapsulated *Artemia* cysts for feeding prawn post-larvae. Aquac. Int. 6, 421–440.
Sorgeloos, P., Bossuyt, E., Laviña, E., et al., 1977. Decapsulation of *Artemia* cysts: a simple technique for the improvement of the use of brine shrimp in aquaculture. Aquaculture 12, 311–315.
Sorgeloos, P., Coutteau, P., Dhert, P., et al., 1998. Use of brine shrimp, *Artemia* spp., in larval crustacean nutrition: a review. Rev. Fish. Sci. 6, 55–68.
Tinh, N.T.N., Asanka Gunasekara, R.Y.S., Boon, N., et al., 2007. N-acyl homoserine lactone-degrading microbial enrichment cultures isolated from *Penaeus vannamei* shrimp gut and their probiotic properties in *Brachionus plicatilis* cultures. FEMS Microbiol. Ecol. 62, 45–53.
Van Stappen, G., 1996. Introduction, biology and ecology of *Artemia*. In: Lavens, P., Sorgeloos, P. (Eds.), Manual on Production and Use of Live Food for Aquaculture. Food and Agriculture Organization of the United Nations, p. 108.
Vanhaecke, P., Lavens, P., Sorgeloos, P., 1983. International study on *Artemia*. XVIII. Energy consumption in cysts and early larval stages of various geographical strains of *Artemia*. Annls. Soc. R. Zool. Belg. 113, 155–164.
Verschuere, L., Rombaut, G., Huys, G., Dhont, J., Sorgeloos, P., Verstraete, W., 1999. Microbial control of the culture of *Artemia* juveniles through preemptive colonization by selected bacterial strains. Appl. Environ. Microbiol. 65, 2527–2533.
Yang, F., Chen, S., Dai, Z.M., et al., 2013. Regulation of trehalase expression inhibits apoptosis in diapause cysts of *Artemia*. Biochem. J. 456, 185–194.

Regional Studies in Marine Science 102 (2026) 105436

Contents lists available at ScienceDirect

Regional Studies in Marine Science

journal homepage: www.elsevier.com/locate/rsma

Optimization of dietary marigold (*Tagetes erecta*) carotenoid levels on growth performance, feed utilization, skin pigmentation, and digestive enzyme activities of juvenile golden trevally (*Gnathanodon speciosus*)

Dung Van Tran [a], Trang Le Thi Tran [a], Dang Duyen Thi Thach [a], Dai Quang Tran [a], Manh Van Ngo [a], Dai Trong Vu [a], Hung Quoc Pham [a], Thanh Trung Dang [b,*]

[a] Department of Aquaculture, School of Fisheries and Life Sciences, Nha Trang University, Khanh Hoa, Vietnam
[b] Department of Food Technology, School of Fisheries and Life Sciences, Nha Trang University, Khanh Hoa, Vietnam

ARTICLE INFO

Keywords:
Carotenoids
Marigold
Gnathanodon speciosus
Skin pigmentation
Digestive enzymes
Marine aquaculture

ABSTRACT

Color fading under captivity substantially reduces the market value of golden trevally (*Gnathanodon speciosus*), a tropical marine fish of high ornamental and food value. This study determined the optimum dietary level of marigold (*Tagetes erecta*) carotenoids for juvenile golden trevally. Fish (2.92 ± 0.06 cm; 0.51 ± 0.04 g) were fed six diets supplemented with carotenoids at 0, 200, 400, 600, 800, and 1000 mg/kg (triplicate) for 8 weeks. Final body weight, specific growth rate (SGR), feed conversion ratio (FCR), and protein efficiency ratio improved significantly ($P < 0.05$), peaking at 600–800 mg/kg. Skin yellowness (b*) rose 3.3–3.4-fold and plateaued near 800 mg/kg. Carotenoid deposition was strongly tissue-specific (skin ≫ whole body > muscle), with a skin-to-muscle ratio of 35–69-fold. Intestinal protease and lipase activities increased 1.9- and 2.3-fold, respectively, whereas amylase was unaffected. Crude protein increased (≥ 400 mg/kg) and crude lipid decreased (≥ 600 mg/kg) significantly. Survival exceeded 94% across all treatments. Model selection (quadratic models selected via AICc-based comparison among eight candidates) estimated optima of 646 mg/kg for specific growth rate (SGR_W) and 761 mg/kg for skin yellowness, while pigment accumulation and lipase activity saturated within 600–800 mg/kg. A practical range of 600–800 mg/kg is recommended. This is the first dose–response study of marigold carotenoids in golden trevally, providing a scientific basis for natural-pigment aquafeed in tropical marine aquaculture.

1. Introduction

Tropical marine aquaculture is diversifying rapidly, with marine ornamental and high-value food fish gaining particular attention (Araujo et al., 2022). Beyond growth and survival, external appearance - especially body coloration - has become a key determinant of market value in both sectors, reflecting health and nutritional status and directly influencing consumer acceptance (Mehar et al., 2020; Mitra et al., 2021). Nutritional strategies that simultaneously optimize growth and color are therefore of high scientific and practical significance.

Golden trevally (*Gnathanodon speciosus* Forsskål, 1775) belongs to the Carangidae, the largest family of the order Carangiformes (~148 species), which occur across tropical, subtropical, and temperate waters of the Atlantic, Indian, and Pacific Oceans (Na-Nakorn et al., 2023). The species has a broad Indo-Pacific range, extending from the Red Sea and East Africa through Southeast Asia and northward to Japan, and is characterized by a golden-yellow body with alternating black bands that confers high aesthetic value in the ornamental market (Dharma et al., 2025). Although carangids such as pompano (*Trachinotus* spp.) and yellowtail (*Seriola quinqueradiata*) dominate marine finfish aquaculture, golden trevally remains an emerging, minor-volume species, with a reported global output of only a few tonnes per year, and hatchery and cage-culture protocols are still being developed across Southeast Asia (Na-Nakorn et al., 2023; Dharma et al., 2025). Its rapid growth, good flesh quality, and adaptability to captivity nonetheless make it a promising candidate for diversifying tropical mariculture (Pham et al.,

"Given their role as Co-Guest Editor, Quoc-Hung Pham had no involvement in the peer review of this article and had no access to information regarding its peer review. Full responsibility for the editorial process for this article was delegated to another journal editor."

* Corresponding author.
E-mail address: thanhdt@ntu.edu.vn (T.T. Dang).

https://doi.org/10.1016/j.rsma.2026.105436
Received 31 May 2026; Received in revised form 4 September 2026; Accepted 7 September 2026
Available online 11 September 2026

2026). However, cultured fish commonly exhibit color fading relative to wild counterparts because of the absence of dietary carotenoids in formulated feeds (Tran et al., 2024b), markedly reducing market value - a problem documented across many brightly colored species (Luo et al., 2021; Shastak and Pelletier, 2023).

Carotenoids are the principal natural pigments responsible for yellow–red coloration in aquatic animals (Elbahnaswy and Elshopakey, 2024). Because fish cannot synthesize carotenoids de novo, they must acquire them from the diet. Dietary carotenoids are absorbed across the intestinal epithelium partly via lipid-transporter–mediated pathways (e.g., SR-B1/CD36), incorporated into lipoproteins, and delivered through the circulation to peripheral tissues (Guo et al., 2024; Liao et al., 2025). In the skin, they are selectively retained and stabilized within dermal chromatophores (xanthophores and erythrophores) by carotenoid-binding proteins, whereas cleavage enzymes (e.g., BCO1/BCO2) and differential tissue affinity determine how much pigment is deposited, metabolically converted, or stored in each tissue (Liao et al., 2025). This differential partitioning explains the pronounced skin-over-muscle accumulation reported in many teleosts and underlies the tissue-specific deposition examined in the present study. Beyond pigmentation, carotenoids contribute to antioxidant defence, immunity, and stress tolerance (Elbahnaswy and Elshopakey, 2024).

Plant-derived carotenoids enhance coloration in diverse species, including clownfish, goldfish, gilthead sea bream, koi carp, and leopard coral grouper (Tiewsoh et al., 2019; Tran et al., 2024a; Wassef et al., 2010; Zhang et al., 2023). However, responses are highly species-specific, depending on source, bioavailability, biotransformation, and tissue partitioning (Liao et al., 2025), so each species requires dedicated optimization. Recent reports also suggest carotenoids may enhance digestive enzyme activity and feed utilization (Ansarifard et al., 2018; Xu et al., 2022), although this relationship remains poorly characterized in tropical marine fish.

In our previous screening (Tran et al., 2024b), five floral carotenoid sources were tested at a fixed level (250 mg/kg), and marigold proved superior for skin pigmentation (CIE b* = 18.8) and growth. That single-dose design, however, could not establish the dose–response relationship. Determining the optimum dose is essential for translating these findings into aquafeed production, particularly because golden trevally is being developed for marine cage culture across Southeast Asia (Viet Nam, Indonesia, the Philippines), where marigold is widely cultivated and thus a locally available, cost-effective pigment source.

Building on this, the present study determined the optimum marigold carotenoid level (0–1000 mg/kg) for growth, feed utilization, skin coloration, tissue accumulation, digestive enzyme activities, and whole-body composition of juvenile golden trevally. We hypothesized that (i) appropriate supplementation would improve growth and feed utilization partly through enhanced digestive enzymes; (ii) carotenoids would be preferentially deposited in skin, enhancing yellowness with a saturation threshold; and (iii) the optimum dose for growth would differ from that for pigmentation.

2. Materials and methods

2.1. Ethical statement

All procedures complied with Vietnamese regulations on animal use in research (Livestock Law 2018; Decree 32/2006/NĐ-CP), under which marine fish experiments are exempt from ethics approval. Husbandry, handling, and sampling were performed to minimize stress.

2.2. Carotenoid extraction

Marigold (*Tagetes erecta* L.) was selected based on its superior performance in our previous screening (Tran et al., 2024b). Fresh flowers collected in Khanh Hoa Province, Vietnam, were washed, dried (40 °C, 8–12 h), and ground to powder. Carotenoids were extracted and quantified following: 20 g of powder was extracted with hexane (5:1 v/w, 40 °C, 4 h), filtered, and re-extracted 4–5 times until colorless; pooled extracts were rotary-evaporated (40 °C) and stored in amber bottles at 4 °C. Total carotenoid content was determined by UV-Vis spectrophotometry (Libra S60, Biochrom Ltd., Cambridge, UK) at 450 nm using: Total carotenoid (μg/g) = $(A \times V \times D \times 10^4)/(W \times E_{1\ cm}^{1\%})$, where $E_{1\ cm}^{1\%} = 2500$.

2.3. Experimental diets

A basal diet was formulated to be isonitrogenous (~50% crude protein) and to a target crude lipid of ~9%, meeting the established nutrient requirements of juvenile marine carnivorous finfish (Nankervis et al., 2022; Nguyen et al., 2022). Marigold was selected as the carotenoid source based on our preliminary screening of candidate plant pigments (Tran et al., 2024b) and its high xanthophyll (lutein) content. The complete ingredient composition is given in Table 1.

Protein was supplied by an imported Peruvian anchovy (*Engraulis*

Table 1
Ingredient formulation of the basal diet.

Ingredient	g/kg
Fish meal (Peru)[4]	385.0
Fish meal (Vietnam)[4]	150.0
Squid meal	160.0
Corn gluten meal	100.0
Rice bran	20.0
Wheat flour	110.7
Soybean oil[1]	40.0
Vitamin premix[2]	15.0
Mineral premix[3]	5.3
Binder (polymethylurea)	10.0
Sargassum (seaweed) meal	3.3
L-Lysine[5]	0.5
DL-Methionine[5]	0.2
Total	**1000**

[1] Soybean oil is the sole supplemental lipid; ~20 mL/kg is delivered as the carotenoid top-coat carrier (Table 2), with the remainder incorporated into the dry base, keeping total dietary lipid constant across treatments. [2] Vitamin premix composition (per kg premix; included at 15 g premix/kg diet): Vitamin A 1000,000 IU; D3 300,000 IU; Vitamin C monophosphate 10,000 mg; Pantothenic acid 2500 mg; Vitamin E 2000 mg; B3 2000 mg; K3 500 mg; B1 500 mg; B6 500 mg; B2 320 mg; Folic acid 200 mg; Biotin 20 mg; B12 5 mg; Inositol 10 mg; Choline chloride 5 mg. [3] Mineral premix composition (per kg premix; included at 5.3 g premix/kg diet): Zn (ZnO) 4750 mg; Mn ($MnSO_4 \cdot H_2O$) 1900 mg; Mg (MgO) 1050 mg; Co ($CoCO_3$) 47.5 mg; Se (Na_2SeO_3) 47.5 mg; I ($Ca(IO_3)_2 \cdot H_2O$) 19 mg; P ($CaHPO_4 \cdot 2H_2O$) 0.7%; Ca ($CaHPO_4 \cdot 2H_2O$) 0.8%; Moisture 10%; Ash 2%; Carrier (dextrose) to 100% (w/w of premix). The premix specified for the present trial was ethoxyquin-free (Section 2.3).
[4] Peruvian fish meal: imported anchovy (Engraulis ringens) meal, 65% crude protein. Vietnamese fish meal: commercially produced, mixed-source marine fish meal of 55% crude protein (Long Sinh Co., Ltd., Khanh Hoa Province, Vietnam), manufactured from low-value whole fish and bycatch landed by local coastal capture fisheries together with trimmings (heads and frames) recovered from domestic tuna processing. Protein contents are the manufacturers' product specifications for the batches used; the analysed proximate composition of the finished diets is given in Table 3. Both meals were used as single batches across all six diets.
[5] Crystalline L-lysine and DL-methionine were included at identical levels (0.5 and 0.2 g/kg) in all six diets. Calculated dietary lysine (≈3.5%) and methionine + cystine (≈1.9%, as-fed), derived from tabulated ingredient amino acid composition (NRC, 2011), exceeded the requirements reported for juvenile marine carangids.

ringens) fish meal (385 g/kg; 65% crude protein) and a locally produced Vietnamese marine fish meal of 55% crude protein (150 g/kg; Long Sinh Co., Ltd., Khanh Hoa Province, Vietnam), squid meal, and corn gluten meal; rice bran and wheat flour served as carbohydrate and binder sources; soybean oil was the sole supplemental lipid (40 g/kg); and Sargassum meal, crystalline L-lysine and DL-methionine, a pellet binder (polymethylurea), and vitamin and mineral premixes completed the formulation.

As is characteristic of commercially produced Vietnamese fish meal, the local meal was of mixed origin, being manufactured from low-value whole fish and bycatch landed by coastal capture fisheries together with trimmings (heads and frames) recovered from domestic tuna processing; reflecting this bone-rich processing fraction, it carries a higher mineral content than the imported meal. The two meals were combined deliberately: the imported meal served as the principal source of high-quality protein and palatability for a fast-growing marine carnivore, whereas the locally produced meal - which returns processing residues to the feed chain - kept the formulation representative of, and economically realistic for, feeds that can be manufactured in Vietnam and the wider region (Section 4.5). Both meals were used as single batches, and all six diets were prepared from one common dry-ingredient base, so ingredient origin and inclusion were identical across treatments; the analysed proximate composition of the finished diets is reported in Table 3.

Crystalline L-lysine (0.5 g/kg) and DL-methionine (0.2 g/kg) were retained from the standard basal formulation used in our laboratory for this species as a small precautionary margin, principally to offset the low lysine density of the plant fraction (100 g/kg corn gluten meal, in which lysine accounts for < 2% of crude protein, together with 130.7 g/kg wheat flour and rice bran) and to buffer batch-to-batch variation in the locally sourced fish meal. Their contribution was nevertheless marginal (0.05% and 0.02% of the diet), and the calculated dietary lysine (≈3.5%) and methionine + cystine (≈1.9%, as-fed) already exceeded reported requirements for juvenile marine carangids (NRC (National Research Council), 2011); because both were added at identical levels to all six diets, they cannot have contributed to any treatment difference.

No synthetic antioxidant was added at any stage of diet formulation or top-coating, and an ethoxyquin-free mineral premix was specified for the present trial, so that carotenoid stability, tissue deposition, and recovery could be evaluated without an added synthetic-antioxidant confounder. Any residual antioxidant carried over with commercial marine ingredients as part of suppliers' standard stabilisation practice was necessarily identical across all six diets, since all were manufactured from a single common dry-ingredient base and differed only in the level of top-coated marigold extract (Table 2). Oxidative protection during processing and storage instead relied on freshly prepared extract, gentle oven-drying, and light-protected refrigerated storage, consistent with the 87.0–91.4% carotenoid recovery (Table 3).

For full transparency relative to our earlier screening study (Tran et al., 2024b), in which five floral pigment sources were compared at a single fixed level, the basal diet used here was re-formulated and manufactured as a single new batch specifically for the present dose-response trial, and is documented independently and in full in Tables 1–3. Two nominal differences with respect to that report should be noted. First, the pellet binder is the same material - a urea–formaldehyde condensation binder included at 10 g/kg - and is designated here as polymethylurea, an alternative name used interchangeably with polymethylcarbamide for this same resin in commercial aquafeed manufacture. Second, the mineral premix specified for the present trial was formulated without ethoxyquin or any other synthetic antioxidant, in contrast to the commercial premix used in that earlier study, so that the carotenoid stability, tissue deposition, and net recovery reported here (Table 3) could be assessed without a synthetic-antioxidant confound (Table 1, footnote 3). For clarity, all constituents in Table 1, footnotes 2 and 3, are expressed per kilogram of premix, together with the corresponding dietary inclusion rate (15 g premix/kg diet and 5.3 g premix/kg diet, respectively).

Table 2
Isovolumetric carotenoid top-coat applied to each diet.

Target supplemental (mg/kg)	Marigold extract (mL/kg)[a]	Soybean oil (mL/kg)	Total oil-phase (mL/kg)
0 (Control)	0	20.0	20
200	3.1	16.9	20
400	6.3	13.7	20
600	9.4	10.6	20
800	12.5	7.5	20
1000	15.6	4.4	20

[a] Extract standardized to 64 mg total carotenoids/mL; volume = target ÷ 64. Soybean oil balanced each top-coat to a constant 20 mL/kg, so added lipid was identical and only carotenoid level varied.

Six diets were prepared from a single, identical dry-ingredient base and differed only in supplemental marigold carotenoids (0, 200, 400, 600, 800, 1000 mg/kg), applied by post-pelleting top-coating. A marigold extract standardized to 64 mg total carotenoids/mL served as the pigment stock; the required volume was calculated as (target, mg/kg) ÷ (64 mg/mL), and soybean oil was co-added to bring every top-coat to a constant 20 mL/kg (isovolumetric design; Table 2). Because the extract is oil-based, total added lipid was identical across treatments and only carotenoid level varied.

All dry ingredients except the carotenoid extract and the vitamin premix were weighed, finely ground, and homogenized in a commercial mixer (Lifeng B20, Guangdong, China) for 15–20 min. The mash was steam-conditioned at 90–95 °C for 20 min to gelatinize starch and reduce microbial load, then pelleted (not extruded) through a 3.0-mm die (S150, Binh Quan T&M Co., Ltd., Vietnam). Pellets were oven-dried (60 °C, ~8 h) to ~10% moisture, cooled, crumbled, and sieved to 0.8–1.0 mm to match the mouth gape of golden trevally juveniles.

The carotenoid–oil solution and the vitamin premix were then surface-applied by a two-step manual top-coating: the oil dose was first pipetted onto 10–20% of the pellets and hand-mixed for 3–5 min, then blended into the remaining pellets and mixed for a further 5–10 min to ensure homogeneity. Coated diets were briefly re-dried (60 °C) to ~10% moisture, portioned into daily-ration bags, air-expelled, wrapped in opaque/foil bags to exclude light, and stored frozen (−20 °C) until use. Proximate composition and total carotenoids were analyzed in triplicate on the final coated diets (Table 3).

2.4. Animals, rearing, and experimental design

Hatchery-produced *Gnathanodon speciosus* juveniles were obtained from the Marine Fish Hatchery of Duong De (Nha Trang), located immediately adjacent to the experimental facility and sharing the same natural-seawater source and water-treatment procedure; transport therefore lasted only a few minutes. Fish selected for uniform size and health were held in a single common tank connected to the experimental recirculating aquaculture system (RAS) and acclimated for 5 days under conditions identical to those of the subsequent trial (temperature 29.0 ± 1.0 °C; salinity 33 ± 1‰; pH 8.0 ± 0.2; dissolved oxygen 5.3 ± 0.2 mg/L). Because the fish originated from this neighbouring hatchery and were already adapted to the local seawater and climate, this period was sufficient for full acclimation. Throughout acclimation all fish were fed the carotenoid-free control diet (0 mg/kg) to apparent satiation, thereby standardising the initial pigment status of the whole stock before the treatments began. At the end of acclimation (day 0), immediately before stocking, all fish were measured individually for total length and body weight (initial total length, $L_1 = 2.92 \pm 0.06$ cm; initial body weight, $W_1 = 0.51 \pm 0.04$ g); these values constitute the baseline for the 56-day trial.

Rearing was carried out in a RAS comprising 18 rectangular glass tanks (55 × 35 × 38 cm; 65 L effective volume) connected to a central ~500-L sump. The sump housed a sequential filtration train - filter wool for mechanical removal of solids, followed by biological media (bio-

Table 3
Experimental diet design and analyzed composition.

Parameter	Dietary supplemental carotenoid level (mg/kg)					
	0 (Control)	200	400	600	800	1000
Crude protein (%)	50.38 ± 0.21	50.42 ± 0.18	50.29 ± 0.24	50.51 ± 0.20	50.35 ± 0.23	50.44 ± 0.19
Crude lipid (%)	9.15 ± 0.11	9.18 ± 0.09	9.12 ± 0.12	9.22 ± 0.12	9.16 ± 0.11	9.20 ± 0.08
Ash (%)	9.52 ± 0.09	9.48 ± 0.08	9.55 ± 0.11	9.50 ± 0.07	9.53 ± 0.09	9.47 ± 0.08
Moisture (%)	10.08 ± 0.10	10.12 ± 0.12	9.96 ± 0.09	10.05 ± 0.13	10.14 ± 0.09	10.02 ± 0.11
Analyzed carotenoids (mg/kg)	13.8 ± 1.2	196.5 ± 6.8	374.8 ± 10.5	547.6 ± 13.2	718.4 ± 17.6	883.9 ± 21.4

Values are means ± SD (n = 3). All diets shared an identical dry-ingredient base (Table 1) and differed only in top-coated marigold carotenoids (Table 2). Proximate composition did not differ among diets ($P > 0.05$), confirming the diets were isonitrogenous and isolipidic. The 13.8 mg/kg measured in the control represents endogenous carotenoids from corn gluten meal (lutein/zeaxanthin) and the marine meals (fish and squid meal), and is low relative to the supplemented diets. Net recovery of supplemental carotenoids - calculated as (analyzed total - 13.8 mg/kg endogenous baseline) ÷ nominal supplemental level - ranged from 87.0% to 91.4%.

balls, Ø 40 mm, and coral rubble) colonised by nitrifying bacteria. Treated water was returned to each tank by a submersible pump (Life-tech AP5300, 80 W), with inflow regulated at 1.4–1.6 L/min per tank (≈ 31–35 tank volumes/day). Each tank received continuous aeration through one air stone supplied by a central blower (Hailea ACO-009, 120 W; 120 L/min). The system was placed under a translucent roof on a natural 12 L:12D photoperiod, supplemented during low-light periods by an LED array (eight 40-W tubes and one 60-W bulb, ~150 cm above the water surface) that provided a uniform surface irradiance of 1000–1500 lux across all tanks.

The trial followed a completely randomised design (6 dietary treatments × 3 replicates; 18 experimental units) over 56 days. Fish were randomly allocated to the 18 tanks at 30 fish per tank (0.5 fish/L), and the stocked group weight per tank was recorded to provide tank-specific initial biomass for growth and feed-efficiency calculations; initial mean weight did not differ among treatments ($P > 0.05$). Fish were fed to apparent satiation four times daily (07:30, 10:00, 13:30, 16:30) and feed intake was recorded. Tank bottoms were siphoned twice daily and 30–50% of the system water was renewed weekly. Water quality was monitored every other day between 08:00 and 09:00 h. Temperature, pH, salinity, and dissolved oxygen were measured in situ with a LAQUA WQ-300-series smart handheld water quality meter (model WQ-310-K; HORIBA Advanced Techno Co., Ltd., Kyoto, Japan), fitted with the corresponding smart sensor heads: a combination pH/temperature head, a conductivity head reporting salinity on the seawater scale, and an optical (fluorescence-based) dissolved-oxygen head with automatic salinity compensation derived from the conductivity reading. The meter was calibrated before each sampling occasion using the manufacturer's pH buffers (pH 4.01, 6.86, and 9.18) and conductivity standard, and following the manufacturer's dissolved-oxygen calibration procedure. Total ammonia nitrogen (TAN), nitrite (NO_2^--N), and nitrate (NO_3^--N) were determined colorimetrically on filtered water samples with a double-beam UV-Vis spectrophotometer (Libra S60, Biochrom Ltd., Cambridge, UK) following APHA (American Public Health Association), (2012): the indophenol-blue (phenate) method for TAN (4500-NH_3 F), diazotization for nitrite (4500-NO_2^- B), and cadmium reduction for nitrate (4500-NO_3^- E). Un-ionised ammonia (NH_3) was not measured directly but calculated from TAN together with the concurrently measured pH, temperature, and salinity, using the seawater ammonia-ionization relationships of Bower and Bidwell (1978), which incorporate the salinity-dependent shift in the ammonium pK_a and are therefore appropriate to the full-strength seawater used here. All parameters were maintained within optimal ranges throughout (temperature 29.0 ± 1.0 °C; salinity 33 ± 1‰; pH 8.0 ± 0.2; dissolved oxygen 5.3 ± 0.2 mg O_2/L; total ammonia nitrogen 0.45 ± 0.20 mg N/L; un-ionised ammonia, NH_3, 0.02 ± 0.01 mg N/L; nitrite, NO_2^--N, 0.15 ± 0.08 mg N/L; nitrate, NO_3^--N, 12.5 ± 4.6 mg N/L), with no differences among tanks.

2.5. Sampling and analyses

On day 56, fish were fasted 24 h and anaesthetized (2-phenoxyethanol, 500 ppm).

Growth and feed utilization. All fish were measured for TL and BW. Indices: $SGR_L = 100 \times (\ln L_2 - \ln L_1)/t$; $SGR_W = 100 \times (\ln W_2 - \ln W_1)/t$; condition factor $CF = 100 \times W/L^3$; survival $SR = 100 \times N_2/N_1$; $FCR = FI/(W_2 + D - W_1)$; $PER = (W_2 - W_1)/(FI \times P)$, where t = 56 d and P is dietary protein (decimal). Coefficients of variation (CV_L, CV_W) were also computed.

Skin color. Colour was measured on live, freshly anaesthetized fish (i.e., no post-mortem interval); for each fish, measurements were taken within ~5–10 s of anaesthesia, immediately after TL and BW were recorded. Prior to measurement, each fish was individually dip-netted and blotted on absorbent paper to remove surface water, with no other skin preparation. Colour was recorded with a CR-400 Chroma Meter (Konica Minolta; D65 illuminant, CR-A33F glass light-projection tube; manufacturer's default settings) in CIE L*a*b* space, on the left flank at two regions (Region 1, between the pectoral- and pelvic-fin bases; Region 2, above and anterior to the anal fin), each in triplicate with the mean used as the representative value. Derived indices: chroma $C^*_{ab} = (a^{*2} + b^{*2})^{½}$; hue $h^*_{ab} = \arctan(b^*/a^*)$; and total colour difference ΔE^*_{ab} relative to the control (Tomasevic et al., 2019).

Tissue carotenoids. Three fish per tank were sampled (n = 3 tanks/treatment) for skin, muscle, and whole-body carotenoids, extracted in acetone with anhydrous Na_2SO_4 (Tran et al., 2024b), centrifuged (10,000 rpm, 4 °C, 15 min), and quantified at 450 nm using the same double-beam UV-Vis spectrophotometer (Libra S60, Biochrom Ltd., Cambridge, UK) described in Section 2.2.

Whole-body composition. Five fish per tank were randomly sampled and pooled (n = 3 tanks/treatment), stored at −80 °C, and homogenized (T10 Ultra-turrax®, IKA, Germany). Pooled samples were analysed for crude protein (Kjeldahl, N × 6.25), crude lipid (Soxhlet), ash (550 °C), and moisture (105 °C) per AOAC International (2005), in triplicate (% wet weight).

Digestive enzymes. Five fish per tank were randomly sampled, and their entire digestive tract (stomach and intestine, excluding the liver and other accessory organs) was excised. Because of the small size of the fish (7.0–9.0 cm; 7.5–10.0 g), the tracts from the five fish were pooled into a single composite sample per tank (n = 3/treatment). Samples were homogenized in cold phosphate buffer (1:10) and centrifuged (15,000 × g, 4 °C, 30 min). Protease (Anson method, casein; Kunitz, 1947), lipase (pH-stat, olive oil; Tambekar et al., 2013), and amylase (DNS, starch; Bernfeld, 1955) were assayed; soluble protein by Bradford (1976). Activities are expressed as U/mg protein.

2.6. Statistical analysis

Normality and homogeneity were verified (Shapiro-Wilk; Levene); survival was arcsine-transformed. One-way ANOVA with Duncan's test ($P < 0.05$) was applied in SPSS 26.0. The four dietary carotenoid

dose–response relationships reported in Table 7 - SGR_W, skin carotenoid concentration, skin yellowness (b*), and intestinal lipase activity - were analysed using the individual replicate-tank observations (n = 18) by fitting and comparing eight candidate models: linear, quadratic, cubic, linear broken-line, quadratic broken-line, asymptotic, Michaelis–Menten, and four-parameter logistic. The polynomial models were fitted by ordinary least squares and the segmented and non-linear models by non-linear least squares (Python 3.10.12; NumPy 2.2.6 and SciPy 1.15.3); the second-order polynomial fit reproduced the original SPSS 26.0 Curve-Estimation result. Competing models were ranked by the second-order Akaike information criterion (AICc), with ΔAICc, Akaike weights (w_i) and adjusted R^2 as supporting indicators and residual normality confirmed (Shapiro–Wilk); the best-supported model was selected, and where models were similarly supported (ΔAICc < 2) the more parsimonious, biologically interpretable model was retained (Supplementary Appendix). For models with a quadratic term, the optimum dietary level was estimated as $x_{opt} = -b/(2a)$. Results are means ± SE (n = 3).

3. Results

3.1. Growth performance, survival, and feed utilization

Carotenoid supplementation significantly affected growth in both length and weight ($P < 0.05$; Table 4). Relative to the control, final total length and body weight were significantly higher from 400 mg/kg onward ($P < 0.05$), whereas the 200 mg/kg group was intermediate and did not differ significantly from the control in final size; the highest values occurred at 600 mg/kg, with no significant differences among the 400–800 mg/kg groups. Specific growth rate showed the same overall response: SGR_W rose from 4.81%/day in the control to a maximum of 5.26%/day at 600 mg/kg, and although it declined numerically to 5.07%/day at 1000 mg/kg, this value did not differ significantly from the 600 mg/kg peak; the overall dose–response was best described by a quadratic function (Section 3.4). Condition factor, the coefficients of variation for length and weight, and survival (94.45–97.78%) did not differ significantly among treatments ($P > 0.05$).

Feed intake did not differ significantly among treatments (6.83–7.29 g/fish; $P > 0.05$), indicating that the improved growth was not driven by greater feed consumption. Relative feeding rate (% BW/day) was significantly lower at 400–800 mg/kg than in the control, FCR was significantly reduced (lowest at 600 mg/kg, 0.79, vs. 0.97 in the control), and PER was significantly increased (up to 2.53 at 600 mg/kg vs. 2.07 in the control); together these indicate more efficient feed conversion rather than higher intake. The lower relative feeding rate is consistent with the greater body mass attained on the supplemented diets at a comparable absolute intake (Table 4).

3.2. Skin coloration and tissue carotenoid accumulation

Supplementation significantly affected most colour indices ($P < 0.05$; Table 5; Fig. 1). Skin yellowness (b*) increased markedly with dose, reaching maxima of 43.50 and 41.75 at 800 and 600 mg/kg, respectively (3.4- and 3.3-fold above the control), which did not differ significantly from each other; b* at 1000 mg/kg (36.64) was significantly lower than at 800 mg/kg but did not differ significantly from that at 600 mg/kg. The a* values were negative in all groups and most negative at 600–800 mg/kg, and chroma (C^*_{ab}) closely paralleled b*. Hue angle (h^*_{ab}) did not differ significantly among treatments ($P > 0.05$), indicating that the fundamental yellow tone was preserved, whereas the total colour difference from the control (ΔE^*_{ab}) was greatest at 800 and 600 mg/kg (not significantly different from each other), far exceeding the perceptibility threshold.

Total carotenoids accumulated dose-dependently in all tissues ($P < 0.05$; Table 5), predominantly in the skin (11.7→109.3 μg/g; a 9.3-fold increase), far exceeding muscle and whole body. In every tissue, concentrations at 600, 800, and 1000 mg/kg did not differ significantly (sharing the same statistical grouping), indicating that deposition had saturated by ~600 mg/kg.

3.3. Whole-body composition and digestive enzyme activities

Whole-body moisture and ash did not differ significantly among treatments ($P > 0.05$; Table 6). Crude protein was significantly higher than the control from 400 mg/kg onward (17.1–17.9% vs. 15.5%; $P < 0.05$), the 200 mg/kg group being intermediate and not significantly different from the control. Crude lipid was significantly lower than the control from 600 mg/kg onward (4.60–4.62% vs. 5.21%; $P < 0.05$), with no significant differences among the 600–1000 mg/kg groups.

Intestinal protease and lipase activities were significantly enhanced by supplementation ($P < 0.05$), whereas amylase showed a numerical upward trend that was not statistically significant ($P = 0.06$; Table 6). Protease increased ~1.9-fold (from 2.87 to a maximum of 5.53 U/mg) and lipase ~2.3-fold (from 2.95 to a maximum of 6.72 U/mg); for both enzymes, activities at 600, 800, and 1000 mg/kg did not differ significantly from one another, indicating a plateau at the higher doses. Amylase increased only numerically (9.65→13.0 U/mg; $P = 0.06$).

3.4. Dose–response regression analysis

Among the eight candidate models, the quadratic model had the

Table 4
Growth performance, survival, and feed utilization of juvenile golden trevally (*Gnathanodon speciosus*) fed diets supplemented with graded levels of marigold carotenoids for 56 days.

Parameter	Dietary supplemental carotenoid level (mg/kg)					
	0 (Control)	200	400	600	800	1000
L_2 (cm)	7.75 ± 0.10^{a}	7.96 ± 0.10^{ab}	8.22 ± 0.05^{c}	8.36 ± 0.06^{c}	8.25 ± 0.03^{c}	8.15 ± 0.04^{bc}
W_2 (g)	7.57 ± 0.04^{a}	8.24 ± 0.27^{ab}	9.06 ± 0.25^{bcd}	9.73 ± 0.20^{d}	9.37 ± 0.25^{cd}	8.74 ± 0.11^{bc}
SGR_L (%/day)	1.74 ± 0.02^{a}	1.79 ± 0.02^{b}	1.85 ± 0.01^{c}	1.88 ± 0.01^{c}	1.86 ± 0.01^{c}	1.84 ± 0.01^{bc}
SGR_W (%/day)	4.81 ± 0.10^{a}	4.97 ± 0.06^{ab}	5.13 ± 0.05^{bc}	5.26 ± 0.04^{c}	5.19 ± 0.05^{c}	5.07 ± 0.02^{bc}
CF (g/cm^3)	1.62 ± 0.03	1.63 ± 0.02	1.63 ± 0.02	1.66 ± 0.02	1.67 ± 0.02	1.62 ± 0.01
SR (%)	95.55 ± 2.22	94.45 ± 2.22	95.56 ± 2.94	96.67 ± 1.93	97.78 ± 1.11	96.67 ± 1.93
FI (g/fish)	6.83 ± 0.35	7.07 ± 0.36	7.02 ± 0.37	7.29 ± 0.30	7.14 ± 0.44	7.20 ± 0.26
FCR	0.97 ± 0.03^{d}	0.91 ± 0.02^{cd}	0.82 ± 0.02^{ab}	0.79 ± 0.02^{a}	0.81 ± 0.03^{ab}	0.88 ± 0.02^{bc}
FR (%BW/day)	3.02 ± 0.09^{b}	2.88 ± 0.06^{b}	2.62 ± 0.07^{a}	2.54 ± 0.06^{a}	2.57 ± 0.10^{a}	2.78 ± 0.07^{ab}
PER	2.07 ± 0.07^{a}	2.19 ± 0.04^{ab}	2.44 ± 0.06^{cd}	2.53 ± 0.05^{d}	2.50 ± 0.10^{cd}	2.29 ± 0.05^{bc}

Initial $L_1 = 2.92 \pm 0.06$ cm and $W_1 = 0.51 \pm 0.04$ g were measured individually at the end of the 5-day acclimation, immediately before stocking (30 fish per tank). Coefficients of variation for length (9.01–10.04%) and weight (16.78–19.74%) did not differ among treatments ($P > 0.05$). L_2, W_2: final length and weight; SGR_L, SGR_W: specific growth rate in length and weight; CF: condition factor; SR: survival; FI: feed intake; FR: feeding rate; FCR: feed conversion ratio; PER: protein efficiency ratio. Means ± SE (n = 3); different superscripts within a row differ ($P < 0.05$).

Table 5
Skin color parameters (CIE L*a*b*) and total carotenoid concentration (μg/g wet weight) in tissues of juvenile golden trevally fed graded marigold carotenoid levels for 56 days.

Parameter	Dietary supplemental carotenoid level (mg/kg)					
	0 (Control)	**200**	**400**	**600**	**800**	**1000**
L*	60.05 ± 0.65^{a}	61.06 ± 0.96^{a}	62.86 ± 0.69^{ab}	64.30 ± 0.85^{b}	65.84 ± 1.15^{b}	60.42 ± 1.21^{a}
a*	-3.01 ± 0.32^{c}	-5.46 ± 0.38^{b}	-6.39 ± 0.74^{b}	-8.59 ± 0.69^{a}	-8.43 ± 0.43^{a}	-6.46 ± 0.71^{b}
b*	12.66 ± 1.13^{a}	23.76 ± 2.67^{b}	32.02 ± 1.83^{c}	41.75 ± 2.63^{de}	43.50 ± 2.04^{e}	36.64 ± 1.78 ^{cd}
C^*_{ab}	13.04 ± 1.04^{a}	24.38 ± 2.69^{b}	32.69 ± 1.63^{c}	42.66 ± 2.44^{de}	44.31 ± 2.08^{e}	37.21 ± 1.87 ^{cd}
h^*_{ab}	103.69 ± 2.48	103.08 ± 0.68	101.48 ± 1.98	101.81 ± 1.62	100.96 ± 0.04	99.93 ± 0.62
ΔE^*_{ab}	-	11.48 ± 2.71^{a}	19.95 ± 1.52^{b}	29.98 ± 2.55 ^{cd}	31.86 ± 2.25^{d}	24.30 ± 1.82^{bc}
Skin carotenoid	11.7 ± 0.75^{a}	53.3 ± 2.60^{b}	77.6 ± 5.19^{c}	100.4 ± 5.05^{d}	109.3 ± 3.21^{d}	107.7 ± 3.03^{d}
Muscle carotenoid	0.17 ± 0.04^{a}	0.85 ± 0.10^{b}	1.36 ± 0.12^{c}	2.85 ± 0.11^{d}	3.06 ± 0.24^{d}	3.09 ± 0.14^{d}
Whole-body carotenoid	2.16 ± 0.31^{a}	3.49 ± 0.36^{a}	10.69 ± 1.31^{b}	25.74 ± 2.01^{c}	27.83 ± 2.16^{c}	26.12 ± 1.96^{c}

L*: lightness; a*: redness–greenness; b*: yellowness–blueness; C^*_{ab}: chroma; h^*_{ab}: hue angle; ΔE^*_{ab}: total color difference vs. control. Means ± SE (n = 3); different superscripts within a row differ ($P < 0.05$).

Fig. 1. Representative photographs of skin coloration of juvenile golden trevally (*Gnathanodon speciosus*) fed diets supplemented with marigold (*Tagetes erecta*) carotenoids at (A) 0 (control), (B) 200, (C) 400, (D) 600, (E) 800, and (F) 1000 mg/kg diet for 56 days.

Table 6
Whole-body proximate composition (% wet weight) and gastrointestinal digestive enzyme specific activities (U/mg protein) of juvenile golden trevally fed graded marigold carotenoid levels for 56 days.

Parameter	Dietary supplemental carotenoid level (mg/kg)					
	0 (Control)	**200**	**400**	**600**	**800**	**1000**
Moisture (%)	71.4 ± 0.55	70.1 ± 0.77	70.9 ± 0.61	69.7 ± 0.42	70.0 ± 0.68	69.8 ± 0.49
Protein (%)	15.5 ± 0.37^{a}	16.3 ± 0.48^{ab}	17.1 ± 0.45^{bc}	17.8 ± 0.18^{c}	17.9 ± 0.22^{c}	17.8 ± 0.22^{c}
Lipid (%)	5.21 ± 0.06^{b}	5.14 ± 0.07^{b}	4.82 ± 0.08^{ab}	4.62 ± 0.18^{a}	4.60 ± 0.19^{a}	4.62 ± 0.15^{a}
Ash (%)	3.11 ± 0.13	2.85 ± 0.31	2.88 ± 0.16	3.04 ± 0.30	2.92 ± 0.36	2.97 ± 0.13
Amylase	9.65 ± 1.04	10.6 ± 0.37	11.6 ± 0.93	12.7 ± 0.36	13.0 ± 0.64	12.0 ± 0.83
Protease	2.87 ± 0.35^{a}	3.93 ± 0.27^{b}	4.82 ± 0.18^{bc}	5.35 ± 0.28^{c}	5.53 ± 0.43^{c}	5.08 ± 0.21^{c}
Lipase	2.95 ± 0.27^{a}	4.55 ± 0.58^{b}	5.87 ± 0.41^{c}	6.70 ± 0.24^{c}	6.72 ± 0.27^{c}	6.51 ± 0.54^{c}

Means ± SE (n = 3); different superscripts within a row differ ($P < 0.05$).

lowest AICc for SGR_W, skin carotenoid concentration, and intestinal lipase activity. For skin yellowness (b*), the cubic model had the lowest AICc; however, the quadratic model remained similarly supported (ΔAICc = 1.23; evidence ratio ≈ 1.8) and was retained as the more parsimonious and biologically interpretable representation. The retained quadratic models explained 74.1–97.7% of the variation in the four responses ($P < 0.001$; Table 7; Supplementary Appendix; Fig. 2). Broken-line models were also competitive for skin carotenoid concentration (ΔAICc = 0.25) and lipase activity (ΔAICc = 0.09), supporting interpretation of these responses as saturation rather than a genuine post-peak decline. Skin carotenoid concentration and b* were strongly linearly associated ($R^2 = 0.923$, $P < 0.001$; Fig. 3). The estimated optima were 646 mg/kg for SGR_W and 761 mg/kg for b*, whereas the fitted vertices for skin carotenoid and lipase (887 and 782 mg/kg) represent saturation ceilings rather than dietary requirements (Table 7; Section 4.4).

Table 7
Retained regression models for the dietary carotenoid dose–response relationships and the association between skin carotenoid concentration and skin yellowness (b*) (n = 18). The four dose–response models were retained following AICc-based comparison of eight candidate models (Supplementary Appendix).

Response	Model	Equation	R^2	p	Optimum (mg/kg)
SGR_W	Quadratic	$y = 4.783 + 1.344 \times 10^{-3}x - 1.040 \times 10^{-6}x^2$	0.741	< 0.001	646
Skin carotenoid	Quadratic	$y = 12.257 + 2.196 \times 10^{-1}x - 1.238 \times 10^{-4}x^2$	0.977	< 0.001	887[a]
b*	Quadratic	$y = 11.338 + 7.868 \times 10^{-2}x - 5.171 \times 10^{-5}x^2$	0.901	< 0.001	761
Lipase	Quadratic	$y = 2.903 + 9.962 \times 10^{-3}x - 6.368 \times 10^{-6}x^2$	0.849	< 0.001	782[a]
b* vs. skin carotenoid	Linear	$y = 8.568 + 3.020 \times 10^{-1}x$	0.923	< 0.001	—

For quadratic dose–response models, x = dietary carotenoid level (mg/kg); for the b* vs. skin carotenoid model, x = skin carotenoid (μg/g). Optimum = −b/(2a). [a] For skin carotenoid and lipase, the tabulated value is the fitted quadratic vertex (≈ saturation ceiling), not the recommended dietary dose (see Section 4.4 for practical optimum).

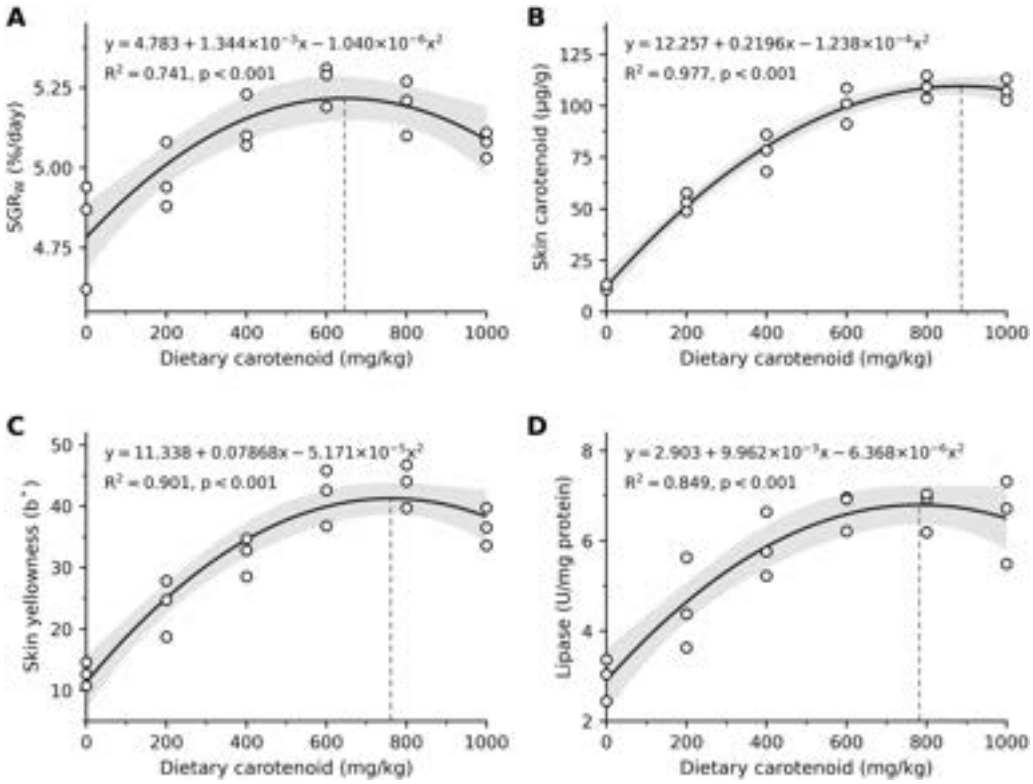

Fig. 2. Regression relationships between dietary carotenoid level and key response variables after 56 days (shaded band = 95% CI): quadratic fits for (A) specific growth rate (SGR_W, %/day), (B) skin carotenoid concentration (μg/g), (C) skin yellowness (b*), and (D) lipase specific activity (U/mg protein). Open circles represent individual replicate tank means (n = 18); curves/lines denote fitted regressions. Equations, R^2, and significance levels are displayed in each panel.

4. Discussion

4.1. Growth performance and feed utilization

Marigold carotenoids at 400–800 mg/kg significantly improved growth and feed utilization, optimally at 600 mg/kg, with a quadratic SGR_W response (optimum 646 mg/kg). This non-linear pattern is consistent with reports for many ornamental and food fish (Liao et al., 2025). Positive growth effects of carotenoids have been documented with astaxanthin in golden pompano, red-spotted grouper, and red porgy (Fang et al., 2021; Kalinowski et al., 2011; Song et al., 2021) and with marigold in koi carp, orange chromide, and Indian major carp (Chhaba et al., 2024; Jagadeesh et al., 2014; Swian et al., 2014), although null effects also occur (e.g., gilthead sea bream, electric yellow cichlid), reflecting dependence on species, source, dose, and life stage (Yeşilayer et al., 2020).

Several mechanisms may underlie the growth benefit. First, the antioxidant activity of carotenoids reduces energy diverted to oxidative repair (Elbahnaswy and Elshopakey, 2024). Second - and supported here - carotenoid supplementation was associated with higher protease and lipase activities (Section 4.3), which coincided with improved FCR and PER. Third, carotenoids contribute to immune modulation and overall health (Lim et al., 2023). The slight, mostly non-significant decline at 1000 mg/kg suggests a mild pro-oxidant effect at excessive doses, as reported in discus, golden pompano, large yellow croaker, and spotted sea bass (Black et al., 2020; Fang et al., 2021; Song et al., 2017; Xu et al., 2022; Yu et al., 2021). High, uniform survival (94.45–97.78%) confirms the safety of marigold carotenoids within the tested range.

4.2. Skin coloration and carotenoid accumulation

A central finding is the effective enhancement of yellow coloration: b* rose 3.3–3.4-fold at 600–800 mg/kg, with ΔE^*_{ab} far above the perceptibility threshold, indicating a commercially meaningful colour change.

Mechanistically, this pronounced yellowing is the direct optical expression of xanthophyll deposition in the skin. Marigold pigment is dominated by the yellow xanthophylls lutein and zeaxanthin (≈80–90%

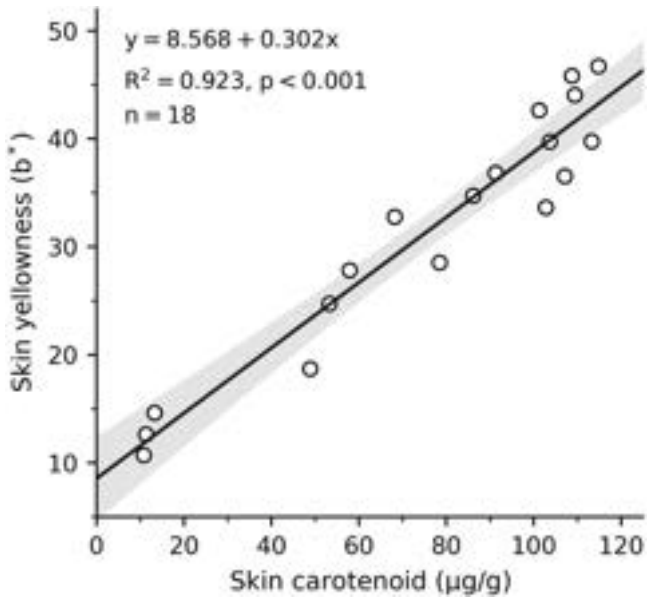

Fig. 3. Linear relationship between skin carotenoid concentration (μg/g) and skin yellowness (b*) across all dietary treatments after 56 days (shaded band = 95% confidence interval). Open circles represent individual replicate tank means (n = 18); the line denotes the fitted regression. The equation, R^2, and significance level are displayed in the panel.

of total carotenoid), whose extended conjugated double-bond systems absorb maximally in the blue region (~445–450 nm) and consequently reflect strongly in the yellow waveband - the physical basis of a high CIE b* (Eghlima and Seyed Hajizadeh, 2026). After intestinal uptake via lipid-transporter–mediated pathways (SR-B1/CD36), incorporation into circulating lipoproteins, and delivery to the integument, these xanthophylls are selectively retained and stabilised by carotenoid-binding proteins within dermal xanthophores (Guo et al., 2024; Liao et al., 2025). Progressive loading of the xanthophore layer raises yellow reflectance in near-direct proportion to the amount deposited, which explains the tight linear coupling between skin carotenoid concentration and b* observed here (R^2 = 0.923; Fig. 3). Because golden trevally naturally possesses a dense, high-affinity xanthophore population - the basis of its golden phenotype - the skin acts as an efficient sink for dietary lutein/zeaxanthin, accounting for both the steep rise in b* and the strong skin-over-muscle partitioning (35–69-fold; Table 5). Notably, hue angle (h^*_{ab}) was unchanged across all doses, indicating that the deposited pigment remained chemically yellow and was not oxidatively converted to red ketocarotenoids - unlike astaxanthin or canthaxanthin in species equipped with the requisite ketolase (CYP2J-/BCO2-type) machinery (Liao et al., 2025); supplementation therefore intensified, rather than re-hued, the natural golden coloration.

Consistent with a finite deposition capacity, carotenoid accumulation and b* plateaued from ~600 mg/kg. This ceiling reflects saturable steps along the deposition pathway - transporter-mediated intestinal uptake, lipoprotein carrying capacity, and the limited number of carotenoid-binding sites within the xanthophore layer - beyond which additional dietary pigment cannot be further deposited (Liao et al., 2025). Similar preferential, saturable skin deposition has been reported in goldfish, koi carp, large yellow croaker, and rainbowfish (Besen et al., 2019; Yi et al., 2016; Yuangsoi et al., 2011). Supplementation beyond 600–800 mg/kg therefore yields no further colour gain and is unlikely to be cost-effective.

The significantly lower b* at 1000 mg/kg than at 800 mg/kg, despite comparable skin carotenoid concentrations and coinciding with reduced lightness (L*), is consistent with concentration-dependent optical and chemical effects at high dermal pigment loads - self-association/aggregation of xanthophylls that broadens and dampens reflectance, and/or partial pigment degradation under the mild pro-oxidant conditions that can arise at excessive carotenoid doses (Black et al., 2020; Liao et al., 2025). The stable hue angle confirms that these effects modulated colour intensity without altering the underlying yellow tone.

4.3. Digestive enzymes and whole-body composition

Marigold carotenoids markedly stimulated protease (1.9-fold) and lipase (2.3-fold), complementing recent reports in large yellow croaker, yellow river carp, and Nile tilapia (Hassaan et al., 2021; Ren et al., 2025; Xu et al., 2022). Proposed mechanisms include carotenoid interaction with intestinal epithelial membranes improving fluidity and enzyme secretion (Guo et al., 2024), antioxidant protection of luminal enzymes (Mansour et al., 2020), and modulation of gut microbiota (Zhao et al., 2022). Amylase was unaffected, consistent with the carnivorous digestive physiology of carangids, which prioritizes protein and lipid over carbohydrate hydrolysis.

The concurrent rise in protease and lipase explains the improved FCR/PER and the shift toward higher body protein and lower lipid: the higher proteolytic activity may contribute to protein accretion, while greater lipolysis promotes fatty-acid oxidation. Digestive lipase activity tended to be inversely related to whole-body lipid content across treatments. As neither variable represents a graded dose–response function of dietary carotenoid, this association is noted only as a descriptive, correlated physiological observation and was not fitted as a requirement model (Table 7); we interpret it as a co-varying physiological outcome rather than a carotenoid-dependent optimum. This carotenoid-mediated metabolic regulation parallels reports in red porgy, rainbow trout, and snow trout (Jha et al., 2012; Kalinowski et al., 2011; Zhao et al., 2022); mechanistically, carotenoids and apocarotenoids may activate PPAR/RXR nuclear receptors to stimulate β-oxidation and suppress lipogenesis (Ikeuchi et al., 2007), while enhanced protein digestion supplies amino-acid substrates for synthesis.

4.4. Optimum dose and practical implications

Because skin carotenoid and lipase responses plateaued from 600 mg/kg (Tables 5 and 6), their quadratic vertices (887 and 782 mg/kg) should be interpreted as upper-bound saturation estimates rather than dietary requirements; the biologically and economically relevant optimum is the plateau onset at 600–800 mg/kg. The higher optimum for pigmentation than growth - widely reported (Liao et al., 2025) - reflects priority allocation: at low-to-moderate doses carotenoids serve antioxidant and metabolic functions (growth), and only surplus is deposited for pigmentation (Lim et al., 2023). For commercial ornamental production requiring both growth and color, 600–800 mg/kg is recommended, achieving near-maximal growth, strong coloration, optimal FCR, and saturated enzyme activity, whereas higher doses may add cost without proportional benefit.

4.5. Novelty, limitations, and future directions

This is the first comprehensive dose–response study of marigold carotenoids in golden trevally, extending beyond growth and pigmentation to digestive physiology. The robust b*–skin carotenoid relationship (R^2 = 0.923) offers a non-invasive colorimetric proxy for tissue pigment content. Regionally, marigold is a low-cost, locally available alternative to synthetic or microalgal carotenoids, providing a direct basis for Southeast Asian aquafeed formulation.

Limitations include the 56-day juvenile-stage duration, which may not capture long-term color retention; the absence of individual carotenoid profiling (lutein, zeaxanthin, esters), immune/oxidative biomarkers, and gene expression; and the laboratory setting. Future work should assess color fade-out dynamics after withdrawal, HPLC tissue profiling, immune and stress responses, expression of carotenoid transport/metabolism genes (*scarb1*, *cd36*, *bco1*, *bco2*), grow-out efficacy,

and comparison with astaxanthin or microalgal sources.

5. Conclusion

Dietary marigold (*Tagetes erecta*) carotenoids at 600–800 mg/kg significantly improved growth, feed utilization, and skin yellowness in juvenile golden trevally without affecting survival. Carotenoid accumulation was tissue-specific, with skin as the preferential deposition site, and stimulation of intestinal protease and lipase provided an indirect route to improved feed utilization alongside higher body protein and lower lipid. With distinct optima for growth and pigmentation, 600–800 mg/kg is recommended for combined objectives, providing a practical basis for natural-pigment aquafeed in tropical marine aquaculture where marigold is an abundant, low-cost source.

CRediT authorship contribution statement

Dung Van Tran: Writing – original draft, Visualization, Supervision, Methodology, Formal analysis, Conceptualization. **Trang Le Thi Tran:** Writing – review & editing, Resources, Project administration, Funding acquisition. **Dang Duyen Thi Thach:** Investigation, Data curation. **Dai Quang Tran:** Visualization, Investigation. **Manh Van Ngo:** Resources, Investigation. **Dai Trong Vu:** Validation, Investigation. **Hung Quoc Pham:** Writing – review & editing, Supervision, Conceptualization. **Thanh Trung Dang:** Writing – original draft, Supervision, Methodology, Investigation, Formal analysis.

Funding

This research was funded by Nha Trang University, Vietnam (Grant TR2024–13–32 to Trang Le Thi Tran).

Declaration of Competing Interest

The authors declare no competing interests.

Acknowledgements

The authors thank Mrs. Nguyen Thi Nhat Anh and Mr. Duong Nguyen Hoang from the Marine Ornamental Fish Hatchery of Vinh Hoa, Nha Trang University, for assistance in fish husbandry. This work contributes to the celebration of the 50th anniversary of Nha Trang University, located in Nha Trang City, Khanh Hoa Province, Viet Nam.

Appendix A. Supporting information

Supplementary data associated with this article can be found in the online version at doi:10.1016/j.rsma.2026.105436.

Data availability

Data will be made available on request.

References

Ansarifard, F., Rajabi Islami, H., Shamsaie Mehrjan, M., Soltani, M., 2018. Effects of *Arthrospira platensis* on growth, skin color and digestive enzymes of koi, *Cyprinus carpio*. *Iran*. J. Fish. Sci. 17, 381–393. https://doi.org/10.22092/ijfs.2018.115878.

AOAC International, 2005. Official Methods of Analysis of AOAC International, 18th ed. AOAC International, Gaithersburg, MD.

APHA (American Public Health Association), 2012. Standard Methods for the Examination of Water and Wastewater, 22nd ed. APHA/AWWA/WEF, Washington, DC.

Araujo, G.S., Silva, J.W.A.D., Cotas, J., Pereira, L., 2022. Fish farming techniques: current situation and trends. J. Mar. Sci. Eng. 10, 1598. https://doi.org/10.3390/jmse10111598.

Bernfeld, P., 1955. Amylases, α and β. In: Colowick, S.P., Kaplan, N.O. (Eds.), Methods in Enzymology, 1. Academic Press, New York, pp. 149–158. https://doi.org/10.1016/0076-6879(55)01021-5.

Besen, K.P., Melim, E.W.H., da Cunha, L., Favaretto, E.D., Moreira, M., Fabregat, T.E.H. P., 2019. Lutein as a natural carotenoid source: effect on growth, survival and skin pigmentation of goldfish juveniles (*Carassius auratus*). Aquac. Res. 50, 2200–2206. https://doi.org/10.1111/are.14101.

Black, H.S., Boehm, F., Edge, R., Truscott, T.G., 2020. The benefits and risks of certain dietary carotenoids that exhibit both anti- and pro-oxidative mechanisms—a comprehensive review. Antioxidants 9, 264. https://doi.org/10.3390/antiox9030264.

Bower, C.E., Bidwell, J.P., 1978. Ionization of ammonia in seawater: effects of temperature, pH, and salinity. J. Fish. Res. Board. Can. 35, 1012–1016. https://doi.org/10.1139/f78-165.

Bradford, M.M., 1976. A rapid and sensitive method for the quantitation of microgram quantities of protein utilizing the principle of protein–dye binding. Anal. Biochem. 72, 248–254. https://doi.org/10.1016/0003-2697(76)90527-3.

Chhaba, B., Goud, E.A., Das, S.A., Karmakar, S., Rout, S.K., Kachave, V.C., 2024. The effects of tulsi and marigold as dietary supplement on growth, haematological and biochemical parameters in *Labeo rohita* (Hamilton). Int. J. Adv. Biochem. Res. 8, 135–143. https://doi.org/10.33545/26174693.2024.v8.i4b.971.

Dharma, T.S., Hutapea, J.H., Mahardika, K., Supii, A., 2025. Prospect of Kuwe fish (*Gnathanodon speciosus* Forsskal) hatchery supports to the aquaculture development. In: Nugroho, Imron, E., Gunadi, Rosmiati, B., Syahputra, K. (Eds.), Aquaculture Development in Archipelago: Domestication and Cultivation of Freshwater and Marine Fishes in Indonesia. Springer Nature, Singapore, pp. 225–232. https://doi.org/10.1007/978-981-95-1084-9_24.

Eghlima, G., Seyed Hajizadeh, H., 2026. Variability in lutein and zeaxanthin content, fatty acid and phytosterols profiles, and genetic parameters of some *Tagetes* spp. cultivars. BMC Plant. Biol. 26, 198. https://doi.org/10.1186/s12870-025-08061-w.

Elbahnaswy, S., Elshopakey, G.E., 2024. Recent progress in practical applications of a potential carotenoid astaxanthin in aquaculture industry: a review. Fish. Physiol. Biochem. 50, 97–126. https://doi.org/10.1007/s10695-022-01167-0.

Fang, H., Xie, J., Zhao, W., Liu, Z., Liu, Y., Tian, L., Niu, J., 2021. Study supplementation of astaxanthin in high-fat diet on growth performance, antioxidant ability, anti-inflammation, non-specific immunity and intestinal structure of juvenile *Trachinotus ovatus*. Aquac. Nutr. 27, 2575–2586. https://doi.org/10.1111/anu.13386.

Guo, Z., Liu, Y., Luo, Y., 2024. Mechanisms of carotenoid intestinal absorption and the regulation of dietary lipids: lipid transporter-mediated transintestinal epithelial pathways. Crit. Rev. Food Sci. Nutr. 64, 1791–1816. https://doi.org/10.1080/10408398.2022.2119204.

Hassaan, M.S., Mohammady, E.Y., Soaudy, M.R., Sabae, S.A., Mahmoud, A.M.A., El-Haroun, E.R., 2021. Comparative study on the effect of dietary β-carotene and phycocyanin extracted from *Spirulina platensis* on immune-oxidative stress biomarkers, genes expression and intestinal enzymes, serum biochemical in Nile tilapia, *Oreochromis niloticus*. Fish. Shellfish. Immunol. 108, 63–72. https://doi.org/10.1016/j.fsi.2020.11.012.

Ikeuchi, M., Koyama, T., Takahashi, J., Yazawa, K., 2007. Effects of astaxanthin in obese mice fed a high-fat diet. Biosci. Biotechnol. Biochem. 71, 893–899. https://doi.org/10.1271/bbb.60521.

Jagadeesh, T.D., Murthy, H.S., Swain, S.H., Chethan, N., Manjunatha, A.R., Baglodi, V., 2014. Effect of marigold oleoresin on growth, survival and pigmentation in orange chromide, *Etroplus maculatus* (Bloch, 1795). Fish. Technol. 51, 25–30.

Jha, G.N., Sarma, D., Qureshi, T.A., Akhtar, M.S., 2012. Effect of marigold flower and beetroot meals on growth performance, carcass composition, and total carotenoids of snow trout (*Schizothorax richardsonii*). Isr. J. Aquac. Bamidgeh 64, 20622. https://doi.org/10.46989/001c.20622.

Kalinowski, C.T., Robaina, L.E., Izquierdo, M.S., 2011. Effect of dietary astaxanthin on the growth performance, lipid composition and post-mortem skin colouration of red porgy *Pagrus pagrus*. Aquac. Int. 19, 811–823. https://doi.org/10.1007/s10499-010-9401-0.

Kunitz, M., 1947. Crystalline soybean trypsin inhibitor: II. General properties. J. Gen. Physiol. 30, 291–310. https://doi.org/10.1085/jgp.30.4.291.

Liao, Y., Zhang, B., Wang, D., Jiang, D., Zhu, C., Deng, S., Chen, H., Li, G., Shi, H., 2025. Metabolism, function, molecular mechanism, and application of carotenoids in coloration of aquatic animals. Rev. Aquac. 17, e70016. https://doi.org/10.1111/raq.70016.

Lim, K.C., Yusoff, F.M., Karim, M., Natrah, F.M., 2023. Carotenoids modulate stress tolerance and immune responses in aquatic animals. Rev. Aquac. 15, 872–894. https://doi.org/10.1111/raq.12767.

Luo, M., Lu, G., Yin, H., Wang, L., Atuganile, M., Dong, Z., 2021. Fish pigmentation and coloration: molecular mechanisms and aquaculture perspectives. Rev. Aquac. 13, 2395–2412. https://doi.org/10.1111/raq.12583.

Mansour, A.T., El-Feky, M.M., El-Beltagi, H.S., Sallam, A.E., 2020. Synergism of dietary co-supplementation with lutein and bile salts improved the growth performance, carotenoid content, antioxidant capacity, lipid metabolism, and lipase activity of the marbled spinefoot rabbitfish, *Siganus rivulatus*. Animals 10, 1643. https://doi.org/10.3390/ani10091643.

Mehar, M., Mekkawy, W., McDougall, C., Benzie, J.A., 2020. Fish trait preferences: a review of existing knowledge and implications for breeding programmes. Rev. Aquac. 12, 1273–1296. https://doi.org/10.1111/raq.12382.

Mitra, S., Khatun, M.N., Prodhan, M.M.H., Khan, M.A., 2021. Consumer preference, willingness to pay, and market price of capture and culture fish: do their attributes matter? Aquaculture 544, 737139. https://doi.org/10.1016/j.aquaculture.2021.737139.

Na-Nakorn, U., Kamcharoen, M., Santos, B.S., Torres, S.K.M., Nakajima, M., Senanan, W., Gonzales-Plasus, M.M., Zeng, C., 2023. Current status of carangid aquaculture and way forward. Agric. Nat. Resour. 57, 541–558. https://doi.org/10.34044/j.anres.2023.57.3.18.

Nankervis, L., Cobcroft, J.M., Nguyen, N.V., Rimmer, M.A., 2022. Advances in practical feed formulation and adoption for hybrid grouper (*Epinephelus fuscoguttatus* ♀ × *E. lanceolatus* ♂) aquaculture. Rev. Aquac. 14, 288–307. https://doi.org/10.1111/raq.12598.

Nguyen, M.C., Fotedar, R., Pham, H.D., 2022. Effects of dietary protein and lipid levels on growth performance, feed utilization and body composition of juvenile giant trevally (*Caranx ignobilis* Forsskal, 1775). Aquac. Res. 53 (17), 6254–6263. https://doi.org/10.1111/are.16098.

NRC (National Research Council), 2011. Nutrient Requirements of Fish and Shrimp. National Academies Press, Washington, DC. https://doi.org/10.17226/13039.

Pham, H.Q., Le, H.M., Van Phan, U., Van Nguyen, M., Dinh, K.V., 2026. Seasonal dynamics of plasma estradiol 17β level, gonadosomatic index, and ovarian development in female golden trevally (*Gnathanodon speciosus*). Sci. Rep. 16, 713. https://doi.org/10.1038/s41598-025-30370-1.

Ren, H., Cao, X., Guo, X., Yuan, P., 2025. Supplementation of Yellow River carp diet with lutein and ferrous fumarate: growth performance, digestive enzyme activity, skin pigmentation, and intestinal microbiota. Isr. J. Aquac. Bamidgeh 77, 10–18. https://doi.org/10.46989/001c.127435.

Shastak, Y., Pelletier, W., 2023. Captivating colors, crucial roles: astaxanthin's antioxidant impact on fish oxidative stress and reproductive performance. Animals 13, 3357. https://doi.org/10.3390/ani13213357.

Song, J.H., Cho, Y.S., Park, J.Y., Kim, G.D., Lim, H.K., 2021. Effects of astaxanthin produced by *Paracoccus haeundaensis* on growth and body color in *Epinephelus akaara*. Isr. J. Aquac. Bamidgeh 73, 1422474. https://doi.org/10.46989/001c.24456.

Song, X., Wang, L., Li, X., Chen, Z.Z., Liang, G., Leng, X., 2017. Dietary astaxanthin improved the body pigmentation and antioxidant function but not the growth of discus fish (*Symphysodon* spp.). Aquac. Res. 48, 1359–1367. https://doi.org/10.1111/are.13200.

Swian, H.S., Senapati, S.R., Meshram, S.J., Mishra, R., Murthy, H.S., 2014. Effect of dietary supplementation of marigold oleoresin on growth, survival and total muscle carotenoid of koi carp, *Cyprinus carpio* L. J. Appl. Nat. Sci. 6, 430–435. https://doi.org/10.31018/jans.v6i2.478.

Tambekar, D.H., Mundekar, S.P., Bombode, V.B., 2013. Partial characterization and optimization of lipase production from *Bacillus cereus* isolated from haloalkaliphilic Lonar Lake. Int. J. Life Sci. Biotechnol. Pharma Res. 2, 249–256.

Tiewsoh, W., Singh, E., Nath, R., Surnar, S.R., Priyadarshini, A., 2019. Effect of carotenoid in growth and colour enhancement in gold fish, *Carassius auratus* (L.). J. Exp. Zool. India 22, 765–771.

Tomasevic, I., Tomovic, V., Milovanovic, B., Lorenzo, J., Đorđević, V., Karabasil, N., Djekic, I., 2019. Comparison of a computer vision system vs. traditional colorimeter for color evaluation of meat products with various physical properties. Meat Sci. 148, 5–12. https://doi.org/10.1016/j.meatsci.2018.09.015.

Tran, D.V., Luong, H.T., Pham, K.T., Dang, T.T., Hua, N.T., Pham, H.Q., 2024a. Plant-based carotenoid supplementation: growth, feed utilization efficiency, and coloration in false clownfish (*Amphiprion ocellaris*). Isr. J. Aquac. Bamidgeh 76, 1–12. https://doi.org/10.46989/001c.94193.

Tran, T.L.T., Tran, D.V., Ngo, M.V., Hoang, T.T., Luong, H.T., Dang, T.T., 2024b. Influence of floral-derived natural pigments on the growth, coloration, and biochemical profiles of golden trevally (*Gnathanodon speciosus* Forsskål, 1775). Fish. Aquat. Sci. 27, 622–633. https://doi.org/10.47853/FAS.2024.e59.

Wassef, E.A., Chatzifotis, S., Sakr, E.M., Saleh, N.E., 2010. Effect of two natural carotenoid sources in diets for gilthead seabream, *Sparus aurata*, on growth and skin coloration. J. Appl. Aquac. 22, 216–229. https://doi.org/10.1080/10454438.2010.497741.

Xu, W., Liu, Y., Huang, W., Yao, C., Yin, Z., Mai, K., Ai, Q., 2022. Effects of dietary supplementation of astaxanthin (Ast) on growth performance, activities of digestive enzymes, antioxidant capacity and lipid metabolism of large yellow croaker (*Larimichthys crocea*) larvae. Aquac. Res. 53, 4605–4615. https://doi.org/10.1111/are.15933.

Yeşilayer, N., Mutlu, G., Yıldırım, A., 2020. Effect of nettle (*Urtica* spp.), marigold (*Tagetes erecta*), alfalfa (*Medicago sativa*) extracts and synthetic xanthophyll (zeaxanthin) carotenoid supplementations into diets on skin pigmentation and growth parameters of electric yellow cichlid (*Labidochromis caeruleus*). Aquaculture 520, 734964. https://doi.org/10.1016/j.aquaculture.2020.734964.

Yi, X., Li, J., Xu, W., Zhang, W., Mai, K., 2016. Effects of dietary lutein/canthaxanthin ratio on the growth and pigmentation of large yellow croaker *Larimichthys croceus*. Aquac. Nutr. 22, 683–690. https://doi.org/10.1111/anu.12289.

Yu, W., Lin, H., Yang, Y., Zhou, Q., Chen, H., Huang, X., Zhou, C., Huang, Z., Li, T., 2021. Effects of supplemental dietary *Haematococcus pluvialis* on growth performance, antioxidant capacity, immune responses and resistance to *Vibrio harveyi* challenge of spotted sea bass *Lateolabrax maculatus*. Aquac. Nutr. 27, 355–365. https://doi.org/10.1111/anu.13189.

Yuangsoi, B., Jintasataporn, O., Areechon, N., Tabthipwon, P., 2011. The pigmenting effect of different carotenoids on fancy carp (*Cyprinus carpio*). Aquac. Nutr. 17, e306–e316. https://doi.org/10.1111/j.1365-2095.2010.00764.x.

Zhang, J., Tian, C., Zhu, K., Liu, Y., Zhao, C., Jiang, M., Zhu, C., Li, G., 2023. Effects of natural and synthetic astaxanthin on growth, body color, and transcriptome and metabolome profiles in the leopard coralgrouper (*Plectropomus leopardus*). Animals 13, 1252. https://doi.org/10.3390/ani13071252.

Zhao, W., Guo, Y.C., Huai, M.Y., Li, L., Man, C., Pelletier, W., Wei, H.L., Yao, R., Niu, J., 2022. Comparison of the retention rates of synthetic and natural astaxanthin in feeds and their effects on pigmentation, growth, and health in rainbow trout (*Oncorhynchus mykiss*). Antioxidants 11, 2473. https://doi.org/10.3390/antiox11122473.

Regional Studies in Marine Science 102 (2026) 105385

Contents lists available at ScienceDirect

Regional Studies in Marine Science

journal homepage: www.elsevier.com/locate/rsma

Chitosan nanoparticles derived from molted shrimp shells as biodegradable adjuvants for *Vibrio harveyi* vaccination in Asian sea bass (*Lates calcarifer*)

Tran Vi Hich [a], Khuong V. Dinh [a,b,*], Nguyen Thi Kim Cuc [a], Nguyen Thi Thuy Giang [a], Pham Thi Dan Phuong [b], Nguyen Cong Minh [c,d], Trang Si Trung [c,**]

[a] *Institute of Aquaculture Research, Nha Trang University, Vietnam*
[b] *Department of Biosciences, University of Oslo, Norway*
[c] *Faculty of Food Technology, Nha Trang University, Vietnam*
[d] *Institute of Biotechnology and Environment, Nha Trang University, Vietnam*

ARTICLE INFO

Dataset link: Valorization of molted shrimp shells: Comparative adjuvanticity of soluble chitosan derivatives versus nanoparticles in Vibrio harveyi vaccine for Asian sea bass (Lates calcarifer)

Keywords:
Chitosan nanoparticles
Molted shrimp shells
Vaccine adjuvant
Vibrio harveyi
Biodegradability
Structure-property relationship

ABSTRACT

The development of biodegradable adjuvants is crucial for aquaculture vaccination, yet it is still understudied. This study evaluated the comparative adjuvanticity of three chitosan derivatives prepared from molted shrimp shells (*Litopenaeus vannamei*), low viscosity chitosan (LV-chitosan), water-soluble chitosan lactate (Chi-L), and ionically cross-linked chitosan nanoparticles (Chi-N), in an inactivated *Vibrio harveyi* vaccine for Asian sea bass (*Lates calcarifer*), a major aquaculture species in Asia. Following intraperitoneal injection, the immune response was monitored against phosphate-buffered saline (PBS) and Freund's Complete Adjuvant (FCA) controls. The results showed that soluble derivatives (LV-chitosan and Chi-L) did not induce higher antibody titers than the PBS control by day 28 post-vaccination. Chi-N elicited antibody titers ($2^{3.29} \pm 0.1$) that were lower than the FCA benchmark ($2^{4.73} \pm 0.1$), but significantly higher than the PBS control, suggesting immune enhancement. In addition, Chi-N significantly enhanced serum lysozyme activity compared with the PBS control, indicating stimulation of innate immunity. Macroscopic examination showed no visible persistent residues in the Chi-N group, whereas FCA produced obvious intra-abdominal residues. These observations are consistent with the expected biodegradability of nanochitosan, although in vivo biodegradation needed to be confirmed by histological examination or quantitative assessment of material degradation. Overall, these findings suggest that valorizing molted shrimp shells into nanoparticulate chitosan enhances adjuvant performance compared with soluble chitosan derivatives, highlighting the importance of the structure–property relationship among chitosan formulations and supporting the potential of nanochitosan as a sustainable alternative for aquaculture vaccination.

1. Introduction

The global aquaculture sector is a critical component of food security and economic development. Shrimp farming is one of the most valuable aquaculture industries worldwide, but processing also generates substantial quantities of byproducts (50–60% of raw shrimp weight), specifically molted shrimp shells accumulated in culture ponds (NIRMAL et al., 2020). Unlike conventional exoskeletons obtained from processing plants, these molted shells possess significantly lower protein levels (12.7%) compared to peeled shells (28.8%) and have been demonstrated to be a promising source for the production of high-purity chitin and chitosan under relatively mild extraction conditions (PHUONG et al., 2022). Furthermore, chitosan derived from molted shrimp shells has low crystallinity and low viscosity (LV-chitosan), characteristics that are highly advantageous for chemical modification and pharmaceutical applications (PHUONG et al., 2022).

Asian seabass (*Lates calcarifer*) is a highly economically valuable species in marine aquaculture of Asia and Australia (COPLAND and GREY, 1986; PEARSON, 1987). However, a rapid expansion of intensive Asian seabass farming is associated with increased diseases caused by bacteria, especially vibriosis. *Vibrio harveyi* is a major pathogen in warm-adapted fish such as (*Acanthopagrus cuvieri*), orange-spotted

* Corresponding author at: Department of Biosciences, University of Oslo, Norway.
** Corresponding author.
E-mail addresses: van.k.dinh@ibv.uio.no (K.V. Dinh), trungts@ntu.edu.vn (T.S. Trung).

https://doi.org/10.1016/j.rsma.2026.105385
Received 23 May 2026; Received in revised form 22 July 2026; Accepted 21 August 2026
Available online 24 August 2026

grouper (*Epinephelus tauvina*) (Saeed, 1995), yellow grouper (*Epinephelus awoara)*(WANG et al., 2002; QIN et al., 2006), common dentex (*Dentex dentex),* Senegalese sole (*Solea senegalensis*)(ZORRILLA et al., 2003), as well as Japanese seabass (*Lateolabrax japonicus*), causing substantial economic losses (MOHD YAZID et al., 2021). While vaccination is a key control strategy, inactivated vaccines often show limited immunogenicity and require adjuvants to elicit a robust protective immune response (TAFALLA et al., 2013). Traditionally, oil-based adjuvants like Freund's Complete Adjuvant (FCA) are used as a gold standard in eliciting a high potency (Stills, 2005). However, their application in commercial aquaculture is often restricted due to potential side effects and persistent tissue residues, which raise concerns regarding animal welfare and food safety (MIDTLYNG et al., 1996). It is recommended that FCA should be replaced by other adjuvants when possible (GUY, 2007).

Several classes of vaccine adjuvants have been investigated for aquaculture applications, including mineral salts, emulsions, liposomes, polymeric nanoparticles, and immunostimulatory compounds such as β-glucans and CpG oligodeoxynucleotides (TAFALLA et al., 2013). Although these formulations can improve vaccine efficacy, many remain limited by relatively short antigen retention, formulation instability, high production costs, injection-site reactions, or regulatory constraints that restrict their widespread commercial application (TAFALLA et al., 2013; DMOUR and ISLAM, 2022; GUY, 2007). As a result, there is a growing interest in chitosan and its derivatives as biodegradable alternatives. Chitosan-based adjuvants can enhance vaccine efficacy by facilitating mucosal adhesion and stimulating immune cell recruitment (DMOUR and ISLAM, 2022). However, the efficacy of chitosan is heavily dependent on its physicochemical form. Previous studies suggest that chitosan nanoparticles may enhance antigen retention and cellular uptake (NANDHAKUMAR et al., 2025; WU et al., 2020), however, their efficacy remains dependent on formulation characteristics and target species.

Despite this potential, the comparative efficacy of LV-chitosan derived specifically from molted shells and its modified forms, specifically water-soluble chitosan lactate versus particulate chitosan nanoparticles, as injectable adjuvants for marine aquaculture fish such as Asian sea bass remains underexplored. Specifically, it is unclear how the solubility and particle size of these derivatives influence the trade-off between immune sustainment and rapid biodegradation. In inactivated bacterial vaccines, the induction of antigen-specific antibodies represents one of the principal correlates of adaptive immune protection in teleost fish and is therefore widely used to evaluate adjuvant efficacy (TAFALLA et al., 2013; YE et al., 2013). Although other immune parameters, including innate immune responses and pathogen challenge tests, provide complementary information, comparative antibody responses offer a robust first assessment of the capacity of different adjuvant formulations to enhance vaccine-induced humoral immunity (TAFALLA et al., 2013; YE et al., 2013).

In this study, we explored the valorization of molted shrimp shell waste for the development of sustainable chitosan-based vaccine adjuvants. Using intraperitoneal injection, we aimed to assess the comparative immunostimulatory effects of LV-chitosan, chitosan lactate (Chi-L), and chitosan nanoparticles (Chi-N) on the humoral immune response against *Vibrio harveyi* in Asian sea bass. We hypothesize that nanoparticulate chitosan, but not soluble chitosan derivatives, enhances vaccine-induced humoral immunity in Asian sea bass by acting as a biodegradable antigen depot that prolongs immune stimulation compared to non-adjuvanted vaccines. The findings from this assessment will provide baseline data to determine the feasibility of utilizing these modified chitosan forms in aquaculture health management.

2. Materials and methodology

2.1. Ethical statement

All experimental procedures involving live fish were conducted in accordance with the Vietnamese legislation on animal welfare, including Decree No. 33/2005/ND-CP and the Law on Animal Husbandry (Law No. 79/2015/QH13). The study was carried out under the approval of the Scientific Committee of Nha Trang University as part of the university-level research project TR2021–13–10. Under current national regulations, separate approval from an institutional animal ethics committee is not required for scientific research involving aquaculture fish. All efforts were made to minimize stress and suffering. Fish were anesthetized using ethylene glycol monophenyl ether (100–150 mg L^{-1}) during handling and blood collection, and all procedures were performed by trained personnel. After completion of sampling, surviving fish were monitored during a recovery period before being transferred to designated holding tanks.

2.2. Preparation of chitosan derivatives and nanoparticles

Chitosan was isolated from molted shrimp shells (*Litopenaeus vannamei*) collected from intensive farming waste, following the protocol described by PHUONG et al., 2022 (PHUONG et al., 2022). Low-Viscosity Chitosan (LV-chitosan) was prepared from chitosan extracted from molted shrimp shells using the solid-state depolymerization method described by (MINH et al., 2017). Chitosan powder (100 mesh) was swollen in 0.2% (w/v) NaOH solution for 8 h at a chitosan-to-NaOH solution ratio of 1:10 (w/v). Subsequently, 0.3% (w/v) H_2O_2 solution was added at a volume ratio of 1:10 (H_2O_2 solution: NaOH suspension), and depolymerization was performed for 6 h at room temperature. The obtained LV-chitosan was filtered, washed with distilled water until neutral pH, dried at 40°C, and stored for subsequent use. The resulting LV-chitosan exhibited a degree of deacetylation (DA) of 88% and a weight-average molecular weight (M_w) of 215 kDa.

Chitosan lactate (Chi-L) was synthesized via a solid-state reaction between the prepared LV-chitosan and lactic acid, as reported by Trung et al. (TRUNG et al., 2023) with slight modifications. Briefly, chitosan obtained from molted shrimp shells was ground and sieved through a 35-mesh screen. The powder was then soaked in 70% ethanol at a chitosan-to-solvent ratio of 1:10 (w/v) for 4 h at room temperature. After soaking, the ethanol was removed by centrifugation at 5000 rpm, and 1 M lactic acid was added at a ratio of 1:10 (w/v, chitosan:lactic acid solution). The mixture was allowed to react for 2 h at room temperature. The resulting product was filtered through cloth, washed with 85% ethanol to remove residual lactic acid, and dried at 40 °C for 12 h before storage.

Chitosan nanoparticles (Chi-N) were produced using the ionic gelation method adapted from Cuong et al. (CUONG et al., 2022). Briefly, 25 mL of 0.5% (w/v) TPP solution was added dropwise into 500 mL of 0.1% (w/v) LV-chitosan solution over 30 min under continuous stirring at 500–600 rpm at room temperature (25 ± 2°C). The formulation corresponded to a chitosan-to-TPP mass ratio of 4:1 (w/w). After complete addition of the TPP solution, the suspension was stirred for an additional 30 min under the same conditions. The final suspension had a pH of 5.5 ± 0.1 and was used immediately after preparation. Particle size, polydispersity index (PDI), and zeta potential were determined using a Horiba SZ-100 Nano Particle Analyzer. Measurements were performed on freshly prepared nanoparticle suspensions immediately after preparation. Each sample was analyzed in triplicate, and the reported values represent the mean ± standard deviation.

2.3. Experimental fish

Healthy Asian seabass (*Lates calcarifer*) were obtained from a local hatchery in Khanh Hoa province, Vietnam. Prior to the experiment, 30 fish were randomly sampled to determine the initial body weight, which averaged 9.9 ± 1.4 g (n = 30). Before the experiment, the fish were screened for *Vibrio harveyi* using bacteriological methods, and only fish that tested negative were included in the study. Subsequently, the fish were transported to the Center for Experiments on Aquatic Breeding and

Diseases, Nha Trang University, and acclimatized for 14 days. During this period, fish were maintained in 2000 L tanks under controlled environmental conditions, with natural water temperature ranging from 28 to 32°C which are representative of those encountered in local Asian seabass aquaculture systems (DOAN et al., 2018; DINH et al., 2026), pH 7.9–8.3, and dissolved oxygen (DO) > 5 mg L^{-1} . The fish were fed a commercial diet (UP 5001) twice daily, and approximately 50% of the water was exchanged every two days to maintain water quality.

2.4. Preparation of inactivated vaccine formulations

The pathogenic strain *Vibrio harveyi* (Aus K0917), originally isolated from the kidneys of *L. calcarifer* exhibiting hemorrhagic and ulcerative symptoms in Van Ninh, Khanh Hoa, Vietnam (September 2017). This strain was maintained in TSB including 20% glycerol at −80 °C at the Center for Research on Aquatic Breeding and Diseases, Nha Trang University, Vietnam. For vaccine preparation, the bacteria were cultured in Tryptic Soy Broth (TSB) supplemented with 1.5% NaCl at 30°C for 18 h. Subsequently, the culture was inactivated using 0.5% (v/v) formalin for 24 h. Complete bacterial inactivation was confirmed by plating aliquots of the formalin-treated bacterial suspension onto TSA and TCBS agar. No bacterial growth was observed after incubation, confirming complete inactivation before vaccine preparation. The inactivated bacterial cells were harvested by centrifugation at 7000 $\times$ g for five minutes and washed three times with sterile phosphate-buffered saline (PBS, pH 7.4). The final pellet was resuspended in PBS and adjusted to an optical density of OD600 = 1.1, corresponding to approximately 2×10^9 CFU/mL.

To prepare the experimental vaccines, the bacterial suspension was mixed with the respective adjuvant solutions (PBS, Freund's Complete Adjuvant, or 0.1% chitosan derivatives: LV-chitosan, chitosan lactate, and chitosan nanoparticles) at a 1:1 (v/v) ratio. For the FCA formulation, the bacterial suspension and adjuvant were emulsified using a homogenizer equipped with a DS-160/5 dispersing shaft at approximately 18,000 rpm for 4 min. Emulsification was continued until a stable water-in-oil emulsion was obtained, as confirmed by the water-drop test. The preparation of chitosan-based vaccines was adapted from the protocol described by Kitiyodom et al. (KITIYODOM et al., 2019). This resulted in five vaccine formulations containing a final bacterial concentration approximately 1×10^9 CFU/mL.

2.5. Experimental design and vaccination protocol

To test the efficiency of using chitosan-based adjuvants, we conducted a completely randomized design experiment with six experimental treatments (see below), each of which had three replications, resulting in a total of 18 experimental units. Asian sea bass were acclimatized in 18 × 250 L tanks; each contained 200 L of seawater and 25 fish juveniles. Water quality parameters were maintained as during the acclimation period. Fish were intraperitoneally (IP) injected with 0.1 mL of the respective formulations. The treatments included:

Negative Control: Injected with sterile physiological saline (PBS) only.
Non-adjuvanted Control (PBS group): Injected with inactivated *V. harveyi* suspended in PBS.
Chi: Injected with inactivated *V. harveyi* + LV-chitosan.
Chi-L: Injected with inactivated *V. harveyi* + chitosan lactate.
Chi-N: Injected with inactivated *V. harveyi* + chitosan nanoparticles.
Positive Control (Freu): Injected with inactivated *V. harveyi* emulsified with Freund's Complete Adjuvant.

2.6. Sample collection

Sampling was conducted on days 21 and 28 post-vaccination (dpv). At each time point, ten fish were randomly selected from each tank and anesthetized using 100 ppm 2-phenoxyethanol (Merck). Blood samples were drawn from the caudal vein using 1 mL sterile syringes and transferred to 1.5 mL Eppendorf tubes. The blood was allowed to clot at 4°C overnight and then centrifuged at 5000 rpm for 10 min to separate the serum. The serum was collected and stored at −20°C until analyzed for specific antibody titers and lysozyme activity. Sampled fish were removed from the experiment after blood collection and transferred to a separate 2-m^3 holding tank.

2.7. Analytical methods used for characterization of chitosan derivatives

The physicochemical properties of chitosan and its derivatives were characterized using standard protocols. UV-Vis spectra (200–800 nm) were recorded using a DR2800 spectrophotometer (KUMIRSKA et al., 2010). Particle size, polydispersity index (PDI), and zeta potential were determined using a Horiba SZ-100 Nano Particle Analyzer. Apparent viscosity was measured at 25 °C using a Brookfield LVT viscometer (KUBOTA et al., 2000), while solution pH (1% w/v) was monitored with a digital pH meter.

The average molecular weight (Mw) was determined by intrinsic viscosity measurements in acetate buffer (pH 4.75) using a Ubbelohde viscometer. Mw was derived from the Mark-Houwink equation $[\eta] = K \times M^a$, with constants $K = 1.424 \times 10^{-5}$ dL/g and a = 0.96 (ZHANG and NEAU, 2001). The degree of deacetylation (DD) was assessed via zero-order UV spectrophotometry at 210 nm following dissolution in 85% H_3PO_4, based on the method by WU and Zivanovic, (2008) (WU and ZIVANOVIC, 2008). Finally, functional groups were identified using FTIR spectroscopy (diamond ATR) over the range of 500–4000 cm^{-1} (32 scans, resolution 16 cm^{-1}).

2.8. Methods of analyzing humoral immune parameters

2.8.1. Determination of serum lysozyme activity

Serum lysozyme activity was determined using a turbidimetric assay based on the lysis of *Micrococcus lysodeikticus* (Sigma), using chicken egg white lysozyme (Sigma) as the standard. Briefly, 25 μL of each serum sample was added to triplicate wells of a 96-well plate. A standard curve was established using lysozyme concentrations ranging from 0.3125 to 20 μg mL^{-1} . Subsequently, 175 μL of a 0.075% (w/v) *M. lysodeikticus* suspension (prepared in phosphate buffer) was added to each well and mixed immediately. The reduction in turbidity was monitored by measuring the absorbance at 450 nm every 30 s for 5 min using a spectrophotometer (Titertek multiskan MK II, Flow laboratories, Switzerland).

2.8.2. Determination of specific antibody titers

The specific antibody response in fish serum was assessed using a bacterial agglutination assay in 96-well U-bottom microplates, following the method of Plumb and Areechon (PLUMB and AREECHON, 1990). First, 50 μL of serum was added to the first well, and 25 μL of Phosphate Buffered Saline (PBS) was dispensed into the remaining wells. Two-fold serial dilutions were performed by transferring 25 μL from the first well to the second, mixing well, and continuing the process across the row. Finally, 25 μL of inactivated *V. harveyi* suspension was added to all wells. The plates were gently shaken and incubated overnight at 4°C. The agglutination titer was defined as the reciprocal of the highest serum dilution exhibiting visible agglutination. For statistical analysis and data presentation, these titer values were log-transformed (log_2) as titers were determined from serial two-fold dilutions. The final results are expressed as the geometric mean (2^{mean}) of the log-transformed titers to correspond with the serial dilution scale.

2.9. Statistical analysis

Data quality control and statistical analyses were performed using Microsoft Excel 2016 and SPSS version 19.0 (IBM Corp., Armonk, NY,

USA). Prior to statistical analysis, all datasets were tested for normality and homogeneity of variance before performing ANOVAs. Differences in serum lysozyme activity and specific antibody titers among treatment groups were evaluated using one-way Analysis of Variance (ANOVA), with tanks considered experimental units for all statistical analyses. Where significant differences were detected, Tukey's HSD post-hoc test was applied to identify specific pairwise differences. A probability value of $P < 0.05$ was considered statistically significant. Results are presented in tables and graphs as mean ± standard deviation (SD).

3. Results and discussions

3.1. Physicochemical characteristics of chitosan derivatives

The results indicated distinct variations in pH, viscosity, and electrokinetic potential, reflecting the structural modifications of each derivative. LV-chitosan required an acidic medium for dissolution (pH = 4.0 ± 0.1), which is consistent with the protonation requirements of the amine groups in the chitosan backbone (RINAUDO, 2006; DASH et al., 2011). In contrast, chitosan lactate showed a higher pH (5.5 ± 0.2), characteristic of its water-soluble salt form, providing advantageous solubility at near-neutral pH for biological applications (RINAUDO, 2006; DASH et al., 2011). Both LV-chitosan and chitosan lactate demonstrated relatively low viscosity values (< 50 cP, Table 1). Notably, the nanochitosan solution showed the lowest viscosity, which was approximately 4 times lower than that of LV-chitosan and chitosan lactate (Table 1). This significantly lower viscosity can be attributed to the compact hydrodynamic volume of the crosslinked nanoparticles compared to the extended chain conformation of the polymer solutions (RINAUDO, 2006).

All chitosan derivative samples showed positive surface charges, confirming their cationic nature. Nanochitosan showed the highest stability with a zeta potential 34% and 50% higher than that of chitosan lactate and LV-chitosan, respectively (Table 1). The elevated positive charge on the nanoparticles suggests strong electrostatic repulsion between particles, a critical factor for preventing aggregation and ensuring long-term colloidal stability in suspension (RAMPINO et al., 2013; BENAMER OUDIH et al., 2023). Dynamic light scattering (DLS) analysis further revealed the successful formation of nanochitosan with an average particle size of 210.3 ± 5.4 nm and a polydispersity index (PDI) of 0.454 ± 0.014, indicating a relatively narrow and uniform size distribution. Such particle sizes and PDI values are generally considered acceptable for nanoparticle suspensions intended for biological applications (RAMPINO et al., 2013).

Both the LV-chitosan and the chitosan lactate formed clear solutions (Figs. 1a, 1b). However, a critical distinction lies in the solvent required. LV-chitosan required 1% acetic acid to achieve dissolution due to its rigid crystalline structure at neutral pH. The chitosan lactate derivative was fully soluble in distilled water (Fig. 1b), suggesting that lactic acid successfully improved water solubility, eliminating the need for acidic solvents, which can be irritant in parenteral administration. In contrast to the clear molecular solutions of the derivatives, the nanochitosan preparation (Fig. 1c) showed a distinct milky appearance. This turbidity is a macroscopic indicator of the ionic gelation process, where the formation of crosslinked nanoparticles scatters light (Tyndall effect), distinguishing the colloidal suspension from the true solutions observed in Figs. 1a and 1b.

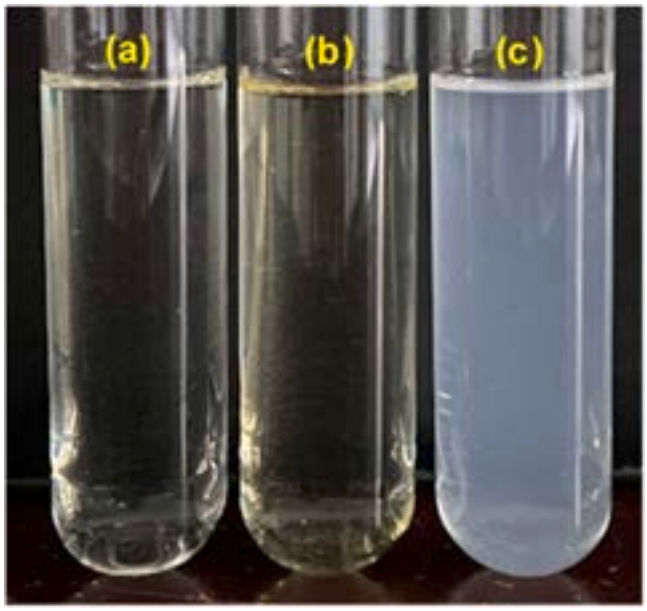

Fig. 1. Visual appearance of the experimental formulations. **(a)** LV-chitosan dissolved in 1% acetic acid (clear solution); **(b)** Water-soluble chitosan lactate dissolved in distilled water (clear solution); and **(c)** Chitosan nanoparticle suspension exhibiting characteristic opalescence (Tyndall effect).

The spectrum of LV-chitosan displayed a sharp absorption peak at approximately 202 nm, while remaining highly transparent in the visible region (Fig. 2). Chitosan lactate exhibited intense absorption below 240 nm, likely due to the presence of the lactate counter-ion, but maintained a flat baseline in the range of 400–800 nm, confirming its

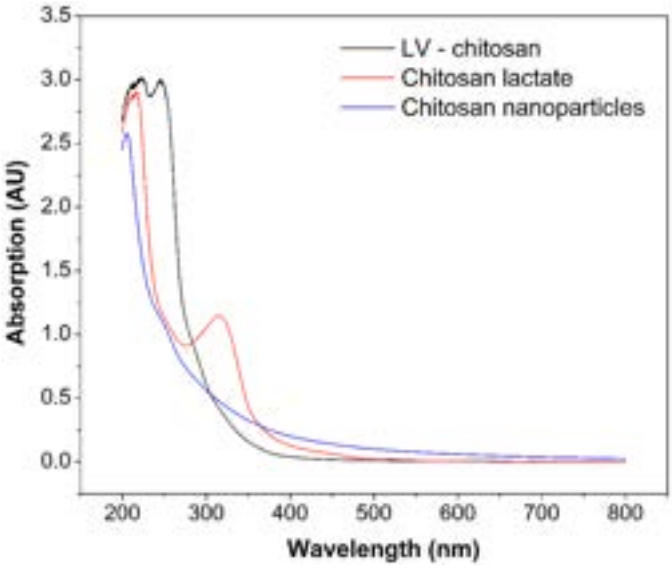

Fig. 2. UV-Vis spectra of chitosan derivatives.

Table 1
Physicochemical characteristics of chitosan derivatives.

Chitosan derivatives	Physocochemical characteristics				
	pH	Viscosity (Cp)	Zeta potential (mV)	Particle size (nm)	Polydispersity Index (PDI)
LV-chitosan	4.0 ± 0.1	47.5 ± 3	33.2 ± 0.2	NA	NA
Chitosan lactate	5.5 ± 0.2	48.4 ± 5	43.6 ± 0.8	NA	NA
Chitosan nanoparticles	5.0 ± 0.1	12.4 ± 2	66.2 ± 0.5	210.3 ± 5.4	0.241 ± 0.014

complete dissolution as a homogeneous solution. In contrast, the spectrum of nanochitosan was distinct, showing a "scattering tail" in the visible region (400–800 nm) and a broad shoulder between 280 and 320 nm. This optical behavior is a hallmark of the Tyndall effect, providing strong evidence for the presence of colloidal nanoparticles rather than a true molecular solution.

Fourier Transform Infrared (FTIR) spectroscopy provided the chemical modifications in the derivatives (Fig. 3). For LV-chitosan, the spectrum showed characteristic bands at ~1655 cm^{-1} (Amide I) and ~1590 cm^{-1} (-NH2 bending), confirming the presence of free amine groups. In the spectrum of chitosan lactate, the reaction with lactic acid was evidenced by the disappearance of the -NH2 bending peak and the concurrent emergence of intense bands at ~1580 cm^{-1} and ~1400 cm^{-1}. These bands correspond to the asymmetric and symmetric stretching vibrations of the carboxylate group (-COO-), confirming the protonation of amino groups and the successful formation of the lactate salt. For nanochitosan, the ionic gelation process induced a shift in the amide peak to ~1540 cm^{-1}. Furthermore, specific phosphate fingerprints were observed at ~1215 cm^{-1} (P = O stretching) and ~890 cm^{-1} (P-O-P stretching), verifying the electrostatic crosslinking between the cationic chitosan chains and the anionic tripolyphosphate (TPP) molecules.

The DLS analysis revealed that the synthesized nanochitosan formed a highly uniform colloidal system, characterized by a distinct unimodal distribution (Fig. 4). The nanoparticles showed a Z-average diameter of ~210 nm with a low Polydispersity Index (PDI) of 0.241. This size range aligns perfectly with previous reports on chitosan-TPP ionic gelation (typically 130–300 nm) (QI et al., 2004), confirming the successful formation of crosslinked nanoparticles. Furthermore, the hydrodynamic diameter obtained by DLS is considered more physiologically relevant than dry-state imaging (SEM) for vaccine delivery. As emphasized by Wolfbeis (WOLFBEIS, 2015), DLS accounts for the hydration shell and swelling of hydrophilic polymers in aqueous media, thereby providing a reliable estimation of the effective particle size when interacting with biological membranes.

3.2. Effects of chitosan types on lysozyme content in fish serum

Serum lysozyme concentration was not different among treatment groups compared to the control and PBS at day 21 post-vaccination ($P > 0.05$, Fig. 5). Specifically, fish vaccinated with chitosan-based adjuvants exhibited lysozyme levels comparable to those in the PBS negative control and the Freund's adjuvant positive control. While this observation indicates that long-term non-specific immunity was not

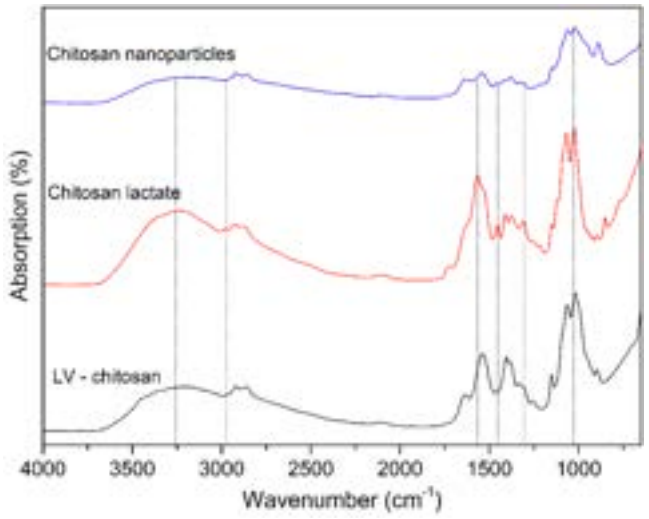

Fig. 3. FTIR spectra of chitosan derivatives.

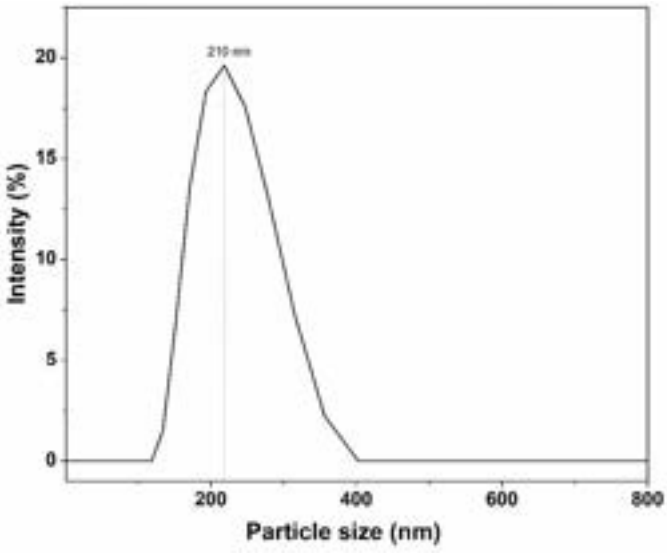

Fig. 4. Particle size distribution of chitosan nanoparticles (Chi-N) determined by DLS. The unimodal peak with a low PDI (0.241) confirms a highly uniform colloidal suspension with a Z-average diameter of ~210 nm.

elevated, it aligns with the temporal kinetics of the innate immune response. Lysozyme is a primary component of acute innate defense, typically exhibiting a rapid spike immediately after stimulation, followed by a decline as homeostasis is restored (SAURABH and SAHOO, 2008). In tilapia, lysozyme activity significantly decreases after just 3 and 7 days post-challenge with *Streptococcus agalactiae* injection, then stabilizes at low levels (BILLER et al., 2021). Therefore, the absence of significant differences on day 21 likely indicates that the immune response had transitioned from the initial non-specific inflammatory phase to a specific adaptive phase (SAURABH and SAHOO, 2008; MAGNADÓTTIR, 2006), rather than reflecting a lack of adjuvant efficacy. However, serum lysozyme activity was assessed only at 21 days post-vaccination, which limits interpretation of the earlier kinetics of innate immune stimulation. Because lysozyme responses may peak within the first several days following vaccination (BILLER et al., 2021) and subsequently return toward baseline, additional sampling at earlier time points, such as 1, 3, and 7 days post-vaccination, would have provided a more complete assessment of the acute innate immune response induced by the different chitosan formulations. Furthermore, the return of lysozyme activity to baseline levels suggests the biocompatibility of the chitosan-based adjuvants. Persistently elevated lysozyme levels at this stage could indicate chronic inflammation or stress caused by the injected material (MAGNADÓTTIR, 2006). The observed physiological stabilization suggests that the chitosan nanoparticles were well-tolerated by the host tissue and did not induce prolonged inflammatory stress, a critical requirement for safe vaccine delivery systems.

3.3. Specific humoral immune response (serum antibody titers)

Serum antibody titers against *Vibrio harveyi* differed significantly among the experimental groups on both days 21 and 28 post-vaccination (Fig. 6), reflecting the different physicochemical forms of the adjuvants. At day 21, most vaccinated groups exhibited antibody titers comparable to or slightly higher than the PBS control. However, by day 28, a distinct divergence in immune sustainment was recorded. The antibody titers in groups vaccinated with soluble chitosan derivatives, including LV-chitosan and chitosan lactate (Chi-L), failed to maintain high levels. Specifically, the Chi-L group exhibited titers ($2^{2.62}$) that were statistically lower than the PBS control ($2^{2.93}$) ($P < 0.05$). This significant decline suggests that the high water solubility of chitosan lactate may lead to rapid dissociation and clearance of the antigen from the injection

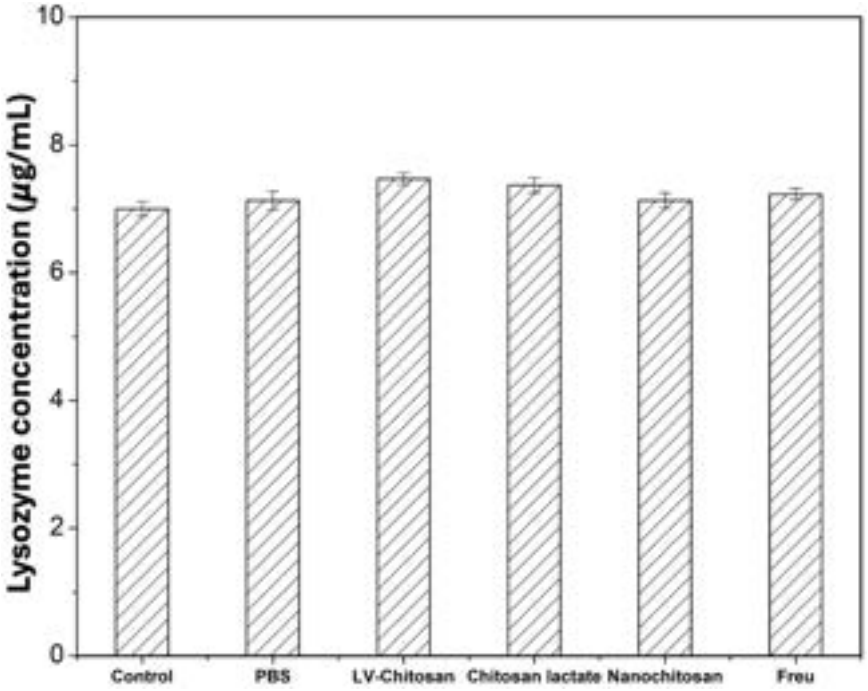

Fig. 5. Serum lysozyme concentration of sea bass at 21 days post-vaccination. Bars represent mean ± SD (n = 3). No significant differences were observed among treatments ($P > 0.05$).

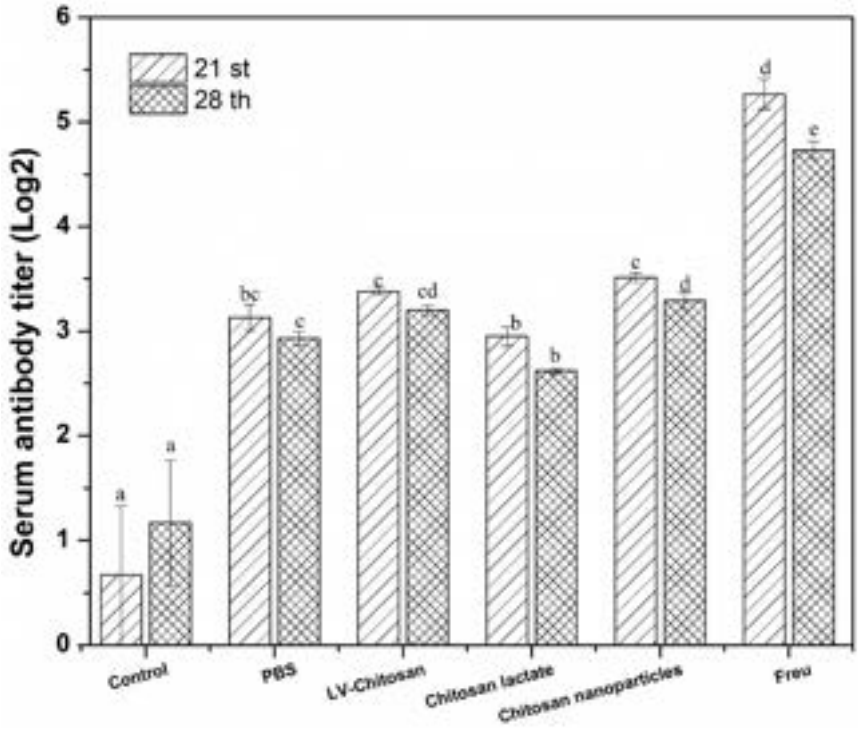

Fig. 6. Specific serum antibody titers (Log2) of Asian sea bass (*Lates calcarifer*) against *Vibrio harveyi* on days 21 and 28 post-vaccination. Note: Data are presented as mean ± SD (n = 3). Different lowercase letters indicate statistically significant differences between experimental groups of the same day ($P < 0.05$). Abbreviations: PBS: Phosphate-buffered saline (negative control); Chi: LV-chitosan; Chi-L: Chitosan lactate; Chi-N: Nanochitosan; Freu: Freund's Complete Adjuvant (positive control).

site, thereby limiting the duration of immune stimulation. It is also possible that prolonged elevation of antibody titers can impose significant metabolic costs in fish, leading to a strategic down-regulation of humoral responses once protective immunity is established. Such immune modulation is consistent with energy trade-offs between immune function and other vital biological processes (MAGNADÓTTIR, 2006; LOCHMILLER and DEERENBERG, 2000; SHELDON and VERHULST, 1996)

Regarding the nanochitosan (Chi-N) formulation, it demonstrated a clear and significant adjuvant effect compared to the negative controls, although it did not reach the peak magnitude of the oil-based positive control. Indeed, the level of antibody titer of the Chi-N group ($2^{3.29}$) was significantly higher than both the PBS and Chi-L groups ($P < 0.05$) on day 28 post-vaccination. While this level remained statistically lower than that of Freund's Complete Adjuvant (FCA) ($2^{4.73}$), which maintained the highest titers throughout the experiment. Chi-N distinguished itself as the only biodegradable formulation to elicit a response significantly superior to the PBS control. These results reflect a clear hierarchy in long-term adjuvant potency: FCA > Nanochitosan > PBS ≥ Soluble Derivatives.

The superior antibody response induced by Chi-N is consistent with previous findings in other fish species. In orally vaccinated turbot, the chitosan/aluminum formulation was the only treatment to produce a significant serum antibody increase at 20 days post-vaccination and generated the highest response at day 26 (JIN et al., 2021). In Nile tilapia, an antigen-loaded chitosan/β-glucan nanovaccine elicited significantly higher specific serum IgM than the formalin-inactivated vaccine and control groups at 14 and 28 days post-vaccination (NANDHAKUMAR et al., 2025). Likewise, a chitosan-coated nanoemulsion produced significantly higher serum IgM than a formalin-killed bacterin in striped catfish throughout 1–21 days post-vaccination, with the systemic response increasing toward day 21 (KITIYODOM et al., 2025). Although differences in species, vaccination route, vaccine composition, and antibody assays prevent direct numerical comparison, these findings collectively support the capacity of particulate chitosan formulations to enhance sustained humoral immunity. The present results further demonstrate that nanochitosan is more effective than soluble LV-chitosan and chitosan lactate when the formulations are compared using the same antigen, administration route, and chitosan source.

The superiority of FCA is attributed to its composition containing non-biodegradable mineral oils, which form a permanent depot at the injection site, continuously releasing antigens over a prolonged period (MIDTLYNG et al., 1996; GUY, 2007). However, this high potency comes at the cost of local reactions, as evidenced by the intra-abdominal residues (see Fig. 7). In contrast, while nanochitosan did not match the potency of the oil emulsion, its performance was higher than that of soluble chitosan forms. This difference may be related to the "structure-property relationship", particularly its particle size and electrostatic characteristics. Based on previous studies, particulate chitosan formulations have been proposed to function as temporary antigen depots, potentially prolonging antigen retention at the injection site and facilitating antigen uptake by antigen-presenting cells (AGNIHOTRI et al., 2004; BACHMANN and JENNINGS, 2010). Although this biodegradable depot eventually breaks down, resulting in lower long-term titers than the permanent Freund's depot, it offers a residue-free alternative that still significantly boosts immunity compared to non-adjuvanted vaccines.

Therefore, while nanochitosan has not yet achieved equivalence to the "gold standard" FCA in terms of antibody magnitude, it represents a promising biodegradable alternative, offering a balanced trade-off between immunogenicity and biological safety.

3.4. Comprehensive evaluation and future perspectives

The findings of this study reveal that, among the chitosan derivatives derived from molted shrimp shells, chitosan nanoparticles (Chi-N) is a promising candidate for vaccine delivery. The effectiveness of chitosan-based adjuvants is dependent on their physicochemical properties, including particle size, surface charge, and cross-linking density, which are largely determined by the preparation process (KUMAR et al., 2004). Therefore, future studies should focus on adjusting these parameters to maximize the immunogenic potential of nanochitosan.

In terms of comparative efficacy, although Chi-N demonstrated the best performance among the biodegradable groups, it did not fully equal the potency of Freund's Complete Adjuvant (FCA) due to its non-biodegradable mineral oil composition, which creates a permanent antigen depot. FCA left significant macroscopic residues within the peritoneal cavity, while Chi-N provides a substantial immune boost, without leaving any visible persistent residues. Although these macroscopic observations are consistent with the biodegradable nature of nanochitosan, histological examination or quantitative assessment of material degradation would be required in future studies to confirm in vivo biodegradation. Nevertheless, these findings suggest that nanochitosan achieves a favorable balance between immunogenicity and biodegradability, highlighting its potential as a sustainable vaccine adjuvant for aquaculture.

Nevertheless, the present study has several limitations. Although enhanced antibody responses demonstrated improved humoral immunogenicity, protective efficacy against *Vibrio harveyi* infection could not be directly confirmed because a pathogen challenge experiment was not performed. Furthermore, the immunological evaluation was limited to serum antibody titers and lysozyme activity, which were selected as established indicators of adaptive and innate immune responses (TAFALLA et al., 2013) to compare the relative adjuvant performance of the different chitosan formulations. Additional immune parameters, including complement activity, respiratory burst activity, and cytokine expression, were not investigated and could provide further mechanistic

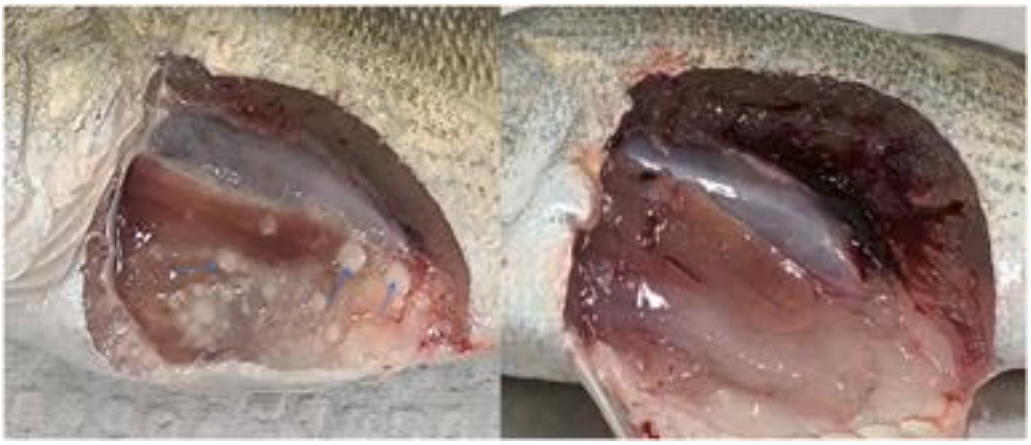

Fig. 7. Macroscopic observation of the peritoneal cavity of Asian sea bass at 28 days post-vaccination. (Left) Fish injected with Freund's Complete Adjuvant (FCA), showing persistent white nodular aggregates (blue arrows), characteristic of non-biodegradable oil depots. (Right) Fish injected with Nanochitosan (Chi-N) adjuvant showing a clean abdominal cavity with no visible residues.

insight into the immunostimulatory effects of nanochitosan (TAFALLA et al., 2013). Likewise, the proposed mechanisms underlying the enhanced humoral response of nanochitosan, including prolonged antigen retention, depot formation, and improved antigen presentation, were not directly evaluated. Consequently, the enhanced antibody response observed in the Chi-N group should be interpreted as being consistent with these proposed mechanisms. Future studies should therefore combine bacterial challenge experiments (LE et al., 2021) with broader immunological analyses, antigen-release kinetics, histological evaluation, and cellular immune assays to comprehensively assess both the protective efficacy and the mechanisms of action of nanochitosan as a vaccine adjuvant.

4. Conclusion

This study successfully demonstrated the potential of valorizing molted shrimp shells, an abundant yet undervalued byproduct, into high-value vaccine adjuvants for aquaculture. The comparative assessment revealed that the adjuvanticity of chitosan is strictly governed by its physicochemical form. While soluble derivatives (LV-chitosan and Chi-L) failed to sustain long-term immunity, the particulate engineering of chitosan into nanoparticles (Chi-N) significantly enhanced antibody production against *Vibrio harveyi*, achieving titers significantly higher than the non-adjuvanted control. Although the immune response elicited by nanochitosan did not reach the magnitude of the oil-based Freund's Complete Adjuvant (FCA), it offered a favorable safety profile. Unlike FCA, which resulted in the accumulation of persistent macroscopic residues in the peritoneal cavity, no visible macroscopic residues were observed in fish vaccinated with nanochitosan. This observation is consistent with the expected biodegradability of chitosan but does not directly demonstrate in vivo biodegradation. These findings suggest that Chi-N can be a promising alternative adjuvant that balances the trade-off between immunogenicity with biological compatibility. Future work should focus on optimizing particle characteristics to further bridge the efficacy gap with commercial oil adjuvants, paving the way for sustainable "green" vaccination strategies in fish farming.

CRediT authorship contribution statement

Hich Tran Vi: Writing – review & editing, Writing – original draft, Visualization, Validation, Investigation, Formal analysis, Data curation, Conceptualization. **Trung Trang Si:** Writing – review & editing, Writing – original draft, Supervision, Project administration, Investigation, Funding acquisition, Formal analysis, Data curation, Conceptualization. **Minh Nguyen Cong:** Writing – review & editing, Writing – original draft, Visualization, Validation, Resources, Methodology, Investigation, Funding acquisition, Formal analysis, Data curation, Conceptualization. **Phuong Pham Thi Dan:** Writing – review & editing, Writing – original draft, Visualization, Validation, Project administration, Methodology, Formal analysis, Data curation, Conceptualization. **Giang Nguyen Thi Thuy:** Writing – review & editing, Visualization, Methodology, Formal analysis, Conceptualization. **Cuc Nguyen Thi Kim:** Writing – review & editing, Writing – original draft, Visualization, Validation, Methodology, Formal analysis, Conceptualization. **Dinh Khuong V.:** Writing – review & editing, Writing – original draft, Visualization, Supervision, Formal analysis, Conceptualization.

Declaration of Generative AI and AI-Assisted Technologies in the Manuscript Preparation Process

During the preparation of this work, the author(s) used Gemini in order to refine grammar, improve the clarity and conciseness of the text. After using this tool/service, the author(s) reviewed and edited the content as needed and take(s) full responsibility for the content of the published article.

Declaration of Competing Interest

The authors declare that they have no known competing financial interests or personal relationships that could have appeared to influence the work reported in this paper

Acknowledgement

The authors gratefully acknowledge the financial support provided by Nha Trang University, Vietnam, under the university-level scientific research project (Code: TR2021–13–10).

Data availability

Research Link Provided

Valorization of molted shrimp shells: Comparative adjuvanticity of soluble chitosan derivatives versus nanoparticles in Vibrio harveyi vaccine for Asian sea bass (Lates calcarifer) (Figshare)

References

AGNIHOTRI, S.A., MALLIKARJUNA, N.N., AMINABHAVI, T.M., 2004. Recent advances on chitosan-based micro-and nanoparticles in drug delivery. J. Control. Release 100, 5–28.

BACHMANN, M.F., JENNINGS, G.T., 2010. Vaccine delivery: a matter of size, geometry, kinetics and molecular patterns. Nat. Rev. Immunol. 10, 787–796.

BENAMER OUDIH, S., TAHTAT, D., NACER KHODJA, A., MAHLOUS, M., HAMMACHE, Y., GUITTOUM, A.E., KEBBOUCHE GANA, S., 2023. Chitosan nanoparticles with controlled size and zeta potential. Polym. Eng. & Sci. 63, 1011–1021.

BILLER, J.D., POLYCARPO, G.D.V., MOROMIZATO, B.S., SIDEKERSKIS, A.P.D., SILVA, T.D.D., REIS, I.C.D., FIERRO-CASTRO, C., 2021. Lysozyme activity as an indicator of innate immunity of tilapia (Oreochromis niloticus) when challenged with LPS and Streptococcus agalactiae. Rev. Bras. De. Zootec. 50, e20210053.

COPLAND, J., GREY, D., 1986. Management of wild and cultured sea bass/barramundi (Lates calcarifer). ACIAR, Australia.

CUONG, H.N., MINH, N.C., HOA, N.V., GIANG, D.H., HIEU, N.V., NAM, P.V., 2022. Antifungal activity of squid pen chitosan nanoparticles against three fungal pathogens in various citrus fruits in vitro and in vivo. Coatings 12, 235.

DASH, M., CHIELLINI, F., OTTENBRITE, R.M., CHIELLINI, E., 2011. Chitosan—A versatile semi-synthetic polymer in biomedical applications. Progress. Polym. Sci. 36, 981–1014.

DINH, K.V., DOAN, N.X., VU, M.T.T., LE, M.-H., 2026. Tropical copepod culture under climate change: live feed production and optimization. Aquac. Fish. (In press.).

DMOUR, I., ISLAM, N., 2022. Recent advances on chitosan as an adjuvant for vaccine delivery. Int. J. Biol. Macromol. 200, 498–519.

DOAN, N.X., VU, M.T.T., NGUYEN, H.T., TRAN, H.T.N., PHAM, H.Q., DINH, K.V., 2018. Temperature- and sex-specific grazing rate of a tropical copepod *Pseudodiaptomus annandalei* to food availability: implications for live feed in aquaculture. Aquac. Res. 49, 3864–3873.

GUY, B., 2007. The perfect mix: recent progress in adjuvant research. Nat. Rev. Microbiol. 5, 396–397.

JIN, P., SUN, F., LIU, Q., WANG, Q., ZHANG, Y., LIU, X., 2021. An oral vaccine based on chitosan/aluminum adjuvant induces both local and systemic immune responses in turbot (Scophthalmus maximus). Vaccine 39, 7477–7484.

KITIYODOM, S., KAEWMALUN, S., NITTAYASUT, N., SUKTHAM, K., SURASSMO, S., NAMDEE, K., RODKHUM, C., PIRARAT, N., YATA, T., 2019. The potential of mucoadhesive polymer in enhancing efficacy of direct immersion vaccination against Flavobacterium columnare infection in tilapia. Fish. & Shellfish. Immunol. 86, 635–640.

KITIYODOM, S., KAMBLE, M.T., YOSTAWONKUL, J., SUKKARUN, P., THOMPSON, K.D., PIRARAT, N., 2025. Effects of immersion vaccination in striped catfish (*Pangasianodon hypophthalmus)* using a cationic lipid-based mucoadhesive nanovaccine against Edwardsiella ictaluri. Fish. & Shellfish. Immunol. 165, 110540.

KUBOTA, N., TATSUMOTO, N., SANO, T., TOYA, K., 2000. A simple preparation of half N-acetylated chitosan highly soluble in water and aqueous organic solvents. Carbohydr. Res. 324, 268–274.

KUMAR, M.R., MUZZARELLI, R.A., MUZZARELLI, C., SASHIWA, H., DOMB, A., 2004. Chitosan chemistry and pharmaceutical perspectives. Chem. Rev. 104, 6017–6084.

KUMIRSKA, J., CZERWICKA, M., KACZYNSKI, Z., BYCHOWSKA, A., BRZOZOWSKI, K., THOMING, J., STEPNOWSKI, P., 2010. Application of spectroscopic methods for structural analysis of chitin and chitosan. Mar. Drugs 8, 1567–1636.

LE, M.-H., DINH, K.V., PHAM, D.H., PHAN, V.U., TRAN, V.H., 2021. Extreme temperature differently alters the effects of dietary vitamin C on the growth, immunity and pathogen resistance of Waigieu seaperch, *Psammoperca waigiensis*. Aquac. Res. 52, 5383–5396.

LOCHMILLER, R.L., DEERENBERG, C., 2000. Trade-offs in evolutionary immunology: just what is the cost of immunity? Oikos 88, 87–98.

MAGNADÓTTIR, B., 2006. Innate immunity of fish (overview). Fish. & Shellfish. Immunol. 20, 137–151.
MIDTLYNG, P., REITAN, L., SPEILBERG, L., 1996. Experimental studies on the efficacy and side-effects of intraperitoneal vaccination of Atlantic salmon (Salmo salarL.) against furunculosis. Fish. & Shellfish. Immunol. 6, 335–350.
MINH, N.C., CUONG, H.N., PHUONG, P.T.D., SCHWARZ, S., STEVENS, W.F., VAN HOA, N., TRUNG, T.S., 2017. Swelling-assisted reduction of chitosan molecular weight in the solid state using hydrogen peroxide. Polym. Bull. 74, 3077–3087.
MOHD YAZID, S.H., MOHD DAUD, H., AZMAI, M.N.A., MOHAMAD, N., MOHD NOR, N., 2021. Estimating the economic loss due to vibriosis in net-cage cultured Asian seabass (Lates calcarifer): Evidence from the East coast of peninsular Malaysia. Front. Vet. Sci. 8, 644009.
NANDHAKUMAR, K., GUHA, R., LAKSHMI, S., ELUMALAI, P., 2025. Immunogenicity and protective efficacy of chitosan/β-glucan nanoparticle encapsulated inactivated Streptococcus agalactiae oral vaccine for Nile tilapia (Oreochromis niloticus). Comp. Immunol. Rep., 200254
NIRMAL, N.P., SANTIVARANGKNA, C., RAJPUT, M.S., BENJAKUL, S., 2020. Trends in shrimp processing waste utilization: An industrial prospective. Trends Food Sci. & Technol. 103, 20–35.
PEARSON, R., 1987. Barramundi breeding research–laying the foundations for industry. Aust. Fish. 46, 2–3.
PHUONG, P.T.D., TRUNG, T.S., STEVENS, W.F., MINH, N.C., BAO, H.N.D., HOA, N.V., 2022. Valorization of heavy waste of modern intensive shrimp farming as a potential source for chitin and chitosan production. Waste Biomass-.-. Valoriz. 13, 823–830.
PLUMB, J.A., AREECHON, N., 1990. Effect of malathion on humoral immune response of channel catfish. Dev. & Comp. Immunol. 14, 355–358.
QI, L., XU, Z., JIANG, X., HU, C., ZOU, X., 2004. Preparation and antibacterial activity of chitosan nanoparticles. Carbohydr. Res. 339, 2693–2700.
QIN, Y., WANG, J., SU, Y., WANG, D., CHEN, X., 2006. Studies on the pathogenic bacterium of ulcer disease in Epinephelus awoara. Acta Oceanol. Sin. /Haiyang Xuebao 23, 154–159.
RAMPINO, A., BORGOGNA, M., BLASI, P., BELLICH, B., CESÀRO, A., 2013. Chitosan nanoparticles: Preparation, size evolution and stability. Int. J. Pharm. 455, 219–228.
RINAUDO, M., 2006. Chitin and chitosan: Properties and applications. Progress. Polym. Sci. 31, 603–632.
Saeed, M.O., 1995. Association of Vibrio harveyi with mortalities in cultured marine fish in Kuwait. Aquaculture 136, 21–29.
SAURABH, S., SAHOO, P., 2008. Lysozyme: an important defence molecule of fish innate immune system. Aquac. Res. 39, 223–239.
SHELDON, B.C., VERHULST, S., 1996. Ecological immunology: costly parasite defences and trade-offs in evolutionary ecology. Trends Ecol. & Evol. 11, 317–321.
Stills Jr., H..F, 2005. Adjuvants and Antibody Production: Dispelling the Myths Associated with Freund's Complete and Other Adjuvants. ILAR J. 46 (3), 280–293.
TAFALLA, C., BØGWALD, J., DALMO, R.A., 2013. Adjuvants and immunostimulants in fish vaccines: current knowledge and future perspectives. Fish. & Shellfish. Immunol. 35, 1740–1750.
TRUNG, T.S., PHUONG, P.T.D., MINH, N.C., THUONG, N.T.N., PRINYAWIWATKUL, W., BAO, H.N.D., VAN HOA, N., 2023. Swollen-state preparation of chitosan lactate from moulted shrimp shells and its application for harvesting marine microalgae Nannochloropsis sp. Int. J. Biol. Macromol. 244, 125337.
WANG, B., YU, J., LI, Y., JI, W., XU, H., 2002. Isolation and identification of pathogen (Vibrio harveyi) from sea perch, Lateolabrax japonicus. J. Fish. Sci. China 9, 52–55.
WOLFBEIS, O.S., 2015. An overview of nanoparticles commonly used in fluorescent bioimaging. Chem. Soc. Rev. 44, 4743–4768.
WU, Y., RASHIDPOUR, A., ALMAJANO, M.P., METÓN, I., 2020. Chitosan-based drug delivery system: Applications in fish biotechnology. Polymers 12, 1177.
WU, T., ZIVANOVIC, S., 2008. Determination of the degree of acetylation (DA) of chitin and chitosan by an improved first derivative UV method. Carbohydr. Polym. 73, 248–253.
YE, J., KAATTARI, I.M., MA, C., KAATTARI, S., 2013. The teleost humoral immune response. Fish. & Shellfish. Immunol. 35, 1719–1728.
ZHANG, H., NEAU, S.H., 2001. vitro degradation of chitosan by a commercial enzyme preparation: effect of molecular weight and degree of deacetylation. Biomaterials 22, 1653–1658.
ZORRILLA, I., ARIJO, S., CHABRILLON, M., DIAZ, P., MARTINEZ-MANZANARES, E., BALEBONA, M., MORINIGO, M., 2003. Vibrio species isolated from diseased farmed sole, Solea senegalensis (Kaup), and evaluation of the potential virulence role of their extracellular products. J. Fish. Dis. 26, 103–108.

Regional Studies in Marine Science 101 (2026) 105314

Contents lists available at ScienceDirect

Regional Studies in Marine Science

journal homepage: www.elsevier.com/locate/rsma

Antiparasitic effects of silver nanoparticles on *Cryptocaryon irritans* and toxicity in juvenile *Trachinotus* spp.

Kim Minh Anh [a], Vu Duc Manh [a], Ngo Van Manh [b], Truong Dinh Hoai [a], Nguyen Manh Hung [c], Kim Van Van [a,*]

[a] Faculty of Fisheries, Vietnam National University of Agriculture, Vietnam
[b] School of Fisheries and Life Sciences, Nha Trang University, Vietnam
[c] Institute of Biology, Graduate University of Science and Technology, Vietnam Academy of Science and Technology, Vietnam

ARTICLE INFO

Dataset link: Raw data supporting the study: Antiparasitic effects of silver nanoparticles on Cryptocaryon irritans and toxicity in juvenile Trachinotus spp.

Keywords:
Acute toxicity
Cryptocaryon irritans
Marine aquaculture
Silver nanoparticles
Trachinotus spp

ABSTRACT

White spot disease caused by *Cryptocaryon irritans* remains a major challenge in marine aquaculture, particularly in intensive cage-culture systems. This study evaluated the antiparasitic activity of silver nanoparticles (AgNPs) against two critical developmental stages of *C. irritans* and assessed their acute toxicity in juvenile golden pompano (*Trachinotus* spp.). AgNPs were tested in seawater at concentrations of 0, 0.25, 0.50, 1.00, 2.00, and 5.00 ppm. Protomont-to-tomont development was monitored after 24 and 48 h of exposure, whereas theront survival was evaluated after 1 h. Acute toxicity to juvenile *Trachinotus* spp. was assessed during a 96-h immersion exposure. AgNPs significantly inhibited protomont-to-tomont development in a concentration-dependent manner. Tomont formation was markedly suppressed at concentrations $\geq$ 1.00 ppm and completely inhibited at 5.00 ppm. Theronts were susceptible to AgNP exposure, with survival decreasing from 83.3 $\pm$ 5.8% in the control to 4.7 $\pm$ 2.9% at 0.50 ppm, while complete mortality occurred at concentrations $\geq$ 1.00 ppm. Toxicity assays in juvenile fish showed no mortality at 0.25 and 0.50 ppm, whereas the 96-h LC_{50} was estimated at 1.42 ppm. These findings demonstrate that AgNPs can inhibit the development and survival of *C. irritans* under experimental seawater conditions, particularly during the theront stage. However, the relatively narrow margin between antiparasitic activity and host toxicity highlights the need for further optimization of exposure conditions and safety evaluation prior to practical application in marine aquaculture.

1. Introduction

White spot disease caused by *Cryptocaryon irritans* remains one of the major constraints to intensive marine fish aquaculture, particularly in coastal cage-culture systems and industrial-scale hatchery production (Dan et al., 2006; Yin et al., 2019). This ciliate parasite primarily infects the skin and gills of fish, causing epithelial damage, respiratory dysfunction, reduced growth performance, and severe mortality under heavy infection intensity (Li et al., 2022; Noga, 2010). In Vietnam, together with the rapid expansion of marine aquaculture, particularly for high-value species such as groupers, cobia, and golden pompano (*Trachinotus* spp.), outbreaks of *C. irritans* have become increasingly common and economically significant for farmers (Anh et al., 2025b).

Current control strategies for marine white spot disease remain limited due to the complex life cycle of *C. irritans*. The life cycle of *C. irritans* includes three major developmental stages: the trophont on the host, the encysted tomont in the environment, and the free-swimming theront. Mature trophonts develop within the epithelial tissues of the skin and gills and subsequently leave the fish as protomonts, which settle on the substrate and encyst as tomonts or tomocysts. Within the tomocyst, repeated division produces numerous tomites, which later emerge as infective theronts and seek a new host. Theronts are free-swimming infective stages that are relatively sensitive to chemical treatments, whereas tomonts exhibit high resistance because of their protective cyst wall and prolonged survival capability in the benthic environment (Colorni and Burgess, 1997; Dung, 2022; Fridman, 2022). These differences in susceptibility among developmental stages often result in only temporary treatment efficacy and make it difficult to completely interrupt the parasite transmission cycle in marine farming systems.

In recent years, silver nanoparticles (AgNPs) have attracted increasing attention for aquatic disease control because of their broad-

* Correspondence to: Vietnam National University of Agriculture, Gia Lam, Ha Noi, Vietnam.
E-mail address: kvvan@vnua.edu.vn (K. Van Van).

https://doi.org/10.1016/j.rsma.2026.105314
Received 29 May 2026; Received in revised form 11 July 2026; Accepted 27 July 2026
Available online 4 August 2026

spectrum antimicrobial and antiparasitic properties (Marambio-Jones and Hoek, 2010; Márquez et al., 2018). Due to their nanoscale size (1–100 nm) and high surface area-to-volume ratio, AgNPs can interact with microbial cell membranes and release Ag^+ ions, thereby disrupting cellular structure and physiological function in pathogenic organisms (Morones et al., 2005; Rai et al., 2009). In aquaculture, AgNPs have been investigated for controlling bacterial, fungal, and parasitic pathogens, particularly in studies evaluating alternative approaches to disease management in intensive farming systems (Márquez et al., 2018; Saad et al., 2024).

However, the effectiveness of AgNPs in marine environments remains controversial. High salinity and ionic strength can alter the surface characteristics of AgNPs, affecting Ag^+ release and the bioavailability of silver in aquatic systems (Behra et al., 2013). Under chloride-rich conditions, AgNPs may also undergo chlorination, forming AgCl or AgClx complexes, thereby altering their biological toxicity (Levard et al., 2013). In addition, seawater may promote aggregation and precipitation of AgNPs, reducing nanoparticle stability and limiting biological interactions (Zhang et al., 2018). For *C. irritans*, these limitations may be even more pronounced because the tomont stage is enclosed within a thick cyst wall that provides high resistance against chemotherapeutics and adverse environmental conditions (Colorni and Burgess, 1997; Yin et al., 2019). Therefore, evaluating the susceptibility of *C. irritans* at different developmental stages to AgNPs under seawater conditions is necessary to better understand both the antiparasitic potential and the practical limitations of these nanomaterials in marine aquaculture.

Despite their promising applications, the use of AgNPs in aquaculture also raises concerns regarding biosafety and environmental toxicity. Exposure to AgNPs may induce oxidative stress, impair physiological functions, and cause tissue damage in fish when exposure exceeds safe thresholds (Gagné et al., 2012). Moreover, the toxicity of AgNPs to fish gill cells can vary considerably depending on environmental composition and nanoparticle aggregation status (Yue et al., 2015). In marine fish, the risk of toxicity may be greater because osmoregulatory physiology requires continuous seawater intake, potentially increasing metal uptake and accumulation.

Golden pompano (*Trachinotus* spp.) is one of the most economically important marine fish species cultured in Vietnam and is particularly sensitive during the juvenile stage to environmental fluctuations and chemical exposure (Boi et al., 2025; Van Quang and Binh, 2023). Nevertheless, scientific information regarding the acute toxicity and safety thresholds of AgNPs for this species remains limited.

Therefore, the present study aimed to: (i) evaluate the effects of AgNPs on the survival and development of *C. irritans* during two critical life-cycle stages (protomont/tomont and theront) under *in vitro* conditions; and (ii) determine the acute toxicity and 96-h LC_{50} of AgNPs in juvenile golden pompano (*Trachinotus* spp.). Rather than proposing immediate therapeutic application, this preliminary study aimed to evaluate parasite susceptibility and identify potential biosafety limitations of AgNP exposure under seawater conditions.

2. Materials and methods

2.1. Experimental materials

The parasite *C. irritans* used in this study was isolated from three naturally infected cage-cultured golden pompano (*Trachinotus* spp.; n = 3), which were used as the source of parasite, and maintained under laboratory conditions following the method described by (Anh et al., 2025b). In general, infected fish were maintained in aerated seawater tanks to allow the parasite to complete its life cycle. Protomonts detached naturally from infected fish and settled onto the tank bottom, where they developed into tomonts under controlled conditions. Theronts released from mature tomonts were collected periodically and used for subsequent *in vitro* experiments. Prior to each experiment, parasite developmental stages were morphologically identified under light microscopy.

Healthy juvenile golden pompano were obtained from a marine fish hatchery in Quang Ninh Province, Vietnam. Fish had an average body length of 5.5–6.5 cm and body weight of 4.0–6.0 g. Prior to the experiments, individuals were clinically examined and screened for parasitic infections by fresh examination of skin and gill samples.

Fish were acclimated in 250-L plastic tanks at a density of 50 individuals per tank for 14 days before experimentation. Filtered and disinfected natural seawater was used and maintained at a salinity of 30 ± 1‰. Water quality parameters, including temperature, pH, dissolved oxygen (DO), NH_4^+/NH_3, and NO_2^-, were monitored daily. During the acclimation period, the fish were fed a commercial pellet diet containing 40% crude protein twice daily at approximately 5% of total body weight.

All experimental procedures involving animals were conducted to minimize stress and unnecessary adverse effects on the experimental fish.

2.2. Preparation of AgNPs

The silver nanoparticle formulation used in this study was a self-synthesized AgNPs–chitosan suspension containing AgNPs at a stock concentration of 2000 ppm and 0.1% (w/v) chitosan as a stabilizing agent. Before use, the suspension was gently homogenized and diluted with sterile seawater (30‰) to obtain final experimental concentrations of 0, 0.25, 0.50, 1.00, 2.00, and 5.00 ppm AgNPs. The corresponding volumes of stock solution added to the treatment media were 0.125, 0.25, 0.50, 1.00, and 2.50 mL/L sterile seawater, respectively.

The selected concentrations were based on previous studies on the biological activity and toxicity of AgNPs in aquatic organisms, particularly nanosilver concentrations of 0.1–1.5 ppm tested against *Ichthyophthirius multifiliis* and acute toxicity ranges reported for juvenile fish, and were further adjusted based on seawater conditions and preliminary screening results from this study (Dung, 2022; Johari et al., 2013; Yue et al., 2015; Zhang et al., 2018). During preparation and exposure, treatments were periodically observed for visible changes in color, aggregation, or precipitation of AgNPs in seawater.

2.3. Preparation of Cryptocaryon irritans protomonts and theronts

After trophonts detached from the host fish, protomonts were collected using a bottom-collection system and filtered through a 30–50 μm mesh to remove organic debris and impurities.

Samples were lightly centrifuged at 1500 rpm for 3 min, and the pellet containing protomonts was retained and incubated in sterile seawater at 28–30°C for 18–24 h to allow development into tomonts.

Morphologically normal protomonts were selected under a light microscope and transferred into Falcon 24-well plates at a density of 10 individuals per well in 2 mL sterile seawater. Each well was considered an independent experimental unit.

Theronts were collected immediately after tomont excystment and used for subsequent experiments.

2.4. In vitro exposure experiments

Two independent experiments were conducted to evaluate the susceptibility of critical developmental stages of *C. irritans*: (1) protomont-to-tomont development, and (2) theront survival following exposure to AgNPs. Experimental procedures were designed to evaluate the direct response of the parasite to AgNPs with minor modifications based on the method described by Kim et al. (2026).

2.4.1. Effect of AgNPs on protomont-to-tomont development

This experiment was conducted to evaluate the effects of AgNPs on the development of protomonts into mature tomonts and the subsequent

development of the parasite.

Each well of a 24-well plate contained 10 protomonts in 2 mL sterile seawater supplemented with AgNPs at concentrations of 0, 0.25, 0.50, 1.00, 2.00, and 5.00 ppm. Each treatment was performed in triplicate.

The plates were incubated at 28–30°C. Tomont formation and subsequent development were observed after 24 and 48 h under a light microscope. Tomonts were considered successfully developed when a complete cyst wall was formed, and internal cell division activity was observed within the cyst.

2.4.2. Effect of AgNPs on theront survival

This experiment was conducted to evaluate the direct effects of AgNPs on theront survival, representing the infective stage of *C. irritans*.

Theronts released from tomonts were collected and quantified using a Neubauer counting chamber. Each well contained approximately 20–25 theronts in 2 mL sterile seawater supplemented with AgNPs at concentrations identical to those used in the protomont-to-tomont development experiment. Each treatment was conducted in triplicate.

After 1 h exposure at 28°C, theronts were examined microscopically. Theronts were considered alive when active swimming behavior and normal morphology were maintained. Immobile, deformed, or non-swimming individuals were recorded as dead.

2.5. Acute toxicity test on juvenile Trachinotus spp

The acute toxicity assay was conducted according to OECD guideline 203 (Fish Acute Toxicity Test) with minor modifications appropriate for marine fish conditions. A total of 144 juvenile fish were used in the acute toxicity assay, followed the method described by Anh et al. (2025a), with six treatments, three replicates per treatment and eight fish per tank. Fish were maintained in 20-L plastic tanks containing 15 L seawater at 30‰ salinity with AgNP concentrations of 0, 0.25, 0.50, 1.00, 2.00, and 5.00 ppm.

The experiment was conducted under a semi-static exposure system, in which 50% of the water volume was renewed every 24 h and replenished with the corresponding AgNP concentration to maintain relatively stable exposure conditions and minimize water quality fluctuations.

Fish mortality was recorded at 24, 48, and 96 h post-exposure. Behavioral and physiological indicators, including swimming activity, response to external stimuli, equilibrium status, respiratory activity, and mucus secretion, were periodically monitored throughout the experiment. Dead fish were removed immediately after detection to minimize deterioration of water quality and effects on the remaining fish.

2.6. Statistical analysis

Data were analyzed using SPSS version 27.0 (IBM Corp., USA). Protomont-to-tomont development data were analyzed using one-way ANOVA followed by Tukey's post hoc test to determine differences among treatments ($p < 0.05$). Theront survival data were analyzed using the Kruskal-Wallis test. Results are presented as mean ± standard deviation (SD).

The 96-h LC_{50} value was estimated using Probit analysis with 95% confidence intervals (95% CI). Kärber's formula (1931) was additionally used as a supplementary reference method for rapid LC_{50} estimation when appropriate (Vu et al., 2024). Kaplan-Meier survival analysis was used to evaluate the probability of fish survival during AgNP exposure.

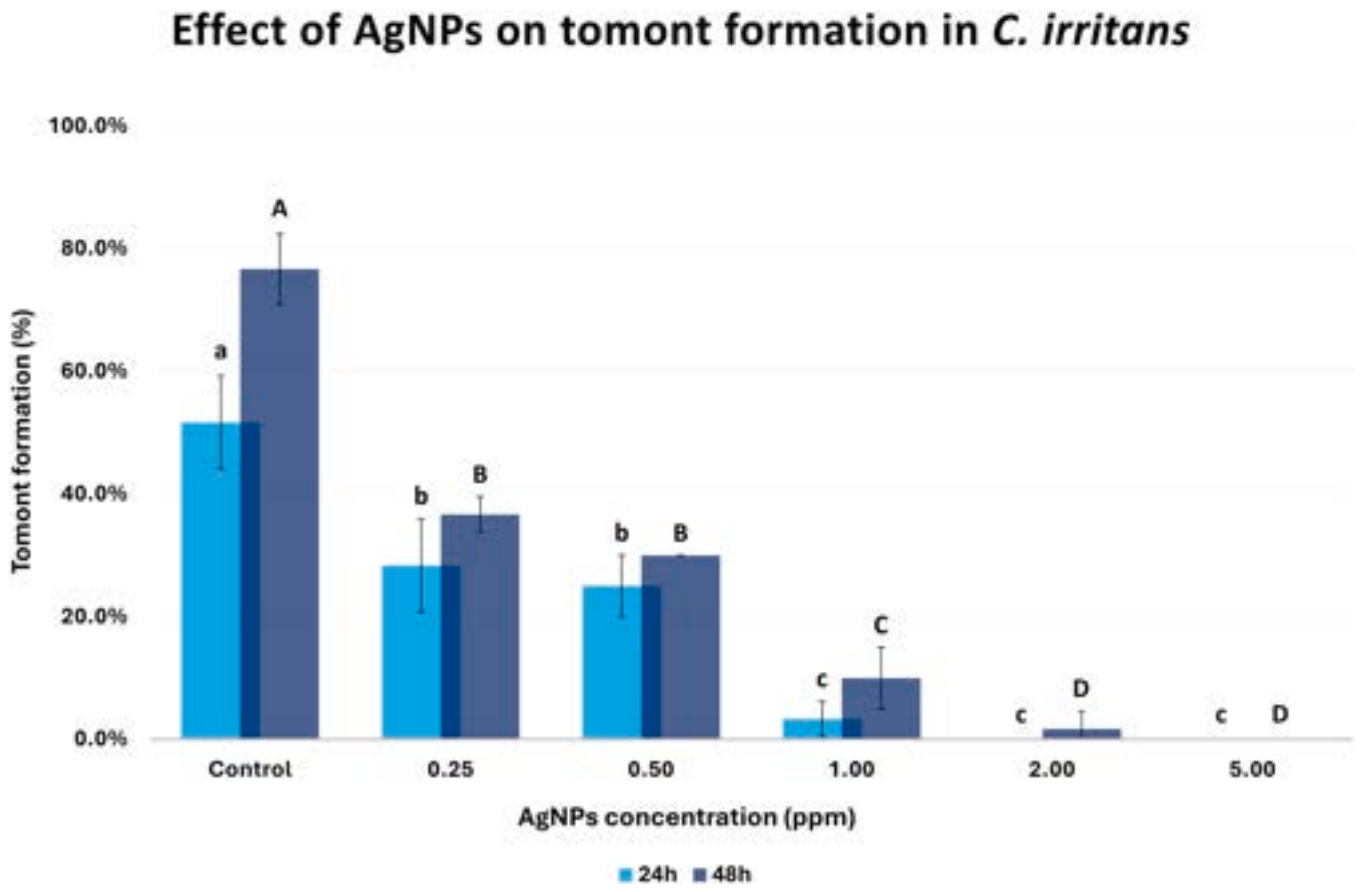

Fig. 1. Effect of AgNP exposure on tomont formation of *Cryptocaryon irritans* after 24 and 48 h incubation. Values are presented as mean ± SD (n = 3). Different lowercase and uppercase letters indicate significant differences among treatments at 24 h and 48 h, respectively (Tukey's test, $p < 0.05$).

3. Results

3.1. Effects of AgNPs on tomont formation of Cryptocaryon irritans

Exposure of protomonts to AgNPs significantly reduced their ability to develop into tomonts in a concentration-dependent manner (Fig. 1). In the control treatment, tomont formation remained high, reaching 51.7 ± 7.6% and 76.7 ± 5.8% after 24 and 48 h, respectively.

At lower AgNP concentrations (0.25–0.50 ppm), tomont formation was significantly reduced compared with the control group ($p < 0.05$). After 24 h exposure, tomont formation rates at 0.25 and 0.50 ppm were 28.3 ± 7.6% and 25.0 ± 5.0%, respectively, while corresponding values after 48 h increased to 36.7 ± 2.9% and 30.0 ± 0.0%.

A pronounced inhibitory effect on parasite development was observed at concentrations ≥ 1.00 ppm. At 1.00 ppm, tomont formation decreased to 3.3 ± 2.9% and 10.0 ± 5.0% after 24 and 48 h exposure, respectively. At 2.00 ppm, tomont formation was almost completely inhibited, with only 1.7% recorded after 48 h. No tomont formation was observed at 5.00 ppm throughout the experimental period.

Tukey's post hoc analysis revealed significant differences among treatments at both observation times ($p < 0.05$). After 24 h, the control group differed significantly from all AgNP-treated groups, while treatments ≥ 1.00 ppm exhibited strong inhibitory effects on protomont development. A similar trend was observed after 48 h, with increasing inhibition at higher AgNP concentrations.

During host infection, trophonts were observed between gill lamellae, exhibiting a spherical morphology, active movement, and attachment to host gill tissues (Fig. 2A). Localized hemorrhage, gill tissue damage, and excessive mucus secretion were observed at infection sites.

Following incubation under experimental conditions, tomonts in the control group maintained normal morphology, characterized by a regular spherical shape, distinct cyst wall, and homogeneous internal structure (Fig. 2B). No deformation or structural disruption was observed.

In contrast, tomonts exposed to AgNPs for 24 h exhibited marked morphological abnormalities (Fig. 2C). Treated tomonts lost their characteristic spherical morphology, while the cyst structure became disrupted, and internal contents appeared disorganized compared with the control group. In addition, floc-like aggregates of organic material were observed surrounding the tomonts, which may be associated with cellular degradation and/or AgNP aggregation under seawater conditions.

3.2. Effects of AgNPs on theront survival

AgNP exposure significantly reduced theront survival after 1 h exposure (Fig. 3). Theront survival remained high in the control group (83.5 ± 7.8%) and decreased markedly with increasing AgNP concentration.

At 0.25 ppm, theront survival decreased to 47.7 ± 6.0%, which was significantly lower than the control group ($p < 0.05$). Increasing the concentration to 0.50 ppm further reduced survival to 4.6 ± 4.5%. Complete immobilization of theronts was observed at concentrations ≥ 1.00 ppm, where no surviving theronts were detected during the observation period.

Statistical analysis revealed significant differences among treatments ($p < 0.05$) and demonstrated that theronts were substantially more sensitive to AgNP exposure than were tomonts.

3.3. Acute toxicity of AgNPs in juvenile Trachinotus spp

Water quality parameters remained stable throughout the experiment, with no significant differences observed between the control and AgNP-treated groups. pH ranged from 7.7 to 8.3, temperature from 25.0 to 29.0°C, dissolved oxygen from 4.0 to 7.0 mg/L, and salinity was maintained at 30‰. NH_4^+/NH_3 and NO_2^- concentrations remained within acceptable ranges for marine fish culture. Overall, environmental conditions were maintained within suitable physiological ranges for the experimental fish. Therefore, changes in survival and clinical signs observed in the treatments were considered primarily associated with AgNP exposure rather than environmental fluctuations.

During the experiment, fish exposed to higher AgNP concentrations exhibited several abnormal behavioral and physiological signs. At 2.00 and 5.00 ppm, fish showed reduced swimming activity, slower response to external stimuli, increased respiratory activity, and excessive mucus secretion prior to mortality. These signs appeared earlier and were more severe at 5.00 ppm.

The acute toxicity assay demonstrated that AgNP-induced mortality was concentration- and time-dependent (Fig. 4). No mortality was observed in the control, 0.25 ppm, or 0.50 ppm treatments throughout the 96-h exposure period.

At 1.00 ppm, cumulative mortality remained low at 4.2% after 96 h of exposure. In contrast, fish mortality at 2.00 ppm increased progressively over time. Kaplan-Meier analysis showed that fish survival decreased from 79.2% at 24 h to 58.3% at 48 h, and then further declined to 20.8% at 96 h of exposure. At the highest concentration (5.00 ppm), AgNPs caused severe acute toxicity, with survival probability decreasing to 4.2% after 24 h and complete mortality occurring before 48 h exposure. The 96-h LC_{50} value was estimated at 1.42 ppm by probit analysis ($p > 0.05$), indicating that AgNPs exert acute toxicity toward juvenile golden pompano under seawater conditions.

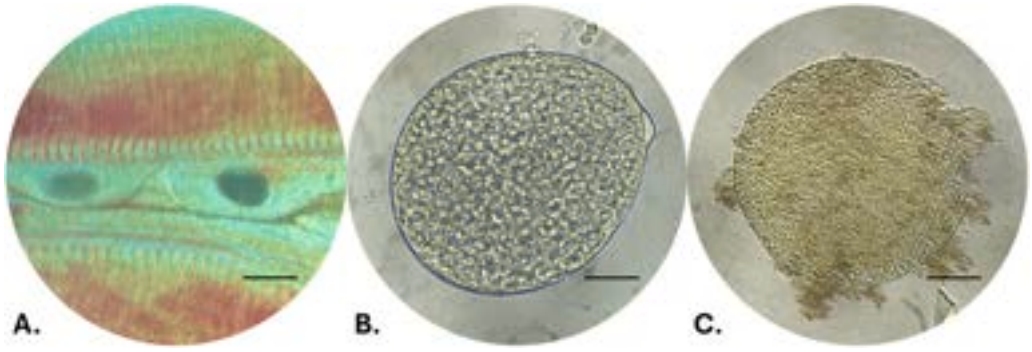

Fig. 2. Microscopic morphology of *Cryptocaryon irritans* following exposure to AgNPs. (A) Trophonts attached to the gill tissue of infected fish; (B) Normal tomont morphology observed in the control group, showing an intact spherical structure and homogeneous internal contents; (C) Damaged tomont following AgNP exposure, showing irregular morphology and disrupted cyst structure, and leakage/disorganization of internal contents. (A: 4x magnification, Scale bar = 200 μm; B–C: 40 × magnification, Scale bar = 50 μm).

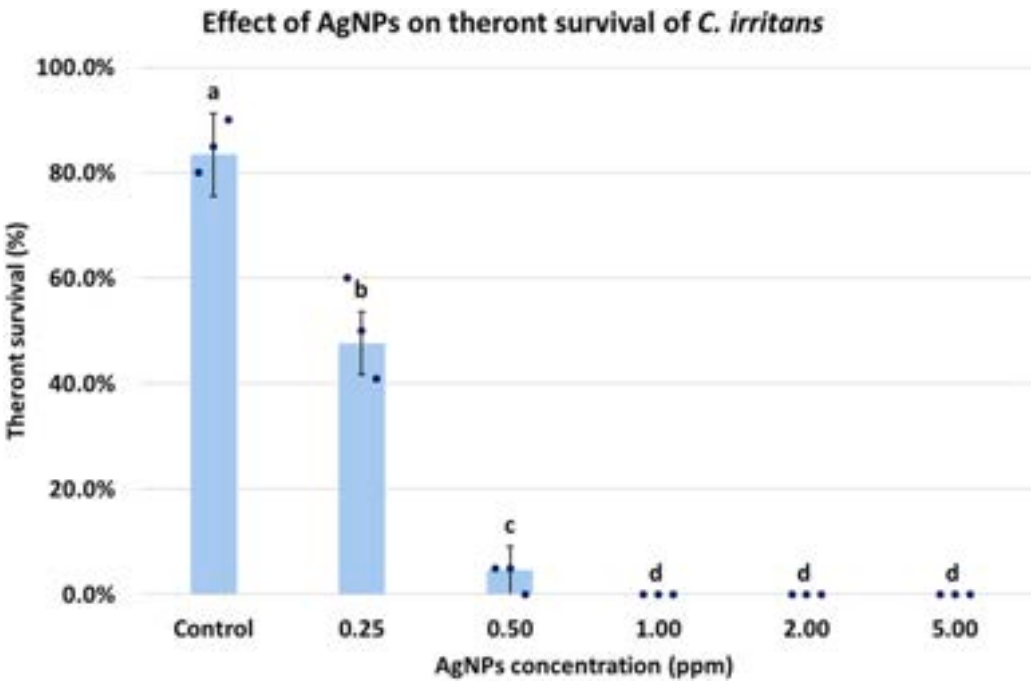

Fig. 3. Effect of AgNPs on theront survival of *Cryptocaryon irritans* after 1 h exposure Bars represent mean ± SD (n = 3), while dots indicate individual replicates. Different lowercase letters indicate significant differences among treatments ($p < 0.05$).

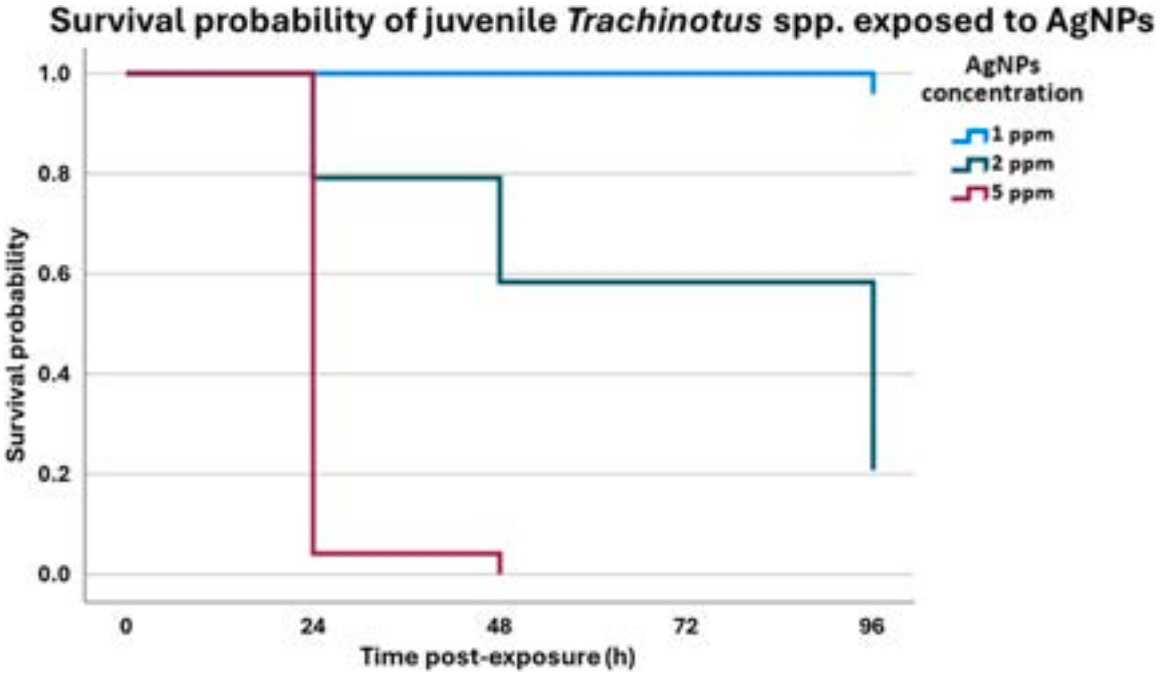

Fig. 4. Kaplan-Meier survival curves of juvenile *Trachinotus* spp. exposed to different concentrations of AgNPs during a 96-h acute toxicity assay.

4. Discussion

The present study demonstrated that AgNP exposure inhibited the development and survival of multiple developmental stages of *Cryptocaryon irritans* under seawater conditions (30‰), although parasite susceptibility varied substantially among life stages. Theronts were markedly more sensitive than protomonts/tomonts, exhibiting complete loss of motility at concentrations ≥ 1.00 ppm after short-term exposure. However, the concentrations associated with antiparasitic activity were relatively close to those inducing acute toxicity in juvenile golden pompano, highlighting a relatively narrow biosafety margin for AgNP application under marine aquaculture conditions.

AgNPs significantly inhibited the development of protomonts into mature tomonts, particularly at concentrations ≥ 1.00 ppm. These findings are consistent with the study of Saleh et al. (2017) on *Ichthyophthirius multifiliis*, a freshwater parasitic ciliate with a life cycle relatively similar to that of *C. irritans*. Their study demonstrated that AgNPs could kill theronts and suppress tomont reproduction after short-term exposure. Similarly, Dung (2022) reported that silver nanoparticles effectively affected the trophont and tomont stages of

I. multifiliis infecting snakehead fish, *Channa argus*, under in vitro conditions. The similarity among these studies suggests that free-living and reproductive transition stages of parasitic fish ciliates may share a relatively similar sensitivity to AgNPs.

Morphological observations in the present study showed that AgNP-treated protomonts exhibited deformation of cyst-like structures, loss of their characteristic spherical morphology, and leakage of internal contents compared with the intact structures observed in the control group. These alterations suggest that AgNP exposure may interfere with normal parasite development and could be associated with structural or physiological disruption of parasite cells. This interpretation is consistent with previously proposed mechanisms of AgNP toxicity, including disruption of membrane permeability, oxidative stress, and interactions between Ag^{+} ions and sulfhydryl (-SH)-containing membrane proteins (Marambio-Jones and Hoek, 2010; Morones et al., 2005; Rai et al., 2009).

The biological activity of AgNPs in seawater should be interpreted within the context of silver transformation processes in ion-rich environments. The bioavailability of AgNPs and Ag^{+} may be substantially altered by oxidation, dissolution, complex formation, and interactions with chemical constituents in the aquatic environment. Behra et al. (2013) and Zhang et al. (2018) demonstrated that AgNPs may undergo several transformation processes in aquatic systems, including oxidative dissolution, chlorination, sulfidation, and aggregation, thereby altering particle size, dispersion state, bioavailability, and toxicity. In addition, Levard et al. (2013) reported that the ionic composition of the environment, particularly chloride ions, plays an important role in controlling the chemical speciation and behavior of silver in seawater. Therefore, the aggregated organic-like materials observed around the protomont surface in the present study may reflect both parasite cell degradation and AgNP transformation under seawater conditions.

Another factor that should be considered is the role of the chitosan coating in the AgNPs–chitosan system used in this study. Chitosan may improve nanoparticle dispersion and reduce aggregation in aqueous environments, while its positive charge may influence interactions between the nanoformulation and parasite cell surfaces. Consequently, the antiparasitic activity observed in the present study may not be solely attributable to AgNPs themselves but could also be influenced by the surface characteristics of the chitosan-coated nanoformulation. However, under highly ionic seawater conditions, the dispersion behavior of the AgNPs–chitosan system may change substantially, thereby affecting the bioavailability and biological activity of the nanoparticles. This may partly explain the appearance of floc-like structures or aggregated organic materials surrounding the protomonts in the present study. Nevertheless, because a chitosan-only control treatment was not included, the individual contribution of the chitosan coating to the observed antiparasitic activity could not be completely distinguished from the effects of AgNPs. Therefore, further studies are required to specifically evaluate the role of chitosan coating in the stability, antiparasitic activity, and biological toxicity of AgNPs under seawater conditions.

Theronts were considerably more sensitive to AgNP exposure than protomonts/tomonts. After only 1 h of exposure, theronts in treatments ≥ 1.00 ppm completely lost motility and exhibited obvious structural deformation in the aquatic environment. This may be related to the biological characteristics of theronts, which are free-swimming stages with small body size and lack the protective cyst wall of tomonts, making them more vulnerable to direct exposure to AgNPs and Ag^{+} ions in the surrounding water. These findings are consistent with the study of Saleh et al. (2017), in which AgNPs showed pronounced inhibitory effects against theronts of *I. multifiliis* following short-term exposure. In addition, Kumari et al. (2025) reported antiparasitic effects of AgNPs against the fish ectoparasite *Argulus siamensis*. Although the target organism in that study was a crustacean ectoparasite rather than a protozoan ciliate, the findings suggest that AgNP-based nanoformulations may have broader applicability against aquatic parasites.

Abnormal behavioral responses observed in *Trachinotus* spp. exposed to AgNPs included reduced swimming activity, delayed responses to external stimuli, increased respiratory activity, and excessive mucus secretion, suggesting that AgNPs may affect respiratory function and gill physiology in fish. Gagné et al. (2012) reported that AgNPs could induce biological responses in rainbow trout associated with oxidative stress and inflammatory pathways. Furthermore, Yue et al. (2015) demonstrated that environmental composition and nanoparticle aggregation state may substantially influence the toxicity of AgNPs toward fish gill cells. This is particularly important under seawater conditions, where salinity and ionic composition may simultaneously alter nanoparticle dispersion, bioavailability, and toxicity.

Although AgNPs demonstrated inhibitory activity against *C. irritans*, the present study also demonstrated considerable acute toxicity to juvenile golden pompano. The 96-h LC_{50} value was determined to be 1.42 ppm, indicating acute toxicity of AgNPs under seawater conditions. This toxicity level is comparable to that reported in several previous studies on fish species. Johari et al. (2013), for example, reported a 96-h LC_{50} value of 2.16 mg/L for AgNPs in juvenile rainbow trout *Oncorhynchus mykiss*. Differences among studies may be related to fish species, developmental stage, nanoparticle characteristics, stabilizing coatings, salinity, and exposure conditions. These findings suggest that the biosafety margin of AgNPs under seawater conditions may be relatively narrow, particularly for juvenile marine fish.

The narrow gap between concentrations effective against the parasite and those toxic to fish suggests that the biosafety margin of AgNPs may be relatively limited. Therefore, prolonged treatment strategies in marine aquaculture systems should be interpreted with caution. Future studies should combine comparative cost–benefit analysis with assessments of efficacy, chronic toxicity, bioaccumulation potential, environmental persistence, biosafety, and environmental risk, as well as optimization of exposure conditions and delivery strategies. Such information will be necessary to determine whether AgNP-based approaches can be developed into safe, environmentally acceptable, and economically feasible tools for marine aquaculture.

From an economic and practical perspective, the use of AgNPs for fish disinfection or disease control should be interpreted with caution. Although the present findings demonstrate antiparasitic activity against *C. irritans* under experimental conditions, the feasibility of commercial application remains uncertain and will depend on several factors, including product cost, effective dose, treatment frequency, labor requirements, environmental management, and overall cost-effectiveness relative to existing treatment and disinfection methods. These limitations may be particularly important in open marine cage-culture systems, where continuous water exchange, dilution, currents, and tidal movements make it difficult to maintain an effective treatment concentration. Under such conditions, repeated applications or larger quantities of AgNPs may be required, potentially increasing treatment costs and reducing practical feasibility. Because the present study did not include an economic assessment, no conclusions can yet be drawn regarding the commercial viability or widespread adoption of AgNP-based treatments. At the current stage, controlled hatchery systems, short-term water treatment, or localized reduction of theront density may represent more realistic settings for further evaluation than routine application in open or large-scale mariculture systems.

Several limitations of the present study should be considered when interpreting these findings. First, the study evaluated only short-term acute toxicity and did not assess chronic effects, bioaccumulation in fish tissues, or silver residue in rearing environments. Second, the physicochemical properties of AgNPs in seawater, including particle size distribution, zeta potential, and aggregation behavior, were not characterized during the experiments. In addition, the study was conducted under *in vitro* and semi-controlled conditions without field-scale validation. Therefore, the present findings should be regarded as preliminary evidence obtained under controlled experimental conditions

rather than direct support for the field-scale therapeutic application of AgNPs in marine aquaculture systems.

5. Conclusion

This study demonstrated that AgNPs can inhibit the development and survival of *Cryptocaryon irritans* under experimental conditions, particularly during the infective theront stage, while suppressing protomont-to-tomont development in a concentration-dependent manner. However, the relatively narrow margin between antiparasitic activity and acute toxicity in juvenile *Trachinotus* spp. highlights the importance of further optimization and biosafety evaluation before practical application in mariculture systems.

The findings suggest that AgNPs may be more suitable for selective or short-term applications, such as hatchery disinfection or localized theront control, rather than prolonged whole-system treatments. In addition, the results emphasize the importance of considering nanoparticle transformation, aggregation behavior, and coating stability under seawater conditions when evaluating the biological performance of AgNP-based treatments.

Further studies on chronic toxicity, bioaccumulation, nanoparticle stability, and optimized delivery strategies are required to clarify the long-term feasibility and biosafety of AgNP applications in marine fish farming.

CRediT authorship contribution statement

Vu Duc Manh: Writing – review & editing, Validation, Methodology, Investigation, Conceptualization. **Ngo Van Manh:** Validation, Investigation, Conceptualization. **Kim Minh Anh:** Writing – original draft, Visualization, Methodology, Investigation, Formal analysis, Data curation, Conceptualization. **Kim Van Van:** Writing – review & editing, Supervision, Project administration, Methodology, Funding acquisition. **Truong Dinh Hoai:** Writing – review & editing, Supervision, Methodology. **Nguyen Manh Hung:** Writing – review & editing, Supervision, Methodology, Conceptualization.

Declaration of Generative AI and AI-assisted technologies in the writing process

During the preparation of this manuscript, the authors used ChatGPT (OpenAI) for language improvement and grammatical editing. All generated content was subsequently reviewed, verified, and edited by the authors, who take full responsibility for the final content of the manuscript.

Ethics statement

All experimental procedures involving fish were conducted under project number KHCN-FF−2025–09-O7TD in accordance with institutional guidelines for the care and use of aquatic animals and were designed to minimize stress and unnecessary suffering.

Funding

This research was financially supported under project number KHCN-FF−2025–09-O7TD through the project “Institutional Support Programme to Strengthen Vietnam National University of Agriculture’s Research and Training Capacity in the Fields of Animal Science, Aquaculture and Socio-economic”, funded by ARES, Belgium.

Declaration of Competing Interest

The authors declare that they have no known competing financial interests or personal relationships that could have appeared to influence the work reported in this paper.

Acknowledgement

This work contributes to the celebration of the 50th anniversary of Nha Trang University, located in Nha Trang City, Khanh Hoa Province, Viet Nam.

Data availability

Data will be made available on request.

Raw data supporting the study: Antiparasitic effects of silver nanoparticles on Cryptocaryon irritans and toxicity in juvenile Trachinotus spp. (Google Sheets)

References

Anh, K.M., et al., 2025a. Evaluation of the acute toxicity of Ivermectin on juvenile Golden Pompano (*Trachinotus* spp.). J. Agric. Environ. 10, 101–109. https://doi.org/10.71254/hrmpzt50.

Anh, K.M., et al., 2025b. Infection and Propagation of *Cryptocaryon irritans* on Golden Pompano (*Trachinotus* spp.) in Vietnam. Vietnam. J. Agric. Sci. 8 (4), 2715–2722. https://doi.org/10.31817/vjas.2025.8.4.04.

Behra, R., et al., 2013. Bioavailability of silver nanoparticles and ions: from a chemical and biochemical perspective. J. R. Soc. Interface 10 (87), 15. https://doi.org/10.1098/rsif.2013.0396.

Boi, V.N., et al., 2025. Effect of processing parameters to the product quality during manufacturing of fermented salting snubnose pompano (*Trachinotus blochii*). Fish. Aquat. Sci. 28 (1), 54–64. https://doi.org/10.47853/FAS.2025.e6.

Colorni, A., Burgess, P., 1997. *Cryptocaryon irritans* Brown 1951, the cause of ‘white spot disease’in marine fish: an update. Aquar. Sci. Conserv. 1, 217–238. https://doi.org/10.1023/A:1018360323287.

Dan, X., et al., 2006. A standardized method to propagate *Cryptocaryon irritans* on a susceptible host pompano *Trachinotus ovatus*. Aquaculture 258 (1-4), 127–133. https://doi.org/10.1016/j.aquaculture.2006.04.026.

Dung, L.V., 2022. Testing the Antiprotozoal Potential of Nanosilver Against *Ichthyophthirius multifiliis* on Snakehead Fish (*Channa argus*). Vietnam. J. Agric. Sci. 20 (2), 235–245.

Fridman, S., 2022. title (in: (Eds.)). Aquaculture Pathophysiology. Elsevier, Place, pp. 505–512 (in: (Eds.)).

Gagné, F., et al., 2012. Toxicity of silver nanoparticles to rainbow trout: a toxicogenomic approach. Chemosphere 89 (5), 615–622. https://doi.org/10.1016/j.chemosphere.2012.05.063.

Johari, S.A., et al., 2013. Toxicity comparison of colloidal silver nanoparticles in various life stages of rainbow trout (*Oncorhynchus mykiss*). Iran. J. Fish. Sci. 12 (1), 76–95.

Kim, A.M., et al., 2026. *In vitro* evaluation of the survival and development of *Cryptocaryon irritans* under ivermectin exposure. J. Aquac. Bamidgeh 78 (1), 136–143. https://doi.org/10.46989/001c.155623.

Kumari, P., et al., 2025. Anti-parasitic efficacy of green-synthesized silver nanoparticles on *Argulus siamensis*: an ectoparasite of fish and their effect on the expression of ion channel genes. Aquac. Int. 33 (2), 83. https://doi.org/10.1007/s10499-024-01675-1.

Levard, C., et al., 2013. Sulfidation of silver nanoparticles: natural antidote to their toxicity. Environ. Sci. Technol. 47 (23), 13440–13448. https://doi.org/10.1021/es403527n.

Li, Y., et al., 2022. *Cryptocaryon irritans* (Brown, 1951) is a serious threat to aquaculture of marine fish. Rev. Aquac. 14 (1), 218–236. https://doi.org/10.1111/raq.12594.

Marambio-Jones, C., Hoek, E.M., 2010. A review of the antibacterial effects of silver nanomaterials and potential implications for human health and the environment. J. Nanopart. Res. 12 (5), 1531–1551. https://doi.org/10.1007/s11051-010-9900-y.

Márquez, J.C.M., et al., 2018. Silver nanoparticles applications (AgNPS) in aquaculture. Int. J. Fish. Aquat. Stud. 6 (2), 5–11.

Morones, J.R., et al., 2005. The bactericidal effect of silver nanoparticles. Nanotechnology 16 (10), 2346–2353. https://doi.org/10.1088/0957-4484/16/10/059.

Noga, E.J., 2010. Fish Disease: Diagnosis and Treatment, Second edition ed. Wiley-Blackwell.

Quang, Van, N.,Binh, T.T., 2023. Mariculture development in Vietnam: present status and prospects. VMOST J. Social. Sci. Humanit. 65 (3), 11–20. https://doi.org/10.31276/VMOSTJOSSH.65(3).11-20.

Rai, M., Yadav, A., Gade, A., 2009. Silver nanoparticles as a new generation of antimicrobials. Biotechnol. Adv. 27 (1), 76–83. https://doi.org/10.1016/j.biotechadv.2008.09.002.

Saad, M.F., et al., 2024. Biocontrol of multidrug resistant pathogens isolated from fish farms using silver nanoparticles combined with hydrogen peroxide insight to its modulatory effect. Sci. Rep. 14 (1), 7971. https://doi.org/10.1038/s41598-024-58349-4.

Saleh, M., et al., 2017. Antiprotozoal effects of metal nanoparticles against *Ichthyophthirius multifiliis*. Parasitology 144 (13), 1802–1810. https://doi.org/10.1017/S0031182017001184.

Vu, M.D., et al., 2024. Using Ivermectin for treating channel catfish (*Ictalurus punctatus*) infected with *Dollfustrema bagarii*. Fish. Aquat. Sci. 27 (9), 614–621. https://doi.org/10.47853/FAS.2024.e58.

Yin, F., et al., 2019. Antiparasitic effect of copper alloy surface on *Cryptocaryon irritans* in aquaculture of *Larimichthys crocea*. Appl. Environ. Microbiol. 85 (3), e01982-18. https://doi.org/10.1128/AEM.01982-18.

Yue, Y., et al., 2015. Toxicity of silver nanoparticles to a fish gill cell line: role of medium composition. Nanotoxicology 9 (1), 54–63. https://doi.org/10.3109/17435390.2014.889236.

Zhang, W., Xiao, B., Fang, T., 2018. Chemical transformation of silver nanoparticles in aquatic environments: mechanism, morphology and toxicity. Chemosphere 191, 324–334. https://doi.org/10.1016/j.chemosphere.2017.10.016.

Regional Studies in Marine Science 99 (2026) 105108

Contents lists available at ScienceDirect

Regional Studies in Marine Science

journal homepage: www.elsevier.com/locate/rsma

Development of chitosan-red onion peel extract coatings for enhancing the quality and shelf life of houndfish (*Tylosurus crocodilus*) during ice storage

Nguyen Thi Nhu Ha [a,*], Nguyen Cong Minh [b], Vuong Thanh Tung [a]

[a] College of Aquaculture and Fisheries, Can Tho University, Can Tho, Vietnam
[b] Institute for Biotechnology and Environment, Nha Trang University, Nha Trang City, Vietnam

ARTICLE INFO

Keywords:
Antioxidant and antibacterial properties
Chitosan-red onion peel extract coatings
Fish preservation
Houndfish

ABSTRACT

This study investigated the effectiveness of 1.5% (w/v) chitosan coatings incorporated with red onion peel extract (ROPE) in improving the quality and shelf life of houndfish (*Tylosurus crocodilus*) during ice storage. The incorporation of ROPE significantly enhanced the antioxidant capacity of chitosan coatings, increasing DPPH radical scavenging activity from 31.6% to 74.0%. Chitosan showed antibacterial activity against *Bacillus cereus* and *Salmonella enterica* with an MIC of 234 μg/mL. The addition of ROPE significantly improved its effectiveness, lowering the MIC to 29 μg/mL (chitosan combined with 125 μg/mL ROPE). This substantial reduction highlights a strong synergistic interaction between chitosan and ROPE-derived phenolic compounds, significantly improving antibacterial activity. During 24 days of ice storage, ROPE-enriched coatings, particularly at 500–1000 μg/mL, effectively delayed quality deterioration by suppressing microbial growth, protein degradation, and lipid oxidation. These treatments maintained lower pH, total volatile basic nitrogen (TVBN), and total viable counts (TVC), while reducing TCA-soluble peptide formation and preserving myofibrillar protein integrity, as confirmed by SDS-PAGE. In addition, lipid oxidation was significantly reduced, with lower peroxide value (PV) and TBARS than in control and chitosan-only samples. Furthermore, ROPE incorporation improved water holding capacity, maintained texture, and extended sensory acceptability for up to 24 days. Pearson correlation analysis revealed strong negative relationships between sensory quality and spoilage indicators (pH, TVBN, TVC, PV, TBARS, and TCA-soluble peptides), while texture showed a positive correlation with overall acceptability, confirming the effectiveness of CROPE in delaying quality deterioration. Overall, 1.5% chitosan combined with ROPE represents a promising bioactive coating strategy for enhancing seafood quality and shelf life stability during ice storage.

1. Introduction

Seafood is an essential source of high-quality protein and micronutrients, playing a critical role in global food security. However, its high content of unsaturated fatty acids makes it highly susceptible to oxidative spoilage if not adequately preserved (Ebirim and Long, 2024; Siddiqui et al., 2024). Conventional preservatives such as salt, vinegar, and synthetic additives are widely used to extend seafood shelf life but may compromise sensory quality and raise safety concerns due to potential chemical hazards. Additionally, seafood is commonly packaged in plastic films to maintain freshness; however, petroleum-based materials pose environmental and potential health risks (Ceballos-Santos et al., 2024; Rustagi et al., 2011).

Biodegradable materials include biopolymers such as polysaccharides (e.g., chitosan), lipids, and proteins, which are readily degradable, abundant, and sustainable in nature (Kumar et al., 2022). Among these, chitosan, derived from chitin obtained from aquatic exoskeletons, has attracted considerable interest due to its antimicrobial activity, biodegradability, biocompatibility, and low toxicity (Jiménez-Gómez and Cecilia, 2020; Shahidi, 2007). Chitosan has been widely applied as an edible coating to inhibit microbial spoilage in seafood and meat products; however, quality deterioration during storage also involves oxidative reactions associated with post-mortem enzymatic autolysis (Özogul et al., 2004; Yaghoubi et al., 2021). Consequently, chitosan-based systems combined with plant-derived polyphenols have gained increasing interest as sustainable preservation materials because of their synergistic antioxidant and antimicrobial properties (Eranda et al., 2024; Wang et al., 2022).

* Corresponding author.
E-mail address: nhuha@ctu.edu.vn (N.T.N. Ha).

https://doi.org/10.1016/j.rsma.2026.105108
Received 13 April 2026; Received in revised form 27 May 2026; Accepted 28 May 2026
Available online 1 June 2026

Global onion production is approximately 100 million tons per year, generating over one million tons of waste such as peels, roots, and damaged bulbs, putting pressure on the environment if not properly managed (Jaganmohanrao, 2025).Red onion peel is a rich source of flavonoids and polyphenolic compounds, including quercetin, with strong antioxidant and antimicrobial potential (Barbosa et al., 2023; Roy et al., 2022). Previous studies demonstrated that onion peel extracts incorporated into chitosan films enhanced radical scavenging activity and inhibited foodborne pathogens such as *Staphylococcus aureus* and *Escherichia coli* (Wang et al., 2022). Moreover, polyphenolic compounds may interact with chitosan through hydrogen bonding and complex formation, contributing to improved film compactness and bioactivity, while pH-dependent release kinetics may support the sustained release of active compounds during storage (Popa et al., 2000). Nevertheless, the application of chitosan coatings enriched with red onion peel extract (ROPE) for seafood preservation remains limited, particularly for marine fish species.

Houndfish (*Tylosurus crocodilus*), found in oceans worldwide (Froese and Pauly, 2024), is a nutritionally valuable marine species but is highly perishable and susceptible to rapid spoilage without proper preservation, highlighting its suitability for seafood preservation studies. Furthermore, the species was selected because houndfish are readily available in the Mekong Delta region of southern Vietnam. Since most production originates from offshore fishing, inadequate preservation during postharvest handling can result in substantial quality deterioration and economic losses before inland processing. Despite these challenges, effective and sustainable preservation strategies for houndfish remain limited. Therefore, this study aimed to investigate the antimicrobial and antioxidant efficacy of a 1.5% (w/v) chitosan coating incorporated with different concentrations of red onion peel extract and to evaluate its effectiveness in maintaining the quality of houndfish during ice storage.

2. Materials and methods

2.1. Materials

Fresh houndfish (*T. crocodilus*) caught in Nam Du, Vietnam. The chitosan, from *Penaeus vannamei* shrimp produced by Nha Trang University, has a molecular weight of 185 ± 15 kDa, medium molecular weight (MMW) chitosan, 88.3 ± 2.2% deacetylation, viscosity of 169 ± 5.25 mPa·s (1% CTS prepared in 1% acetic acid), over 99% solubility, mineral content of 0.82 ± 0.05%, and protein of 0.67 ± 0.07%. Red onion peels are collected locally.

2.2. Coating solution preparation

Red onion peel extract (ROPE) and 1.5% w/v chitosan solution (CTS) were prepared following our previous publications (Ha et al., 2025, 2024). In this study, chitosan coating solutions (1.5%, w/v) were combined with ROPE at concentrations of 27 μg/mL, 500 μg/mL, and 1000 μg/mL, designated CROPE1, CROPE2, and CROPE3, respectively. The viscosities of CTS, CROPE1, CROPE2, and CROPE3 were 504.6 ± 4.5; 495.6 ± 3.1; 491.9 ± 7.2; 466.3 ± 7.5 mPa·s, respectively. All coating treatments were applied under identical immersion conditions to minimize potential variability.

2.3. Determination of antioxidant and antibacterial properties

DPPH radical-scavenging activity was measured by Sharma and Bhat (2009), with modifications. 100 μL of DPPH (6×10^{-4} M) was combined with 100 μL of test samples (including ROPE and CROPE (CTS combined with ROPE), where ROPE consists of extracts at concentrations of 0, 10, 15, 20, 25, and 30 μg/mL; CROPE is a 1.5% w/v chitosan solution mixed with ROPE) and left to incubate in the dark at room temperature for 60 min. Absorbance was measured at 517 nm to calculate antioxidant DPPH free radical neutralization activity (%): E (%) = (ODc - ODm) / ODc × 100, where ODc is the negative control, and ODm is the sample.

The antibacterial activity of CTS and CROPE was evaluated using the dilution method of Sarker et al. (2007). Chitosan solution (15, 000 μg/mL, equivalent to 1.5%, w/v) was prepared in 1% (v/v) acetic acid (equivalent to 10,000 μg/mL). Resazurin and gentamicin solutions were made in sterile distilled water at concentrations of 0.1 mg/mL and 100 mg/mL, respectively. *Bacillus cereus* (ATCC 11778) and *Salmonella enterica* (ATCC 13076) were cultured in Mueller Hinton Broth (MHB) at 37°C for 24 h. Afterward, the broth was centrifuged, and pellets were resuspended in saline (0.85%). Subsequently, the bacterial suspensions were diluted to achieve a final density of 5×10^6 CFU/mL in MHB medium. The CTS and CROPE test solutions were prepared by serial dilution to achieve final CTS concentrations ranging from 3750 to 7 μg/mL. In all CROPE samples, the final ROPE concentration was 125 μg/mL. Each well received a reaction mixture made of 50 μL of test solution, 50 μL of bacterial solution, and 20 μL of resazurin solution. After incubation at 37°C for 18 h, the plates were examined to determine the lowest CTS concentration, in the absence or presence of ROPE, that inhibited bacterial growth. The shift in color from bluish-purple to pink was regarded as a crucial indicator of the MIC value. The measurement was repeated three times to confirm accuracy.

2.4. Application of CROPE in the preservation of houndfish

Each houndfish was immersed in CROPE1, CROPE2, or CROPE3 solutions (1:1, w/v) for 2 min, while control samples were dipped in distilled water (DW) or 1.5% chitosan (CTS) for the same duration. After treatment, the fish were drained, hung vertically, and air-dried for 30 min at below 20 °C. Then, they were individually packed in PA bags and stored in polystyrene boxes with alternating layers of fish and ice, kept below 4 °C. A total of 105 houndfish were divided into five treatments (DW, CTS, CROPE1, CROPE2, CROPE3), with 21 fish per treatment. Samples were analyzed at days 0, 4, 8, 12, 16, 20, and 24, with three independent replicates per treatment at each time point. Before analysis, the fish was filleted, removing bones and skin. The core temperature of the houndfish ranged from 1.43 ± 0.12–2.27 ± 0.06 °C during storage, which was maintained by daily ice addition and removal of meltwater from the boxes.

2.5. Quality assessment of houndfish

2.5.1. pH measurement

The pH was measured using a pH meter (Mettler Toledo, Columbus, USA) in a homogenate prepared from 15 g of fish mince and 15 mL of 0.15 M KCl (Hultmann et al., 2012).

2.5.2. Total volatile basic nitrogen (TVBN)

TVBN was determined as described by Velho (2001). A 5 g sample was placed in a Kjeldahl tube, followed by the addition of 2 g MgO and 50 mL deionized water. The mixture was distilled for 5 min, and the distillate was collected in boric acid containing a mixed indicator (35 mg methyl red and 50 mg bromocresol green). After standing for 5 min, the solution was titrated with 0.1 N sulfuric acid.

2.5.3. Water holding capacity (WHC)

Water holding capacity (WHC) was determined according to Hultmann et al. (2012). Briefly, 1.5 g of minced fish was placed in a 15 mL centrifuge tube and centrifuged at 300 × g and 4 °C for 10 min (Mikro 22-R, Hettich Zentrifugen, Tuttlingen, Germany). WHC was expressed as the percentage of bound water remaining after centrifugation relative to the total water content.

$$\%WHC = 100 - \left(\left(\frac{M_2 - M_3}{M_2 - M_1} \right) \times 100 \right)$$

Where M_1 is the mass of the empty centrifuge tube (g), and M_2 and M_3 represent the masses of the tube with the sample before and after centrifugation, respectively (g).

2.5.4. Hardness

Texture analysis was performed using a TA-XT2i texture analyzer (Stable Micro Systems, Godalming, UK) with a 75 mm diameter cylindrical probe (P75) in a double compression test (TPA) (Saavedra et al., 2017). Fish fillets (30 × 30 × 10 mm) were equilibrated at 4 °C and compressed to 50% of their original height. Pre-test, test, and post-test speeds were set at 1.0, 2.0, and 5.0 mm/s, respectively

2.5.5. Trichloroacetic acid-soluble (TCA-soluble) peptides

TCA-soluble peptide content was determined according to Benjakul et al.(2002). Briefly, 3 g of the sample was homogenized with 27 mL of chilled 5% TCA at 11,000 rpm for 1 min, followed by incubation on ice for 30 min and centrifugation at 5000 × *g* and 4 °C for 20 min. The peptide content in the supernatant was quantified using the Lowry method (Lowry et al., 1951) and expressed as μmol tyrosine/g muscle.

2.5.6. Sodium dodecyl sulfate-polyacrylamide gel electrophoresis (SDS-PAGE)

SDS-PAGE was performed according to Laemmli (1970) with slight modifications. Fish muscle (0.5 g) was solubilized in 20 mL of SDS-urea buffer (20 mM Tris-HCl, pH 8.8, 2% SDS, 8 M urea, and 2% β-mercaptoethanol) and stirred overnight. Electrophoresis was conducted on 10% resolving and 4% stacking polyacrylamide gels at a constant current of 20 mA per gel using a Criterion system (Bio-Rad, Hercules, California, USA). Protein samples (10 μg) were loaded per well. Gels were stained with 0.1% Coomassie Brilliant Blue R−250 in methanol/acetic acid/-water (30:10:60, v/v/v) and subsequently destained using the same solvent system without dye.

2.5.7. Peroxide value (PV)

PV was determined using the ferric thiocyanate method (IDF, 2006). Fish samples (7.5 g) were extracted with 30 mL chloroform:methanol (2:1, v/v) for 3 h, followed by centrifugation at 700 × *g* and 25 °C for 5 min. The lower phase was collected for fat determination and used as the sample extract. An aliquot (1 mL) was mixed with 3.9 mL chloroform:methanol (2:1, v/v), followed by sequential addition of 50 μL 0.018 M Fe^{2+} and 50 μL 30% NH_4SCN, and vortexed for 15 s. Absorbance was measured at 480 nm against a reagent blank. PV (meq peroxide/kg lipid) was calculated from Fe^{3+} concentration using a standard regression equation ($y = ax + b$) and the fat content of the samples.

2.5.8. Thiobarbituric acid reactive substances (TBARS)

The TBARS were determined following the spectrophotometric method of Raharjo et al. (1993). Samples were homogenized and extracted with 5% TCA, then centrifuged at 1050 x*g* and 4 °C for 15 min. The supernatant was collected and adjusted to a final volume of 50 mL. An aliquot (2 mL) was mixed with 2 mL of 80 mM TBA, vortexed for 15 s, and heated in a water bath at 94 °C for 5 min. After cooling, absorbance was measured at 530 nm. A standard curve was constructed using TEP (0–10 μM). Results were expressed as mg malondialdehyde (MDA)/kg sample.

2.5.9. Total viable count (TVC)

The fish sample (25 g) underwent a decimal dilution under sterile conditions. The diluted samples were combined with the plate count media in a Petri dish, which was incubated at 30 °C for 48 h. The number of viable aerobic microorganisms per gram of sample was calculated based on the number of colonies on the Petri dish. TVC was determined using the pour plate method (NMKL, 2013).

2.5.10. Sensory assessment

Fish fillets were prepared and steamed for 10 min, then cut into pieces of approximately 3.0 × 2.0 cm for sensory evaluation, following the method of Piedrahíta Márquez et al. (2019) with minor modifications. The sensory panel consisted of 10 trained members who followed ISO 8586:2012 standards to identify quality parameters and descriptive attributes and to use scoring scales, with eight training sessions totaling 18 h. Cooked fish samples were presented on white paper plates under white fluorescent lighting at room temperature and were randomly coded with three-digit numbers. Samples were evaluated for odor, color, texture, appearance, and overall acceptability using a five-point hedonic scale (1 = dislike extremely; 2 = dislike; 3 = neutral; 4 = like; 5 = like extremely).

2.6. Data analysis

All data were shown as mean ± standard deviation. Data were analyzed using one-way ANOVA followed by Tukey's multiple comparison test at a significance level of $p < 0.05$. Statistical analyses were performed using Minitab 20.0 and GraphPad Prism 10.0.0. Pearson correlation assessed parameter relationships.

3. Results and discussion

3.1. DPPH radical scavenging activity of ROPE and CROPE

The antioxidant activity of CROPE solutions was evaluated using the DPPH radical scavenging assay (Fig. 1a), based on the reduction of DPPH radicals and the corresponding decrease in absorbance (Gulcin, 2025). The 1.5% (w/v) chitosan solution exhibited a scavenging activity of 29.7%, attributed to the interaction of its amino groups (-NH_2) with free radicals (Farajzadeh et al., 2016). Red onion peel extract (ROPE) showed strong antioxidant capacity, with an IC_{50} of 27 μg/mL and a total phenolic content of 467 mg GAE/g (Ha et al., 2025). Incorporation of ROPE into chitosan significantly enhanced DPPH scavenging activity, increasing from 31.6% to 74.0% with ROPE concentrations of 10–30 μg/mL ($p < 0.0001$), corresponding to a 1.1–2.5 fold increase compared to chitosan alone. Notably, CROPE exhibited 9–18% higher activity than ROPE alone at equivalent concentrations. While ROPE showed no significant difference between 10 and 15 μg/mL, CROPE exhibited significantly higher values at 15 μg/mL than at 10 μg/mL ($p < 0.0001$). In addition, both CROPE concentrations were higher than their corresponding ROPE concentrations, indicating improved antioxidant efficiency. This synergistic effect probably results from interactions between chitosan and polyphenols, enhancing radical scavenging through hydrogen bonds and functional group interactions (Bertolo et al., 2021). Similar enhancements have been reported for chitosan films enriched with plant extracts (Wang et al., 2022), highlighting the potential of ROPE as an effective additive in bioactive coatings.

3.2. The antibacterial activity of CTS and CROPE

Antibacterial activity of chitosan (CTS) and CROPE against *Bacillus cereus* and *Salmonella enterica* is illustrated in Fig. 1b. Chitosan is a cationic polysaccharide whose positively charged amino groups enable electrostatic interactions with negatively charged bacterial cell components, such as lipopolysaccharides (LPS) in Gram-negative bacteria and teichoic acids in Gram-positive bacteria, leading to membrane disruption and leakage of intracellular contents (Helander et al., 2001).

The initial samples (column A) were subjected to a two-fold serial dilution to column N, resulting in progressively decreasing concentrations. Pink coloration indicated bacterial growth, while unchanged wells indicated inhibition. For both *B. cereus* (ATCC 11778) and *S. enterica* (ATCC 13076), chitosan exhibited antibacterial activity at wells E4-E6 (234 ppm), where no color change was observed, indicating an MIC of

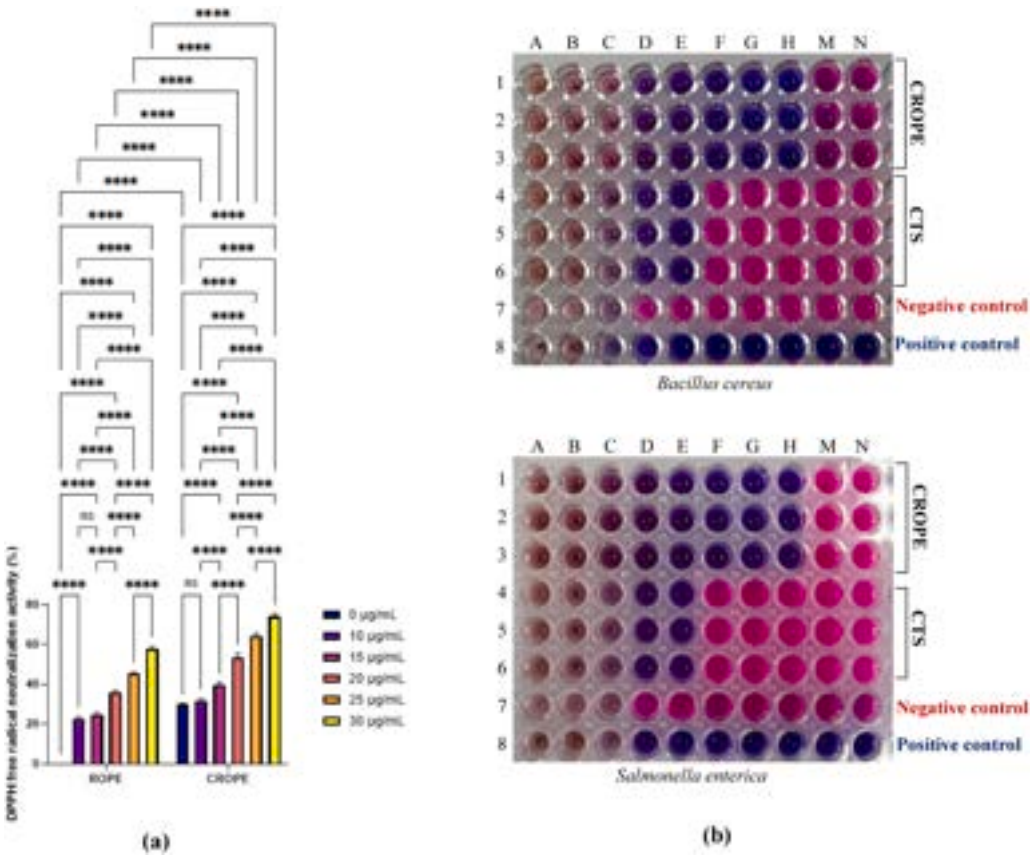

Fig. 1. Antioxidant and antibacterial activities. **(a)** DPPH free radical neutralization activity (%) of ROPE and CROPE; ROPE: red onion peel extract; CROPE: chitosan solution combined with ROPE, where ROPE concentrations of 0, 10, 15, 20, 25, and 30 µg/mL; ns: no significance; **** ($p < 0.0001$). **(b)** Antibacterial activity of chitosan (CTS) and CROPE on *Bacillus cereus* and *Salmonella enterica*; CROPE: chitosan was serially diluted in wells A-N (3750−7 µg/mL) + 125 µg/mL ROPE + indicator + bacteria; CTS: chitosan was serially diluted in wells A-N (3750−7 µg/mL) + indicator + bacteria; Negative control: Acetic acid was serially diluted in wells A-N (2500−5 µg/mL) + indicator + bacteria; Positive control: Gentamicin was serially diluted in wells A-N (25,000−49 µg/mL) + indicator + bacteria.

234 µg/mL. In contrast, acetic acid at the corresponding concentration (156 µg/mL, well E7) showed no inhibitory effect, with its MIC of 625 µg/mL (well C7), confirming that the antibacterial activity at 234 µg/mL was primarily due to the chitosan solution.

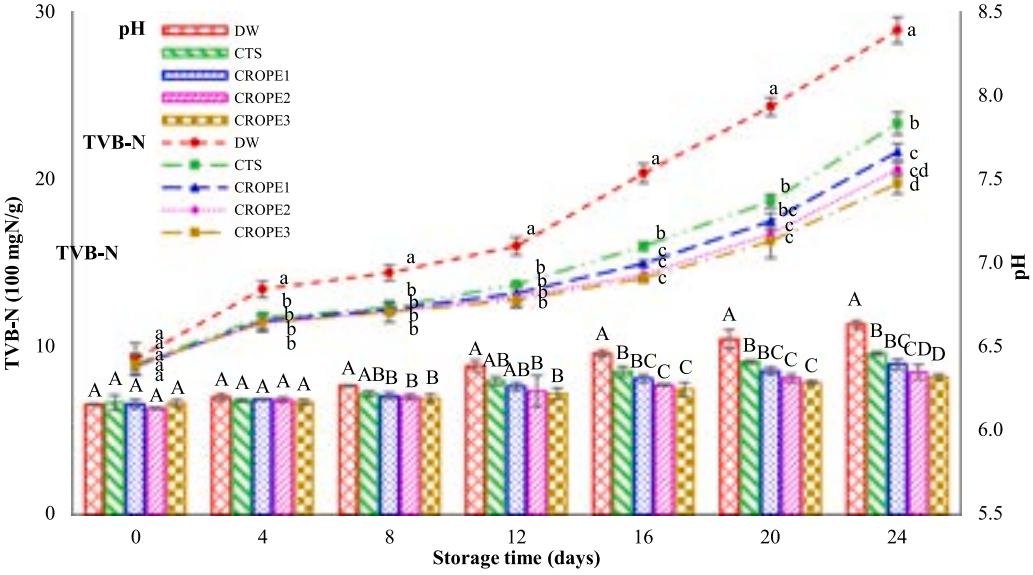

Fig. 2. Changes in pH and TVB-N of houndfish treated with DW, CTS, CROPE1, CROPE2, and CROPE3 during ice storage (mean ± SD, n = 3). Statistical significance among treatments was $p < 0.05$ and was indicated with capital letters for data obtained from pH and lowercase letters for data obtained from TVB-N. DW: houndfish treated with distilled water; CTS: houndfish treated with chitosan (1.5%, w/v); CROPE1, CROPE2, CROPE3: houndfish treated with chitosan solution combined with ROPE at the concentrations of 27, 500, 1000 µg/mL, respectively.

CROPE exhibited stronger antibacterial activity, with MIC values at wells H1–H3 (29 μg/mL chitosan combined with 125 μg/mL ROPE). The substantial reduction in MIC compared with chitosan alone provides strong evidence of synergistic effects between chitosan and ROPE polyphenols, resulting in markedly enhanced antibacterial potency. These synergistic effects may be associated with the combined actions of chitosan-mediated membrane disruption and polyphenol-induced impairment of membrane integrity and cellular metabolism. Moreover, interactions between chitosan and polyphenols may contribute to the formation of a more compact antimicrobial matrix and pH-dependent release kinetics, potentially enabling sustained antibacterial activity during storage (Helander et al., 2001; Popa et al., 2000; Wang et al., 2015).

3.3. Quality assessment of houndfish

3.3.1. pH

On the first day of storage, no significant differences in pH were observed among treatments ($p > 0.05$) (Fig. 2), indicating that chitosan and CROPE coatings did not affect the initial pH of houndfish. During cold storage, pH values in all samples gradually increased from 6.13 to 6.17–6.32–6.63 over 24 days (Fig. 2), mainly due to the degradation of proteins and amino acids, which produced volatile basic compounds (Hultmann et al., 2012). From day 8 onwards, DW exhibited significantly higher pH values compared to CROPE-treated samples ($p < 0.05$). After 16 days, CROPE2 and CROPE3 maintained significantly lower and more stable pH values than the 1.5% (w/v) chitosan-treated samples ($p < 0.05$), whereas no significant difference was observed between CROPE1 and chitosan alone throughout storage ($p > 0.05$). The addition of ROPE at 500 and 1000 μg/mL to CTS effectively slowed the increase in pH, thereby improving quality stability compared to DW and CTS samples. This effect is attributed to the high phenolic content of ROPE, which inhibits microbial growth and reduces the formation of basic nitrogenous compounds such as ammonia and trimethylamine (Ha et al., 2025; Zolfaghari et al., 2010).

3.3.2. TVBN

The degradation of proteins and other nitrogenous compounds by endogenous enzymes and spoilage microorganisms generates volatile bases, including ammonia, trimethylamine, and dimethylamine, collectively referred to as TVBN (Ha et al., 2025). Accordingly, TVBN values in all treatments increased progressively during storage due to microbial activity and proteolysis (Ruiz-Capillas and Moral, 2005), consistent with the observed rise in pH. Initial TVBN values ranged from 8.8 to 9.3 mg N/100 g (Fig. 2), and by day 4, DW exhibited significantly higher TVBN than all coated samples ($p < 0.05$), confirming the antimicrobial effect of the coatings in suppressing protein degradation and oxidative deamination (Fan et al., 2008). From day 16 onward, the CTS samples showed higher TVBN than the CROPE samples ($p < 0.05$). This result is consistent with the antibacterial effects of the CTS and CROPE solutions tested as mentioned above (Fig. 1B). At the end of storage, CROPE2 and CROPE3 reduced TVBN by 28.8–31.6% and 11.7–15.3% compared to DW and CTS, respectively, while further reductions were observed relative to CROPE1. These results demonstrate that ROPE at 500–1000 μg/mL effectively retarded protein degradation due to bioactive compounds, including flavonols (quercetin, kaempferol) and allicin (Chadorshabi et al., 2022). Notably, TVBN values in all treatments remained below the rejection limit of 30 mg N/100 g throughout 24 days of storage (Zolfaghari et al., 2010).

3.3.3. TVC

Total viable counts (TVC) increased progressively in all treatments during 24 days of storage but remained below the acceptability limit of 7 $\log_{10}$ CFU/g (ICMSF, 1986), except for DW, which reached 7.44 $\log_{10}$ CFU/g at the end of storage (Table 1). From day 12, CROPE2 and CROPE3 exhibited significantly lower TVC than DW and CTS, and from

Table 1
Changes in hardness (gramf), TVC (log10 CFU/g), and WHC (percentage) of houndfish treated with DW, CTS, CROPE1, CROPE2, and CROPE3 during ice storage.

Stoarge time (days)	Samples	Hardness (g_f)	TVC ($\log_{10}$ CFU/g)	WHC (%)
0	DW	18,560 ± 100^{a}	2.43 ± 0.03^{a}	83.0±0.6^{a}
	CTS	18,404 ± 148^{a}	2.27 ± 0.08^{a}	83.3±1.2^{a}
	CROPE1	18,067 ± 188^{a}	2.30 ± 0.08^{a}	83.1±1.4^{a}
	CROPE2	18,408 ± 349^{a}	2.28 ± 0.08^{a}	82.9±0.4^{a}
	CROPE3	18,136 ± 131^{a}	2.32 ± 0.21^{a}	83.1±0.8^{a}
4	DW	16,881 ± 211^{a}	2.81 ± 0.09^{a}	84.1±1.1^{a}
	CTS	17,082 ± 195^{a}	2.45 ± 0.04^{b}	83.6±0.4^{a}
	CROPE1	17,289 ± 280^{a}	2.39 ± 0.04^{b}	83.6±1.7^{a}
	CROPE2	17,274 ± 271^{a}	2.39 ± 0.04^{b}	83.3±0.7^{a}
	CROPE3	17,290 ± 211^{a}	2.37 ± 0.09^{b}	83.3±1.8^{a}
8	DW	14,519 ± 65^{d}	3.53 ± 0.10^{a}	86.7±1.2^{a}
	CTS	15,406 ± 151^{c}	2.89 ± 0.05^{b}	84.2±0.4^{ab}
	CROPE1	16,060 ± 151^{b}	2.78 ± 0.08^{bc}	83.8±0.8^{b}
	CROPE2	16,518 ± 319^{ab}	2.70 ± 0.03^{bc}	83.6±1.5^{b}
	CROPE3	16,697 ± 178^{a}	2.63 ± 0.11^{c}	83.3±1.2^{b}
12	DW	12,228 ± 287^{d}	4.68 ± 0.06^{a}	88.0±0.7^{a}
	CTS	13,136 ± 131^{c}	3.51 ± 0.08^{b}	84.9±1.0^{b}
	CROPE1	14,409 ± 301^{b}	3.35 ± 0.11^{bc}	84.7±0.7^{b}
	CROPE2	15,593 ± 163^{a}	3.22 ± 0.07^{c}	84.2±1.4^{b}
	CROPE3	15,786 ± 194^{a}	3.14 ± 0.06^{c}	83.8±1.5^{b}
16	DW	10,559 ± 104^{d}	5.92 ± 0.06^{a}	90.7±1.3^{a}
	CTS	12,161 ± 91^{c}	4.13 ± 0.14^{b}	86.7±0.7^{b}
	CROPE1	13,412 ± 300^{b}	3.85 ± 0.12^{c}	85.8±0.4^{b}
	CROPE2	14,337 ± 229^{a}	3.55 ± 0.09^{d}	85.6±1.0^{b}
	CROPE3	14,730 ± 268^{a}	3.45 ± 0.08^{d}	84.9±0.8^{b}
20	DW	7928 ± 153^{e}	6.99 ± 0.05^{a}	93.3±0.7^{a}
	CTS	10,407 ± 149^{d}	5.43 ± 0.04^{b}	87.6±0.8^{b}
	CROPE1	12,167 ± 237^{c}	5.01 ± 0.08^{c}	86.9±0.8^{b}

(continued on next page)

Table 1 (*continued*)

Stoarge time (days)	Samples	Hardness (g_f)	TVC (log_{10} CFU/g)	WHC (%)
	CROPE2	13,154 ± 307^{b}	4.65 ± 0.18^{d}	86.0±1.2^{b}
	CROPE3	13,838 ± 177^{a}	4.56 ± 0.04^{d}	85.6±0.4^{b}
24	DW	6894 ± 221^{e}	7.44 ± 0.09^{a}	95.1±0.4^{a}
	CTS	9072 ± 179^{d}	6.34 ± 0.06^{b}	90.0±0.8^{b}
	CROPE1	10,731 ± 278^{c}	6.08 ± 0.06^{c}	89.6±0.8^{bc}
	CROPE2	11,634 ± 268^{b}	5.83 ± 0.11^{d}	88.2±0.8^{bc}
	CROPE3	12,492 ± 164^{a}	5.75 ± 0.09^{d}	87.3±1.3^{c}

*Values are mean ± SD (n = 3). Values with different superscripts within the same sampling day are significantly different ($p < 0.05$). DW: houndfish treated with distilled water; CTS: houndfish treated with chitosan (1.5%, w/v); CROPE1, CROPE2, CROPE3: houndfish treated with chitosan solution combined with ROPE at the concentrations of 27, 500, 1000 μg/mL, respectively.

day 16, lower than CROPE1 ($p < 0.05$), indicating enhanced antimicrobial efficacy at higher ROPE concentrations (500–1000 μg/mL). By the end of storage, TVC values for CROPE2 (5.83 log_{10} CFU/g) and CROPE3 (5.75 log_{10} CFU/g) were not significantly different and were comparable to DW at day 16, indicating a marked delay in bacterial growth. Phenolic compounds can damage cell walls, increase membrane permeability, induce leakage of intracellular constituents, alter lipid structures, and interfere with nucleic acid synthesis and protein transport. This antimicrobial effect is enhanced by the synergistic interaction between chitosan and ROPE, whereby phenolics impair microbial membranes and metabolic functions (Shan et al., 2007), while chitosan binds to negatively charged cell surfaces, leading to membrane destabilization and intracellular leakage (Helander et al., 2001). These findings agree with Raeisi et al. (2020), TVC of the control sample reached 8.40 log CFU/g after 12 days of cold storage, whereas chitosan-coated samples enriched with plant extracts ranged from 4.93 to 6.13 log CFU/g.

3.3.4. WHC and texture

Water holding capacity (WHC), defined as the proportion of water retained after centrifugation, increased progressively in all treatments during storage, indicating reduced water retention associated with protein degradation and structural breakdown. This change might also be attributed to collagen fiber degradation and disruption of protein cross-links caused by microbial proteases (Olsson et al., 2003). No significant differences were observed within the first 4 days; however, variations became significant thereafter ($p < 0.05$). At the end of storage, the DW sample exhibited the highest WHC (95.1%), indicating greater water loss than the CTS (90.0%) and CROPE-treated samples (87.3–89.6%) ($p < 0.05$). The effectiveness of chitosan-coated samples in maintaining water retention has been reported previously (Ha et al., 2024). Notably, the CROPE3 sample retained more water than the CTS sample ($p < 0.05$). This is due to polyphenol compounds in ROPE interacting with the hydroxyl and amino groups of chitosan via hydrogen bonds, forming a denser polymer network (Wang et al., 2022).

Texture analysis showed a continuous decline in hardness from 18,067 to 18,560 g_f to 6894–12,492 g_f over 24 days (Table 1). During the initial 4 days, there was no significant difference, whereas from day 8 onward, DW exhibited significantly lower hardness than coated samples ($p < 0.05$). This softening is primarily attributed to protein degradation induced by oxidative and microbial activity (Ge et al., 2016; Piedrahíta Márquez et al., 2019). Notably, CROPE2 and CROPE3 maintained higher hardness values from day 16 ($p < 0.05$), suggesting that the combined antioxidant and antimicrobial effects of chitosan and ROPE effectively limited muscle degradation. The presence of phenolic compounds, such as quercetin, may further contribute to texture preservation by inhibiting proteolytic enzymes (e.g., cysteine cathepsin) (Xu et al., 2015)

3.3.5. TCA-soluble peptides and SDS-PAGE

TCA-soluble peptides, an indicator of protein degradation, increased from 0.24 to 0.27–1.43–3.41 μmol tyrosine/g during 24 days of storage (Fig. 3A), reflecting progressive proteolysis in houndfish muscle. The increase occurred in two phases: an initial stage dominated by endogenous enzymatic activity, followed by a later stage involving both enzymes and microbial activity (Ge et al., 2016; Yi and Xie, 2022). In the control (DW), rapid peptide accumulation was observed after day 8, whereas CTS- and CROPE-treated samples showed a delayed increase, becoming more pronounced after day 12. This delay may be attributed to chitosan's ability to inhibit enzymatic activity through hydrogen bonding and metal ion interactions (Piedrahíta Márquez et al., 2019), as well as the antimicrobial effect of ROPE (Ha et al., 2025). After 16 days, CTS and CROPE1 exhibited significantly higher peptide contents (1.42 and 1.31 μmol tyrosine/g) than CROPE2 and CROPE3 (1.13 and 1.05 μmol tyrosine/g), indicating more advanced protein degradation. No significant difference was observed between CROPE2 and CROPE3, suggesting comparable inhibitory effects at ROPE concentrations of 500 and 1000 μg/mL.

SDS-PAGE patterns of myofibrillar proteins from houndfish under different treatments on days 0 and 24 are shown in Fig. 3B. Major protein bands, including myosin heavy chain (MHC), actin, α-actinin, tropomyosin, and troponin, were clearly identified. Myosin and actin are the predominant proteins that play a key role in determining the functional properties of myofibrillar proteins. At day 0, all samples displayed comparable SDS-PAGE profiles. By day 24, additional protein bands in the 100–250 kDa range (bands I and II) and a band at approximately 75 kDa (band III) became more evident. Notably, bands I, II, III, and two bands within the range of 37–50 kDa (band IV) were absent in the DW sample but were clearly retained in the CTS- and CROPE-treated samples, indicating improved preservation of myofibrillar proteins. Moreover, CROPE2 and CROPE3 exhibited markedly higher intensities for bands I, II, III, and α-actinin than CTS and CROPE1, suggesting enhanced inhibition of proteolytic degradation. These results suggest that CROPE treatments effectively delayed proteolytic degradation of MHC and its fragments. Consistent with Ha et al. (2025) ROPE incorporation inhibited myofibrillar protein degradation during storage. Moreover, higher ROPE concentrations (500–1000 μg/mL) combined with chitosan exhibited greater protective effects than lower ROPE concentrations, indicating concentration-dependent efficacy in preserving protein structure.

3.3.6. Lipid oxidation during storage periods

Lipid oxidation plays a critical role in fish spoilage during storage, causing rancidity, discoloration, and flavor deterioration due to the high levels of unsaturated fatty acids (Ali et al., 2019; Ha et al., 2025). A critical step in lipid oxidation is the reaction between oxygen and unsaturated fatty acids, leading to the formation of hydroperoxides. PV is widely used to monitor primary oxidation, reflecting both the formation and subsequent decomposition of hydroperoxides (Ali et al., 2019; Yerlikaya et al., 2004). In this study, initial PV values ranged from 3.46 to 3.54 meq/kg and increased to 7.28–13.77 meq/kg after 24 days. In DW and CTS samples, PV increased from day 0–4, declined until day 12, and then rose again, whereas in CROPE-treated samples, this pattern was delayed by approximately 4 days (increase to day 8, decline to day 16, then increase). On day 4, CROPE2 and CROPE3 exhibited significantly lower PV than DW and CTS ($p < 0.05$). The PV of DW exceeded the acceptability threshold of 10 meq O_2/kg by day 16, while CTS and CROPE1 reached this level on day 24. In contrast, CROPE2 and CROPE3 remained below this limit throughout storage, indicating enhanced

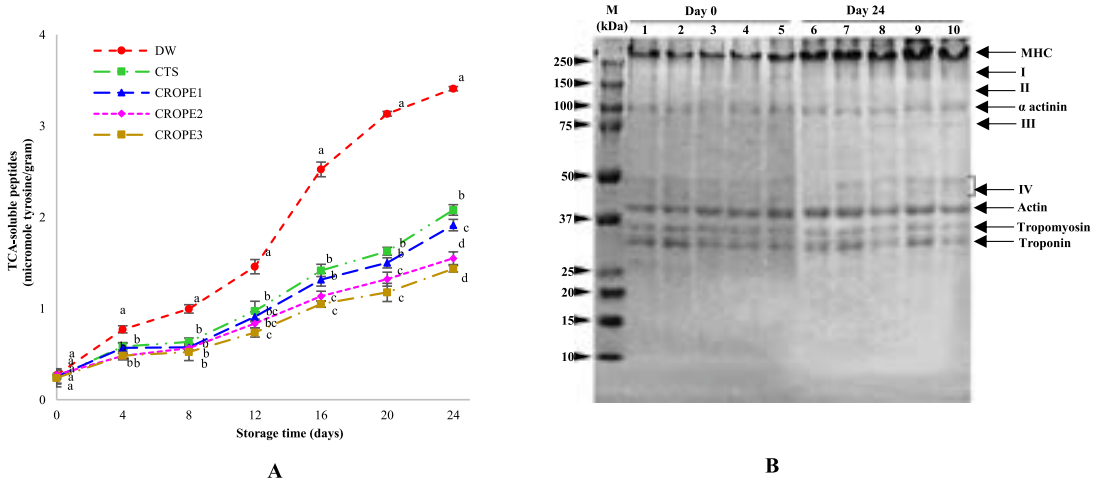

Fig. 3. Changes in TCA-soluble peptides (A) and SDS-PAGE patterns (B) of houndfish treated with DW, CTS, CROPE1, CROPE2, and CROPE3 during ice storage (mean ± SD, n = 3). Values with different superscripts among treatments are statistically significant ($p < 0.05$). DW: houndfish treated with distilled water; CTS: houndfish treated with chitosan (1.5%, w/v); CROPE1, CROPE2, CROPE3: houndfish treated with chitosan solution combined with ROPE at the concentrations of 27, 500, 1000 μg/mL, respectively; M: Marker; 1, 6: houndfish treated with DW; 2, 7: houndfish treated with CTS; 3, 8: houndfish treated with CROPE1; 4,9: houndfish treated with CROPE2; 5,10: houndfish treated with CROPE3.

oxidative stability Fig. 4.

The improved performance is attributed to the synergistic antioxidant effects of chitosan and ROPE. Chitosan can chelate metal ions and scavenge free radicals (Farajzadeh et al., 2016), while phenolic compounds in ROPE, particularly quercetin derivatives, inhibit lipid oxidation by donating hydrogen and interrupting radical chain reactions (Ali et al., 2019; Kim and Kim, 2006; Tang and Cronin, 2007). Consequently, CROPE-treated samples showed PV reductions of 14.04–38.04% compared to CTS and 26.65–47.13% compared to DW after 24 days, consistent with previous reports on polyphenol-enriched coatings (Ha et al., 2025; Raeisi et al., 2020; Zhang et al., 2020).

TBARS values (Table 2) increased during the first 12 days of storage, followed by a decline in the later stage, likely due to the decomposition of secondary oxidation products (Haghighi and Yazdanpanah, 2020). The initial increase can be attributed to the accumulation of free iron, pro-oxidants, and aldehydes generated from hydroperoxide breakdown. From days 8–24, DW and CTS samples exhibited significantly higher TBARS values than CROPE-treated samples ($p < 0.05$), indicating a faster lipid oxidation rate. This trend is consistent with previous studies reporting reduced TBARS in chitosan coatings enriched with plant-derived antioxidants (Haghighi and Yazdanpanah, 2020; Raeisi et al., 2020).

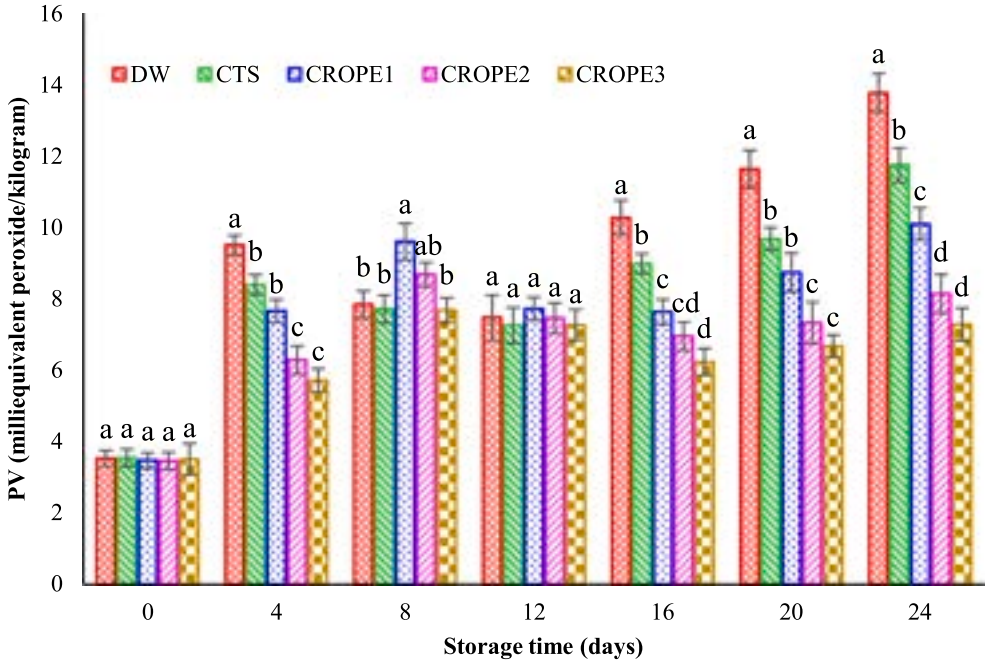

Fig. 4. Changes in peroxide value (milliequivalent peroxide/kilogram) of houndfish treated with DW, CTS, CROPE1, CROPE2, and CROPE3 during ice storage. Values with different superscripts among treatments are statistically significant ($p < 0.05$). DW: houndfish treated with distilled water; CTS: houndfish treated with chitosan (1.5%, w/v); CROPE1, CROPE2, CROPE3: houndfish treated with chitosan solution combined with ROPE at the concentrations of 27, 500, 1000 μg/mL, respectively.

Table 2
Changes in thiobarbituric acid reactive substances (milligram MDA/kilogram) of houndfish treated with DW, CTS, CROPE1, CROPE2, and CROPE3 during ice storage.

Samples	Storage time (days)						
	0	4	8	12	16	20	24
DW	0.67 ± 0.09^{a}	1.16 ± 0.04^{a}	2.15 ± 0.03^{a}	2.85 ± 0.08^{a}	2.32 ± 0.04^{a}	2.22 ± 0.06^{a}	2.03 ± 0.08^{a}
CTS	0.69 ± 0.04^{a}	1.02 ± 0.05^{b}	1.51 ± 0.06^{b}	2.11 ± 0.13^{b}	1.72 ± 0.03^{b}	1.59 ± 0.04^{b}	1.54 ± 0.04^{b}
CROPE1	0.67 ± 0.08^{a}	0.91 ± 0.05^{bc}	1.35 ± 0.04^{c}	1.79 ± 0.01^{c}	1.50 ± 0.05^{c}	1.39 ± 0.05^{c}	1.32 ± 0.02^{c}
CROPE2	0.64 ± 0.04^{a}	0.83 ± 0.07^{cd}	1.22 ± 0.04^{d}	1.46 ± 0.02^{d}	1.37 ± 0.03^{d}	1.25 ± 0.02^{d}	1.19 ± 0.04^{d}
CROPE3	0.66 ± 0.05^{a}	0.76 ± 0.05^{d}	1.10 ± 0.04^{d}	1.31 ± 0.03^{d}	1.27 ± 0.03^{d}	1.17 ± 0.05^{d}	1.09 ± 0.05^{d}

* Values are mean ± SD (n = 3). Values with different superscripts within the same sampling day are significantly different ($p < 0.05$). DW: houndfish treated with distilled water; CTS: houndfish treated with chitosan (1.5%, w/v); CROPE1, CROPE2, CROPE3: houndfish treated with chitosan solution combined with ROPE at the concentrations of 27, 500, 1000 μg/mL, respectively.

By day 24, TBARS values for DW, CTS, and CROPE1 reached 2.03, 1.54, and 1.32 mg MDA/kg, respectively, which were significantly higher than those of CROPE2 (1.09 mg MDA/kg) and CROPE3 (1.19 mg MDA/kg) ($p < 0.05$). The enhanced oxidative stability in CROPE samples can be attributed to the synergistic effects of chitosan and ROPE, in which chitosan acts as a barrier to oxygen transfer and scavenges free radicals, while the phenolic compounds in ROPE further inhibit oxidative reactions (Farajzadeh et al., 2016). Importantly, all samples remained below the acceptability threshold of 5 mg MDA/kg throughout storage (Sallam, 2007), indicating that product quality was maintained.

3.3.7. Sensory evaluation

Sensory evaluation using a hedonic scale indicated that storage time significantly affected all sensory attributes of houndfish (Fig. 5). Off-odor, a key indicator of spoilage, is commonly associated with lipid oxidation and the formation of volatile compounds such as alcohols, aldehydes, ketones, pyrazines, and furans (Pan et al., 2018; Sae-leaw and Benjakul, 2014). The DW sample showed the earliest quality deterioration, with odor and texture scores falling below the acceptability threshold (score 3) by day 12, followed by color, appearance, and overall acceptability by day 16. Chitosan coating delayed sensory decline, extending acceptability to day 20 for odor and day 24 for the remaining attributes. These findings are consistent with Ha et al. (2024), who reported sensory rejection of untreated samples after 16 days, while chitosan-coated samples (1.5–2%) maintained acceptable quality up to 20 days under iced storage. Notably, the combination of chitosan with red onion peel extract (ROPE) further enhanced preservation efficiency. While CTS and CROPE1 extended overall acceptability to day 24, higher ROPE concentrations (CROPE2 and CROPE3) maintained all sensory attributes above the acceptability threshold (>3) throughout 24 days of storage, indicating a synergistic effect in inhibiting lipid oxidation and microbial spoilage.

3.3.8. Pearson correlation

The Pearson correlation coefficients were used to assess relationships

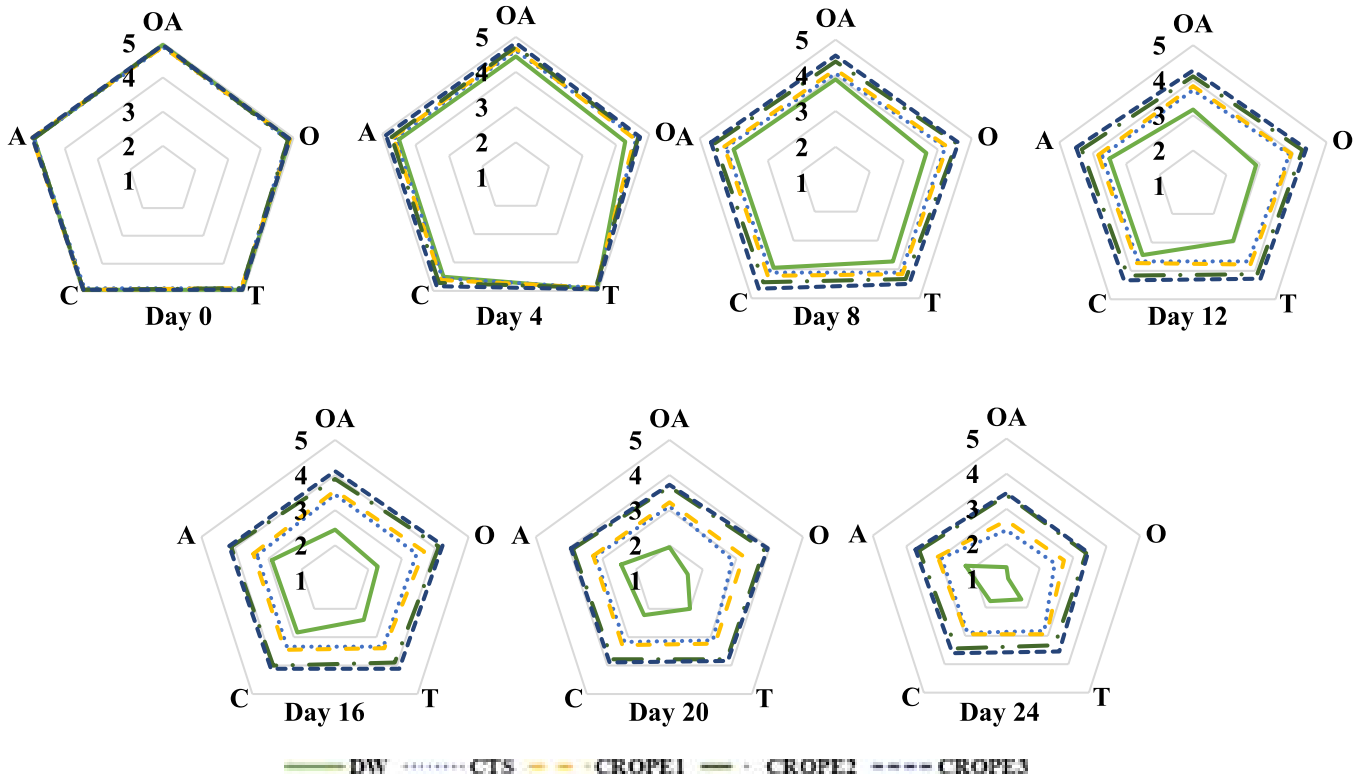

Fig. 5. Changes in sensory acceptance of color (C), odor (O), texture (T), appearance (A), and overall acceptability (OA) of houndfish treated with DW, CTS, CROPE1, CROPE2, and CROPE3 during ice storage.
DW: houndfish treated with distilled water; CTS: houndfish treated with chitosan (1.5%, w/v); CROPE1, CROPE2, CROPE3: houndfish treated with chitosan solution combined with ROPE at the concentrations of 27, 500, 1000 μg/mL, respectively.

among sensory properties, microbial load, and physicochemical characteristics, to evaluate fish freshness and quality (Ha et al., 2025). Generally, a positive correlation was observed between overall acceptability (OA) and hardness (H) ($r \geq 0.96$, $p < 0.01$), whereas the physicochemical parameters (e.g., pH, TVBN, TCA-soluble peptides, PV, and TBARs) and TVC in the samples were negatively correlated with OA (r ranged from −0.55 to −0.99, $p < 0.05$) (Fig. 6). These findings indicate that increases in quality deterioration parameters were associated with reductions in sensory quality and texture during storage. The DW and CTS samples exhibited strong correlations ($r \geq 0.8$, $p < 0.01$) for most quality parameters, except for TBARS (r ranged from 0.44 to 0.68, $p < 0.05$). In contrast, the CROPE samples showed weak to moderate correlations between PV/TBARS and other quality parameters, suggesting that ROPE supplementation may have helped retard oxidative deterioration during storage. Furthermore, TVC showed strong positive correlations with protein degradation parameters TVBN and TCA-soluble peptides ($r \geq 0.93$, $p < 0.01$), and significant negative correlations with OA and hardness ($p < 0.01$). These results suggest that the combination of CTS and ROPE effectively delayed the deterioration of fish muscle quality by suppressing microbial growth and reducing protein degradation.

4. Conclusion

The incorporation of ROPE into 1.5% (w/v) chitosan coatings markedly enhanced the preservation of houndfish during ice storage through synergistic antioxidant and antimicrobial effects. ROPE-enriched coatings, particularly at 500–1000 μg/mL, effectively inhibited bacterial growth, protein degradation, and lipid oxidation while preserving texture, water holding capacity, and sensory attributes. Overall, the synergistic interaction between chitosan and ROPE demonstrates strong potential as a sustainable, efficient strategy for extending the shelf life of houndfish during ice storage.

Funding

The study did not receive any funding.

CRediT authorship contribution statement

Nguyen Thi Nhu Ha conceptualized, curated, analyzed the data, and wrote the manuscript; **Nguyen Cong Minh** and **Vuong Thanh Tung** reviewed and edited the manuscript.

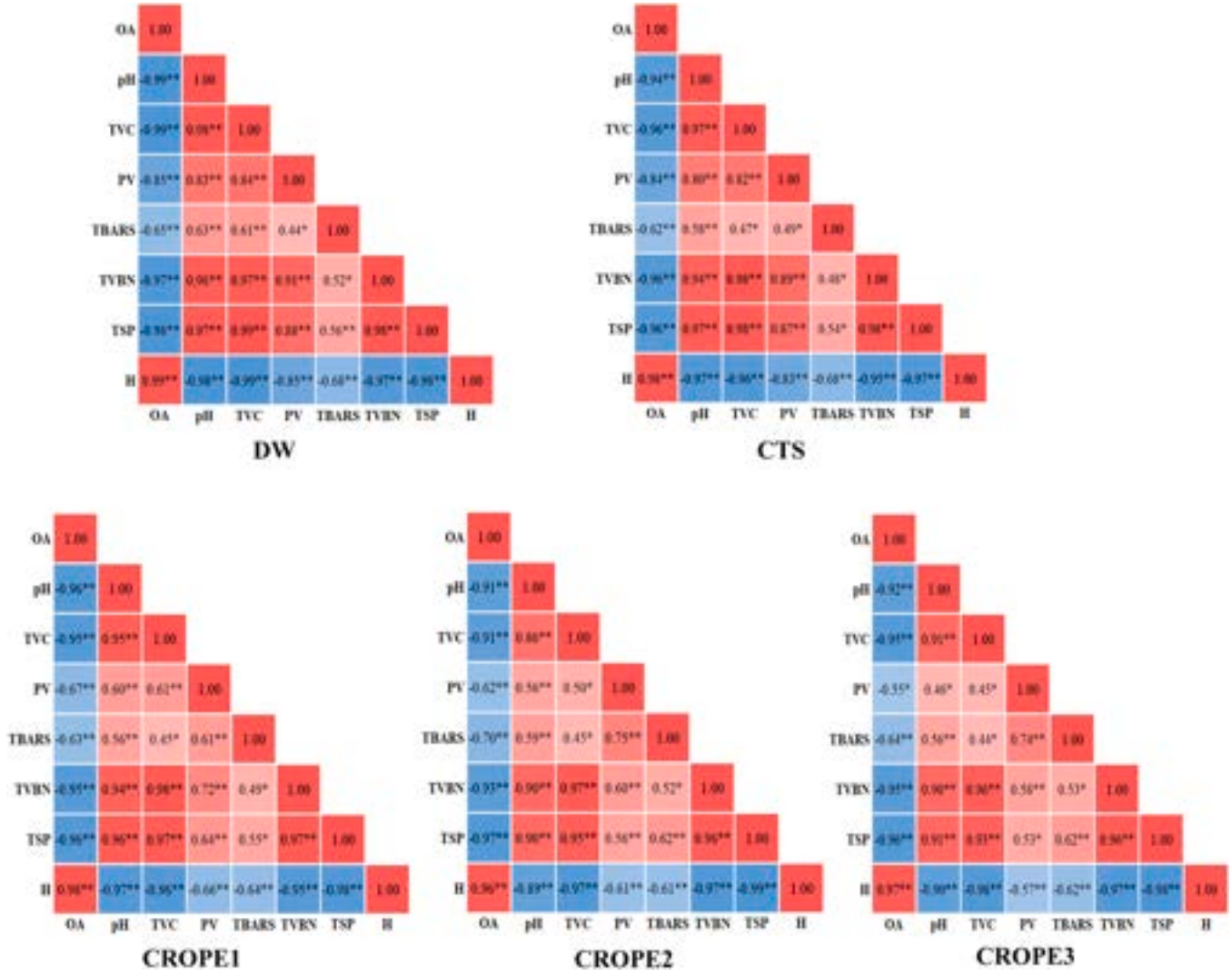

Fig. 6. Correlation coefficients between overall acceptability, pH, TVC, PV, TBARS, TVB-N, TCA-soluble peptides, and hardness in houndfish treated with DW, CTS, CROPE1, CROPE2, and CROPE3 during ice storage. Note: DW: houndfish treated with distilled water; CTS: houndfish treated with chitosan (1.5%, w/v); CROPE1, CROPE2, CROPE3: houndfish treated with chitosan solution combined with ROPE at the concentrations of 27, 500, 1000 μg/mL, respectively. Abbreviations: OA, overall acceptability; TVC, total viable count; PV, peroxide value; TBARS, thiobarbituric acid reactive substances; TVB-N, total volatile basic nitrogen; TSP, TCA-soluble peptides; H, hardness. *Correlation is significant at the 0.05 level (two-tailed). **Correlation is significant at the 0.01 level (two-tailed).

CRediT authorship contribution statement

Vuong Thanh Tung: Writing – review & editing. **Nguyen Cong Minh:** Writing – review & editing. **Nguyen Thi Nhu Ha:** Writing – review & editing, Writing – original draft, Data curation, Conceptualization.

Declaration of Competing Interest

The authors declare that they have no known competing financial interests or personal relationships that could have appeared to influence the work reported in this paper.

Acknowledgments

This work contributes to the celebration of the 50th anniversary of Nha Trang University, located in Khanh Hoa Province, Viet Nam.

Data availability

Data will be made available on request.

References

Ali, M., Imran, M., Nadeem, M., Khan, M.K., Sohaib, M., Suleria, H.A.R., Bashir, R., 2019. Oxidative stability and sensoric acceptability of functional fish meat product supplemented with plant-based polyphenolic optimal extracts. Lipids Health Dis. 18. https://doi.org/10.1186/S12944-019-0982-Y.

Barbosa, M.L., de Oliveira, L.M., Paiva, R., Dametto, A.C., Dias, D. dos S., Ribeiro, C.A., Wrona, M., Nerín, C., Barud, H. da S., Cruz, S.A., 2023. Evaluation the potential of onion/laponite composites films for sustainable food packaging with enhanced UV protection and antioxidant capacity. Molecules 28, 6829. https://doi.org/10.3390/MOLECULES28196829.

Benjakul, S., Veessanguan, W., Leelapongwattana, K., 2002. Characteristics of muscle from two species of bigeye snapper, Priacanthus tayenus and Priacanthus macracanthus. J. Food Biochem. 26, 307–326. https://doi.org/10.1111/J.1745-4514.2002.TB00756.X.

Bertolo, R., Martins, V., Plepis, A., Bogusz, J., 2021. Rheological study of the incorporation of grape seed extract in chitosan and gelatin coatings. J. Appl. Polym. Sci. 138, 50052. https://doi.org/10.1002/APP.50052;SUBPAGE:STRING:FULL.

Ceballos-Santos, S., de Sousa, D.B., García, P.G., Laso, J., Margallo, M., Aldaco, R., 2024. Exploring the environmental impacts of plastic packaging: a comprehensive life cycle analysis for seafood distribution crates. Sci. Total. Environ. 951, 175452. https://doi.org/10.1016/J.SCITOTENV.2024.175452.

Chadorshabi, S., Hallaj-Nezhadi, S., Ghasempour, Z., 2022. Red onion skin active ingredients, extraction and biological properties for functional food applications. Food Chem. 386. https://doi.org/10.1016/J.FOODCHEM.2022.132737.

Ebirim, R.I., Long, W., 2024. Evaluation of antimicrobial and preservative effects of cinnamaldehyde and clove oil in catfish (Ictalurus punctatus) fillets stored at 4 °C. Foods 13, 1445. https://doi.org/10.3390/FOODS13101445.

Eranda, D.H.U., Chaijan, M., Panpipat, W., Karnjanapratum, S., Cerqueira, M.A., Castro-Muñoz, R., 2024. Gelatin-chitosan interactions in edible films and coatings doped with plant extracts for biopreservation of fresh tuna fish products: a review. Int. J. Biol. Macromol. 280, 135661. https://doi.org/10.1016/J.IJBIOMAC.2024.135661.

Fan, W., Chi, Y., Zhang, S., 2008. The use of a tea polyphenol dip to extend the shelf life of silver carp (Hypophthalmicthys molitrix) during storage in ice. Food Chem. 108, 148–153. https://doi.org/10.1016/J.FOODCHEM.2007.10.057.

Farajzadeh, F., Motamedzadegan, A., Shahidi, S.A., Hamzeh, S., 2016. The effect of chitosan-gelatin coating on the quality of shrimp (Litopenaeus vannamei) under refrigerated condition. Food Control. 67, 163–170. https://doi.org/10.1016/J.FOODCONT.2016.02.040.

Froese, R., Pauly, D., 2024. A global information system on fishes [WWW Document]. URL ⟨https://www.fishbase.org⟩.

Ge, L., Xu, Y., Xia, W., Jiang, Q., Jiang, X., 2016. Differential role of endogenous cathepsin and microorganism in texture softening of ice-stored grass carp (Ctenopharyngodon idella) fillets, 96, 3233–3239. https://doi.org/10.1002/JSFA.7506.

Gulcin, İ., 2025. Antioxidants: a comprehensive review. Arch. Toxicol. 99, 1893–1997. https://doi.org/10.1007/S00204-025-03997-2.

Ha, N.T.N., Dao, N.L.A., Truc, T.T., 2025. Assessing red onion (Allium cepa L.) peel extract as an antioxidant and antimicrobial agent for ice storage of tilapia (Oreochromis niloticus) fillets. J. Food Process. Preserv. 2025, 6642585. https://doi.org/10.1155/JFPP/6642585.

Ha, N.T.N., Phuong, P.T.D., Minh, N.C., Nguyen, V.T., Giao, N.T.H., Thuy, L.T.M., 2024. Effect of medium molecular weight chitosan coating on quality of houndfish (Tylosurus crocodilus) during ice storage. Fish. Aquat. Sci. 27, 600–613. https://doi.org/10.47853/FAS.2024.E57.

Haghighi, M., Yazdanpanah, S., 2020. Chitosan-based coatings incorporated with cinnamon and tea extracts to extend the fish fillets shelf life: validation by FTIR spectroscopy technique. J. Food Qual. 2020, 8865234. https://doi.org/10.1155/2020/8865234.

Helander, I.M., Nurmiaho-Lassila, E.L., Ahvenainen, R., Rhoades, J., Roller, S., 2001. Chitosan disrupts the barrier properties of the outer membrane of gram-negative bacteria. Int. J. Food Microbiol. 71, 235–244. https://doi.org/10.1016/S0168-1605(01)00609-2.

Hultmann, L., Phu, T.M., Tobiassen, T., Aas-Hansen, O., Rustad, T., 2012. Effects of pre-slaughter stress on proteolytic enzyme activities and muscle quality of farmed Atlantic cod (Gadus morhua). Food Chem. 134, 1399–1408. https://doi.org/10.1016/J.FOODCHEM.2012.03.038.

ICMSF, 1986. Sampling plans for fish and shellfish. Microorganisms in Foods. Sampling for Microbiological Analysis: Principles and Scientific Applications, 2nd ed. University of Toronto Press, Toronto.

IDF, 2006. International Dairy Federation, International IDF Standards, sec. 74A [WWW Document]. URL ⟨https://cdn.standardsiteh.ai/samples/38685/159c4127dd004c50aada548310eef61a/ISO-3976-2006.pdf⟩.

Jaganmohanrao, L., 2025. Valorization of onion wastes and by-products using deep eutectic solvents as alternate green technology solvents for isolation of bioactive phytochemicals. Food Res. Int. 206, 115980. https://doi.org/10.1016/J.FOODRES.2025.115980.

Jiménez-Gómez, C.P., Cecilia, J.A., 2020. Chitosan: a natural biopolymer with a wide and varied range of applications. Molecules 25, 3981. https://doi.org/10.3390/MOLECULES25173981.

Kim, S., Kim, G., 2006. Quantification of quercetin in different parts of onion and its DPPH radical scavenging and antibacterial activity -food science and biotechnology | Korea Science. Food Sci. Biotechnol. 15, 39–43.

Kumar, A.V., Hasan, M., Mangaraj, S., M, P., Verma, D.K., Srivastav, P.P., 2022. Trends in edible packaging films and its prospective future in food: a review. Appl. Food Res. 2, 100118. https://doi.org/10.1016/J.AFRES.2022.100118.

Laemmli, U.K., 1970. Cleavage of structural proteins during the assembly of the head of bacteriophage T4 227, pp. 680–685.

Lowry, O.H., Rosebrough, N.J., Farr, A.L., Randall, R.J., 1951. Protein measurement with the folin phenol reagent. J. Biol. Chem. 193, 265–275. https://doi.org/10.1016/S0021-9258(19)52451-6.

NMKL, 2013. Nordic Committee on Food Analysis. Method 86. Aerobic microorganisms. Determination in foods at 37°C, 30°C, 25°C, 20°C, 17/7°C or 6.5°C by the colony count method. Bergen.

Olsson, G.B., Ofstad, R., Lødemel, J.B., Olsen, R.L., 2003. Changes in water-holding capacity of halibut muscle during cold storage. LWT - Food Sci. Technol. 36, 771–778. https://doi.org/10.1016/S0023-6438(03)00098-7.

Özogul, F., Polat, A., Özogul, Y., 2004. The effects of modified atmosphere packaging and vacuum packaging on chemical, sensory and microbiological changes of sardines (Sardina pilchardus). Food Chem. 85, 49–57. https://doi.org/10.1016/J.FOODCHEM.2003.05.006.

Pan, J., Jia, H., Shang, M., Li, Q., Xu, C., Wang, Y., Wu, H., Dong, X., 2018. Effects of deodorization by powdered activated carbon, β-cyclodextrin and yeast on odor and functional properties of tiger puffer (Takifugu rubripes) skin gelatin. Int. J. Biol. Macromol. 118, 116–123. https://doi.org/10.1016/J.IJBIOMAC.2018.06.023.

Piedrahíta Márquez, D.G., Fuenmayor, C.A., Suarez Mahecha, H., 2019. Effect of chitosan-propolis edible coatings on stability of refrigerated cachama (Piaractus brachypomus) vacuum-packed fish fillets. Packag. Technol. Sci. 32, 143–153. https://doi.org/10.1002/PTS.2422.

Popa, M.I., Aelenei, N., Popa, V.I., Andrei, D., 2000. Study of the interactions between polyphenolic compounds and chitosan. React. Funct. Polym. 45, 35–43. https://doi.org/10.1016/S1381-5148(00)00009-2.

Raeisi, M., Hashemi, M., Aminzare, M., Ghorbani Bidkorpeh, F., Ebrahimi, M., Jannat, B., Tepe, B., Noori, S.M.A., 2020. Effects of sodium alginate and chitosan coating combined with three different essential oils on microbial and chemical attributes of rainbow trout fillets. J. Aquat. Food Product. Technol. 29, 253–263. https://doi.org/10.1080/10498850.2020.1722777.

Raharjo, S., Sofos, J.N., Schmidt, G.R., 1993. Solid-phase acid extraction improves thiobarbituric acid method to determine lipid oxidation. J. Food Sci. 58, 921–924. https://doi.org/10.1111/J.1365-2621.1993.TB09391.X.

Roy, A., Khan, A., Ahmad, I., Alghamdi, S., Rajab, B.S., Babalghith, A.O., Alshahrani, M. Y., Islam, S., Islam, M.R., 2022. Flavonoids a bioactive compound from medicinal plants and its therapeutic applications. Biomed Res. Int. 2022, 5445291. https://doi.org/10.1155/2022/5445291.

Ruiz-Capillas, C., Moral, A., 2005. Sensory and biochemical aspects of quality of whole bigeye tuna (Thunnus obesus) during bulk storage in controlled atmospheres. Food Chem. 89, 347–354. https://doi.org/10.1016/J.FOODCHEM.2004.02.041.

Rustagi, N., Pradhan, S.K., Singh, R., 2011. Public health impact of plastics: an overview. Indian. J. Occup. Environ. Med. 15, 100. https://doi.org/10.4103/0019-5278.93198.

Saavedra, S., Rohr, R.P., Bascompte, J., Godoy, O., Kraft, N.J., Levine, J.M., 2017. A structural approach for understanding multispecies coexistence. Ecol. Monogr. 87 (3), 470–486. https://doi.org/10.1002/ecm.1263.

Sae-leaw, T., Benjakul, S., 2014. Fatty acid composition, lipid oxidation, and fishy odour development in seabass (Lates calcarifer) skin during iced storage. Eur. J. Lipid Sci. Technol. 116, 885–894. https://doi.org/10.1002/EJLT.201300381.

Sallam, K., 2007. Antimicrobial and antioxidant effects of sodium acetate, sodium lactate, and sodium citrate in refrigerated sliced salmon. Food Control. 18, 566–575. https://doi.org/10.1016/J.FOODCONT.2006.02.002.

Sarker, S.D., Nahar, L., Kumarasamy, Y., 2007. Microtitre plate-based antibacterial assay incorporating resazurin as an indicator of cell growth, and its application in the in vitro antibacterial screening of phytochemicals. Methods 42, 321–324. https://doi.org/10.1016/J.YMETH.2007.01.006.

Shahidi, F., 2007. Chitin and chitosan from marine by-products. Maximising the Value of Marine By-Products 340–373. https://doi.org/10.1533/9781845692087.2.340.

Shan, B., Cai, Y.Z., Brooks, J.D., Corke, H., 2007. The in vitro antibacterial activity of dietary spice and medicinal herb extracts. Int. J. Food Microbiol. https://doi.org/10.1016/j.ijfoodmicro.2007.03.003.

Sharma, O.P., Bhat, T.K., 2009. DPPH antioxidant assay revisited. Food Chem. 113 (4), 1202–1205. https://doi.org/10.1016/j.foodchem.2008.08.008.

Siddiqui, S.A., Singh, S., Bahmid, N.A., Sasidharan, A., 2024. Applying innovative technological interventions in the preservation and packaging of fresh seafood products to minimize spoilage - a systematic review and meta-analysis. Heliyon 10, e29066. https://doi.org/10.1016/J.HELIYON.2024.E29066.

Tang, X., Cronin, D.A., 2007. The effects of brined onion extracts on lipid oxidation and sensory quality in refrigerated cooked turkey breast rolls during storage. Food Chem. 100, 712–718. https://doi.org/10.1016/J.FOODCHEM.2005.10.042.

Velho, N.P.S., 2001. Preparation for obtaining accreditation of analytical methods regarding quality issues as stated in ISO standard ISO/IEC 17025: 1999. Final project report.

Wang, L., Campanella, O., Patel, B., Lu, L., 2015. Preparation and sealing processing of sodium alginate based blending film. Math. Probl. Eng. 2015. https://doi.org/10.1155/2015/895637.

Wang, C., Tian, S., Gao, Z., Li, Z., An, X., Lu, Y., Song, Y., Zhao, Y., 2022. Preparation and characterization of chitosan-based antioxidant composite films containing onion skin ethanolic extracts. J. Food Meas. Charact. 16, 598–609. https://doi.org/10.1007/S11694-021-01187-Z/METRICS.

Xu, Y., Ge, L., Jiang, X., Xia, W., Jiang, Q., 2015. Inhibitory effect of aqueous extract of Allium species on endogenous cathepsin activities and textural deterioration of ice-stored grass carp fillets, 8 Food Bioprocess. Technol. 8 (10), 2171–2175. https://doi.org/10.1007/S11947-015-1564-2.

Yaghoubi, M., Ayaseh, A., Alirezalu, K., Nemati, Z., Pateiro, M., Lorenzo, J.M., 2021. Effect of chitosan coating incorporated with artemisia fragrans essential oil on fresh chicken meat during refrigerated storage, 13, 716 Polymers 2021 13, 716. https://doi.org/10.3390/POLYM13050716.

Yerlikaya, P., Gokoglu, N., Uran, H., 2004. Quality changes of fish patties produced from anchovy during refrigerated storage, 3 220 Eur. Food Res. Technol. 220, 287–291. https://doi.org/10.1007/S00217-004-1035-X.

Yi, Z., Xie, J., 2022. Assessment of spoilage potential and amino acids deamination & decarboxylation activities of Shewanella putrefaciens in bigeye tuna (Thunnus obesus). LWT 156, 113016. https://doi.org/10.1016/J.LWT.2021.113016.

Zhang, X., Liu, Jing, Yong, H., Qin, Y., Liu, Jun, Jin, C., 2020. Development of antioxidant and antimicrobial packaging films based on chitosan and mangosteen (Garcinia mangostana L.) rind powder. Int. J. Biol. Macromol. 145, 1129–1139. https://doi.org/10.1016/j.ijbiomac.2019.10.038.

Zolfaghari, M., Shabanpour, B., Fallahzadeh, S., 2010. Quality preservation of salted, vacuum packaged and refrigerated mahi sefid (Rutilus frisii kutum) fillets using an onion (Allium cepa) extract. Aquac. Res. 41, 1123–1132. https://doi.org/10.1111/J.1365-2109.2009.02395.X.

Regional Studies in Marine Science 102 (2026) 105427

Contents lists available at ScienceDirect

Regional Studies in Marine Science

journal homepage: www.elsevier.com/locate/rsma

LC-MS-based chemical profiling and *in vivo* anti-inflammatory effects of the Vietnamese red alga *Tricleocarpa cylindrica*

Thi Hong Tuoi Do [a,b,1], Thanh Tra Do [a], Huong-Giang Le [a,2], Thi Kim Anh Le [b,3], Van Minh Nguyen [c,4], The Han Nguyen [c,5], Anh Duy Do [d,6], Thi Van Anh Tran [a,*,7]

[a] School of Pharmacy, University of Medicine and Pharmacy at Ho Chi Minh City, Ho Chi Minh City, 70000, Viet Nam
[b] UMP Science and Technology Center - University of Medicine and Pharmacy at Ho Chi Minh City, Ho Chi Minh City, 70000, Viet Nam
[c] Faculty of Food Technology, School of Fisheries and Life Sciences, Nha Trang University, Khanh Hoa Province, 57000, Viet Nam
[d] Northern Research Center for Marine Fisheries (NRCMF), Viet Nam Academy of Fishery Sciences (VAFIS), 224 Le Lai Street, Hai Phong City, 04000, Viet Nam

ARTICLE INFO

Keywords:
Tricleocarpa cylindrica
Marine red alga, anti-inflammatory activity
Carrageenan
Arthritis, sulfated triterpene, molecular networking

ABSTRACT

Inflammation is a protective response to harmful stimuli; however, excessive or persistent inflammation contributes to chronic disease and remains a therapeutic challenge. Marine algae are promising sources of bioactive metabolites, yet the anti-inflammatory potential and oral safety of *Tricleocarpa cylindrica* remain poorly characterized. This study characterized the chemical profile of *T. cylindrica* using LC-MS and GNPS-based molecular networking, identifying triterpene sulfates as the primary bioactive constituents. The *in vivo* anti-inflammatory activity was evaluated using carrageenan-induced paw edema, cotton pellet-induced granuloma, and acute/chronic carrageenan-induced arthritis models. The extract significantly reduced carrageenan-induced paw edema by 34.79 – 40.97% (185 mg/kg) and 35.42 – 57.95% (370 mg/kg). In the granuloma model, the 185 mg/kg group reduced granuloma weights by 22.96%. Furthermore, in acute arthritis, joint swelling decreased by 34–59% and 49–65% at 185 and 370 mg/kg, respectively, while in chronic arthritis treatment with 185 mg/kg, joint circumference decrease by 42–55% from day 3 to day 12. These results highlight the anti-inflammatory potential of *T. cylindrica* and provide promising leads for identifying novel bioactive compounds in this species.

1. Introduction

Marine macroalgae constitute one of the most diverse and underexploited biological resources in coastal and marine ecosystems. Beyond their ecological roles in primary production, habitat formation, and nutrient cycling, macroalgae have increasingly attracted scientific interest as renewable sources of structurally diverse natural products with potential applications in pharmaceuticals, nutraceuticals, cosmeceuticals, and functional foods (Choo et al., 2025, Rocha et al., 2022). Their continuous exposure to intense light, salinity fluctuations, oxidative stress, microbial colonization, and herbivory has driven the biosynthesis of a wide range of secondary metabolites, including fatty acids, sterols, terpenoids, phenolic compounds, pigments, sulfated polysaccharides, and halogenated metabolites (Choo et al., 2025, Rocha et al., 2022, Sunarwidhi et al., 2023). Many of these compounds have been reported to possess antioxidant, antimicrobial, antiviral, antidiabetic, anticancer, immunomodulatory, and anti-inflammatory properties (Choo et al., 2025, Rocha et al., 2022, Sunarwidhi et al., 2023). In this context, tropical and subtropical coastal regions, including the Vietnamese coastline, represent promising but still insufficiently explored reservoirs

* Corresponding author.
E-mail addresses: hongtuoi@ump.edu.vn (T.H.T. Do), dothanhtra0405@gmail.com (T.T. Do), lhgiang@ump.edu.vn (H.-G. Le), lethikimanh@ump.edu.vn (T.K.A. Le), minhnv@ntu.edu.vn (V.M. Nguyen), hannt@ntu.edu.vn (T.H. Nguyen), daduy@rimf.org.vn (A.D. Do), ttvananh@ump.edu.vn (T.V.A. Tran).
[1] https://orcid.org/0000-0002-5445-0694
[2] https://orcid.org/0000-0003-1962-2371
[3] https://orcid.org/0009-0004-4850-3333
[4] https://orcid.org/0000-0001-5316-8067
[5] https://orcid.org/0000-0002-8154-6739
[6] https://orcid.org/0000-0002-9561-9556
[7] https://orcid.org/0000-0001-6998-2450

https://doi.org/10.1016/j.rsma.2026.105427
Received 30 May 2026; Received in revised form 17 July 2026; Accepted 16 August 2026
Available online 10 September 2026

of marine bioactive compounds (Nguyen et al., 2013, Wiriyadamrikul et al., 2013).

Inflammation is an essential biological response to infection, tissue injury, or chemical irritation. However, when inflammatory responses become excessive, unresolved, or chronically activated, they may contribute to progressive tissue damage and the pathogenesis of several chronic diseases, including arthritis, diabetes, cardiovascular disorders, cancer, and autoimmune diseases (Chen et al., 2017). At the cellular and molecular levels, inflammatory activation involves pattern-recognition receptors, downstream signaling pathways such as nuclear factor kappa B, mitogen-activated protein kinases, and Janus kinase/signal transducer and activator of transcription; and the subsequent production of inflammatory mediators, including nitric oxide, prostaglandins, tumor necrosis factor-alpha, interleukins, and reactive oxygen species (Chen et al., 2017; Lawrence, 2009; Li and Wu, 2021; Schaper and Rose-John, 2015; Carlini et al., 2023). Although non-steroidal anti-inflammatory drugs, corticosteroids, and immunosuppressive agents remain widely used, their long-term application is limited by adverse effects such as gastrointestinal bleeding, hepatic and renal impairment, hemodynamic disturbances, osteoporosis, and increased cardiovascular risk (Varga et al., 2017, Buchman, 2001). These limitations have intensified the search for new anti-inflammatory agents from natural sources, particularly marine organisms with distinctive chemical profiles (Choo et al., 2025).

Among marine macroalgae, red algae of the family Galaxauraceae are of interest in marine natural-product research because several members contain lipophilic and steroidal metabolites with reported biological activities (Sunarwidhi et al., 2023, Rocha et al., 2022, González et al., 2015). *Tricleocarpa cylindrica* (J. Ellis & Solander) Huisman & Borowitzka, formerly reported under synonyms such as *Corallina cylindrica* and *Galaxaura cylindrica*, is a red alga belonging to the phylum Rhodophyta and the family Galaxauraceae (Wiriyadamrikul et al., 2013). This species is distributed in tropical and subtropical marine waters, including parts of the Indo-Pacific region (Wiriyadamrikul et al., 2013). In Vietnam, *T. cylindrica* has been recorded from several coastal areas, including Ly Son, Nha Trang, Kien Giang, and Phu Yen, suggesting that it may represent a locally available marine resource for further bioprospecting (Nguyen et al., 2013, Do et al., 2025). Recent taxonomic work on Vietnamese Galaxauraceae has also provided morphological descriptions and images of natural habit, fresh and dried specimens, branch details, and cellular structures, including those of *T. cylindrica* (Do et al., 2025).

Previous phytochemical investigations have indicated that *T. cylindrica* contains several classes of bioactive constituents, including fatty acids, terpenoids, diterpenes, and steroids (Sunarwidhi et al., 2023). Compounds reported from this species include tetradecanoic acid, hexadecanoic acid derivatives, methyl esters of fatty acids, terpenoid hydrocarbons, diterpenoid alcohols, and steroid-related molecules (Sunarwidhi et al., 2023). Although the extract evaluated in the present study was not chemically standardized, the known metabolite profile of *T. cylindrica* supports further testing of its pharmacological activity, particularly in relation to oxidative stress and inflammation (Sunarwidhi et al., 2023, Rocha et al., 2022).

While studies on *T. cylindrica* remain limited, available evidence suggests that this species may possess relevant pharmacological potential. Sunarwidhi et al. (2023) investigated marine algae, including *T. cylindrica*, as potential sources of compounds for conditions involving diabetes and COVID-19 comorbidity. In that study, lipid-rich extracts were obtained using a chloroform:methanol:water solvent system, and *T. cylindrica* extract exhibited hypoglycemic effects in alloxan-induced diabetic mice after 15 days of treatment. Furthermore, the extract displayed moderate *in vitro* antioxidant activity, with IC_{50} values of 252 ± 0.10 μg/mL (DPPH) and 353.22 ± 0.070 μg/mL (ABTS). Although these antioxidant activities were lower than those of ascorbic acid, they were better than those reported for some other marine algae, supporting the potential of *T. cylindrica* as a source of natural antioxidant compounds (Sunarwidhi et al., 2023).

Despite these findings, comprehensive data regarding the chemical composition and anti-inflammatory properties of *T. cylindrica* remain limited and are yet to be fully explored. Therefore, this study aims to investigate the chemical profile of this species using LC/MS techniques and evaluate its anti-inflammatory activity through various *in vivo* models. The finding provides initial pharmaceutical evidence for the potential value of *T. cylindrica* as a marine-derived bioresource from Vietnamese coastal waters.

2. Materials and methods

2.1. Sample collection and preparation

Tricleocarpa cylindrica (J. Ellis & Solander) Huisman & Borowitzka was collected by SCUBA diving from two coastal locations in Vietnam in 2024. The sample coded RVB-LS2–3 was collected in May 2024 at a depth of approximately 4.0 m from Ly Son Island, Quang Ngai Province (15°25′54″ N, 109°04′38″ E). The sample coded VHS-NT3–8 was collected in June 2024 at a depth of approximately 3.5 m from Nha Trang Bay, Khanh Hoa Province (12°11′07″ N, 109°13′40″ E). The algal material was authenticated by morphological comparison, based on external morphology and microscopic anatomical characters, with reference to published descriptions of Galaxauraceae seaweeds distributed in Vietnam (Do et al., 2025). The identification of this species was confirmed by Dr. Do Anh Duy at the Northern Research Center for Marine Fisheries, Viet Nam Academy of Fishery Sciences (VAFIS). After collection, the algal material was washed with seawater to remove sand, epiphytes, and other impurities, shade-dried to a moisture content below 12%, and ground into coarse powder for extraction. Voucher material (AlgaeNT0624) was deposited at the Department of Pharmacognosy and Traditional Pharmacy, Faculty of Pharmacy, University of Medicine and Pharmacy at Ho Chi Minh City, Vietnam.

Algae powder (2.5 kg) was percolated with 96% ethanol (30 L), and the extract was subsequently evaporated to yield 360 g of crude extract. Due to its high salt content, which could potentially interfere with the investigated pharmacological activities, a desalting process was carried out. The crude extract was dissolved in ethanol to form a concentrated solution, mixed with clean sand as the carrier, and evaporated to dryness to obtain a sample powder. This mixture was then loaded onto a column that was packed a layer of reversed-phase silica gel (100 g). Elution was performed with water (2 L) until the eluate was salt-free. Then, the organic components were eluted using 96% ethanol (0.5 L) followed by acetone (0.5 L). The ethanol and acetone eluates were concentrated under reduced pressure to yield the extract (33.25 g) with a moisture content of 10.5% and an ash content of 0.45%. This extract was used for all subsequent experiments.

2.2. Chemicals and reagents

Food-grade ethanol (96%) used for extraction was purchased from OPC Pharmaceutical Joint Stock Company (Vietnam); acetonitrile and formic acid (LC-MS grade) were supplied by Merck (Germany). Diclofenac sodium (Voltaren, VN-13293–11, Novartis, Switzerland) was used as the reference drug in the *in vivo* experiments. Carrageenan (CAS: 9000–07–1) was purchased from Sigma (Germany), and the ELISA kit test TNF-α, IL-10, IL-1β was supplied by BioLegend (USA).

2.3. Animals

Healthy male and female ICR mice, 6–8 weeks old and weighing 20–25 g, were supplied by the Biotechnology Center of Ho Chi Minh City. The animals were acclimatized for at least 5 days before experiments and maintained under standard laboratory conditions with free access to food and water. For the *in vivo* anti-inflammatory experiments, mice were randomly assigned to experimental groups according to each

model. The investigation adheres to the ARRIVE guidelines (Percie Du Sert et al., 2020), ensuring randomization in animal allocation and blinding throughout biochemical analysis. The protocols of the experiments were authorized by the University Ethics Committee. (Approval No. 2448/GCN-HĐĐĐNCTĐV).

2.4. Analysis of chemical profiling by LC-MS

2.4.1. Utilization of ultra-performance liquid chromatography-tandem mass spectrometry (UPLC-MS/MS) for the collection of fragment ions

MS/MS data were acquired using a Waters XEVO G2-XS QTOF mass spectrometer (Waters Corp., USA) equipped with an electrospray ionization (ESI) source operating in negative ion mode. Chromatographic separation was performed on a Waters UPLC C_{18} column (4.6 × 100 mm, 2.7 μm). The mobile phase consisted of water containing 0.1% formic acid (A) and acetonitrile containing 0.1% formic acid (B). The gradient elution program was as follows: 0.01–20 min, 90–50% A; 20–50 min, 50–5% A; 50–60 min, 5% A; 60–63 min, 5–90% A; and 63–65 min, 90% A. The flow rate was maintained at 0.3 mL/min. Samples were prepared by dissolving 5.0 mg of extract in 1 mL methanol and filtering through a 0.22 μm membrane filter prior to analysis. An injection volume of 1 μL was used for UPLC-MS/MS analysis. MSe data were acquired over an *m/z* range of 100–1500 using a data-independent acquisition (DIA) mode with alternating low collision energy (6 eV) and a high-energy ramp of 40–50 eV. Data acquisition and processing were performed using UNIFI 3.15.1 and Progenesis QI 3.1 software (Waters Corp., Milford, MA, USA).

2.4.2. The Global Natural Product Social Molecular Networking (GNPS)-based molecular networking analysis

GNPS-based molecular networking analysis was conducted using the Global Natural Products Social Molecular Networking (GNPS2) web platform (jobID: 4e0c9c53cf714322a4059314fc1393fb). MS/MS spectra were filtered by retaining the top five fragment ions within a ± 50 Da window across the spectrum. A molecular network was then generated using a cosine similarity threshold of 0.70 with a minimum of four matched fragment ions. The generated molecular network was visualized and arranged using Cytoscape 3.10.4 software (NRNB, USA), and putative compound annotations were assigned based on MS/MS fragmentation patterns.

2.5. Acute oral toxicity study

Acute toxicity was evaluated in accordance with the Organization of Economic Co-operation and Development OECD (Guideline No.423 for acute Oral Toxicity, Acute Toxic Class Method) (OECD, 2002). A group of mice (3 males and 3 females) was provided with water ad libitum but fasted for at least 12 h prior to receiving a single maximum testing dose of 5000 mg/kg of the extract. The mice were continuously monitored for 72 h for signs of toxicity, including general movements; abnormal respiratory and gastrointestinal functions (e.g., dyspnea and diarrhea), feeding and drinking reflexes, and mortality rate. If no mortality occurred, the observation period was extended for an additional 14 days.

2.6. Carrageenan-induced paw edema model

The acute anti-inflammatory effect of the extract was evaluated using the carrageenan-induced paw edema model (Fehrenbacher et al., 2012). Healthy male mice were acclimatized for 7 days and randomly divided into five groups, with eight mice per group. The experimental doses were determined based on the extraction yield (1.28%) and the conversion factor for laboratory animals (human/mouse K_m ratio of 37/3) (Nair and Jacob, 2016). Two dosage levels were selected: 185 mg/kg and 370 mg/kg.

+Group 1 (normal control group): received distilled water
+Group 2 (disease control group): received distilled water
+Group 3 (diclofenac-treated group - Diclo): received diclofenac at 10 mg/kg
+Group 4 (test group 1 - AE-185) received the algae extract at 185 mg/kg
+Group 5 (test group 2 - AE-370) received the algae extract at 370 mg/kg

One hour after the administration of the reference drug or algae extracts, mice in groups 2, 3, 4, and 5 were induced with inflammation by a subplantar injection of 25 μL of 1% carrageenan into the right hind paw. Mice in group 1 received an injection of 0.9% NaCl. Paw volume was measured before carrageenan injection and at 1, 3, 5, 24, 48, and 72 h after induction using a plethysmometer. The percentage increase in paw volume (X%) and inhibition of paw edema (Y%) were calculated as follows:

$$X\ (\%) = [(V_t - V_0) / V_0] \times 100 \quad (1)$$

$$Y\ (\%) = [(M_c - M_t) / M_c] \times 100 \quad (2)$$

where V_0 (mL) is the paw volume before carrageenan injection, V_t (mL) is the paw volume at each time point, M_c (%) is the percentage increase in paw volume in the disease control group, and M_t (%) is the percentage increase in paw volume in the treated group.

2.7. Cotton pellet-induced granuloma model

The chronic anti-inflammatory effect of the extract was assessed using the cotton pellet-induced granuloma model (Kumar et al., 2016). Healthy male mice were randomly divided into four groups, with eight mice per group: disease control, diclofenac-treated group, and two extract-treated groups. The disease control group received distilled water, the reference group received diclofenac at 10 mg/kg, and the extract-treated groups received the extract at 185 or 370 mg/kg.

The mice were shaved in the dorsal area (2 ×2 cm), sanitized with alcohol, and locally anesthetized with a subcutaneous injection of 0.04% lidocaine. A small incision was made in the dorsal region, and a sterile cotton pellet weighing 10 ± 1 mg, previously soaked with 100 μL of 1% carrageenan, was implanted subcutaneously. The incision was sutured and disinfected with povidone. The animals were orally treated once daily for 7 days. At the end of the experiment, the mice were euthanized using CO_2, granuloma tissues were collected, dried at 60 °C until reaching a constant weight (18 h), and then weighed. The chronic inflammatory inhibition was calculated as follows:

$$\text{Inhibition}\ (\%) = [(M_{control} - M_{treated}) / M_{control}] \times 100 \quad (3)$$

where $M_{control}$ (mg) is the weight of cotton pellet granuloma in the vehicle control group and $M_{treated}$ (mg) is the weight of cotton pellet granuloma in the mice treated with diclofenac or extract.

Simultaneously, blood samples were collected via cardiac puncture. The levels of IL-1β, IL-10, and TNF-α were quantified using the LEGEND MAX™ Mouse ELISA kit, with concentrations calculated based on the linear regression equation derived from the standard curve.

2.8. Carrageenan-induced acute arthritis model

The anti-arthritic effect of the extract was evaluated using carrageenan-induced acute arthritis in mice (Hansra et al., 2000). Healthy male mice were randomly divided into five groups, following the same protocol as described above.

The circumference of the right knee joint was measured before induction. One hour after oral administration, arthritis was induced by intra-articular injection of 15 μL of 2% carrageenan into the right knee joint in the disease control, diclofenac, and extract-treated groups, while mice in the normal control group received 0.9% NaCl. Treatments were

continued once daily for 3 days. Knee joint circumference was measured at 2, 4, 6, 24, 48, and 72 h after carrageenan injection using millimeter paper.

2.9. Carrageenan-induced chronic arthritis model

Chronic arthritis was induced by repeated intra-articular injection of carrageenan into the right knee joint (Hansra et al., 2000). Mice were assigned to the same five groups as described above. Mice in the disease control, diclofenac, and extract-treated groups received 15 μL of 2% carrageenan into the right knee joint once every 3 days for 18 days, on days 1, 3, 6, 9, 12, 15, and 18. Mice in the normal control group received 15 μL of 0.9% NaCl. Treatments were administered orally once daily for 21 days.

Knee joint circumference was measured before induction and on days 3, 6, 9, 12, 15, 18, and 21. The percentage increase in joint circumference was calculated as follows:

$$X\ (\%) = [(C_t - C_0) / C_0] \times 100 \quad (4)$$

where C_0 (mm) is the knee joint circumference before carrageenan injection and C_t (mm) is the circumference at each evaluation time point. On day 21, mice were euthanized with CO_2. The right knee joint was exposed and evaluated macroscopically using a 0–3 arthritis scoring scale: 0 = no signs of inflammation; 1 = mildly inflamed; 2 = moderately inflamed; and 3 = severely inflamed in 0.25 increments, where 0.25 indicated initial swelling and redness. Scoring was conducted by two independent investigators blinded to the treatment groups (Bileviciute-Ljungar et al., 2006, Marchetti et al., 2018).

2.10. Statistical analysis

Data were analyzed using Microsoft Excel 2021 and SPSS 26.0. Statistical differences among groups were evaluated using one-way ANOVA followed by Tukey's post hoc test for normally distributed data. For non-normally distributed data, Kruskal-Wallis followed by Dunn's test and the Mann-Whitney test were used. A value of $p < 0.05$ was considered statistically significant.

3. Results and discussion

3.1. Characterizing the triterpene sulfates distribution through multi-informative molecular networking (MIMN)

The MIMN analysis was performed using MS/MS data processed on the GNPS2 platform. The resulting molecular network was visualized according to precursor ion *m/z* values, as illustrated in Fig. 1A. A total of five major molecular clusters (A-E) were identified, comprising 5–51 nodes per cluster, predominantly distributed within the *m/z* range of 500–600, consistent with sulfated triterpenoid-type metabolites.

Cluster annotation was performed using a multi-layer dereplication strategy, including GNPS spectral library matching, cosine similarity-based networking, and in silico fragmentation analysis. To ensure transparency and reproducibility of annotations, compounds were classified according to the Metabolomics Standards Initiative (MSI). Nodes with high-confidence spectral library matches (cosine similarity > 0.70 and ≥ 4 matched fragment ions) were assigned as MSI Level 2 annotations, while nodes inferred through network connectivity and structural analogy were classified as MSI Level 3 (putatively characterized compounds).

Cluster A–E showed distinct yet closely related MS/MS fragmentation patterns characterized by diagnostic sulfate-related fragment ions and shared triterpenoid backbone fragments, supporting their structural coherence as a chemical family. Representative nodes from each cluster were selected based on highest degree centrality and MS/MS spectral quality, and their fragmentation spectra are presented in Fig. 1B. Within these clusters, several nodes were successfully dereplicated as previously reported triterpene sulfates (Table 1), including methyl-3β,23(*R*)-dihydroxycycloart-24-en-28-oate 3-sulfate, methyl-3β,23(*R*)-dihydroxy-29-nor-lanosta-8,24-dien-28-oate 3-sulfate, 3β,28-dihydroxycycloart-24-en-23-one 3-sulfate, cycloart-24-en-3β,23(*R*),28-triol 3-sulfate, and related analogues.

Overall, the MIMN results provide a structured and confidence-annotated molecular framework for triterpene sulfate distribution in *T. cylindrica*, thereby strengthening the reliability of compound-level interpretation and supporting subsequent biological correlation.

3.2. Acute toxicity of T. cylindrica extract

The acute toxicity test was performed at the highest dose of 5000 mg/kg in accordance with OECD guidelines. There was no mortality within 72 h or over the subsequent 14-day observation period. The mice exhibited normal behavior and showed a slight weight gain with no signs of weight loss. Therefore, the algae extract can be considered safe, with the lethal dose (LD_{50}) greater than 5000 mg/kg.

3.3. Acute anti-inflammatory effect in carrageenan-induced paw edema model

In the paw-edema model, the disease control group exhibited a significant increase in hind paw volume at all observation time points, confirming the effectiveness of 1% carrageenan as an inflammatory agent in this model. The positive control group (diclofenac 10 mg/kg) exhibited a significant decrease in paw edema volume throughout the observation period, demonstrating potent anti-inflammatory efficacy (inhibition rates ranging from 34.86% to 54.13%). Both test groups administered with algae extract at doses of 185 mg/kg and 370 mg/kg displayed anti-inflammatory activity compared to the control group. The 370 mg/kg dosage group demonstrated a rapid effect at the first hour post-carrageenan injection with an inhibition rate of 57.95%; this inhibitory effect remained up to 72 h and showed no statistically significant difference compared to the diclofenac group ($p = 0.504–0.942 > 0.05$). The 185 mg/kg dosage group showed a delayed onset of action; the inhibition of paw edema volume appeared after 3 h of inflammation induction (34.82%), and then the effect prolonged during the 72-hour observation period (Fig. 2).

3.4. Chronic anti-inflammatory effect in the cotton-pellet-induced granuloma model and serum cytokines

The chronic anti-inflammatory effect was evaluated based on the dry weight of granuloma tissue isolated on day 8th of the model and the quantification of inflammatory mediators (IL-1β, IL-10, and TNF-α). The results for granuloma weight and the expression levels of anti-inflammatory cytokines (IL-1β, IL-10 and TNF-α) are presented in Table 2 and Fig. 3. The results demonstrated that the groups treated with diclofenac and algae extract (185 mg/kg) reduced the dry granuloma weight by 24.03% and 22.96%, respectively, compared to the disease control group ($p = 0.004 < 0.01$). Meanwhile, the algae extract group at a dosage of 370 mg/kg reduced the dry granuloma weight by 12.18% compared to the disease control group ($p = 0.574 > 0.05$), with no significant difference observed compared to the diclofenac group. The quantification of cytokine concentrations revealed that treatment with both diclofenac and algae extracts decreased the levels of IL-1β. Specifically, the group treated with 185 mg/kg of algae extract showed the most significant reduction (57.78% compared to the disease control), followed by the diclofenac group (a reduction of 35.95%), and the 370 mg/kg algae extract group inhibited 26.81%. However, there were no statistically significant differences between the algae extract-treated groups and the diclofenac group ($p = 0.053$ for the 185 mg/kg group and $p = 0.775$ for the 370 mg/kg group). Regarding IL-10 and TNF- α, the treatment groups showed a decreasing trend, but these results were

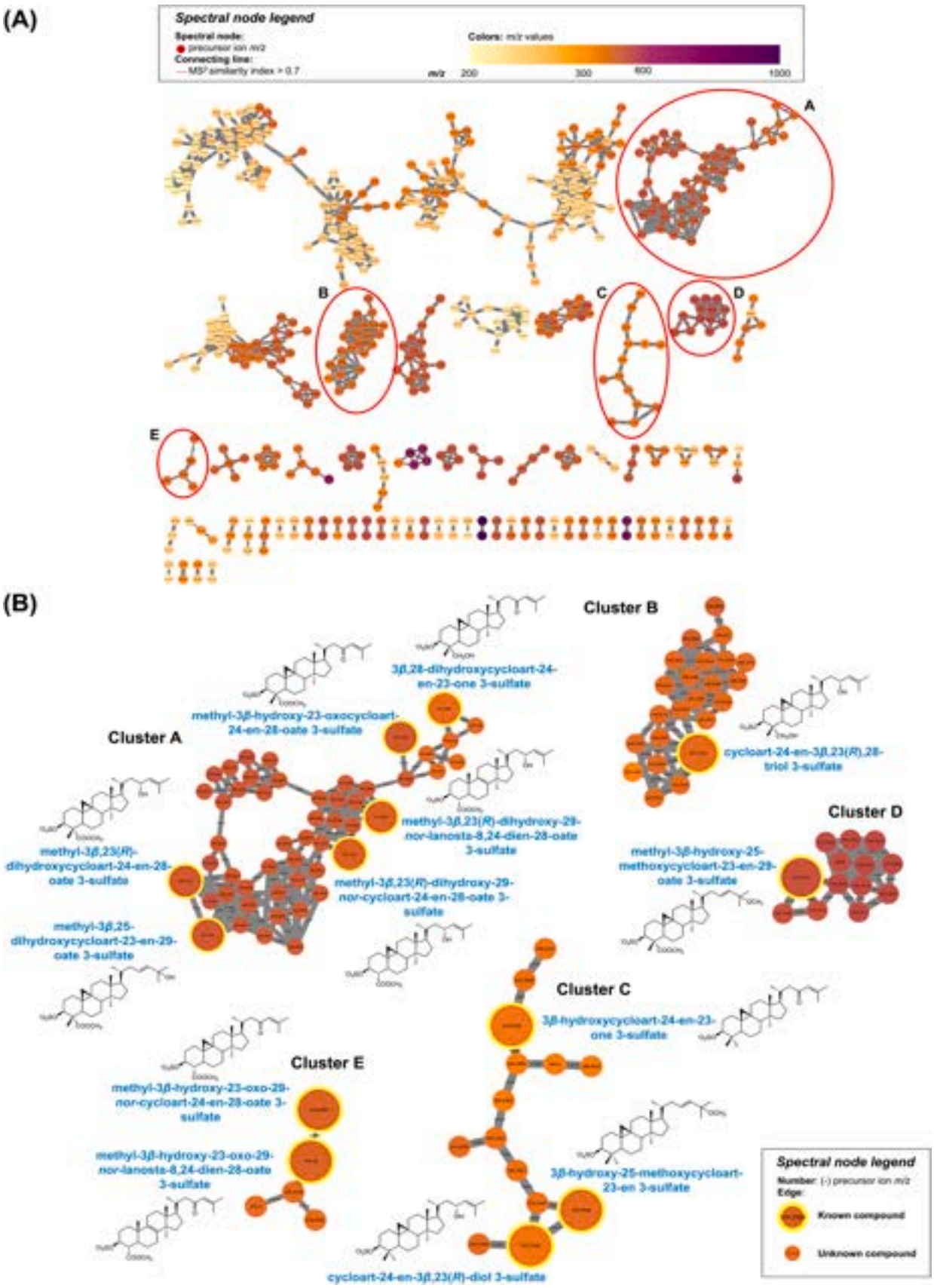

Fig. 1. MS/MS molecular networking (MN) reveals the chemical diversity of triterpene sulfates derived from *Tricleocarpa fragilis*. (**A**) The MN profile is color-coded based on *m/z* values. (**B**) The unique triterpene sulfates identified within clusters A–E are highlighted.

Table 1
The annotated triterpene sulfates originating from the extract of *Tricleocarpa cylindrica*.

No	t_R (min)	Compound name	Ion adduct	Precursor/ Product ion (*m/z*, intensity a.u.)[a]	Molecular formula (error in ppm)	Ref
1	41.20	methyl-3β,23(*R*)-dihydroxycycloart-24-en-28-oate 3-sulfate	$[M]^-$	565.319/ 146.9640 (732), 163.8959 (180), 165.8948 (193), 183.0097 (622), 255.2312 (367), 353.1774 (914), 379.1901 (173), 397.1412 (333), 407.2269 (312), 421.2415 (302), 519.3172 (382), 521.3308 (26020), 531.2478 (287), 533.2562 (236), 535.3027 (301), 537.3162 (296), 547.3124 (825), 549.2963 (757), 563.3019 (708)	$C_{31}H_{49}O_7S^-$ (-1.77)	(Horgen et al., 2000)
2	36.81	methyl-3β-hydroxy-23-oxocycloart-24-en-28-oate 3-sulfate	$[M]^-$	563.304/ 126.9039 (1278), 163.8961 (201), 165.8951 (310), 183.0109 (1229), 255.2340 (650), 281.2473 (387), 339.1976 (202), 366.2306 (125), 505.3024 (784), 519.3129 (338), 521.3270 (353), 531.2540 (330), 536.3115 (187), 537.3259 (421), 547.3087 (463), 549.2886 (321)	$C_{31}H_{47}O_7S^-$ (0.00)	(Horgen et al., 2000)
3	27.65	cycloart-24-en-3β,23(*R*),28-triol 3-sulfate	$[M]^-$	537.325/ 126.9035 (1244), 146.9643 (544), 163.8949 (219), 165.8904 (242), 183.0103 (369), 258.7335 (184), 260.7331 (245), 262.7241 (211), 306.6795 (148), 353.1795 (364), 397.1670 (275), 465.2659 (5040), 495.2738 (1006), 514.3232 (286), 523.2710 (4009), 531.2550 (385)	$C_{30}H_{49}O_6S^-$ (0.00)	(Horgen et al., 2000)
4	39.00	3β,28-dihydroxycycloart-24-en-23-one 3-sulfate	$[M]^-$	535.310/ 126.9039 (782), 146.9667 (531), 163.8960 (260), 174.0006 (168), 183.0106 (664), 255.2309 (293), 339.1974 (59), 353.1756 (340, 379.1953 (199), 397.1682 (289), 421.2406 (251), 505.2986 (982), 519.3172 (291), 521.3297 (7529), 531.2521 (500), 533.2611 (342), 534.2956 (148)	$C_{30}H_{47}O_6S^-$ (1.87)	(Horgen et al., 2000)
5	40.29	cycloart-24-en-3β,23(*R*)-diol 3-sulfate	$[M]^-$	521.334/ 126.9041 (1110), 146.9652 (530), 163.8967 (260), 165.8930 (290), 174.0020 (176), 183.0103 (656), 255.2340 (330), 353.1793 (694), 397.1489 (195), 465.2509 (117), 479.2514 (154), 515.2238 (215), 519.3165 (327)	$C_{30}H_{49}O_5S^-$ (7.67)	(Horgen et al., 2000)
6	47.10	3β-hydroxycycloart-24-en-23-one 3-sulfate	$[M]^-$	519.315/ 126.9032 (1126), 146.9649 (613), 163.8952 (134), 165.8940 (332), 183.0091 (577), 255.2299 (334), 353.1792 (294), 421.2383 (308)	$C_{30}H_{47}O_5S^-$ (1.93)	(Horgen et al., 2000, Tran et al., 2021)
7	38.71	methyl-3β,23(*R*)-dihydroxy-29-*nor*-cycloart-24-en-28-oate 3-sulfate	$[M]^-$	551.304/ 126.9029 (1018), 146.9675 (452), 163.8978 (189), 165.8961 (250), 173.9997 (178), 183.0092 (1015), 255.2337 (335), 279.2344 (266), 339.1851 (147), 353.1790 (367), 379.1927 (182), 397.1630 (229), 421.2448 (270), 505.2978 (2713), 514.3204 (213), 519.3188 (278), 521.3298 (5608), 531.2616 (423), 533.2579 (497), 535.3092 (1006), 537.3071 (195), 547.3064 (806), 550.2907 (263)	$C_{30}H_{47}O_7S^-$ (0.00)	(Horgen et al., 2000)
8	61.84	methyl-3β-hydroxy-23-oxo-29-*nor*-cycloart-24-en-28-oate 3-sulfate	$[M]^-$	549.289/ 126.9047 (372), 146.9658 (1608), 157.0119 (344), 163.8983 (257), 171.9806 (400), 180.9734 (386), 183.0106 (1247), 197.9613 (330), 208.0758 (141), 248.9616 (505), 255.2352 (289), 306.9151 (222), 316.9482 (302), 333.9366 (408), 350.9319 (186), 503.3221 (244), 505.3333 (977), 520.3214 (175), 535.3442 (1077), 547.3073 (909)	$C_{30}H_{45}O_7S^-$ (0.00)	(Horgen et al., 2000)
9	37.21	methyl-3β,23(*R*)-dihydroxy-29-*nor*-lanosta-8,24-dien-28-oate 3-sulfate	$[M]^-$	551.306/ 126.9051 (797), 146.9664 (647), 165.8952 (259), 183.0121 (1936), 339.1990 (413), 353.1726 (165), 397.1639 (214), 505.2999 (571), 507.3153 (499), 521.3316 (756), 531.2662 (229), 533.2611 (252), 535.3083 (429), 537.3224 (524), 547.3150 (369), 548.3055 (305), 549.2949 (559)	$C_{30}H_{47}O_7S^-$ (3.63)	(Horgen et al., 2000)
10	62.14	methyl-3β-hydroxy-23-oxo-29-*nor*-lanosta-8,24-dien-28-oate 3-sulfate	$[M]^-$	549.290/ 126.9036 (364), 146.9653 (1722), 163.8947 (308), 165.8935 (159), 171.9771 (379), 183.0119 (1068), 255.2337 (398), 279.2335 (295), 505.3331 (1629), 521.3231 (151), 531.2521 (223), 533.2571 (205), 535.3460 (1906), 547.3114 (1134)	$C_{30}H_{45}O_7S^-$ (1.82)	(Horgen et al., 2000)
11	40.56	methyl-3β,23(*R*)-dihydroxycycloart-24-en-28-oate 3-sulfate	$[M]^-$	565.319/ 126.9037 (1002), 163.8946 (317), 165.8914 (242), 183.0126 (724), 255.2323 (501), 353.1818 (354), 379.1981 (156), 407.2275 (140), 421.2456 (135), 479.2522 (133), 503.3119 (138), 519.3102 (272), 521.3306 (9843), 531.2565 (209), 533.2540 (371), 535.3109 (753), 537.3213 (214), 547.3105 (820), 563.3058 (2764)	$C_{31}H_{49}O_7S^-$ (-1.77)	(Tran et al., 2021)
12	52.23	methyl-3β-hydroxy-25-methoxycycloart-23-en-29-oate 3-sulfate	$[M]^-$	579.336/ 126.9048 (1226), 146.9652 (411), 171.9828 (103), 174.0002 (239), 183.0117 (965), 248.9614 (225), 255.2321 (403), 519.3209 (191), 521.3296 (503), 549.3283 (1237), 551.3304 (410)	$C_{32}H_{51}O_7S^-$ (0.00)	(Tran et al., 2021)

(*continued on next page*)

Table 1 (*continued*)

No	t_R (min)	Compound name	Ion adduct	Precursor/ Product ion (*m/z*, intensity a.u.)[a]	Molecular formula (error in ppm)	Ref
13	40.03	3β-hydroxy-25-methoxycycloart-23-en 3-sulfate	$[M]^-$	535.345/ 126.9036 (1196), 146.9641 (856), 163.8950 (200), 165.8893 (307), 174.0023 (271), 183.0125 (664), 255.2347 (396), 353.1806 (344), 397.1475 (327), 407.2265 (137), 465.2366 (238), 505.3015 (123), 519.3149 (454), 521.3315 (7706), 531.2515 (153), 533.2570 (316)	$C_{31}H_{51}O_5S^-$ (-1.87)	(Tran et al., 2021)

[a] : Product ions with the highest relative abundance are underlined.

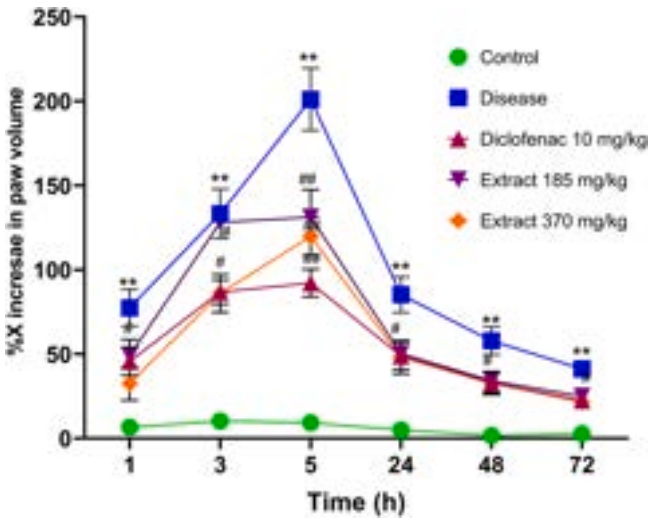

Fig. 2. Effect of *T. cylindrica* extract on carrageenan induced paw edema in mice. Results were presented as Mean ± standard error of mean (SEM), (n = 8). Comparison of the results was performed using analysis of variance (ANOVA) followed by Tukey's post hoc test. * $p < 0.05$, ** $p < 0.01$: compared with the control group. # $p < 0.05$; ## $p < 0.01$ compared with the disease group.

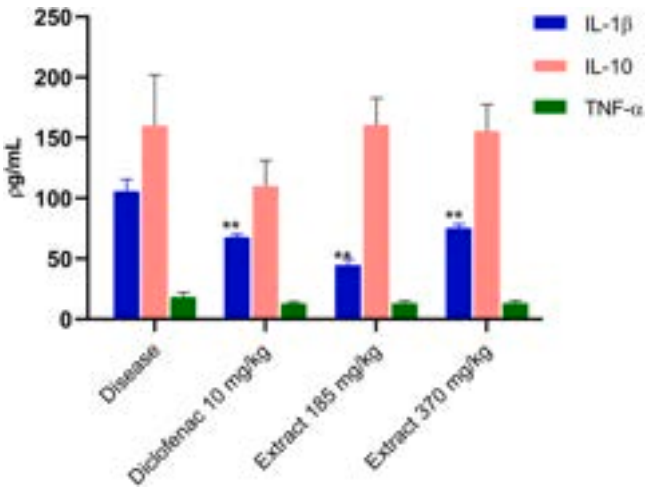

Fig. 3. Concentration of IL-1β, IL-10 and TNF-α in serum of mice. Results were presented as Mean ± standard error of mean (SEM), (n = 8). Comparison of the results was performed using analysis of variance (ANOVA) followed by Tukey's post hoc test the control group; ** $p < 0.01$ compared with the disease group.

Table 2
Effect of the algae extract on cotton pellet granuloma model.

Group	Granuloma dry weight (mg)	Inhibition (%)
Disease control	34.88 ± 2.14	-
Diclofenac 10 mg/kg	**26.50 ± 0.84**##	24.03
Algae extract 185 mg/kg	**26.87 ± 0.88**##	22.96
Algae extract 370 mg/kg	30.63 ± 1.76	12.18

Each value is the mean ± SEM ($n = 8$), ## $p < 0.01$ compared with the disease group

not statistically significant.

3.5. Anti-arthritic effect in acute carrageenan arthritis

The acute anti-arthritic effect was evaluated by measuring joint circumference at 1–72 h carrageenan-induced arthritis. Results showed that the group administered algae extract at 370 mg/kg exhibited a significant reduction in joint swelling, beginning 24 h after induction, with a decrease of 49–65%. The 185 mg/kg dosage group also demonstrated efficacy in reducing joint circumference after 24 h, although the effect was less significant than that of the 370 mg/kg dose at all observed time points. The positive control group (diclofenac) exhibited significant anti-inflammatory action 1 h after injection with a 25.11% decrease, peaked at 24 h (56.00%), and maintained its effect throughout the 72-hour observation period (Fig. 4).

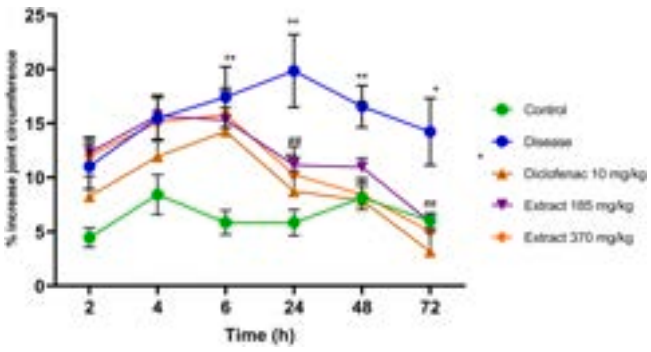

Fig. 4. Effect of *T. cylindrica* extract on carrageenan induced chronic arthritic. Results were presented as Mean ± standard error of mean (SEM), (n = 8). Comparison of the results was performed using analysis of variance (ANOVA) followed by Tukey's post hoc test. * $p < 0.05$, ** $p < 0.01$: compared with the control group. # $p < 0.05$; ## $p < 0.01$ compared with the disease group.

3.6. Anti-arthritic effect in chronic carrageenan arthritis

In the chronic arthritis model, mice were orally administered the algae extract for 21 days, and their body weight was monitored. There were no significant changes in body weight in the algae extract-treated groups compared to other groups.

Anti-inflammatory effects were also assessed by measuring joint circumference every 3 days over the 21-day period. The results indicated that the diclofenac (10 mg/kg) group exhibited anti-arthritic effects at all observation time points, reducing the increase in knee joint circumference by approximately 46–76% compared to the disease

control group ($p = 0.004 – 0.041 < 0.05$), and showing no significant difference compared to the normal control group ($p = 0.485–0.937 > 0.05$). The algae extract at a dose of 185 mg/kg reduced knee joint circumference by approximately 42–55% compared to the disease control group from day 3 to day 12 ($p = 0.026–0.041 < 0.05$); however, from day 15 to day 21, the reduction was approximately 26 – 35% but was not statistically significant ($p = 0.132–0.310 > 0.05$). The group treated with 370 mg/kg of algae extract showed a 41.03% reduction in knee joint circumference on day 3 compared to the disease control group ($p = 0.015 < 0.05$). From day 6 to day 21, the reduction ranged from 9% to 34% compared to the disease control group, but these differences were not statistically significant ($p = 0.093–0.937 > 0.05$) (Fig. 5 and Table 3).

The results of the arthritis scoring scale showed that mice in the disease control group had a mean score approximately 9 times higher than that of the normal control group ($p = 0.001 < 0.01$). The 10 mg/kg diclofenac group had a mean inflammation score 2.9 times lower than the disease control group ($p = 0.009 < 0.05$) and showed no significant difference compared to the normal control group ($p = 0.194 > 0.05$). The groups treated with the algal extract at doses of 185 mg/kg and 370 mg/kg exhibited reductions in the mean arthritis score by 46.08% and 27.19%, respectively, however, there was no significant difference compared to the disease group ($p = 0.555$ and $0.913 > 0.05$) (Table 4).

4. Discussions

4.1. Chemical analysis

Reported studies on *Tricleocarpa fragilis,* a species within the same genus, have indicated that triterpene sulfates are the important class of compounds responsible for its biological activities (Horgen et al., 2000, Tran et al., 2021). Based on the analytical results, it is evident that the chemical constituents of *T. cylindrica* also consist mainly of sulfated triterpenoids, which were previously identified in *T. fragilis*. Interestingly, besides the annotated nodes corresponding to known compounds, these clusters also contained numerous unannotated nodes exhibiting highly similar fragmentation behaviors and close spectral relationships to the identified triterpene sulfates. The occurrence of these unidentified nodes strongly suggests the presence of structurally related metabolites that have not yet been reported in the literature. Since compounds grouped within the same molecular cluster generally possess similar core skeletons and biosynthetic relationships, these unknown nodes were considered potential novel triterpene sulfate derivatives and require further investigation.

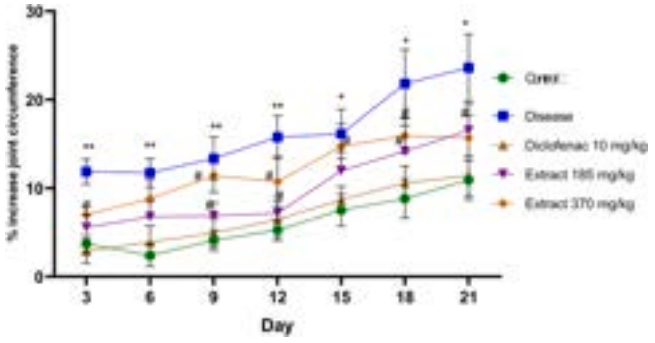

Fig. 5. Effect of *T. cylindrica* extract on carrageenan induced chronic arthritic. Results were presented as Mean ± standard error of mean (SEM), (n = 8). Comparison of the results was performed using analysis of variance (ANOVA) followed by Tukey's post hoc test. * $p < 0.05$, ** $p < 0.01$: compared with the control group. # $p < 0.05$; ## $p < 0.01$ compared with the disease group.

Table 3
Arthritis inhibition (%) of treatment groups relative to disease control in the chronic arthritis model.

Group ($n = 8$)	Day 3	Day 6	Day 9	Day 12	Day 15	Day 18	Day 21
Diclofenac 10 mg/kg	75.57	66.61	62.80	59.15	46.10	51.51	51.57
Algae extract 185 mg/kg	53.07	42.16	48.43	54.59	25.77	35.07	29.97
Algae extract 370 mg/kg	41.03	24.96	14.52	31.86	8.74	27.06	33.62

Table 4
Arthritis scores of the right knee joint in experimental groups on day 21.

Group ($n = 8$)	Normal Control	Disease control	Diclofenac 10 mg/kg	Algae extract 185 mg/kg	Algae extract 370 mg/kg
Inflammation score	0.25 ± 0.11	2.17 ± 0.40**	**0.75 ± 0.28#**	1.17 ± 0.42	1.58 ± 0.40*

Each value is the mean ± SEM ($n = 8$)
*: $p < 0.05$ and ** $p < 0.01$ compared with normal control group, # $p < 0.05$ compared with disease group

4.2. In vivo assay

The carrageenan-induced acute inflammation model exhibits a classic biphasic mechanism. The early phase is triggered by primary vascular mediators like histamine and bradykinin, whereas the delayed, mature phase is sustained by a complex network of prostaglandins, nitric oxide (NO), progressive leukocyte infiltration, and elevated pro-inflammatory cytokines. (Fehrenbacher et al., 2012, Posadas et al., 2004, Lopes et al., 2020). Carrageenan edema also shows differential NO/COX-2 dependence over time (Posadas et al., 2004), and macrophage exposure to carrageenan can engage TLR4-linked cytokine signaling and IL-1β maturation via the canonical NLRP3 inflammasome (Lopes et al., 2020, Swanson et al., 2019). In the present study, the weak 185 mg/kg response at 3 h but clearer efficacy from 5 h to 72 h suggests greater activity during the later prostaglandin/NO/cytokine-dominant phase than during the earliest permeability phase. The dose of 370 mg/kg exhibited a faster onset of action starting from 1 h post-inflammation induction, indicating its ability to neutralize chemical mediators as well as inhibit the production of prostaglandins, NO, and cytokines.

Similarly, in the acute arthritis model, the 370 mg/kg dose exhibited better efficacy than the 185 mg/kg dose, indicating that the constituent compounds in the extract possess an inhibitory effect on delayed-phase mediators. Phytochemical profiling of the algal extract revealed that sulfated triterpenes are the predominant compound class potentially responsible for the observed anti-inflammatory effects. The distinctive structural features of the predicted triterpenes in *T. cylindrica* are the cycloartane skeleton and the sulfate moiety. While there is a lack of reported data regarding the impact of the sulfate group on anti-inflammatory efficacy, the cycloartane skeleton is well-recognized as a structural determinant for this biological activity. Previous studies have shown that cycloartane triterpenes exert anti-inflammatory effects by inhibiting NO, the NLRP3 inflammasome, interleukins, and TNF-α (Wang et al., 2025). These findings are in strong agreement with our *in vitro* anti-inflammatory observations.

However, in the chronic inflammation and chronic arthritis models, the results were different, as the lower dose of 185 mg/kg exhibited better efficacy than the 370 mg/kg dose. This is considered a non-monotonic, bell-shaped dose-response relationship, which is well-documented in pharmacological studies (Calabrese, 2013). The therapeutic mechanisms for acute and chronic inflammation differ based on

the progression of the ongoing inflammatory process. During acute inflammation, chemical mediators (such as histamine, serotonin, NO, and prostaglandins) are massively released; therefore, anti-inflammatory agents must be introduced immediately to rapidly and profoundly neutralize these mediators (Ayoub, 2010). This mechanism explained the algal extract at a dose of 370 mg/kg exhibited superior efficacy compared to the 185 mg/kg dose. However, chronic inflammation is a complex, cell-mediated process involving prolonged macrophage activation, fibroblast proliferation, and intricate cytokine networks (Ayoub, 2010). The administration of high-dose extracts may trigger feedback mechanisms, leading to the down-regulation of target receptors and the shunting of metabolic pathways (Lin et al., 2011, Calabrese, 2013). Furthermore, high-dose administration can induce cellular stress that promotes secondary inflammatory responses, thereby reversing the initial anti-inflammatory effects (Du et al., 2013).

The IL-1β pattern is relevant to chronic inflammation. IL-1β lies downstream of both inflammatory priming and inflammasome-dependent maturation, so a marked fall in IL-1β with a smaller TNF-α effect is compatible with interference at the NF-κB priming step, the NLRP3/caspase-1 processing step, or both (Lopes et al., 2020, Swanson et al., 2019, Yin et al., 2022). The NLRP3/IL-1β axis is recognized as an amplifier in rheumatoid and related chronic synovitides (Swanson et al., 2019, Yin et al., 2022). The present dataset cannot prove NLRP3 inhibition, but the combination of late-phase paw-edema efficacy, IL-1β suppression, and chronic granuloma reduction supports direct protein-level testing in follow-up work.

Regarding the chronic arthritis model, a limitation of the present study is that the evaluation was restricted to knee joint circumference and macroscopic manifestations, without conducting histological analysis or measuring inflammatory mediators. This model relies on carrageenan-induced inflammation in the knee joint, suggesting that its mechanism of action is potentially similar to that of the chronic inflammation model. However, to fully understand the mechanisms of action, an in-depth analysis of molecular expressions at the knee joint is required.

Overall, the algae extract at a dose of 185 mg/kg demonstrated consistent and effective anti-inflammatory activity in both acute and chronic models. The 370 mg/kg dose remained biologically active, but its less stable performance across endpoints argues against simple dose escalation as the next development step.

Based on the obtained results, *T. cylindrica* emerges as a potential natural source exhibiting anti-inflammatory activity, with sulfated triterpenes being the responsible bioactive compounds. The scalability and sustainability of using *T. cylindrica* as a source of triterpene sulfates depend on both biomass availability and environmentally responsible production. This species is relatively widely distributed in tropical and subtropical waters and commonly occurs on rocky substrates and dead coral surfaces in subtidal habitats with moderate-to-strong water movement (Do et al., 2025). In Vietnam, it generally grows well from February to June. Previous observations also suggest relatively rapid growth and the capacity to form substantial biomass within a short period (Tsutsui et al., 2005). However, quantitative data on natural stocks, annual productivity, and recovery after harvesting remain limited. Therefore, future large-scale utilization should be based on resource surveys, seasonal monitoring, suitable harvesting limits, and recovery periods rather than uncontrolled collection from natural populations. The seasonal and geographical variation in triterpene sulfate content should also be evaluated to identify the optimal harvest period.

Controlled cultivation of *T. cylindrica* has not yet been reported. Nevertheless, its relatively rapid growth supports further studies on vegetative propagation, regeneration, attachment to artificial substrates, and land-based or nearshore cultivation. Successful cultivation could provide a more stable raw-material supply and reduce pressure on natural populations. At the processing level, 2.5 kg of dried algal material yielded 33.25 g of desalted extract in the present study. However, the concentrations and recovery yields of individual triterpene sulfates were not quantified. Future work should therefore focus on chemical standardization, batch-to-batch consistency, extraction optimization, greener solvent use, and techno-economic evaluation. At present, *T. cylindrica* should be considered a promising source for further bioprospecting rather than an immediately scalable commercial raw material.

5. Conclusions

Chemical analysis of *T. cylindrica* identified triterpene sulfates as the major constituents, indicating a significant potential for the discovery of novel compounds within this scaffold. *In vivo*, the algae extract reduced carrageenan-induced paw edema, cotton pellet-induced granuloma formation, and joint swelling in acute and chronic carrageenan arthritis. A notable dose-dependent pattern emerged: 370 mg/kg was more active in acute exudative inflammation, whereas 185 mg/kg produced the more favorable profile in chronic granulomatous inflammation, IL-1β suppression, and chronic arthritis endpoints. These findings support *T. cylindrica* from Vietnamese waters as a marine-derived bioresource for further anti-inflammatory research, while also indicating the need for chemical isolation, mechanism-based assays, histopathological confirmation, pharmacokinetic evaluation, and repeat-dose safety studies.

CRediT authorship contribution statement

Thi Hong Tuoi Do: Writing – review & editing, Validation, Supervision, Resources, Methodology. **Thanh Tra Do:** Writing – original draft, Visualization, Investigation, Formal analysis, Data curation. **Huong-Giang Le:** Writing – review & editing, Visualization, Investigation, Formal analysis, Data curation. **Thi Kim Anh Le:** Methodology, Investigation, Formal analysis, Data curation. **Van Minh Nguyen:** Writing – review & editing, Validation, Resources, Project administration. **The Han Nguyen:** Writing – review & editing, Writing – original draft, Validation, Resources, Project administration. **Anh Duy Do:** Resources, Investigation. **Thi Van Anh Tran:** Writing – review & editing, Validation, Supervision, Resources, Methodology.

Ethics approval

All animal experiments were reviewed and approved by the Animal Ethics Committee of the University of Medicine and Pharmacy at Ho Chi Minh City on September 9, 2024, under approval number 2448/GCN-HDDDNCTDV.

Declaration of Generative AI and AI-assisted technologies in the writing process

During the preparation of this work, the authors used Gemini and ChatGPT only to support English language editing, manuscript organization, and formatting. After using this tool, the authors reviewed and edited the content as needed and take full responsibility for the content of the submitted article.

Funding

This work was supported by the Ministry of Education and Training of Vietnam under the project “Study on the chemical composition and selected biological activities of several red algae species of the family Galaxauraceae collected from Vietnamese waters”, grant number B2024-TSN-16. The funder had no role in the study design, data collection, analysis, interpretation, manuscript preparation, or decision to submit the article for publication.

Declaration of Competing Interest

The authors declare that they have no known competing financial

interests or personal relationships that could have appeared to influence the work reported in this paper.

Acknowledgements

The authors gratefully acknowledge MSc. Nguyen Minh Tu for his valuable support in performing the MS analysis. We also thank Waters Corporation for providing access to the Progenesis QI 3.1 software, which was essential for our LC-MS/MS data processing and analysis. This work contributes to the celebration of the 50th anniversary of Nha Trang University, located in Khanh Hoa Province, Viet Nam.

Appendix A. Supporting information

Supplementary data associated with this article can be found in the online version at doi:10.1016/j.rsma.2026.105427.

Data Availability

Data will be made available on request.

References

Ayoub, S., 2010. The inflammatory response – An overview. In: SERHAN, C.N., WARD, P. A., GILROY, D.W. (Eds.), Fundamentals of Inflammation. Cambridge University Press, Cambridge.
Bileviciute-Ljungar, I., Saxne, T., Spetea, M., 2006. Anti-inflammatory effects of contralateral administration of the κ-opioid agonist U-50,488H in rats with unilaterally induced adjuvant arthritis. Rheumatology 45, 295–302.
Buchman, A., 2001. Side Effects of Corticosteroid Therapy. J. Clin. Gastroenterol. 33, 289–294.
Calabrese, E.J., 2013. Biphasic dose responses in biology, toxicology and medicine: Accounting for their generalizability and quantitative features. Environ. Pollut. 182, 452–460.
Carlini, V., Noonan, D.M., Abdalalem, E., Goletti, D., Sansone, C., Calabrone, L., Albini, A., 2023. The multifaceted nature of IL-10: regulation, role in immunological homeostasis and its relevance to cancer, COVID-19 and post-COVID conditions. Front. Immunol. 14, 2023.
Chen, L., Deng, H., Cui, H., Fang, J., Zuo, Z., Deng, J., Li, Y., Wang, X., Zhao, L., 2017. Inflammatory responses and inflammation-associated diseases in organs. Oncotarget 9, 7204.
Choo, M.Z., Chua, J.A., Lee, S.X., Ang, Y., Wong, W.F., Chai, C.L., 2025. Privileged natural product compound classes for anti-inflammatory drug development. Nat. Product. Rep. 42, 856–875.
Do, A.D., Bui, M.T., Dong, T.D., Nguyen, T.H., 2025. Morphological Characteristics of Seaweed Species of Galaxauraceae Family (Nemaliales, Rhodophyta) Distributed in Vietnam. Vietnam. J. Agric. Sci. 23, 161–173.
Du, W.-Y., Chang, C., Zhang, Y., Liu, Y.-Y., Sun, K., Wang, C.-S., Wang, M.-X., Liu, Y., Wang, F., Fan, J.-Y., Li, P.-T., Han, J.-Y., 2013. High-dose chlorogenic acid induces inflammation reactions and oxidative stress injury in rats without implication of mast cell degranulation. J. Ethnopharmacol. 147, 74–83.
Fehrenbacher, J.C., Vasko, M.R., Duarte, D.B., 2012. Models of Inflammation: Carrageenan- or Complete Freund's Adjuvant (CFA)–Induced Edema and Hypersensitivity in the Rat. Curr. Protoc. Pharmacol. 56, 5.4.1-5.4.4.
González, Y., Torres-Mendoza, D., Jones, G.E., Fernandez, P.L., 2015. Marine Diterpenoids as Potential Anti-Inflammatory Agents. Mediat. Inflamm. 2015, 263543.
Hansra, P., Moran, E.L., Fornasier, V.L., Bogoch, E.R., 2000. Carrageenan-induced arthritis in the rat. Inflammation 24, 141–155.
Horgen, F.D., Sakamoto, B., Scheuer, P.J., 2000. New Triterpenoid Sulfates from the Red Alga Tricleocarpa fragilis. J. Nat. Prod. 63, 210–216.
Kumar, R., Gupta, Y.K., Singh, S., 2016. Anti-inflammatory and anti-granuloma activity of Berberis aristata DC. in experimental models of inflammation. Indian. J. Pharmacol. 48, 155–161.
Lawrence, T., 2009. The nuclear factor NF-kappaB pathway in inflammation. Cold Spring Harb. Perspect. Biol. 1 (6), a001651.
Li, D., Wu, M., 2021. Pattern recognition receptors in health and diseases. Signal. Transduct. Target. Ther. 6, 291.
Lin, J.-A., Chen, J.-H., Lee, Y.-W., Lin, C.-S., Hsieh, M.-H., Chang, C.-C., Wong, C.-S., Chen, J.J.-Y., Yeh, G.-C., Lin, F.-Y., Chen, T.-L., 2011. Biphasic Effect of Curcumin on Morphine Tolerance: A Preliminary Evidence from Cytokine/Chemokine Protein Array Analysis. Evid. -Based Complement. Altern. Med. 2011, 452153.
Lopes, A.H., Silva, R.L., Fonseca, M.D., Gomes, F.I., Maganin, A.G., Ribeiro, L.S., Marques, L.M.M., Cunha, F.Q., Alves-Filho, J.C., Zamboni, D.S., 2020. Molecular basis of carrageenan-induced cytokines production in macrophages. Cell. Commun. Signal. 18, 141.
Marchetti, C., Swartzwelter, B., Koenders, M.I., Azam, T., Tengesdal, I.W., Powers, N., De Graaf, D.M., Dinarello, C.A., Joosten, L.A., 2018. NLRP3 inflammasome inhibitor OLT1177 suppresses joint inflammation in murine models of acute arthritis. Arthritis Res. & Ther. 20, 169.
Nair, A.B., Jacob, S., 2016. A simple practice guide for dose conversion between animals and human. J. Basic. Clin. Pharm. 7, 27.
Nguyen, V.T., Le, N.H., Lin, S.-M., Steen, F., De Clerck, O., 2013. Checklist of the marine macroalgae of Vietnam. Bot. Mar. 56, 207–227.
OECD, 2002. Test No. 423: Acute Oral toxicity - Acute Toxic Class Method. OECD Publishing.
Percie Du Sert, N., Hurst, V., Ahluwalia, A., Alam, S., Avey, M.T., Baker, M., Browne, W. J., Clark, A., Cuthill, I.C., Dirnagl, U., Emerson, M., Garner, P., Holgate, S.T., Howells, D.W., Karp, N.A., Lazic, S.E., Lidster, K., Maccallum, C.J., Macleod, M., Pearl, E.J., Petersen, O.H., Rawle, F., Reynolds, P., Rooney, K., Sena, E.S., Silberberg, S.D., Steckler, T., Würbel, H., 2020. The ARRIVE guidelines 2.0: Updated guidelines for reporting animal research. PLOS Biol. 18, e3000410.
Posadas, I., Bucci, M., Roviezzo, F., Rossi, A., Parente, L., Sautebin, L., Cirino, G., 2004. Carrageenan-induced mouse paw oedema is biphasic, age-weight dependent and displays differential nitric oxide cyclooxygenase-2 expression. Br. J. Pharmacol. 142, 331–338.
Rocha, D.H., Pinto, D.C., Silva, A.M., 2022. Macroalgae specialized metabolites: evidence for their anti-inflammatory health benefits. Mar. Drugs 20, 789.
Schaper, F., Rose-John, S., 2015. Interleukin-6: Biology, signaling and strategies of blockade. Cytokine & Growth Factor. Rev. 26, 475–487.
Sunarwidhi, A.L., Rahmaniar, W., Prasedya, E.S., Padmi, H., Widyastuti, S., Pangestu, K. W.J., Ilhami, B.T.K., Handayani, E., Utami, N.W.P., Maulana, F.A., 2023. Vitro Anti-Oxidant, In Vivo Anti-Hyperglycemic, and Untargeted Metabolomics-Aided-In Silico Screening of Macroalgae Lipophilic Extracts for Anti-Diabetes Mellitus and Anti-COVID-19 Potential Metabolites. Metabolites 13, 1177.
Swanson, K.V., Deng, M., Ting, J.P.-Y., 2019. The NLRP3 inflammasome: molecular activation and regulation to therapeutics. Nat. Rev. Immunol. 19, 477–489.
Tran, T.V.A., Nguyen, V.M., Nguyen, T. a N., Nguyen, D.H.T., Tran, D.H., Bui, T.P.T., Pham, V.T., Nguyen, T.H., 2021. New triterpene sulfates from Vietnamese red alga Tricleocarpa fragilis and their α-glucosidase inhibitory activity. J. Asian Nat. Prod. Res. 23, 754–763.
Tsutsui, I., Huynh, Q.N., Nguyen, H.D., Arai, S., Yoshida, T., 2005. Common. Mar. Plants South. Vietnam. Jpn. Seaweed Assoc.
Varga, Z., Rafay Ali Sabzwari, S., Vargova, V., Sabzwari, S.R.A., 2017. Cardiovascular risk of nonsteroidal anti-inflammatory drugs: an under-recognized public health issue. Cureus 9.
Wang, C., Mu, X., Sun, J., 2025. Research progress of cycloartane triterpenoids and pharmacological activities. Arch. der Pharm. 358, e2400923.
Wiriyadamrikul, J., Geraldino, P.J.L., Huisman, J.M., Lewmanomont, K., Boo, S.M., 2013. Molecular diversity of the calcified red algal genus Tricleocarpa (Galaxauraceae, Nemaliales) with the description of T. jejuensis and T. natalensis. Phycologia 52, 338–351.
Yin, H., Liu, N., Sigdel, K.R., Duan, L., 2022. Role of NLRP3 inflammasome in rheumatoid arthritis. Front. Immunol. 13, 931690.

Regional Studies in Marine Science 102 (2026) 105462

Contents lists available at ScienceDirect

Regional Studies in Marine Science

journal homepage: www.elsevier.com/locate/rsma

Bioactive triterpenoid sulfates and carbohydrate derivatives from the Vietnamese red alga *Tricleocarpa cylindrica*

T.V.A. Tran [a,1], Thi Dieu Hien Nguyen [a], Duy Hien Tran [a,2], Thi Kim Anh Le [b,3], Thi Hong Tuoi Do [a,b,4], V.M. Nguyen [c,5], The Han Nguyen [c,*,6]

[a] School of Pharmacy, University of Medicine and Pharmacy at Ho Chi Minh City, Ho Chi Minh, 70000, Vietnam
[b] UMP Science and Technology Center, University of Medicine and Pharmacy at Ho Chi Minh City, 70000, Vietnam
[c] Faculty of Food Technology, School of Fisheries and Life Sciences, Nha Trang University, Khanh Hoa, 57000, Vietnam

ARTICLE INFO

Keywords:
Tricleocarpa cylindrica
Red alga
Triterpenoid sulfate
Carbohydrate derivative
Anti-inflammatory activity

ABSTRACT

Chemical investigation of the marine alga *Tricleocarpa cylindrica* collected in Vietnamese waters led to the structural elucidation of six compounds, including four triterpenoids (methyl-3β-hydroxycycloart-23,25-dien-29-oate-3-sulfate (1), 3β-hydroxycycloart-23,25-dien-3-sulfate (2), 3β-hydroxycycloart-24-en-23-one-3-sulfate (3) and methyl-3β-hydroxycycloart-24-en-23-one-29-oate-3-sulfate (4)) and two carbohydrate derivatives (O-α-galactopyranosyl (1″→6′)-O-β-galactopyranosyl-(1′→1)-glycerol (5) and floridoside (6)). Compounds 1 and 2 were identified as new natural compounds, and all six compounds were reported from *T. cylindrica* for the first time. These compounds were evaluated for their cytotoxic activities using the MTT assay and their anti-inflammatory effects against LPS-induced inflammation in RAW 264.7 cells via the NO inhibition assay. Compounds 3 and 4 exhibited cytotoxicity against the MDA-MB-231 cell line, with IC_{50} values of 66.24 ± 0.09 μM and 62.15 ± 0.25 μM, respectively. Notably, five out of the six isolated compounds demonstrated promising anti-inflammatory potential, with IC_{50} values ranging from 6.76 to 18.07 μM.

1. Introduction

Algae are a huge natural resource with diverse applications across the food, cosmetics, and healthcare industries (Koru et al., 2013). Red algae are regarded as having a greater quantity of natural bioactive chemicals compared to other categories of algae. Over 1600 compounds have been found in Rhodophyta, representing 53% of the bioactive compounds reported in algae (Leal et al., 2013). Vietnam is located in a tropical monsoon region with a coastline of approximately 3260 kilometers and a sea area of 1 million square kilometers, providing optimal conditions for rich marine algal diversity. The checklist of marine macroalgae of Vietnam in 2013 reported 827 species, of which red algae (Rhodophyta) represented nearly 50% of all recorded seaweed species (412 species) (Van Nguyen et al., 2013).

In the report about marine algae of the South China Sea, Vietnam has the highest number of distributed red algae, with 409 species belonging to 36 different families, compared with Indonesia, Malaysia, the Philippines, Singapore and Thailand (Phang et al., 2016). However, the research on bioactive compounds from algae species in Vietnam remains highly limited. Among the red algae, the Galaxauraceae family has over 10 species distributed in Vietnam (Phang et al., 2016). Notably, the species *Tricleocarpa fragilis* has been relatively well-studied for its chemical constituents and biological activities. Sulfated terpenoids have been identified as the main compounds in this species that demonstrated shrimp toxicity, cytotoxicity and α-glucosidase inhibitory activity (Horgen et al., 2000; Tran et al., 2021). Specimens of *T. fragilis* collected

* Corresponding author.
E-mail addresses: ttvananh@ump.edu.vn (T.V.A. Tran), hien153152@gmail.com (T.D.H. Nguyen), tranduyhien@ump.edu.vn (D.H. Tran), lethikimanh@ump.edu.vn (T.K.A. Le), hongtuoi@ump.edu.vn (T.H.T. Do), minhnv@ntu.edu.vn (V.M. Nguyen), hannt@ntu.edu.vn (T.H. Nguyen).
[1] ORCID: https://orcid.org/0000-0001-6998-2450
[2] ORCID: https://orcid.org/0009-0008-5110-2361
[3] ORCID: https://orcid.org/0009-0004-4850-3333
[4] ORCID: https://orcid.org/0000-0002-5445-0694
[5] ORCID: https://orcid.org/0000-0001-5316-8067
[6] ORCID: https://orcid.org/0000-0002-8154-6739

https://doi.org/10.1016/j.rsma.2026.105462
Received 29 May 2026; Received in revised form 9 September 2026; Accepted 9 September 2026
Available online 15 September 2026

from the Andaman Sea (India) were analyzed for the fatty acid composition using GC-MS. The analysis identified a mixture of fatty acids, consisting of one monounsaturated fatty acid (58%), four saturated fatty acids (38%), and one polyunsaturated fatty acid (3.86%) (Banu and Mishra, 2018) and the *n*-hexadecenoic acid was determined as the dominant compound (Banu et al., 2024). Furthermore, phytochemical screening of *T. fragilis* from the Indonesia sea indicated the presence of alkaloids, flavonoids, tannins, triterpenes/steroids and saponins (Singkoh et al., 2019). Besides, *T. fragilis* exhibited potential antibacterial activity. The crude chloroform extract and purified fraction of *T. fragilis* exhibited significant activity against four bacterial pathogens, *Staphylococcus aureus, Pseudomonas aeruginosa, Bacillus cereus* and *Salmonella enterica* Typhimurium, but not against *Listeria monocytogenes.* Fatty acids were considered responsible for this observed activity (Banu et al., 2024).

Tricleocarpa cylindrica, a species within the same genus as *T. fragilis*, is abundantly found in Vietnamese coastal waters such as Ly Son, Nha Trang, and Phu Quy (Do et al., 2024). In a recent biological activity screening of various Vietnamese red algae species, *T. cylindrica* and *T. fragilis* exhibited distinct effects. Specifically, *T. cylindrica* exhibited cytotoxicity against the MDA-MB-231 cell line with an IC_{50} value of 53.87 ± 6.35 μg/mL, while *T. fragilis* displayed weak activity (its IC_{50} value could not be established due to less than 50% inhibition at the highest dose of 100 μg/mL). Furthermore, their anti-inflammatory activities also differed; *T. fragilis* inhibited NO production in LPS-stimulated RAW 264.7 cells with an IC_{50} of 92.76 ± 3.15 μg/mL, but the IC_{50} for *T. cylindrica* could not be determined due to its cytotoxicity to the examined cells (Nguyen et al., 2025). These differences suggest that the two species may contain different chemical constituents and support further investigation of *T. cylindrica*. While the chemical constituents of *T. fragilis* have been extensively reported, data on the phytochemical profile of *T. cylindrica* remain limited. Therefore, the present study aimed to identify the chemical constituents of *T. cylindrica* collected from Vietnamese waters and to evaluate their cytotoxic and anti-inflammatory activities.

2. Materials and methods

2.1. Sample collection and preparation

The samples of *T. cylindrica* were collected from the coastal waters of Ly Son, Quang Ngai Province, Vietnam, using SCUBA diving equipment. The algal samples were collected in two separate batches in July 2023 and May 2024. The specimens were authenticated by Dr. Do Anh Duy at the Northern Research Center for Marine Fisheries, Viet Nam Academy of Fishery Sciences (VAFIS), to ensure the accuracy of the scientific nomenclature. After collection, the algal samples were washed with seawater and then sun-dried. Surface salt crystals were removed from the dried algal material. A voucher specimen is deposited at the Department of Pharmacognosy – Traditional Pharmacy, University of Medicine and Pharmacy at Ho Chi Minh City (voucher numbers AlgaeNT0923 and AlgaeNT1024). To obtain a suitable biomass for extraction, the two batches of algal samples were initially analyzed for chemical consistency by thin-layer chromatography (TLC). Upon confirmation of their similar chemical profiles, the batches were combined for the next extraction process.

2.2. Apparatus and reagents for chemical study

Column chromatography was performed with reverse phase *silica gel* (40 – 63 μm, Merck, Germany), normal *silica gel* (40 – 63 μm, Prolabo, France) and Sephadex LH-20 (GE Healthcare Life, USA). Thin layer chromatography (TLC) was carried out using pre-coated silica gel 60 F_{254} (1.05554.0001, Merck, Germany) and RP-18F_{254} plates (1.15685.0001, Merck, Germany). Spots were identified by using the vanillin-sulfuric reagent and subsequently heating to 105 °C. High-resolution mass spectrometry (HR-ESIMS) was measured on Acquity UPLC-Xevo G2 QTof MS G2 system (Waters, USA). Nuclear magnetic resonance (NMR) spectra were recorded on a Bruker Avance III 600 FT-NMR spectrometer with Tetramethylsilane (TMS) as an internal standard. Optical rotation was measured in Jasco P-2000 digital polarimeter (Jasco, Japan).

2.3. Reagents for bioassay

The RAW 264.7 and MDA-MB-231 cell lines, originally from the American Type Culture Collection (ATCC), were provided by the Pasteur Institute in Ho Chi Minh City, then reactivated and maintained at the UMP Center for Science and Technology. Dulbecco's Modified Eagle Medium (DMEM), fetal bovine serum (FBS), L-glutamine, penicillin-streptomycin, trypsin-EDTA, and phosphate-buffered saline (PBS) were purchased from Gibco (USA). Trypan blue, dexamethasone, and lipopolysaccharide (LPS from *Escherichia coli* O111:B4) were obtained from Sigma-Aldrich (Germany). 3-(4,5-Dimethylthiazol-2-yl)-2,5-diphenyltetrazolium bromide (MTT) was procured from Invitrogen (USA). Doxorubicin was supplied by Ebewe Pharma (Austria). Griess reagent (comprising 1% sulfanilamide, 0.1% N-naphthylethylenediamine dihydrochloride, and 5% phosphoric acid) was purchased from Sigma-Aldrich (Germany). Sodium nitrite (NO_2) standard was obtained from Merck (Germany).

2.4. Extraction, purification, and structural analysis

The seaweed material (2.0 kg) was percolated with 96% ethanol (w/v, 1:15). The solvent was evaporated to obtain the total crude extract (310 g). The extract was dissolved in a solvent to form a concentrated solution, mixed with clean sand as a carrier, and then dried to evaporate the solvent, yielding a powder sample. The column was packed with reversed-phase *silica gel* (50 g) at the bottom, topped with the powder sample. The column was first eluted with water (1 L) to remove salts, followed by ethanol (500 mL) and acetone (500 mL). The ethanol and acetone eluates were combined and concentrated under reduced pressure to yield the extract (24.5 g). The extract was dissolved in $CHCl_3$ and partitioned with 10% H_2SO_4. The $CHCl_3$ layer was washed with water until the washings were neutral, and then evaporated under reduced pressure to afford fraction A (5.22 g). The acidic aqueous layer was neutralized to pH 7 with 10% NaOH and subsequently extracted with $CHCl_3$. The resulting $CHCl_3$ layer was concentrated in vacuo to yield fraction B (4.61 g).

Fraction A was separated over a Sephadex LH-20 column and eluted with 100% MeOH (repeated 10 times on a 3 cm × 100 cm column) to afford 9 subfractions. Fraction A.8 (1.15 g) was subjected to reversed-phase *silica gel* column chromatography, eluting with a water–acetone (6:4, v/v) system to yield 13 subfractions (A.8.1–A.8.13). Fraction A.8.8 (117 mg) was further purified on a reversed-phase column using a water–acetonitrile (6:4, v/v) solvent system to give 12 subfractions. From subfractions A.8.8.3 and A.8.8.7, compound **3** (6.2 mg) and compound **4** (3.5 mg) were obtained, respectively. Fraction A.8.11 (45 mg) was purified over a reversed-phase column with a water–acetone gradient (from 10:0–5:5, v/v) to obtain compound **1** (2.8 mg). Similarly, purification of fraction A.8.13 (31 mg) over a reversed-phase column using a water–acetone gradient (from 9:1–4:6, v/v) yielded compound **2** (3 mg).

Fraction B (4.61 g) was separated by Sephadex LH-20 column chromatography to obtain five fractions (B.1-B.5). Fraction B.3 (44.7 mg) was separated by *silica gel* column, using EtOAc – MeOH - H_2O (8:2:1) as the eluant to obtain compound **5** (3.3 mg) and compound **6** (4.2 mg).

Methyl-3β-hydroxycycloart-23,25-dien-29-oate-3-sulfate (**1**): Colourless gum; α_D^{27} + 17.31 (MeOH, c 0.1); UV λ_{max} (MeOH) 229 nm, ^{1}H-NMR and ^{13}C-NMR data, see Table 1; HR-ESIMS m/z: [M - H]$^-$

Table 1
^{1}H and ^{13}C-NMR data of isolated compounds **1**–**4** (δ in *ppm*; *J* in Hz) (600 MHz for ^{1}H-NMR and 150 MHz for ^{13}C-NMR in CD_3OD).

Position	**1**		**2**		**3**		**4**	
	δ_H (*J* in Hz)	δ_C	δ_H (*J* in Hz)	δ_C	δ_H (*J* in Hz)	δ_C	δ_H (*J* in Hz)	δ_C
1*α*	1.66 m	32.5	1.58 m	32.9	1.57 m	32.9	1.68 m	32.5
1*β*	1.34 m		1.30 m		1.30 m		1.35 m	
2*α*	2.25 m	28.1	2.22 m	28.6	2.21 m	28.6	2.25 m	28.1
2*β*	1.69 m		1.72 m		1.73 m		1.71 m	
3	4.74 dd (4.4, 11.4)	83.3	4.01 dd (4.5, 11.8)	87.2	4.01 dd (4.5, 11.5)	87.4	4.75 dd (4.5, 11.5)	83.3
4	-	55.2	-	41.3	-	41.3	-	55.2
5	2.12 dd (4.5, 12.5)	45.8	1.40 m	48.7	1.40 m	49.0	2.11 m	45.9
6*α*	1.07 m	24.0	1.63 m	22.4	1.63 m	22.2	1.07 m	23.9
6*β*	0.96 m		0.83 m		0.85 m		0.98 m	
7*α*	1.12 m	26.6	1.15 m	27.1	1.13 m	27.1	1.33 m	26.6
7*β*	1.32 m		1.36 m		1.36 m		1.17 m	
8	1.60 m	49.3	1.56 m	49.4	1.57 m	49.4	1.63 m	49.4
9	-	21.3	-	21.3	-	21.2	-	21.2
10	-	26.3	-	26.3	-	26.3	-	26.3
11*α*	2.05 m	27.4	2.05 m	27.5	2.04 m	27.4	2.05 m	27.4
11*β*	1.20 m		1.18 m		1.19 m		1.21 m	
12	1.67 m (2H)	33.9	1.66 m (2H)	34.1	1.67 m (2H)	34.1	1.67 m (2H)	33.9
13	-	46.5	-	46.5	-	46.6	-	46.6
14	-	50.0	-	49.5	-	50.2	-	50.1
15	2.19 m	36.6	2.19 m	36.7	1.35 m	36.6	1.34 m	36.5
	1.35 m		1.37 m					
16*α*	1.96 m	29.0	1.97 m	29.2	1.93 m	29.4	1.93 m	29.3
16*β*	1.36 m		1.36 m		1.33 m		1.35 m	
17	1.64 m	53.4	1.64 m	53.4	1.62 m	53.2	1.67 m	53.9
18	1.02 s (3H)	18.6	1.03 s (3H)	18.6	1.05 s (3H)	18.6	1.04 s (3H)	18.5
19*α*	0.45 d (4.4)	30.1	0.38 d (4.2)	30.8	0.39 d (4.2)	30.8	0.46 d (4.2)	30.6
19*β*	0.65 d (4.4)		0.59 d (4.2)		0.60 d (4.2)		0.65 d (4.2)	
20	1.51 m	38.0	1.53 m	38.0	2.00 m	35.0	1.98 m	35.0
21	0.90 d (6.5) (3H)	18.9	0.90 d (6.4) (3H)	18.9	0.88 d (6.5) (3H)	19.6	0.89 d (6.4) (3H)	19.7
22	1.85 m	40.8	1.85 m	40.7	2.11 m	52.7	2.12 m	52.7
	2.29 m		2.29 m		2.54 m		2.55 dd (3.0, 15.0)	
23	5.66 ddd (15.3, 8.5, 6.3)	130.0	5.66 ddd (15.0, 8.5, 6.2)	130.2	-	204.3	-	204.2
24	6.12 d (15.6)	135.5	6.12 d (15.0)	135.5	6.17 p (1.4)	125.4	6.20 s	125.3
25	-	143.5	-	143.5	-	156.9	-	156.9
26	4.85 s (2H)	114.5	4.83 s (2H)	114.5	1.90 s (3H)	27.5	1.91 s (3H)	27.7
27	1.82 s (3H)	18.9	1.83 s (3H)	18.9	2.14 s (3H)	20.9	2.12 s (3H)	20.8
28	1.17 s (3H)	10.6	0.87 s (3H)	15.4	0.87 s (3H)	15.4	1.17 s (3H)	10.6
29	-	178.0	1.84 s (3H)	26.3	1.02 s (3H)	26.3	-	178.0
30	0.94 s (3H)	19.7	0.94 s (3H)	19.8	0.95 s (3H)	19.7	0.97 s (3H)	19.7
29-OCH_3	3.67 s (3H)	52.4	-	-		-	3.70 s (3H)	52.7

547.30978 (calcd. for $C_{31}H_{47}O_6S^-$ 547.3093).

3*β*-hydroxycycloart-23,25-dien-3-sulfate (**2**) Colourless gum; α_D^{27} + 28.2 (MeOH, c 0.1); UV λ_{max} (MeOH) 230 nm, ^{1}H-NMR and ^{13}C-NMR data, see Table 1; HR-ESIMS m/z: [M - H]$^-$ 503.3168 (calcd. for $C_{30}H_{47}O_4S^-$ 503.3195).

3*β*-hydroxycycloart-24-en-23-one 3-sulfate (**3**) Amorphous white powder; α_D^{27} + 23.0 (MeOH, c 0.1); UV λ_{max} (MeOH) 237 nm, ^{1}H-NMR and ^{13}C-NMR data, see Table 1; HR-ESIMS m/z: [M - H]$^-$ 519.31213 (calcd. for $C_{30}H_{47}O_5S^-$ 519.3144).

Methyl-3*β*-hydroxycycloart-24-en-23-one-29-oate-3-sulfate (**4**) Amorphous white powder; α_D^{27} 38.0 (MeOH, c 0.1); UV λ_{max} (MeOH) 238.5 nm, ^{1}H-NMR and ^{13}C-NMR data, see Table 1; HR-ESIMS m/z: [M-H]$^-$ 563.30412 (calcd. for $C_{31}H_{47}O_7S^-$ 563.30479).

O-*α*-galactopyranosyl (1″→6′)-O-*β*-galactopyranosyl-(1′→1)-glycerol (**5**). Colourless gum; α_D^{27} + 42.9; UV λ_{max} (MeOH) 201 nm, ^{1}H-NMR and ^{13}C NMR, see Table 2; HR-ESIMS m/z: [M-H]$^-$ 415.14378 (calcd. for $C_{15}H_{27}O_{13}^-$ 415.1451).

Floridoside (**6**) Colourless oil; α_D^{27} + 98.4; UV λ_{max} (MeOH) 201 nm, ^{1}H-NMR and ^{13}C-NMR data see Table 2; HR-ESIMS m/z: [M-H]$^-$ 253.09216 (calcd. for $C_9H_{17}O_8^-$ 253.0923).

Table 2
^{1}H and ^{13}C-NMR data of isolated compounds **5** and **6** (δ in *ppm*; *J* in Hz) (600 MHz for ^{1}H-NMR and 150 MHz for ^{13}C-NMR in CD_3OD).

Position	**5**		**6**	
	δ_C	δ_H	δ_C	δ_H
1	64.07	3.60 dd (11.3, 5.3)	62.98	3.70 m (2H)
		3.57 m		
2	70.27	3.77 m	81.59	3.71 m
3	72.21	3.84 m	62.32	3.70 m
		3.70 m		3.66 m
1’	105.21	4.25 d (7.4)	100.42	5.02 d (3.2)
2’	72.59	3.54 m	70.51	3.77 t (3.3)
3’	74.59	3.51 m	71.16	3.88 dd (2.9, 2.3)
4’	70.24	3.86 d (4.3)	71.51	3.78 m
5’	74.69	3.76 m	72.66	4.01, ddd (6.6, 5.0,1.3)
6’	67.83	3.67 m	62.84	3.70 m (2H)
		3.92 m		
1”	100.43	4.86 over l.		
2”	72.34	3.79 m		
3”	71.44	3.76 m		
4”	71.04	3.89 m		
5”	72.48	3.88 m		
6”	62.71	3.71 m (2H)		

2.5. Cytotoxicity assay

The cytotoxic activity of compounds **1**- **6** against the breast cancer cell line (MDA-MB-231) was determined using the MTT assay, with doxorubicin as a positive control. Briefly, compounds were dissolved in DMSO to prepare a stock solution at a concentration of 20 mg/mL, and subsequently diluted in the culture medium to achieve testing

concentrations. 5×10^4 cells/well were seeded into 96-well plates and were treated with the test compounds at different concentrations (100, 50, 25, 12.5 and 6.25 μM). After 72 h, the culture medium was removed, 50 μL MTT (0.5 mg/mL) and 150 μL culture solution were added to each well, followed by incubation at 37°C and 5% CO_2 for 3 h. Subsequently, 200 μL of DMSO was added to solubilize the resulting formazan crystals. The optical density (OD) was measured at 570 nm using a Multiskan™ FC microplate photometer (Denizot and Lang, 1986). IC_{50} values were calculated for each independent experiment from the concentration-response curves using nonlinear regression in GraphPad Prism. The results are expressed as the mean ± standard deviation (SD) of three independent experiments.

2.6. Anti-inflammatory assay

Initially, the test compounds were evaluated for their cytotoxicity against RAW 264.7 cells at various concentrations using the MTT assay. From non-cytotoxic concentrations, subsequent dilutions were prepared from these levels to evaluate the anti-inflammatory activity. NO concentration in the cultured medium was quantified based on the Griess reaction. Briefly, 100 μL of the culture supernatant was mixed with 100 μL of Griess reagents (1% sulfanilamide in 5% phosphoric acid and 0.1% naphthylethylenediamine dihydrochloride in water). The resulting mixture was incubated for 10 min at room temperature in the dark. Then, the absorbance was measured at 540 nm with a microplate reader (Lee et al., 2019).

3. Results

3.1. Identification of isolated compounds

Compound **1** was obtained as a colorless gum. Its molecular formula was determined as $C_{31}H_{48}O_6S$ based on the quasimolecular ion at 547.30978 m/z $[M\text{-}H]^-$ in the HR-ESIMS spectrum. The ^{1}H-NMR spectrum of **1** exhibited characteristic signals of a pair of cyclopropane methylene protons (δ_H 0.45 and 0.65, both d with J = 4.4 Hz), one oxymethine proton (δ_H 4.74, dd, J = 4.4, 11.4 Hz), four tertiary methyls [δ_H 1.82, 1.17, 1.02 and 0.94 (each 3H, s)], a secondary methyl (δ_H 0.90, d, J = 6.5 Hz), a methoxy group (δ_H 3.67, s), two *trans*-olefinic protons (δ_H 5.66, ddd, J = 15.3, 8.5, 6.3 Hz; δ_H 6.12, d, J =15.6 Hz), and two olefinic methylene protons (δ_H 4.85, 2H, s). The ^{13}C-NMR spectrum of **1**, in combination with HSQC data, displayed 31 signals, including a methoxy group (δ_C 52.4), an oxygenated methine carbon (δ_C 83.3), four olefinic carbons (δ_C 143.5, 135.5, 130.0 and 114.5), together with 5 methyl groups (δ_C 19.7, 18.9 (x 2), 18.6 and 10.6) and a carbonyl group (δ_C 178.0). Several key resonances of compound **1** are very close to the sulfated cycloartane triterpenoids reported by Horgen et al. (2000) **(**Fig. 1**)**. The sulfate group was assigned at C-3 when the H-3 (δ_H 4.74) and C-3 (δ_C 83.3) were shifted downfield compared to typical triterpenoids possessing a free hydroxyl group at this position (Lu et al., 2019). Additionally, a pair of cyclopropane methylene protons is characteristic of H_2-19, whereas the -$COOCH_3$ substituent at C-29 induced noticeable shifts in the signals of C-4 (δ_C 55.2), C-5 (δ_C 45.8) and H-5 (δ_H 2.12) compared to those of typical cycloartanes bearing a -CH_3 group at C-29. These signals, when compared with previously reported data (Horgen et al., 2000; Tran et al., 2021), confirmed the cycloartane skeleton. Detailed 2D-NMR analyses (COSY, HSQC, HMBC and NOESY) were performed to unambiguously elucidate the structure. The side chain of compound **1** differed from those of previously reported cycloartanes due to the presence of a terminal double bond, which was confirmed by the exocyclic methylene signals (δ_C 114.5 and δ_H 4.85, s, 2H). The protons at δ_H 4.85 showed HMBC correlations to a methyl group (δ_C 18.9) and an olefinic carbon at δ_C 135.5, while the proton attached to the carbon at δ_C 135.5 exhibited HMBC correlations to the carbons at δ_C 143.5, 114.5 and 130.0. This established the presence of a conjugated diene system. The HMBC correlations from the olefinic proton at δ_H 5.66 to carbon δ_C 143.5 and from the proton δ_H 6.12 to the carbons at δ_C 143.5, 114.5 and 18.9, further supported this deduction. In addition, the proton at δ_H 6.12 showed an HMBC correlation with a methylene carbon at δ_C 40.8, which was further correlated to the protons of the C-21 methyl group (δ_H 0.90). Finally, the COSY correlations between the methylene protons at δ_H 1.85 and 2.29 (attached to the δ_C 40.8) and the olefinic proton (δ_H 5.66) determined that the side chain of compound **1** features a -CH_2- at C-22, two double bonds at C-23/C-24 and C-25/C-26, and a methyl group at C-27 (Fig. 2). The relative stereochemistry of **1** was assigned based on coupling constants and NOESY data. The sulfate group attached to C-3 in β-orientation was due to the coupling constant between H-3 and H-2 ($J_{3a,\ 2a}$ = 11.4 Hz and $J_{3a,\ 2e}$ = 4.4 Hz), which indicated an α-axial orientation for H-3. This was further corroborated by the NOESY cross-peak between H-3 and H-5. Additionally, the NOESY correlation between H-19 (δ_H 0.65) and H_3-28 (δ_H 1.17) supported the β-orientation of 28-CH_3. The coupling constant of H_3-21 (δ_H 0.90, d, J = 6.5 Hz) and NOESY correlations of H_3-30/H-17/H_3-21 indicated the 20 R stereochemistry **(**Fig. 2**).** The NOESY spectroscopic data of compound **1** were similar to those of previously reported cycloartane-type triterpenoids (Horgen et al., 2000; Lu et al., 2019; Tran et al., 2021). Consequently, the structure of compound **1** was determined as methyl-3β-hydroxycycloart-23,25-dien-29-oate-3-sulfate.

Compound **2** showed the HR-ESIMS negative molecular ion at m/z: $[M\text{ - }H]^-$ 503.3168, indicating a molecular formula $C_{30}H_{48}O_4S$. The NMR spectroscopic data of compound **2** were closely related to those of **1**, with the exception of the absence of the methyl ester group and the presence of an additional methyl signal. The HMBC spectrum displayed correlations from the proton H-3 (δ_H 4.01, dd, J = 4.5; 11.8 Hz) to two methyl carbons (δ_C 18.9 and 26.3). Furthermore, the chemical shifts of C-3 (δ_C 87.2), C-4 (δ_C 41.3), and C-5 (δ_C 48.7) of compound **2** were

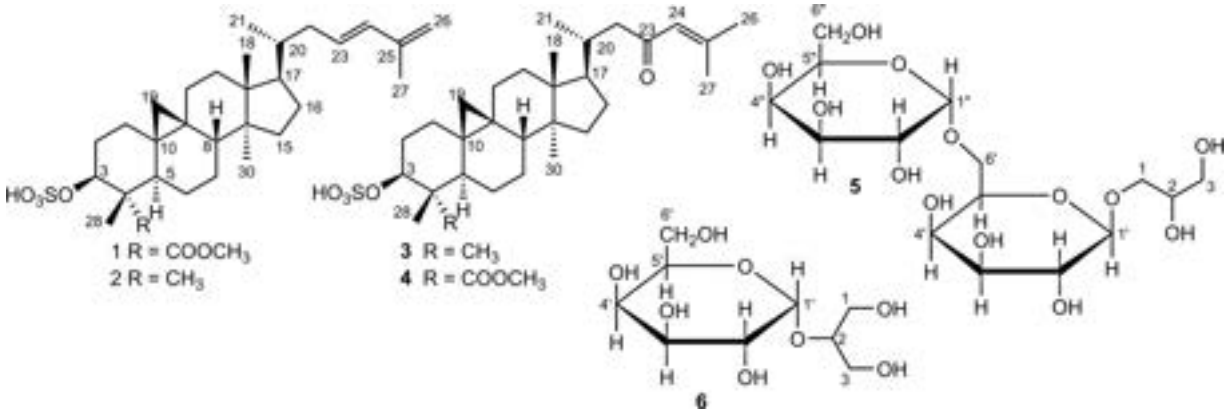

Fig. 1. Structures of isolated compounds (**1** - **6**).

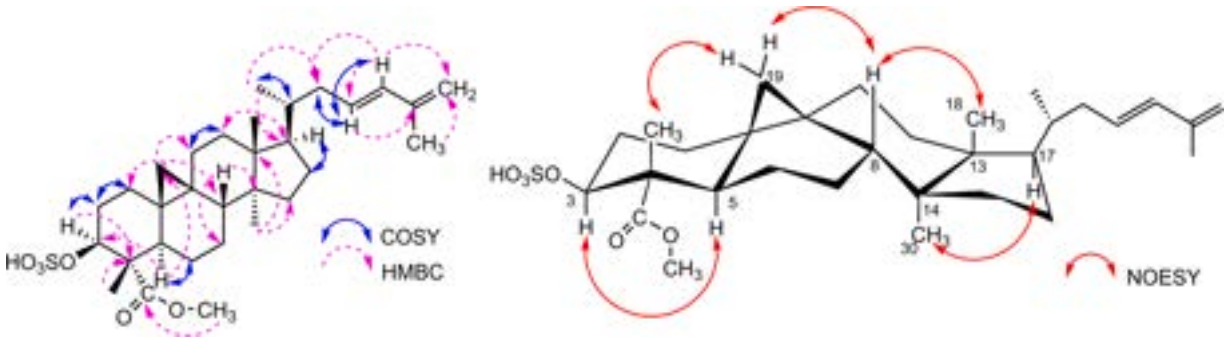

Fig. 2. Key COSY, HMBC and NOESY correlations of compound **1**.

significantly altered compared to compound **1**; specifically, C-3 and C-5 were shifted downfield, whereas C-4 was shifted upfield. These findings indicated that a methyl group substituted the methoxycarbonyl moiety. The key NOESY correlations of compound **2** were identical to those of compound **1**, including H-3 (δ_H 4.01)/ H-5 (δ_H 1.40), H-19 (δ_H 0.59)/H_3-28 (δ_H 0.87), H-19 (δ_H 0.59)/H-8 (δ_H 1.56) and (H-8 (δ_H 1.56)/ H_3-18 (δ_H 1.03). Accordingly, the structure of compound **2** was elucidated as 3β-hydroxycycloart-23,25-dien-3-sulfate. To the best of our knowledge, compounds **1** and **2** were identified as previously undescribed natural products (Fig. 1).

Compound **3** exhibited spectral features similar to those of 3β-hydroxycycloart-24-en-23-one-3-sulfate which was identified from *T. fragilis* (Horgen et al., 2000; Tran et al., 2021). The NMR spectral data of compound **4** closely resembled those of compound **3**; however, compound **4** contained an additional methyl ester group (δ_C 178.0, 52.7 and δ_H 3.70 s, 3H) and lacked a methyl group. Furthermore, the carbon signal at C-3 in **4** was shifted upfield to δ_C 83.3 (compared to δ_C 87.4 in compound **3**). The HMBC correlation from H-3 (δ_H 4.75) to the ester carbonyl carbon (δ_C 178.0) confirmed the replacement of the C-29 methyl group by a methyl ester moiety. Comprehensive analysis of the spectroscopic data led to the elucidation of compound **4** as methyl-3-β-hydroxycycloart-24-en-23-one-29-oate-3-sulfate. Compound **4** has also been previously reported to be isolated from the alga *T. fragilis* (Horgen et al., 2000) (Fig. 1).

Compounds **5** and **6** are two carbohydrate derivatives whose structures were elucidated through NMR spectral analysis and comparison with reported literature data. Compound **5** was identified as *O*-α-galactopyranosyl (1″→6′)-O-β-galactopyranosyl-(1′→1)- *sn*-glycerol (Baruah et al., 1983; Hisamatsu et al., 2005), and compound **6** was determined to be floridoside (Abreu et al., 1997; Karsten et al., 1993). All six compounds were isolated from the alga *T. cylindrica* for the first time (Fig. 1).

3.2. Anti-cancer properties of isolated compounds

The cytotoxic activity of the isolated compounds was evaluated against the breast cancer cell line (MDA-MB-231) at a range of concentrations (100, 50, 25, 12.5, and 6.25 μM). The results indicated that only compounds **3** and **4** exhibited determinable IC_{50} values, which were 66.24 ± 0.09 μM and 62.15 ± 0.25 μM, respectively. The remaining compounds showed inhibition percentages below 50% at the highest tested concentration of 100 μM; therefore, the IC_{50} value could not be determined (Fig. 3). The positive control was doxorubicin, with an IC_{50} value of 1.64 ± 0.01 μM.

3.3. Anti-inflammatory activity of isolated compounds

The cytotoxic activity of the tested compounds against RAW 264.7 cells was evaluated to assess cell viability, ensuring that cytotoxicity would not interfere with the measurement of NO production in LPS-stimulated cells. The cytotoxicity assay results indicated that compounds **3** and **4** induced % inhibition of 22.70% and 35.25% at the concentration of 12.5 μM, respectively. The higher concentrations increased cell death in a dose-dependent manner. Compound **2**

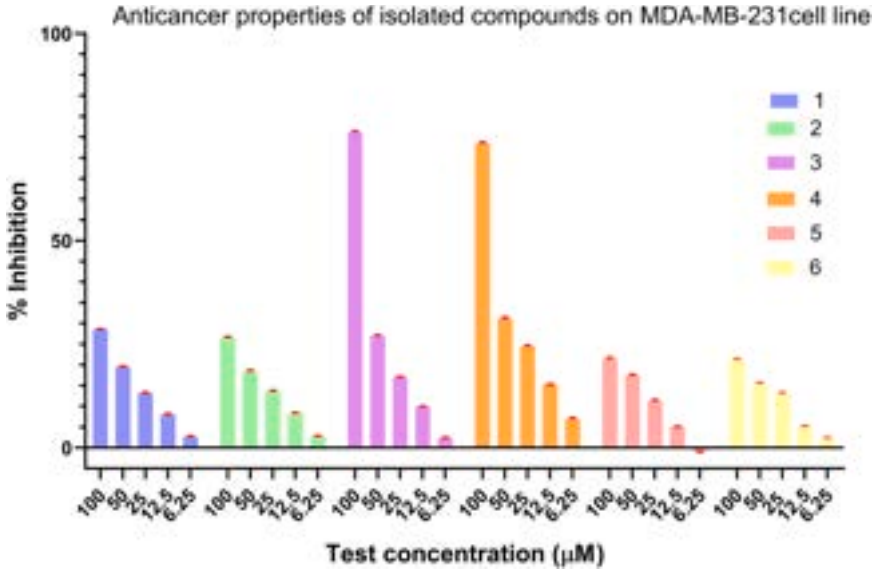

Fig. 3. Anti-cancer properties of compound (**1**- **6**) on MDA-MB-231 cells. The results were presented as mean ± standard deviation (SD), (n = 3).

exhibited inhibition of 20.03% at 12.5 μM whereas compounds **1**, **5**, and **6** were considered safe at concentrations of 50 μM (inhibition of only 22–28%) and lower concentrations (Fig. 4). Based on these findings, the NO inhibitory assay was performed using different concentration ranges. Compounds **3** and **4** were tested at concentrations of 10, 5, 2.5, 1.25, and 0.625 μM. The results showed that compound **3** exhibited only 31.4% inhibition at the highest tested concentration (10 μM) and thus its IC_{50} value could not be determined **(**Fig. 5**).** In contrast, compound **4** inhibited NO production in a concentration-dependent manner, with a calculated IC_{50} value of 6.84 ± 0.61 μM. Compounds **3** and **4** share an identical structural core, differing only in the substituent at C-29. Therefore, the difference in anti-inflammatory activity may be attributed to the structural differences between compound **3** (possessing a 29-CH_3) and compound **4** (possessing a 29-$COOCH_3$ group). However, further experimental studies are required to confirm this hypothesis.

Compound **2** was tested at a concentration range from 25 to 1.56 μM, and the IC_{50} value was determined at 9.01 ± 0.68 μM. Compounds **1**, **5**, and **6** were evaluated over a concentration range from 50 to 3.13 μM, exhibiting concentration-dependent NO inhibitory percentages. Their IC_{50} values were determined to be 18.07 ± 1.85 μM, 7.29 ± 0.86 μM, and 6.76 ± 0.85 μM, respectively (Fig. 6). Besides, the IC_{50} value of positive reference dexamethasone was determined at 12.34 ± 0.15 μM.

4. Discussion

Initial descriptions of the genus *Tricleocarpa* included only two species: *T. fragilis* and *T. cylindrica* (Huisman and Borowitzka, 1990). Currently, the expansion of specimen collection across various marine regions combined with advanced morphological and DNA sequencing analyses has led to the discovery of several novel species, including *T. jejuensis* and *T. natalensis* (Wiriyadamrikul et al., 2013), and *T. confertus* (Liu et al., 2015).

The presence of the marine algal genus *Tricleocarpa* in Vietnam is characterized by two species, *T. cylindrica* and *T. fragilis* (Van Nguyen et al., 2013). While *T. fragilis* has been extensively investigated for both its chemical constituents and biological activities, data regarding *T. cylindrica* remain largely unestablished. Previous studies demonstrated that the main constituents of *T. fragilis* are C-3 sulfated cycloartane-type triterpenoids, which have been proven to exhibit potent cytotoxicity and α-glucosidase inhibitory activities (Horgen et al., 2000; Tran et al., 2021). Based on the taxonomic relationship, evaluating the chemical constituents of *T. cylindrica* represents a highly promising approach to discovering bioactive compounds.

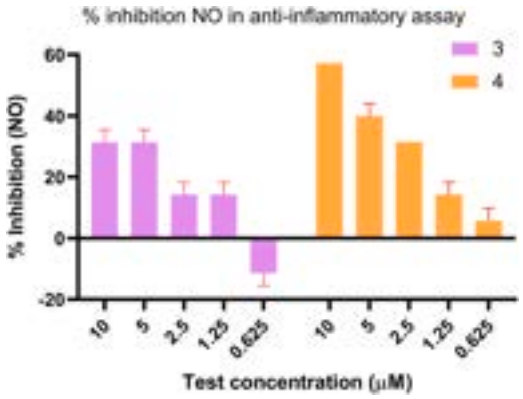

Fig. 5. % inhibition NO of compounds **3** and **4** on LPS-induced RAW 264.7 cell. The results were presented as mean ± standard deviation (SD), (n = 3).

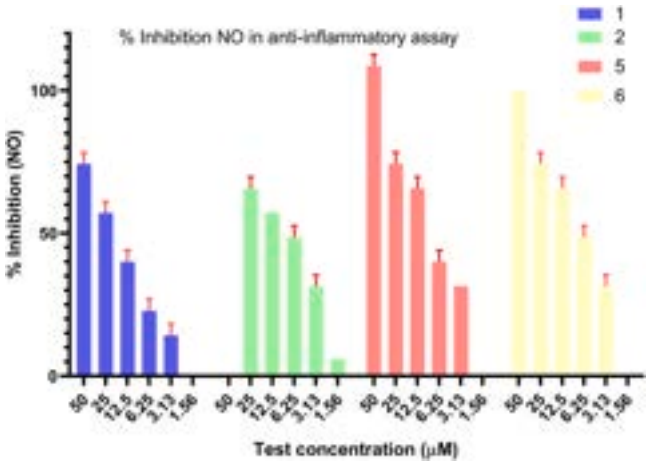

Fig. 6. % inhibition NO of compounds **1, 2, 5** and **6** on LPS-induced RAW 264.7 cell. The results were presented as mean ± standard deviation (SD), (n = 3).

Extraction from marine material often encounters obstacles due to the high accumulation of residual salts in the crude extract. In this study, 96% ethanol was employed as the extraction solvent to minimize the

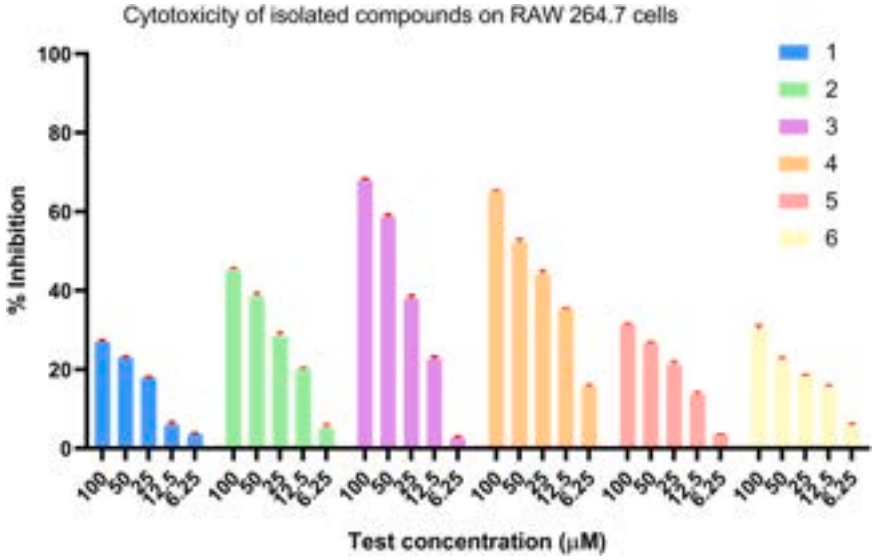

Fig. 4. Cytotoxicity activities of compounds (**1**- **6**) on RAW 264.7 cells. The results were presented as mean ± standard deviation (SD), (n = 3).

extraction of highly polar components; however, the resulting yield still contained a substantial amount of salt. Consequently, a desalting method was developed based on solid-liquid extraction, utilizing clean sand as a carrier matrix for the organic components, followed by water elution. Reversed-phase silica gel was introduced during the elution process to prevent the loss of organic compounds present in the extract. After washing with water, the desalted extract was recovered using 96% ethanol and acetone. This purification process eliminated conventional liquid-liquid partitioning, a process in which the sulfated triterpenoids can act as emulsifiers, making phase separation extremely difficult.

The isolation process successfully yielded six compounds, including four triterpenoids and two carbohydrate derivatives. The structures of the triterpenoids exhibited features similar to those previously identified from *T. fragilis*, characterized by a cycloartane skeleton and a sulfate group at the C-3 position. The structural differences in these compounds are characterized by differences in their side chains and the substituents at C-29. Notably, compounds **3** and **4** demonstrated significant cytotoxic activity against MDA-MB-231 cancer cells, whereas compounds **1** and **2** exhibited weak effects. Furthermore, compounds **3** and **4** also showed more potent cytotoxicity against RAW 264.7 cells. This suggests that the conjugation of the ketone group at C-23 with the C-24/C-25 double bond plays a crucial role in this activity. Previous studies have also indicated that this specific structural feature influences α-glucosidase inhibitory activity (Tran et al., 2021). However, due to the limited number of isolated and evaluated compounds, this hypothesis is considered preliminary. To definitively establish the structure-activity relationships, further screening of a broader library of cycloartane derivatives is required, together with molecular investigations into the interactions between these structural components and the target proteins that mediate cytotoxicity. These preliminary data suggest that cycloartane-type triterpenoids possessing a sulfate group at C-3 contribute to the cytotoxic activity of the *T. cylindrica* extract. Further phytochemical studies on this class of derivatives are needed to elucidate the key structural features responsible for their biological effects.

Regarding the anti-inflammatory activity of the triterpenoids, compounds **1**, **2**, and **4** exhibited notable inhibitory effects on NO production, whereas the IC_{50} value of compound **3** could not be determined within the non-cytotoxic concentration range. Among the triterpenoids tested, compound **4** showed the strongest activity, with an IC_{50} value of 6.84 ± 0.61 μM.

In addition to the triterpenoid constituents, carbohydrate derivatives were also identified from this species for the first time. Compound **5**, *O*-α-galactopyranosyl (1″→6′)-*O*-β-galactopyranosyl-(1′→1)-glycerol, was previously reported from two red algal species, *Polysiphonia fastigiata* and *Corallina officinalis* (Wickberg et al., 1958). Biological activity reports indicated that this compound exhibited weak inhibitory effects on rat lens aldose reductase (Matsuda et al., 1999). Compound **6** was identified as floridoside, which has been found in over 160 red algal species, particularly within the genus Porphyra and Gracilaria. The finding of this compound in a species belonging to the genus *Tricleocarpa* provides additional data for the chemotaxonomic analysis of red algae (Semmouri et al., 2025). Floridoside isolated from *Laurencia undulata* has also been reported to possess antioxidant effects with an IC_{50} value of 39.3 μM (Li et al., 2010). This compound showed no cytotoxicity against several cultured cell lines, including human hepatocyte L-02, BV-2, MRC-5, RAW 264.7, HL-60, and HT-1080 (Semmouri et al., 2025). The findings of the present study are consistent with these reports, as compound **6** was found to be non-cytotoxic to MDA-MB-231 cells. Furthermore, floridoside has been evaluated for its prebiotic potential and it also functions as an artificial sweetener (Semmouri et al., 2025). In this study, both compounds **5** and **6** were found to exhibit potent anti-inflammatory activities. These results provide additional data regarding the biological activities of carbohydrate derivatives discovered in red algae.

5. Conclusion

The phytochemical investigation of *Tricleocarpa cylindrica* led to the isolation and identification of six compounds, including four cycloartane-type triterpenoids and two carbohydrate derivatives. Compounds **1** (methyl-3β-hydroxycycloart-23,25-dien-29-oate-3-sulfate) and **2** (3β-hydroxycycloart-23,25-dien-3-sulfate) are new natural products, and all isolated compounds were reported from this species for the first time. In addition, their cytotoxic and anti-inflammatory activities were evaluated. Only compounds **3** (3β-hydroxycycloart-24-en-23-one 3-sulfate) and **4** (methyl-3β-hydroxycycloart-24-en-23-one-29-oate-3-sulfate), which are characterized by a conjugated system between the ketone group and the double bond in the side chain, exhibited cytotoxicity against MDA-MB-231 cancer cells, whereas the remaining compounds showed weak or no cytotoxic effects. Notably, both the triterpenoids and carbohydrate derivatives displayed potent anti-inflammatory activities in the LPS-stimulated RAW 264.7 assay by suppressing NO production. These findings highlight the potential of the genus *Tricleocarpa* as a promising source of bioactive compounds for further investigation and practical applications.

CRediT authorship contribution statement

T. V. A. Tran: Writing – review & editing, Writing – original draft, Supervision, Investigation, Formal analysis, Data curation. **Thi Dieu Hien Nguyen:** Validation, Investigation. **Duy Hien Tran:** Methodology, Data curation. **Thi Kim Anh Le:** Validation, Investigation. **Thi Hong Tuoi Do:** Methodology, Data curation. **V. M. Nguyen:** Writing – review & editing, Validation, Project administration, Conceptualization. **The Han Nguyen:** Writing – review & editing, Validation, Project administration, Conceptualization.

Declaration of Generative AI and AI-assisted technologies in the manuscript preparation process

During the preparation of this work, the authors used Gemini and ChatGPT for language editing and to improve the readability of the manuscript. After using these tools, the authors reviewed and edited the content as needed and have taken full responsibility for the content of the published article.

Funding

This work was supported by the Ministry of Education and Training of Vietnam under the project “Study on the chemical composition and selected biological activities of several red algae species of the family Galaxauraceae collected from Vietnamese waters”, grant number B2024-TSN-16. The funder had no role in the study design, data collection, analysis, interpretation, manuscript preparation, or decision to submit the article for publication.

Declaration of Competing Interest

The authors declare that they have no known competing financial interests or personal relationships that could have appeared to influence the work reported in this paper.

Acknowledgments

The authors gratefully acknowledge Dr. Do Anh Duy from the Northern Research Center for Marine Fisheries (NRCMF), Viet Nam Academy of Fishery Sciences (VAFIS), for his kind support in the collection and taxonomic identification of *T. cylindrica*, as well as for providing expertise on the morphological authentication of the algal material. This work contributes to the celebration of the 50th anniversary of Nha Trang University, located in Khanh Hoa Province, Viet Nam.

Appendix A. Supporting information

Supplementary data associated with this article can be found in the online version at doi:10.1016/j.rsma.2026.105462.

Data availability

Data will be made available on request.

References

Abreu, P.M., Galindro, J.M., Relva, A.M., Ramos, A.M., 1997. Non-terpenoid compounds from *Plocamium cartilagineum*. Phytochemistry 45 (8), 1601–1603. https://doi.org/10.1016/S0031-9422(97)00200-8.

Banu, V.S., Mishra, J.K., 2018. Fatty acid, micronutrient, proximate composition and phytochemical analysis of red seaweed *Tricleocarpa fragilis* (L.) Huisman & R.A. Towns from Andaman Sea, India. J. Pharmacogn. Phytochem. 7 (4), 2143–2148.

Banu, V.S., Mohan, U., Kumari, R., Kumar, P., Singh, A.K., Siddiqui, M.H., Alamri, S., Siddiqui, M.W., Singh, D.R., 2024. Insights into the physiology, biochemistry and ecological significance of the red seaweed *Tricleocarpa fragilis* in the Andaman Sea. BMC Plant Biol. 24 (1), 765. https://doi.org/10.1186/s12870-024-05452-3.

Baruah, P., Baruah, N.C., Sharma, R.P., Baruah, J.N., Kulanthaivel, P., Herz, W., 1983. A monoacyl galactosylglycerol from *Sonchus arvensis*. Phytochemistry 22 (8), 1741–1744. https://doi.org/10.1016/S0031-9422(00)80262-9.

Denizot, F., Lang, R., 1986. Rapid colorimetric assay for cell growth and survival: modifications to the tetrazolium dye procedure giving improved sensitivity and reliability. J. Immunol. Methods 89 (2), 271–277. https://doi.org/10.1016/0022-1759(86)90368-6.

Do, A.D., Bui, M.T., Dong, T.D., Nguyen, T.H., 2024. Morphological characteristics of seaweed species of Galaxauraceae family (Nemaliales, Rhodophyta) distributed in Vietnam. Vietnam. J. Agric. Sci. 23 (2), 161–173.

Hisamatsu, Y., Goto, N., Sekiguchi, M., Hasegawa, K., Shigemori, H., 2005. Oxylipins arabidopsides C and D from *Arabidopsis thaliana*. J. Nat. Prod. 68 (4), 600–603. https://doi.org/10.1021/np0495938.

Horgen, F.D., Sakamoto, B., Scheuer, P.J., 2000. New triterpenoid sulfates from the red alga *Tricleocarpa fragilis*. J. Nat. Prod. 63 (2), 210–216. https://doi.org/10.1021/np990448h.

Huisman, J.M., Borowitzka, M.A., 1990. A revision of the Australian species of Galaxaura (Rhodophyta, Galaxauraceae), with a description of Tricleocarpa gen. nov. Phycologia 29 (2), 150–172. https://doi.org/10.2216/i0031-8884-29-2-150.1.

Karsten, U., Barrow, K.D., King, R.J., 1993. Floridoside, L-Isofloridoside, and D-Isofloridoside in the Red Alga *Porphyra columbina* (Seasonal and Osmotic Effects). Plant. Physiol. 103 (2), 485–491. https://doi.org/10.1104/pp.103.2.485.

Koru, E., Kılınç, B., Turan, G., Cirik, S., Tekoğul, H., 2013. In: Muzzalupo, I. (Ed.), Seaweeds for food and industrial applications. Food Industry, IntechOpen, London.

Leal, M.C., Munro, M.H.G., Blunt, J.W., Puga, J., Jesus, B., Calado, R., Rosa, R., Madeira, C., 2013. Biogeography and biodiscovery hotspots of macroalgal marine natural products. Nat. Prod. Rep. 30 (11), 1380–1390. https://doi.org/10.1039/c3np70057g.

Lee, T.K., Trinh, T.A., Lee, S.R., Kim, S., So, H.M., Moon, E., Hwang, G.S., Kang, K.S., Kim, J.H., Yamabe, N., Kim, K.H., 2019. Bioactivity-based analysis and chemical characterization of anti-inflammatory compounds from *Curcuma zedoaria* rhizomes using LPS-stimulated RAW264.7 cells. Bioorg. Chem. 82, 26–32. https://doi.org/10.1016/j.bioorg.2018.09.027.

Li, Y.X., Li, Y., Lee, S.H., Qian, Z.J., Kim, S.K., 2010. Inhibitors of oxidation and matrix metalloproteinases, floridoside, and d-isofloridoside from marine red alga *Laurencia undulata*. J. Agric. Food Chem. 58 (1), 578–586. https://doi.org/10.1021/jf902811j.

Liu, S.L., Lin, S.M., Chen, P.C., 2015. Phylogeny, species diversity and biogeographic patterns of the genus Tricleocarpa (Galaxauraceae, Rhodophyta) from the Indo-Pacific region, including *T. confertus* sp. nov. from Taiwan. Eur. J. Phycol. 50 (4), 439–456. https://doi.org/10.1080/09670262.2015.1076892.

Lu, D., Zhang, W., Jiang, Y., Zhang, Y., Pan, D., Zhang, D., Yu, Y., 2019. Two new triterpenoids from *Gardenia jasminoides* fruits. Nat. Prod. Res. 33 (19), 2789–2794. https://doi.org/10.1080/14786419.2018.1502764.

Matsuda, H., Murakami, T., Yashiro, K., Yamahara, J., Yoshikawa, M., 1999. Antidiabetic principles of natural medicines. IV. Aldose reductase and α-glucosidase inhibitors from the roots of *Salacia oblonga* Wall. (Celastraceae): structure of a new friedelane-type triterpene, kotalagenin 16-acetate. Chem. Pharm. Bull. 47 (12), 1725–1729.

Nguyen, T.H., Do, T.H.T., Anh, L.T.K., Anh, T.T.H., Anh, T.T.V., 2025. Screening of acetylcholinesterase inhibitory, cancer cytotoxicity and anti-inflammatory activities of some red algae collected from Vietnamese coastal regions. Ho Chi Minh City J. Med. 28 (6), 12–22. https://doi.org/10.32895/hcjm.p.2025.06.02.

Phang, S.-M., Yeong, H.-Y., Ganzon-Fortes, E.T., Lewmanomont, K., Prathep, A., Hau, L. N., Gerung, G.S., Tan, K.S., 2016. Marine algae of the South China Sea bordered by Indonesia, Malaysia, Philippines, Singapore, Thailand and Vietnam. Raffles Bull. Zool. 34, 13–59.

Semmouri, I., Paepen, R., Janssen, C.R., Asselman, J., 2025. Floridoside originating from red algae (Rhodophyta): review on the occurrence, extraction and potential applications for human health and aquaculture. Algal Res. 92, 104376. https://doi.org/10.1016/j.algal.2025.104376.

Singkoh, M.F.O., Mantiri, D.M.H., Lumenta, C., Manoppo, H., 2019. Biomineral characterization and antibacterial activity of marine algae *Tricleocarpa fragilis* from Kora-kora coastal waters of Minahasa Regency, Indonesia. AACL Bioflux 12 (5), 1814–1822.

Tran, T.V.A., Nguyen, V.M., Nguyen, T.A.N., Nguyen, D.H.T., Tran, D.H., Bui, T.P.T., Pham, V.T., Nguyen, T.H., 2021. New triterpene sulfates from Vietnamese red alga *Tricleocarpa fragilis* and their α-glucosidase inhibitory activity. J. Asian Nat. Prod. Res. 23 (8), 754–763. https://doi.org/10.1080/10286020.2020.1783658.

Van Nguyen, T., Le, N.H., Lin, S.M., Steen, F., De Clerck, O., 2013. Checklist of the marine macroalgae of Vietnam. Bot. Mar. 56 (3), 207–227. https://doi.org/10.1515/bot-2013-0010.

Wickberg, B., Bostrup, O., Jensen, J., Svennerholm, L., Ernster, L., Diczfalusy, E., 1958. Structure of a glyceritol glycoside from *Polysiphonia fastigiata* and *Corallina officinalis*. Acta Chem. Scand. 12, 1183–1186. https://doi.org/10.3891/acta.chem.scand.12-1183.

Wiriyadamrikul, J., Geraldino, P.J.L., Huisman, J.M., Lewmanomont, K., Boo, S.M., 2013. Molecular diversity of the calcified red algal genus Tricleocarpa (Galaxauraceae, Nemaliales) with the description of *T. jejuensis* and *T. natalensis*. Phycologia 52 (4), 338–351. https://doi.org/10.2216/13-155.1.

Regional Studies in Marine Science 101 (2026) 105312

Contents lists available at ScienceDirect

Regional Studies in Marine Science

journal homepage: www.elsevier.com/locate/rsma

Mechanical and Morphological Characterization of Agricultural Waste-Reinforced Recycled HDPE Composites for Offshore Cage Frames

Nguyen Thi Kim Chi [a], Nguyen Van Tai [b], Nguyen Dac Kien [a], Nguyen Van Hoa [a,*]

[a] Department of Chemical and Environmental Engineering, Nha Trang University, Vietnam
[b] Department of Mechanical Engineering, Nha Trang University, Vietnam

ARTICLE INFO

Keywords:
Recycled HDPE
Nano-SiO_2
Wood powder
Coconut fiber
Green composites
Rice husk

ABSTRACT

This study presents the fabrication and properties of eco-friendly composite materials using recycled high-density polyethylene (rHDPE) as the matrix, reinforced with agricultural by-products, including wood powder, coconut fiber, and rice-husk-derived nano-silica (SiO_2). Nano-SiO_2 with a size range of 10–20 nm was successfully extracted from rice husk ash. The composites were prepared via thermal melting and compression molding at 180°C and 5 tons of pressure. Structural and morphological properties were analyzed using scanning electron microscopy (SEM), X-ray diffraction (XRD), and Fourier-transform infrared spectroscopy (FTIR). Mechanical tests revealed that the addition of 2 wt% nano-SiO_2 significantly improved the tensile strength (640.88 MPa) and elastic modulus (1141.48 MPa) compared to those of pure rHDPE, 402.16 and 953.07 MPa, respectively. While increasing the content of wood powder or coconut fiber generally decreased tensile strength, these fillers modified flexural and water absorption properties. The significantly improved tensile and elastic properties confirm that structural requirements for marine aquaculture systems. By utilizing agricultural waste and recycled plastics, this material serves as a potential low-cost substitute for expensive virgin HDPE, drastically reducing the capital investment for offshore cage frame fabrication. These findings support the transition towards sustainable, bio-based engineering solutions for the regional mariculture industry.

1. Introduction

The exponential growth of plastic waste, particularly high-density polyethylene (HDPE), has become a global environmental concern (Geyer et al., 2017). Despite HDPE's widespread use owing to its mechanical strength and chemical resistance, the prevalent linear "take--make-dispose" model has led to vast accumulations of durable waste. Effective recycling of HDPE (rHDPE) is essential for advancing the circular economy and reducing environmental harm (Kumi-Larbi Jnr et al., 2022; Arumugam et al., 2026). Yet, a major challenge is that rHDPE suffers mechanical property losses after repeated processing, restricting its industrial reuse. Addressing this degradation through targeted reinforcement strategies is therefore vital to restoring rHDPE's performance and making recycling a more robust environmental solution (Nasr et al., 2025).

The development of "green" polymer composites reinforced with natural fibers has gained significant traction in materials science due to their sustainability, low cost, and partial biodegradability (Mohanty et al., 2018). Vietnam, as a leading agricultural nation, produces abundant lignocellulosic by-products, including rice husk, wood powder, and coconut fiber. Wood powder and coconut fiber are particularly attractive as fillers due to their high cellulose content, which provides significant stiffness and reduces the composite's overall density and cost (Nadzri et al., 2022). Recent studies by Ogah et al. (2022) highlighted that incorporating agricultural waste into polymer matrices not only addresses waste management issues but also produces materials with specific strengths competitive with those of traditional glass-fiber-reinforced plastics. However, a major bottleneck in natural fiber composites is the inherent incompatibility between the hydrophilic nature of lignocellulosic fibers and the hydrophobic HDPE matrix. This mismatch often leads to poor interfacial bonding, resulting in voids and stress concentration points that compromise the material's long-term durability (Pickering et al., 2016; Kannan and Thangaraju, 2022).

To tackle interface issues, recent research now focuses on making blends that include tiny inorganic particles, such as nanoparticles (Shakil et al., 2026; Chen et al., 2026). Nano-silica (SiO_2) is well known for its large surface area and ability to improve the strength, flexibility, and heat resistance of plastics (Kennedy and Pandian, 2025). Making

* Corresponding author.
E-mail address: hoanv@ntu.edu.vn (N.V. Hoa).

https://doi.org/10.1016/j.rsma.2026.105312
Received 25 May 2026; Received in revised form 13 July 2026; Accepted 30 July 2026
Available online 31 July 2026

nano-silica from rice husk ash, a common farm waste in the Mekong Delta and central Vietnam, offers a more environmentally friendly and cost-effective alternative to using regular silica (Yaqueen et al., 2025). As noted by Sinha et al. (2020), nano-silica can connect parts at the joining surfaces, fill small spaces in the natural fiber-plastic mix, and create a stronger internal structure. This blending effect reduces water infiltration into the material and improves its resistance to tough conditions (Mishra et al., 2025). Besides, it was reported that the HDPE-composite containing SiO_2 offered high flexural strength of 124.82 MPa, a low water absorption rate of 6.01%, and low mass loss at a higher temperature (Venkatesh et al., 2023).

In Vietnam's mariculture industry, there is an urgent need for durable materials to construct offshore cage frames. Traditional materials like bamboo or wood lack longevity, while virgin HDPE pipes are increasingly expensive. Utilizing rHDPE reinforced with nano-SiO_2 and agricultural fibers offers a promising approach to creating high-performance, low-cost materials that withstand harsh marine conditions, including UV radiation and high salinity (Webo et al., 2026a, 2026b; Mullungal and Shaju, 2026). Recent advancements in melt-mixing and compression-molding techniques have enabled precise control over the distribution of these multiscale reinforcements, yet studies focusing on the synergistic interactions among rHDPE, rice-husk-derived nano-SiO_2, and organic fibers, such as wood and coconut, remain limited (Jonathan et al., 2021).

To address these critical research gaps, the primary objective of this study is to systematically evaluate the synergistic effects of rice-husk-derived nano-SiO_2 combined with organic agricultural fillers (wood powder and coconut fiber) on the morphological, chemical, mechanical, and water absorption characteristics of a recycled high-density polyethylene (rHDPE) matrix. It is hypothesized that the incorporation of highly dispersed, amorphous nano-silica will function as an effective nano-filler and interfacial bridge, filling microstructural voids and enhancing stress transfer between the hydrophobic matrix and hydrophilic organic fibers, thereby mitigating the processing-induced mechanical degradation typical of rHDPE. Furthermore, it is expected that while the organic fillers modify the flexural attributes of the matrix, SiO_2 nanoparticles will successfully restrict water infiltration under salinity conditions. This study contributes to the field of sustainable materials science by providing multi-filler rHDPE biocomposites with an eco-friendly and cost-effective material composition for for the regional mariculture industry.

2. Materials and Methods

2.1. Materials

Recycled high-density polyethylene (rHDPE) was obtained from post-consumer plastic waste (plastic bottles), ground to an average particle size of approximately 4 mm, and used as the polymer matrix. Rice husk ash, collected from a biomass combustion process, was used as the precursor for the synthesis of nano-sized SiO_2. Wood powder and coconut fiber were supplied by local agricultural processing facilities. Prior to composite fabrication, the organic fillers were washed thoroughly with distilled water, dried at 75°C overnight to remove moisture, and sieved to obtain a uniform particle size distribution (< 4 mm). All chemical reagents used for nano-SiO_2 synthesis were of analytical grade and used without further purification.

2.2. Composite fabrication

The composites were fabricated via a melt-mixing followed by compression molding process. Recycled HDPE, nano-SiO_2, and organic fillers were blended at various weight ratios (denoted as M1–M9), as summarized in Table 1. The mixtures were heated in a furnace from room temperature to 180°C over 30 min and maintained at this temperature for 15 min to ensure complete melting and homogeneous mixing. Subsequently, the molten materials were compression-molded under a pressure of 5 tons for 10 min, followed by cooling to room temperature inside the mold before demolding.

Table 1
Formulations of recycled HDPE composites with different filler contents.

Sample	rHDPE (wt %)	Wood powder (wt %)	Coconut fiber (wt %)	SiO_2 (wt %)
M1	89	9	0	2
M2	79	19	0	2
M3	69	29	0	2
M4	59	39	0	2
M5	89	0	9	2
M6	79	0	19	2
M7	69	0	29	2
M8	98	0	0	2
M9	100	0	0	0

2.3. Characterization

The morphologies were examined using SEM (Cube II, Tabletop, EMCrafts). Phase composition was then analyzed by XRD (X'Pert-PRO MPD, PANalytical) under Cu Kα radiation. The chemical structure was determined via FTIR (Nicolet iS10, Thermo Scientific) from 525 to 4000 cm^{-1} at a resolution of 16 cm^{-1} for 32 scans. The instrument is equipped with a diamond ATR accessory. Compact tension tests were conducted using an Instron Universal Testing Machine type 3366. The flexural strength and elastic modulus were tested following ASTM standards (AGX−50kNVD, Shimadzu).

The water absorption test specimens measured 80 mm in length, 10 mm in width, and 4 mm in thickness. All specimens were required to have flat surfaces. The test was conducted as per ASTM D570 standard. Prior to measurement, specimens were dried at 80°C until a constant mass was achieved, then cooled in a desiccator before determining the initial mass m_0. The specimens were simultaneously immersed in tap water and seawater (NaCl 0.35 wt%) at ambient conditions to compare water absorption in different environments. The mass of each specimen was recorded after immersion periods of 1, 2, 3, 4, 5, 6, 7, 8, 9, and 10 days. Before weighing, each specimen was wiped dry with a clean cloth and paper.

The water absorption of the specimens was calculated using the following formula:

$$W = \frac{m - m_0}{m_0}(\%)$$

where: W is the water absorption after immersion time t (%); m is mass of the specimen after immersion (g); m_0 is the initial mass of the specimen (g).

3. Results and Discussion

3.1. Recovery and characteristics of nano SiO_2

Rice husk ash is a silica-rich byproduct obtained from burning rice husks, a common agricultural waste. Silica (SiO_2) accounts for about 85–95% of the weight of rice husk ash, depending on the burning conditions. The remainder is carbon and a small amount of metal oxides (Mezan et al., 2021). Nano-SiO_2 is obtained from rice husk ash using NaOH and HCl according to the following reactions:

$$SiO_2 + 2NaOH \rightarrow Na_2SiO_3 + H_2O \quad (1)$$

$$Na_2SiO_3 + 2HCl \rightarrow SiO_2 + 2NaCl + H_2O \quad (2)$$

The shape, size, and structure of the prepared SiO_2 were analyzed using digital photography, SEM, XRD, and FTIR (Fig. 1). From the digital photograph in Fig. 1a, the obtained nano-SiO_2 exhibits a fine, loose, and

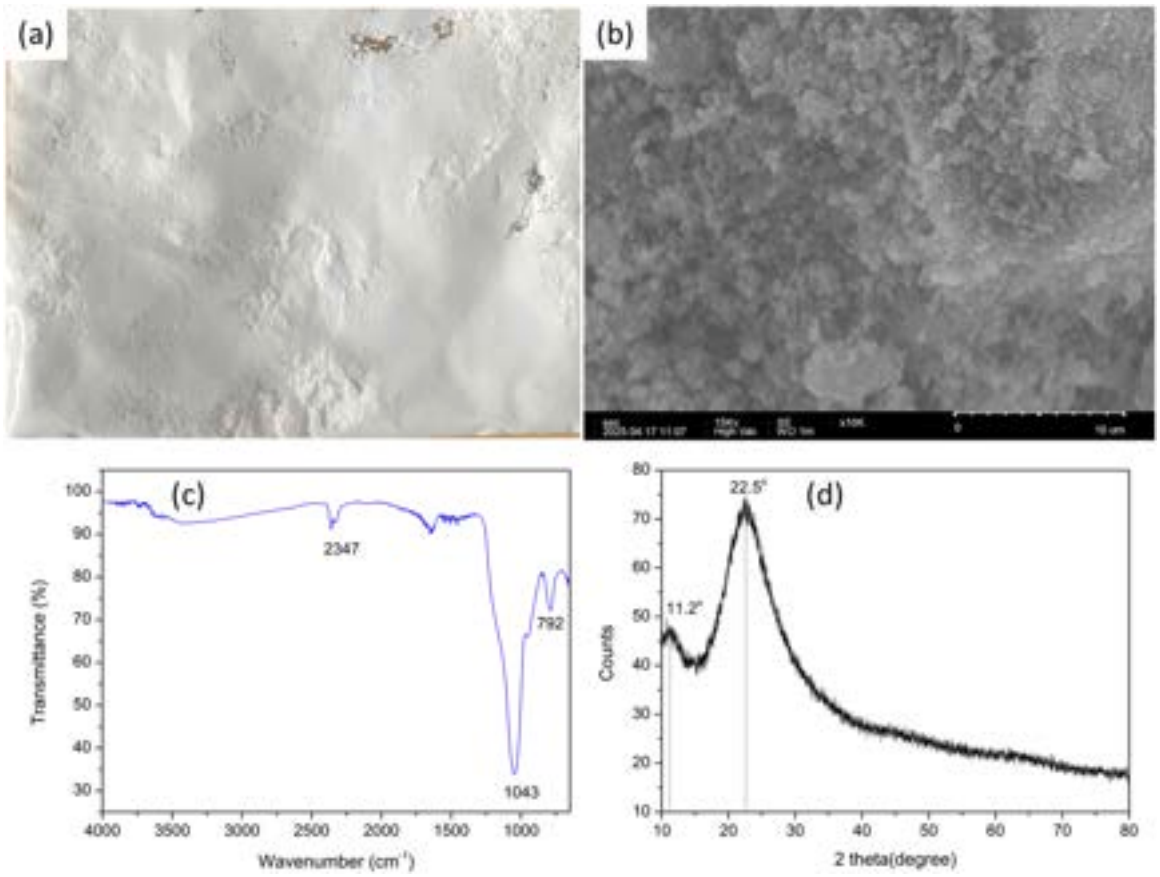

Fig. 1. (a) Digital photo, (b) SEM image, (c) FTIR spectrum, and (d) XRD pattern of as-prepared SiO_2 powder from rice husk ash.

brilliant white powder, qualitatively indicating the high chemical purity and the successful elimination of organic matter and unburnt carbon residues during the alkaline extraction and acid precipitation cycles.

The microscopic morphology is illustrated in the SEM micrograph in Fig. 1b. Due to the high surface energy and nanoscale dimensions typical of rice-husk-derived silica, the SiO_2 nanoparticles exhibit a strong tendency to cluster into agglomerated networks. These clusters create random inter-particle voids and a loose macro-assembly, rather than a strictly defined or verified internal porous framework. Because of this extensive aggregation and the inherent resolution limits of tabletop SEM at these scales, individual particle boundaries are partially obscured within the clusters, making an accurate direct evaluation of primary particle size uniformity difficult from the micrograph alone. This nanoscale morphology is consistent with rice-husk-derived silica observations reported in previous studies (Mezan et al., 2021; Nayak and Datta, 2021).

The chemical framework was verified via the FTIR spectrum in Fig. 1c, which displays prominent peaks at 792 and 1043 cm^{-1} characteristic of the symmetric and asymmetric stretching vibrations of the Si-O-Si siloxane bonds, respectively. The spectral region at approximately 1640 cm^{-1} is the bending vibration of the water molecule (O-H) surrounding the SiO_2 nanoparticle surface (Mezan et al., 2021; Nayak and Datta, 2021). The peak at 2347 cm^{-1} may be due to the C═O stretching vibration of CO_2 in air, a common feature in FTIR spectra. The broad, low-intensity spectral region at approximately 3300 cm^{-1} corresponds to the O-H vibration of water adsorbed on the sample. The exceptional purity of the recovered nano-SiO_2 and the complete elimination of original lignocellulosic organic components from the rice husk are substantiated by multiple lines of evidence across the spectrum. Beyond the total absence of aliphatic C-H stretching peaks in the 2500–3000 cm^{-1} region, there are no detectable absorption bands near 1700 cm^{-1} (indicative of C═O carbonyl stretching from hemicellulose or organic residues) or between 1500–1600 cm^{-1} (indicative of aromatic skeletal vibrations from residual lignin). This high chemical purity aligns with the brilliant white appearance of the powder (Fig. 1a), confirming the absolute volatilization of residual carbon, as well as the clean, single-phase amorphous halo verified via XRD analysis (Fig. 1d).

The phase structure and crystallographic composition of the synthesized SiO_2 were examined via XRD, as shown in Fig. 1d. The diffraction pattern shows two characteristic peaks of SiO2 at 2θ 11.2° and 22.5°. The pattern displays a characteristically broad amorphous diffraction centered near 2θ of 22.5°, confirming the completely disordered, non-crystalline nature of the silica (Azmi et al., 2016; Mohamed et al., 2015). Based on this peak and the Debye–Sherrer formula, the average size of the SiO_2 nanoparticles was calculated to be approximately 20 nm, close to the size observed by SEM above.

3.2. *Fabrication and physiochemical properties of the composites*

The process of making the composite material includes mixing, melting, and pressing, as shown in Fig. 2. This produces sheets whose colors depend on the starting material ratio. Afterward, the samples are checked for microstructure and tested for mechanical properties and water permeability. This method enabled controlled inclusion of varying filler weight ratios, facilitating a direct comparison of the performance of wood powder and coconut fiber reinforcements.

Fig. 3 presents the surface morphology and internal distribution of fillers within the rHDPE matrix, as observed through photographs and SEM images. The macroscopic images reveal distinct color differences: M1 (wood powder) and M5 (coconut fiber) exhibit a dark, textured appearance, suggesting high biomass content, while M8 (rHDPE/nano-SiO_2) displays a more uniform and lighter coloration. SEM analysis at

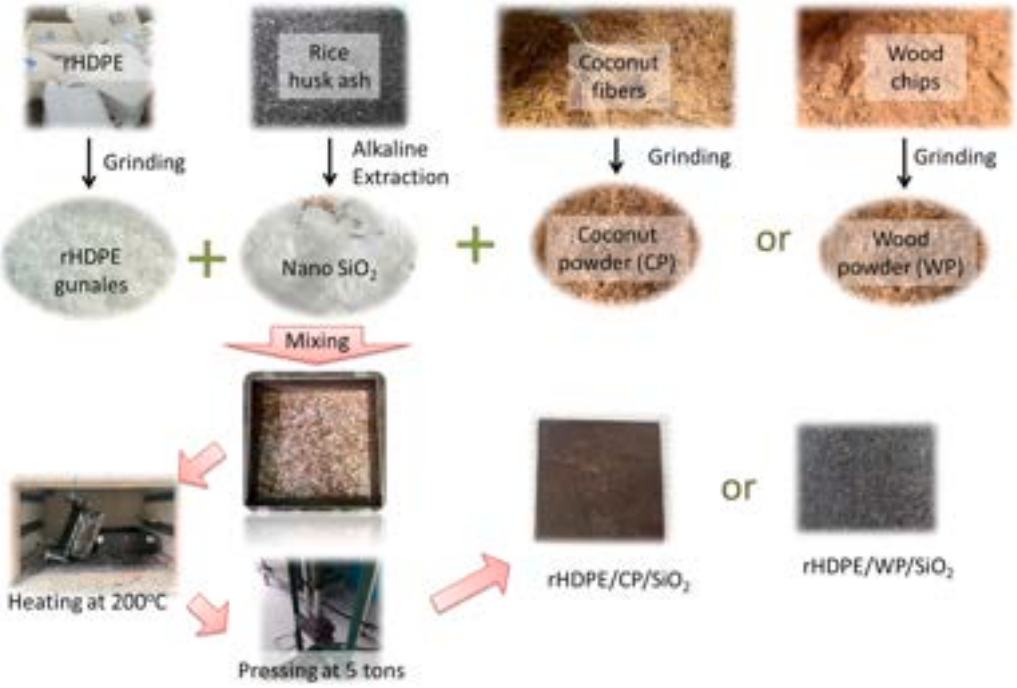

Fig. 2. Schematic illustration of the fabrication process of the composite materials.

higher magnifications indicates that nano-SiO_2 is incorporated relatively smoothly into the polymer matrix in M8, whereas the organic fillers in M1 and M5 produce more complex and heterogeneous surfaces. These fibers and powders modify the interfacial region, which plays a critical role in stress transfer during mechanical loading.

To clarify the influence of the mixing ratio between components on crystallization properties, composite material samples were evaluated using XRD. Fig. 4 shows XRD patterns of obtained materials with different compositions and ratios, but all using HDPE as the substrate. On the XRD pattern, characteristic peaks of HDPE appear at 2θ 21.3° and 23.4°. However, the intensity and location of these peaks differ. The peak positions, peak shifts, and crystallinity values are shown in details in Table S1. This indicates interactions and structural changes in the material when the composition (SiO_2, coconut fiber, wood powder) and their ratios are varied (Table 1). As the concentration of reinforcing substances increases, the peak strength of HDPE decreases. Three-component composite samples (HDPE, SiO_2, and coconut fiber or wood powder) exhibit a shifted peak compared to samples containing only two components (HDPE and SiO_2). This result has also been noted in previous studies (Li and Wang, 2018; Webo et al., 2026a, 2026b; Grozdanov et al., 2007; Lei et al., 2007; Han et al., 2018).

FTIR spectra were used to examine the chemical properties of composite material samples with different compositions and ratios (Fig. 5). The spectrum of the composite material consisting of two components, HDPE and SiO_2 (M8), showed peaks consistent with the FTIR spectrum of polyethylene (Lei et al., 2007; Han et al., 2018). The two peaks observed at 2916 cm^{-1} and 2847 cm^{-1} are characteristic of asymmetric and symmetric C-H vibrations, respectively. The remaining peaks represent out-of-plane vibration modes of the methylene group, where the peak at 1467 cm^{-1} is characteristic of the methylene cross-vibration, and the peak at 723 cm^{-1} is characteristic of the methylene translation vibration. No peak characteristic of the presence of SiO_2 appeared because SiO_2 exists in amorphous form, as observed above. On the other hand, upon the introduction of wood powder and coconut fiber, the characteristic functional groups of these lignocellulosic fillers, such as the broad hydroxyl group (−OH) stretching at 3300 – 3400 cm^{-1} and the carbonyl (C═O) stretching of hemicellulose at about 1735 cm^{-1}, exhibit remarkably low intensities in the composite spectra. This attenuation is primarily governed by two distinct phenomena: (i) The composites were fabricated via thermal compression molding, a process that naturally forces a thin, resin-rich rHDPE polymer layer ('skin') to migrate to the outer mold surface. Besides, because ATR-FTIR analysis relies on a shallow evanescent wave penetration depth, the infrared beam predominantly samples this hydrophobic outer skin layer, effectively masking the embedded filler fibers and reducing their functional group intensities close to the detection baseline. (ii) While the aliphatic C-H stretching bands of the natural fibers are completely obscured by the massive absorption peaks of the rHDPE matrix, the C-O and C-O-C stretching vibrations of the cellulose/hemicellulose carbohydrate rings (1030 – 1050 cm^{-1}) are completely enveloped by the prominent, broad asymmetric stretching band of the Si-O-Si siloxane network at 1043 cm^{-1} originating from the co-blended nano-SiO_2 filler. The slight widening of the 1043 cm^{-1} band in the multi-filler hybrid samples (M2, M4, M7) compared to the binary blend (M8) qualitatively supports the overlapping presence of these cellulosic components, confirming successful physical encapsulation without the formation of unexpected secondary chemical artifacts.

3.3. *Mechanical properties of the composites*

The mechanical performance of the fabricated composites, including tensile strength, elasticity (elastic modulus), and flexural strength, was evaluated to determine their suitability for offshore cage frames. As shown in Fig. 6a, the pure rHDPE matrix (sample M9) exhibited the lowest tensile strength at 402.16 MPa. The incorporation of 2 wt% nano-SiO_2 (sample M8) successfully enhanced the tensile strength to 485.62 MPa, demonstrating the reinforcing efficiency of the synthesized nanoparticles. Interestingly, the addition of wood powder up to 29 wt% yielded a steady increase in tensile strength, with sample M3 reaching the peak value of 640.88 MPa. However, a further increase to 39 wt% wood powder (sample M4) caused a slight drop to 620.20 MPa, likely due to filler agglomeration and localized stress concentrations within the polymer matrix. For the coconut fiber series, incorporating 9 wt% fiber (sample M5) initially increased the tensile strength to 514.68 MPa, but higher loading levels resulted in fluctuations, with sample M6 dropping to 419.12 MPa before recovering slightly to 507.02 MPa in

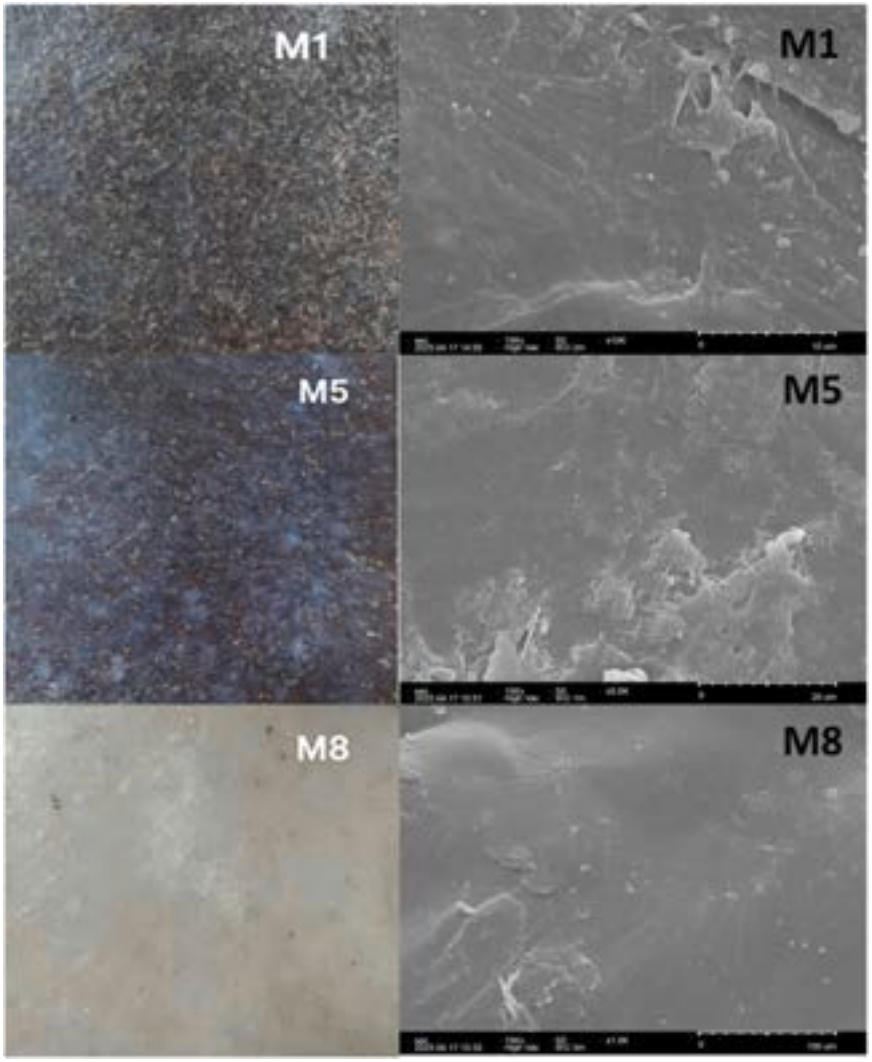

Fig. 3. Photographs (left) and SEM micrographs (right) of various composite samples.

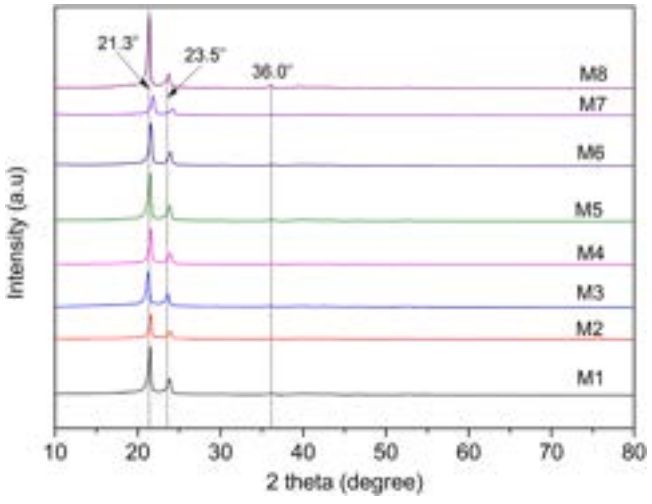

Fig. 4. XRD patterns of different composite samples.

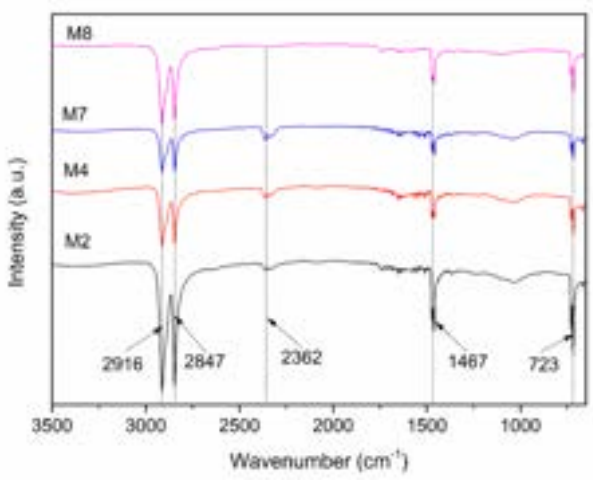

Fig. 5. FTIR spectra of different composite samples.

sample M7. This can be attributed to the complex fibrous morphology of coconut fiber, which tends to clump and hinder uniform dispersion at higher concentrations (Webo et al., 2026a, 2026b; Grozdanov et al., 2007; Lei et al., 2007; Han et al., 2018).

Fig. 6b presents the elasticity (elastic modulus) of the selected composite formulations. Pure rHDPE (M9) possessed a relatively low elastic modulus of 183.15 MPa. The introduction of 2 wt% nano-SiO_2

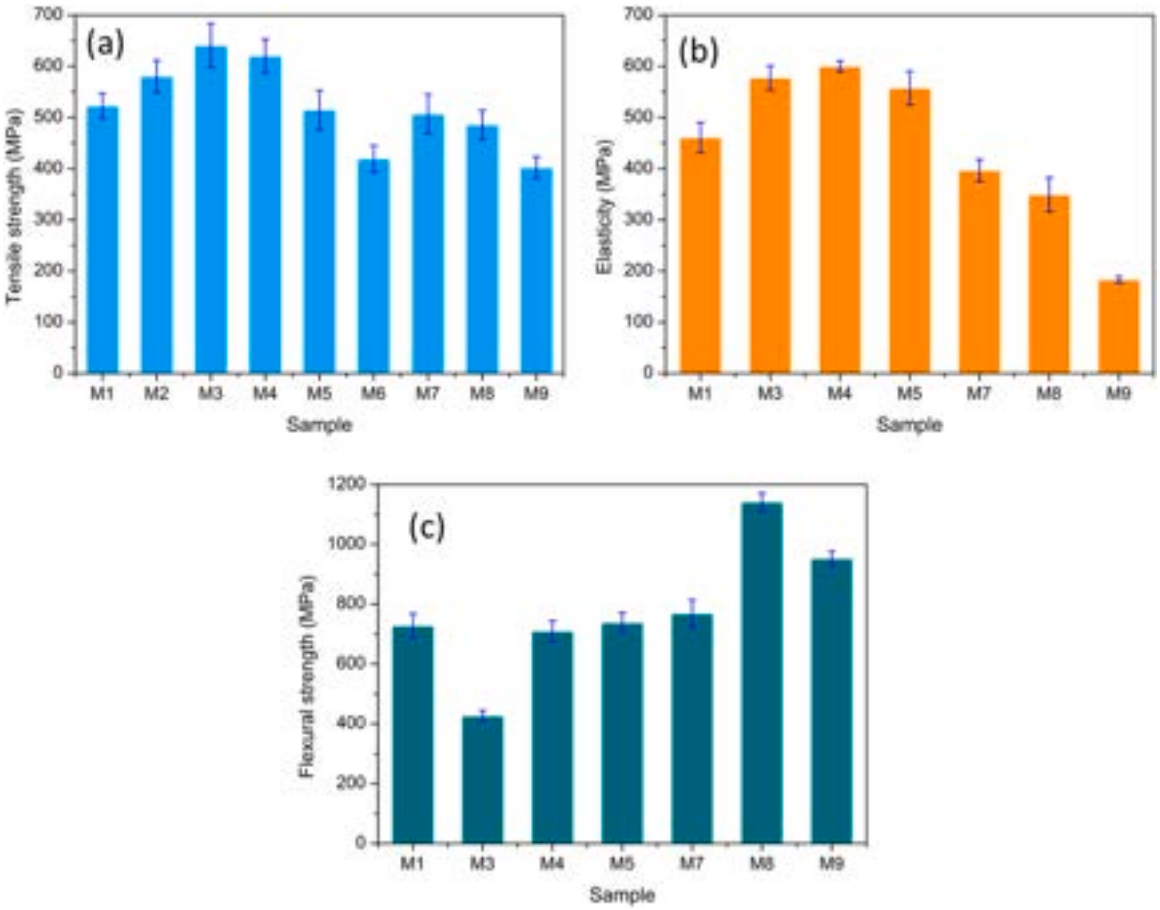

Fig. 6. Effect of composite formulation on (a) tensile strength, (b) elastic modulus, and (c) flexural strength.

(M8) nearly doubled the stiffness, raising the value to 349.42 MPa. The inclusion of lignocellulosic reinforcements further stiffened the material; for the wood powder series, elasticity increased from 460.80 MPa (M1) to a maximum of 600.12 MPa (M4). Similarly, the 9 wt% coconut fiber composite (M5) achieved a high elasticity value of 557.47 MPa, though it decreased to 396.60 MPa at 29 wt% loading (M7), confirming that excessive fiber concentrations lower overall elastic performance.

The flexural strength trends are illustrated in Fig. 6c. Sample M8, composed of 98% rHDPE resin and 2 wt% nano-SiO_2, exhibited the highest overall flexural strength at 1141.48 MPa, clearly surpassing the 953.07 MPa observed for the pure rHDPE control (M9). The addition of agricultural biomass generally resulted in a reduction in flexural strength compared to the nano-SiO_2 reinforced matrix. For the wood powder composites, the flexural strength was 727.48 MPa at 9 wt% loading (M1) but dropped drastically to 426.57 MPa at 29 wt% loading (M3), before recovering slightly to 709.50 MPa at 39 wt% loading (M4). On the other hand, the coconut fiber composites retained stable flexural properties, displaying values of 738.36 MPa (M5) and 768.45 MPa (M7), indicating that the structural length and stiffness of coconut fibers provide better bending resistance than highly loaded wood powder blends.

Water absorption analysis is a crucial step in evaluating the

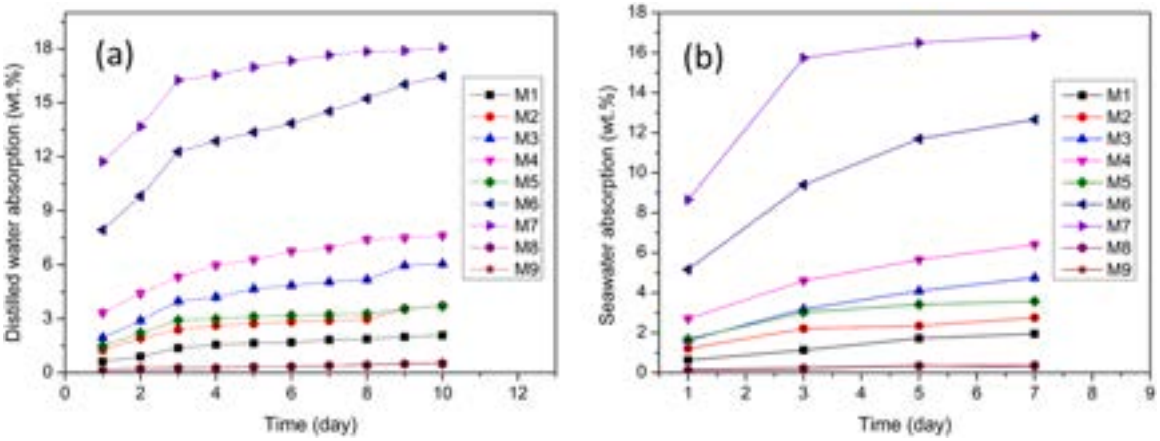

Fig. 7. Effect of composite formulation on (a) distilled water and (b) simulated seawater absorption behavior.

applicability of composite materials (Arumugam et al., 2026; Tkue et al., 2026). Fig. 7 shows that the content of reinforcement (wood powder or coconut fiber) and HDPE resin clearly affects the material's water absorption, including distilled water (Fig. 7a) and simulated seawater (NaCl 0.35 wt%) (Fig. 7b). For both cases, at a ratio of M8 (98% resin, 2% SiO_2), the material has the lowest water absorption, even lower than that of sample M9 (100% resin). This result shows that adding SiO_2 not only increases stiffness but also helps reduce water absorption. When comparing samples using wood powder (M1, M2, M3) with those using coconut fiber (M5, M6, M7), coconut fiber shows much higher water absorption. This is because coconut fiber has a lower density (0.1–0.25 g/cm^3) compared to wood powder (0.3–0.6 g/cm^3), resulting in more voids and higher water retention and absorption capacity. Interestingly, the water absorption contents in seawater were lower than those of distilled water, which suggested the more stability of the obtained composites in the seawater and a high potential application of them as cage frames for the regional mariculture industry.

A comparative analysis between pure rHDPE (M9) and the binary nano-composite containing 2 wt% nano-SiO_2 (M8) demonstrates that even a minor incorporation of nanosilica yields a noticeable reduction in the equilibrium water absorption capacity and diffusion rate. This improved moisture resistance can be explained by two fundamental microstructural mechanisms that alter the water diffusion pathways: (i) In pure rHDPE, water molecules diffuse through the amorphous free-volume regions of the polymer matrix via relatively straight, low-resistance pathways. When 2 wt% of nano-SiO_2 is uniformly dispersed within the matrix, these rigid, impermeable spherical nanoparticles act as physical nano-barriers. Diffusing water molecules cannot penetrate the silica structures and are forced to detour around them. This significantly increases the geometric tortuosity (the ratio of the actual path length to the straight-line distance), effectively extending the travel distance for moisture, lowering the overall diffusion coefficient, and delaying the onset of moisture saturation. (ii) Recycled plastics typically exhibit higher baseline microstructural defects, such as internal micro-voids, weld lines, and free-volume expansion induced by prior thermal degradation cycles. The ultra-fine primary nanoparticles (10–20 nm) physically occupy these micro-voids and intermolecular gaps within the amorphous regions of the rHDPE. By packing into these structural flaws, the nano-SiO_2 reduces the total net volume available for water molecule clustering and capillary condensation, minimizing structural moisture storage capacity. Furthermore, the high surface area of the nano-filler facilitates favorable localized physical anchoring with the surrounding polymer chains, restricting local chain mobility and further suppressing the transient free-volume fluctuations necessary for water transport.

4. Conclusion

This study successfully developed high-performance hybrid composites by reinforcing recycled HDPE with rice-husk-derived nano-SiO_2 and lignocellulosic fibers, specifically engineered for marine-grade applications. Structural analyses confirmed that the 10–20 nm amorphous nano-SiO_2 facilitates superior physical interlocking within the matrix, ensuring structural reliability in aquatic environments. While higher loadings of organic fillers increased water sensitivity, a critical factor for marine durability, the addition of 2 wt% nano-SiO_2 optimized the composite, achieving a peak tensile strength of 640.88 MPa and an elastic modulus of 1141.48 MPa. These findings demonstrate that the proposed composite serves as a robust, low-cost, and sustainable alternative to expensive virgin HDPE and traditional materials. By bridging the gap between waste management and offshore infrastructure, this research provides a scalable solution for the regional mariculture industry, supporting the transition toward a circular blue economy through long-lasting and eco-friendly cage frames.

CRediT authorship contribution statement

Nguyen Thi Kim Chi: Writing – original draft, Investigation, Formal analysis. **Nguyen Van Hoa:** Writing – review & editing, Supervision, Resources, Project administration, Methodology, Funding acquisition, Conceptualization. **Nguyen Dac Kien:** Visualization, Conceptualization. **Nguyen Van Tai:** Data curation.

Declaration of Competing Interest

The authors declare that they have no known competing financial interests or personal relationships that could have appeared to influence the work reported in this paper.

Acknowledgements

The authors thank Nha Trang University for their support and funding (Project No. SV2023–13–37). This work contributes to the celebration of the 50th anniversary of Nha Trang University, located in Khanh Hoa Province, Viet Nam.

Appendix A. Supporting information

Supplementary data associated with this article can be found in the online version at doi:10.1016/j.rsma.2026.105312.

Data availability

Data will be made available on request.

References

Arumugam, A., Zimmermann, J., Weingartz, T., et al., 2026. Polymerization catalyst is key: Predicting molecular changes during mechanical recycling of Phillips and Ziegler-Natta catalyst high-density polyethylene (HDPE). Polym. Degrad. Stab. 247, 111981. https://doi.org/10.1016/j.polymdegradstab.2026.111981.

Azmi, M.A., Ismail, N.A.A., Rizamarhaiza, M., A.A.K., W.M. Hasif., Taib, H., 2016. Characterisation of silica derived from rice husk (Muar, Johor, Malaysia) decomposition at different temperatures. AIP Conf. Proc. 1756, 020005. https://doi.org/10.1063/1.4958748.

Chen, C., Chang, J., Sun, Y., Fatima, A., Huang, J., 2026. Preparation of Pd nanoparticle-modified $FeWO_4$ hollow spheres for highly selective hydrogen sulfide and acetone detection. Front. Mater. Sci. 20 (2), 260762. https://doi.org/10.1007/s11706-026-0762-3.

Geyer, R., Jambeck, J.R., Law, K.L., 2017. Production, use, and fate of all plastics ever made. Sci. Adv. 3 (7), e1700782. https://doi.org/10.1126/sciadv.1700782.

Grozdanov, A., Buzarovska, A., Bogoeva-Gaceva, G., et al., 2007. Rice straw as an alternative reinforcement in polypropylene composites. Agron. Sustain. Dev. 26, 251–255. https://doi.org/10.1051/agro:2006023.

Han, G., Lei, Y., Wu, Q., et al., 2018. Bamboo–fiber filled high density polyethylene composites: effect of coupling treatment and nanoclay. J. Polym. Environ. 16, 123–130. https://doi.org/10.1007/s10924-008-0094-7.

Jonathan, M.K., Osamong, G.A., Butembu, S., et al., 2021. Structural properties of high density polyethylene matrix composites reinforced with open air and furnace rice husks ash. J. Chem. Eng. Mater. Sci. 12, 73–84. https://doi.org/10.5897/JCEMS2020.0349.

Kannan, G., Thangaraju, R., 2022. Recent progress on natural lignocellulosic fiber reinforced polymer composites: A review. J. Nat. Fibers 19, 7100–7131. https://doi.org/10.1080/15440478.2021.1944425.

Kennedy, S.M., Pandian, V.M., 2025. Enhanced mechanical and thermal properties in epoxy-based glass fabric composites via nano silica integration. Polym. -Plast. Technol. Mater. 64, 208–221. https://doi.org/10.1080/25740881.2024.2394828.

Kumi-Larbi Jnr, A., Galpin, R., Manjula, S., et al., 2022. Reuse of waste plastics in developing countries: properties of waste plastic-sand composites. Waste Biomass-.-. Valor 13 (9), 3821–3834. https://doi.org/10.1007/s12649-022-01708-x.

Lei, Y., Wu, Q., Yao, F., 2007. Preparation and properties of recycled HDPE/natural fiber composites. Compos. Part. A. 38, 1664–1674. https://doi.org/10.1016/j.compositesa.2007.02.001.

Li, Y., Wang, B., 2018. Natural fiber-reinforced composites: A review on material. processing and properties. Compos. Part. B Eng. 136, 456–470. https://doi.org/10.1177/0892705719844546.

Mezan, S.O., Al Absi, S.M., Jabbar, A.H., et al., 2021. Synthesis and characterization of enhanced silica nanoparticle (SiO_2) prepared from rice husk ash immobilized of 3-(chloropropyl) triethoxysilanea. Mater. Today Proc. 42, 2464–2468. https://doi.org/10.1016/j.matpr.2020.12.564.

Mishra, B., Varshney, S., Gupta, M.K., 2025. Effect of fillers on the performance of fibre reinforced polymer hybrid composites: A comprehensive review. Polym. -Plast. Technol. Mater. 64, 2179–2213. https://doi.org/10.1080/25740881.2025.2519024.

Mohamed, R.M., Mkhalid, I.A., Barakat, M.A., 2015. Rice husk ash as a renewable source for the production of zeolite NaY and its characterization. Arab. J. Chem. 8 (1), 48–53. https://doi.org/10.1016/j.arabjc.2012.12.013.

Mohanty, A.K., Vivekanandhan, S., Pin, J.M., et al., 2018. Composites from renewable and sustainable resources: Challenges and innovations. Science 362, 536–542. https://doi.org/10.1126/science.aat9072.

Mullungal, M.N., Shaju, S.S., 2026. Advanced polymer composites for eco-friendly marine applications. Macro, Micro and Nanocomposites from sustainable sources: Shrinking environmental footprints. Springer nature Singapore, Singapore, pp. 431–447. https://doi.org/10.1007/978-981-95-2469-3_14.

Nadzri, S.N.I.H.A., Sultan, M.T.H., Shah, A.U.M., et al., 2022. A comprehensive review of coconut shell powder composites: Preparation, processing, and characterization. J. Thermoplast. Compos. Mater. 35, 2641–2664. https://doi.org/10.1177/0892705720930808.

Nasr, A., Wang, J., Duan, Z., et al., 2025. Assessing the visibility and impact of recycled high-density polyethylene (HDPE) fibers in 3D-printed cementitious composites. Constr. Build. Mater. 495, 143639. https://doi.org/10.1016/j.conbuildmat.2025.143639.

Nayak, P.P., Datta, A.K., 2021. Synthesis of SiO_2-nanoparticles from rice husk ash and its comparison with commercial amorphous silica through material characterization. Silicon 13, 1209–1214. https://doi.org/10.1007/s12633-020-00509-y.

Ogah, A.O., Ezeani, O.E., Nwobi, S.C., et al., 2022. Physical and mechanical properties of agro-waste filled recycled high density polyethylene biocomposites. South. Asian Res. J. Eng. Tech. 4, 55–62. https://doi.org/10.36346/sarjet.2022.v04i04.002.

Pickering, K.L., Efendy, M.A., Le, T.M., 2016. A review of recent developments in natural fibre composites and their mechanical performance. Compos. Part. A Appl. Sci. Manuf. 83, 98–112. https://doi.org/10.1016/j.compositesa.2015.08.038.

Shakil, S., Wang, F., Sun, P., Zhou, Z., Lu, X., Du, J., Huang, J., 2026. Metal-organic frameworks as next-generation chemiresistive sensors: From fundamental design to advanced applications. Prog. Chem. 38 (3), 502–531. https://doi.org/10.7536/PC20251208.

Sinha, R.K., Sridhar, K., Purohit, R., et al., 2020. Effect of nano SiO_2 on properties of natural fiber reinforced epoxy hybrid composite: A review. Mater. Today Proc. 26, 183–3186. https://doi.org/10.1016/j.matpr.2020.02.657.

Tkue, T.A., Tesfay, A.G., Gebreselassie, G.T., et al., 2026. Optimizing mechanical performance and water absorption behavior of silica-reinforced recycled thermoplastic composites for rooftile applications, 0(0). J. Thermoplast. Compos. Mater.. https://doi.org/10.1177/08927057261425893.

Venkatesh, R., Roopashree, R., Sur, S., et al., 2023. Investigation and performance study of Hibiscus sabdariffa bast fiber-reinforced HDPE composite enhanced by silica nanoparticles derived from agricultural residues. Fibers Polym. 24 (2023), 2155–2164. https://doi.org/10.1007/s12221-023-00221-9.

Webo, W., Mohlamonyane, R., Mhike, W., et al., 2026b. Development and characterization of sustainable hybrid composites: Recycled HDPE modified with wood powder and calcium carbonate, 0(0). J. Thermoplast. Compos. Mater.. https://doi.org/10.1177/08927057261421154.

Webo, W., Mhike, W., Khoathane, C., 2026a. Fabrication and performance evaluation of sustainable flax fiber-reinforced HDPE bio-composites: A path toward reducing plastic waste, 0(0). J. Thermoplast. Compos. Mater.. https://doi.org/10.1177/08927057261440333.

Yaqueen, M.N., Kuity, A., Ahmed, M.A., 2025. Sustainable nano silica production from agricultural residues: A review of green synthesis techniques and performance in asphalt applications. Inter. J. Pavement Res. Technol. https://doi.org/10.1007/s42947-025-00585-6.

Regional Studies in Marine Science 102 (2026) 105461

Contents lists available at ScienceDirect

Regional Studies in Marine Science

journal homepage: www.elsevier.com/locate/rsma

Vietnamese fishing labour in global perspective: A critical review of social, economic, behavioural, and governance structures

Khanh Q. Nguyen [a,b,*,1], Minh-Hoang Tran [c,d,**,1], Phuong Viet Le [a], Luong T. Nguyen [a]

[a] Nha Trang University, 2 Nguyen Dinh Chieu, North Nha Trang, Khanh Hoa, Vietnam
[b] Fisheries and Oceans Canada, St. John's, NL A1C 5X1, Canada
[c] NTT Hi-Tech Institute, Nguyen Tat Thanh University, Ho Chi Minh City, Vietnam
[d] Nguyen Tat Thanh University Center for Hi-Tech Development, Saigon Hi-Tech Park, Ho Chi Minh City, Vietnam

ARTICLE INFO

Keywords:
Vietnamese fisheries
Fishing labour
Labour informality
Occupational risk
Behavioural responses
Labour governance
Sustainability

ABSTRACT

Marine capture fisheries have contributed significantly to Vietnam's economy through employment, food security, export values, and income generation for coastal communities. However, the labour system remains characterized by informality, economic insecurity, and high occupational risk. We examine Vietnamese fisheries labour through an integrated Fisheries Labour Systems Framework (FLSF) adapted from the Social-Ecological Systems (SES) literature collected from selected Association of Southeast Asia Nations (ASEAN) and Organization for Economic Co-operation and Development (OECD) fisheries. The critical review shows that labour relations in Vietnam are predominantly informal, shaped by community-based recruitment, share-based remuneration, and widespread reliance on informal credit systems. These structural features contribute to income instability, labour dependency, and high mobility. Behavioural dynamics, including risk normalization, masculine occupational identities, and heterogeneous risk perception, further reinforce hazardous working practices. Comparative evidence highlights stark contrasts with OECD fisheries, where formal contracts, institutionalized safety systems, and regulatory oversight have reduced but not eliminated occupational risks. The paper also identifies persistent governance gaps in Vietnam, where fragmented legal frameworks and weak enforcement limit integrating labour protections into fisheries management. By situating Vietnamese fisheries labour within broader regional and global contexts, the study underscores the need for coordinated reforms that address informality, enhance safety, and strengthen labour governance as integral components of sustainable fisheries development.

1. Introduction

Fisheries are simultaneously productive economic sectors, livelihood systems, workplaces, and social institutions. Globally, the fisheries sector supports hundreds of millions of livelihoods across harvesting, processing, trade, and associated value chains. In 2024, an estimated 65.3 million people were directly employed in primary fisheries and aquaculture production, with approximately 85% located in Asia (FAO, 2026). In Vietnam, marine capture fisheries employ approximately 830 thousand workers directly on fishing vessels, in addition to around four million seasonal or temporary workers engaged across the broader value chain, including seafood processing and fisheries-related services (National Statistics Office, 2024; Nguyen et al., 2024a; Bình et al., 2025; Le et al., 2025). Meanwhile, the aquaculture sector provides employment for more than two million people (Bình et al., 2025; FAO, 2026). While fisheries play an important role in social economic development in many coastal countries, fishing remains one of the world's most hazardous occupations, characterized by high levels of occupational risk, income uncertainty, and labour informality. In contrast to OECD countries, where labour relations are generally governed by formal contracts, occupational safety regulations, and institutional oversight, fisheries in many developing countries continue to rely on informal employment arrangements embedded within local social and community networks (Béné, 2003; Henry and Olson, 2014; OECD, 2025).

* Corresponding author at: Nha Trang University, 2 Nguyen Dinh Chieu, North Nha Trang, Vietnam.
** Corresponding author at: NTT Hi-Tech Institute, Nguyen Tat Thanh University, Ho Chi Minh City, Vietnam.
E-mail addresses: khanhnq@ntu.edu.vn (K.Q. Nguyen), tmhoang@ntt.edu.vn (M.-H. Tran).
[1] These authors contributed equally to this work and share first authorship

https://doi.org/10.1016/j.rsma.2026.105461
Received 25 May 2026; Received in revised form 1 September 2026; Accepted 6 September 2026
Available online 15 September 2026

Vietnam is a particularly important case because fisheries combine substantial production and export activity with a labour system that remains strongly embedded in household and community institutions. Existing research describes offshore crews as overwhelmingly male, with occupational entry frequently mediated by kinship and community networks, remuneration commonly linked to catch shares, and employment relationships often established verbally rather than through standardized written contracts (Alonso, 2022; Phuong and Pomeroy, 2025; Le et al., 2026). Informal credit further connects labour and household finance, sometimes creating dependencies between crew members, vessel owners, and intermediaries (Ruddle, 2011). These arrangements are not simply remnants of a traditional sector. They remain economically functional because they lower recruitment costs, facilitate trust, provide flexibility in an uncertain production environment, and connect fishing labour to local social networks. At the same time, these institutional arrangements can reproduce vulnerability. Income depends on catch, prices, costs, and vessel performance; labour mobility may be constrained by social and financial ties; and occupational safety may be subordinated to the need to maintain fishing activity. Empirical evidence indicates that fishers experience substantial injury risks and that inadequate use of personal protective equipment is associated with markedly higher injury risk (Nguyen et al., 2024b). Risk is therefore not generated by weather or vessel technology alone. It is produced through interactions among institutional rules, labour-market organization, economic incentives, occupational culture, and individual and collective decision-making.

The governance context is also changing. Vietnam has strengthened fisheries monitoring and traceability in response to illegal, unreported and unregulated (IUU) fishing concerns, while international supply chains increasingly connect labour conditions with market access and due-diligence expectations (Alonso and Marschke, 2023; Haas et al., 2023; Honniball, 2026). The ILO Work in Fishing Convention, 2007 (C188), provides an international reference point for working conditions, safety, accommodation, food, and other labour protections, but Vietnam has not ratified the Convention (ILO, 2007). These developments make it increasingly difficult to treat fisheries labour as separate from fisheries governance. We therefore conducted this study as a critical review of Vietnam's fisheries labour system rather than a descriptive literature review. The central analytical question is: how do institutional settings shape labour-market structures, how do those structures influence behavioural responses, and how do the resulting interactions affect labour outcomes and governance and sustainability? To answer this question, the paper applies an integrated Fisheries Labour Systems Framework (FLSF) (Basurto et al., 2013; Cinner et al., 2013; McGinnis and Ostrom, 2014) that is adapted from Social-Ecological Systems (SES) (Ostrom, 2009) and uses it as the organizing structure throughout the review. Within each component, Vietnamese evidence is examined first and then compared with selected ASEAN and OECD evidence. The paper also integrates macro-level data from the Food and Agriculture Organization (FAO) and Vietnam's national statistics to provide an empirical context for the literature synthesis.

2. Methodologies

2.1. Literature search and acquisition

This study uses a structured literature review approach to synthesize current knowledge on Vietnamese fishing labour and compare it with labour systems in the ASEAN and OECD countries. Rather than conducting a statistical meta-analysis, the review integrates empirical studies, policy documents, international conventions, and comparative fisheries literature to identify recurring patterns and governance challenges. A structured review was considered appropriate because fishing labour research spans multiple disciplines, including fisheries science, labour studies, sociology, occupational health, governance and others, and therefore requires conceptual rather than quantitative synthesis.

In this study, all information from both peer-reviewed articles, grey literature, technical reports, websites, databases, and other relevant sources was considered. Relevant literature was searched through online sources of databases, such as Web of Science, Scopus, ScienceDirect, Google Scholar, and official government sources and organizations such as FAO, ILO, and OECD, between January and March 2026. This critical review focuses on studies investigating labour characteristics of marine capture fisheries associated with institutional context, labor market structure including recruitment, contracts, remuneration, occupational safety, and governance. Although the primary focus is Vietnam's fisheries labour system, the review also compares Vietnam with neighbouring ASEAN countries and developed OECD countries. The review excludes studies that focus on fisheries biology, stock assessment, gear technology, or aquaculture without labour-related information.

Because official statistics do not consistently separate marine capture employment from the wider agriculture, forestry and fisheries sector, macro-level indicators are used cautiously. For example, Vietnam's national statistics recorded employment in agriculture, forestry and fisheries, whereas FAO reported job opportunities in fisheries and aquaculture (National Statistics Office, 2024; FAO, 2026). These inconsistencies are not directly interchangeable, but together they provide a useful scale for the sector while highlighting a major data gap: the absence of a consistently reported national series for marine capture fish workers alone.

2.2. Analytical framework

The SES framework provides the conceptual starting point because it emphasizes that social and ecological outcomes arise from interactions among resource systems, governance systems, users, and institutions (Ostrom, 2009; Basurto et al., 2013; Cinner et al., 2013; McGinnis and Ostrom, 2014). The present paper does not claim to apply the SES framework in its original form. Instead, it adapts its relational logic to the specific problem of fisheries labour. The resulting analytical anchor is termed the Integrated Fisheries Labour Systems Framework (Fig. 1).

The framework consists of five interconnected components (Basurto et al., 2013; Cinner et al., 2013; McGinnis and Ostrom, 2014; Ostrom, 2009). Institutional settings comprise fisheries legislation, labour law, community institutions, international labour standards, market requirements, and the capacity to inspect and enforce rules. These conditions define the formal and informal rules under which fishing takes place. Labour-market structures translate those rules into recruitment practices, employment contracts, remuneration, access to credit, mobility, and retention. Behavioural responses represent how fishers and vessel organizations interpret and act within these conditions, including occupational identity, risk perception, safety behaviour, communication, and adaptive decision-making. Labour outcomes capture the consequences for income stability, injuries, health, social protection, retention, and well-being. Finally, governance and sustainability outcomes capture whether labour relations become more formal and accountable and whether labour governance becomes integrated with fisheries compliance and long-term sustainability. The components are interconnected rather than sequential in a one-way causal chain. Institutional arrangements shape labour-market incentives, but labour markets can also influence institutional change when shortages, worker mobility, international market requirements, or collective action create pressure for reform. Labour-market insecurity can encourage risk-taking, while occupational culture can normalize those behaviours. Resulting injuries, turnover, or labour shortages can then influence governance responses. Fig. 1 therefore represents feedback as well as pathways. The framework is comparative by design: Vietnam is the primary case, while ASEAN and OECD evidence is used to identify which mechanisms are context-specific and which reflect broader characteristics of fishing as a hazardous and socially embedded occupation.

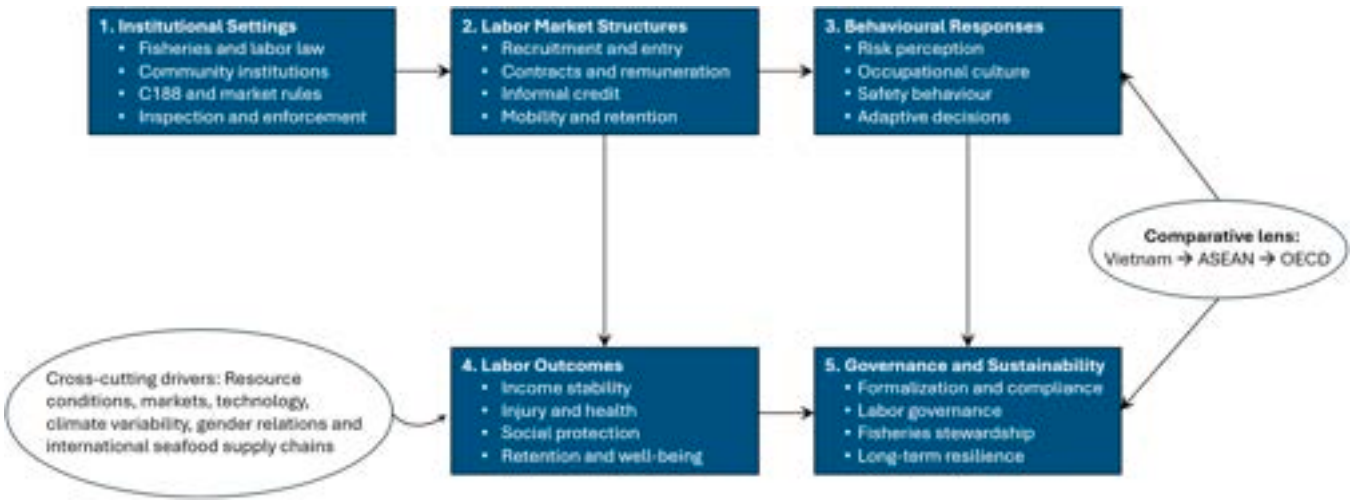

Fig. 1. The organizing structure for the critical review, adapted from SES and FLSF.

3. Context and institutional settings

3.1. Scale, employment context, and institutional landscape in Vietnam

Vietnam's fisheries labour system must first be situated within a much larger national employment structure. In 2024, 51.9 million people were employed nationally, including 13.7 million in agriculture, forestry and fisheries (26.5% of total employment) (National Statistics Office, 2024). FAO's latest employment estimates place Vietnam among the world's major aquatic-sector employers, with approximately 2.8 million people directly employed in fisheries and aquaculture in 2024 (FAO, 2026). The difference between these reports is analytically important: national statistics aggregate agriculture, forestry and fisheries, while FAO's fisheries and aquaculture estimate covers primary aquatic production. Neither data isolate marine capture fishers. Consequently, the manuscript treats sectoral employment estimates as contextual indicators rather than as a precise count of fishing crews.

The broader economic significance of fisheries is nevertheless clear. Vietnam is a major producer and exporter of aquatic products, and capture fisheries remain important to coastal economies and have remained a top ten country for seafood exports in the world during the past two decades (FAO, 2026). Fisheries support not only vessel crews but also processing, trading, transport, repair, ice production, gear supply, and household-based post-harvest work. Women are particularly important in these downstream activities but are less visible in conventional measures of fishing labour (Febri et al., 2017; Torell et al., 2021; Alonso, 2022; Phuong and Pomeroy, 2025; Le et al., 2026). The labour system is therefore larger than the population physically present at sea. Institutionally, fisheries labour is governed through overlapping fisheries, labour, maritime, and local administrative arrangements. The Fisheries Law and Labour Code provide important legal foundations, but fisheries labour has historically been regulated primarily through fisheries-management and vessel-safety instruments rather than through a dedicated and fully integrated labour regime (Cuong et al., 2025; Le et al., 2026). This creates a gap between the formal existence of labour rights and their practical application aboard fishing vessels. The problem is not necessarily an absence of rules; rather, the rules are dispersed across institutions and are difficult to implement in a highly decentralized and geographically dispersed fleet.

Community institutions remain important within this formal system. The historical "Van Chai" system, which is traditional fishing communities, or cultural social organizations, illustrates how coastal communities have long organized fishing activities, cooperation, and resource use (Ruddle, 1998; Nguyen and Ruddle, 2010). Contemporary recruitment continues to rely heavily on kinship, neighbourhood, and long-standing social ties (Phuong and Pomeroy, 2025). These arrangements can substitute for formal labour-market institutions by providing trust and information, but they can also reproduce hierarchy and reduce workers' ability to bargain independently. Thus, community governance should not be treated as simply a weakness to be replaced by state regulation. Its social capital is potentially valuable, but its labour implications depend on how it interacts with formal rights and enforcement. In addition, Vietnam's response to IUU fishing illustrates the changing institutional environment. Since the EU yellow-card decision in 2017, Vietnam has expanded vessel monitoring, traceability, catch documentation, and port controls (Ho and Ngo, 2023). These measures have strengthened surveillance and fisheries compliance, but their labour effects have been less direct because labour rights have not been fully integrated into IUU governance (Alonso and Marschke, 2023). This distinction is central to the framework: institutional modernization in fisheries does not automatically produce labour formalization.

3.2. Comparative institutional context: ASEAN and OECD

The Vietnamese pattern is part of a wider regional continuum. In Indonesia and Myanmar, community-based recruitment and informal labour arrangements remain important, while the Philippines has moved further toward standardized labour agreements in some segments, particularly where migrant and distant-water labour is involved (Belton et al., 2019; Hung et al., 2022; Danial et al., 2024). Thailand provides an important reform case because international scrutiny and trade pressure led to major changes in labour registration, contracts, inspection, and the adoption of ILO C188 (Kadfak and Linke, 2021; MWG, 2021).

OECD fisheries provide a different institutional configuration. Norway, Canada, the United States, and Australia combine fisheries regulation with more formal labour standards, occupational safety systems, professional training, and inspection mechanisms (Håvold, 2010; Henry and Olson, 2014; Håvold and Oltedal, 2018; Shan, 2022). These systems should not be idealized: accidents, fatigue, human error, and labour insecurity remain present. Their importance for Vietnam is instead that institutional capacity changes the consequences of behavioural error. Stronger systems can prevent a risky decision from escalating into a catastrophic outcome through training, vessel standards, communication, emergency response, and enforcement.

4. Labour-market structures

4.1. Occupational entry, demographic structure, and recruitment

Vietnamese fishing labour is socially reproduced to a substantial degree. Offshore crews are overwhelmingly male, commonly concentrated in the 30–50 age range, and often have long fishing experience. Educational attainment is generally lower than in formalized labour markets, while occupational knowledge is transmitted through experience and intergenerational networks (Carruth et al., 2010; Alonso, 2022; Phuong and Pomeroy, 2025; Le et al., 2026). This pattern means that occupational entry is not simply a market transaction between employers and workers; it is also a social process embedded in households and communities. Community-based recruitment reduces search and transaction costs and allows vessel owners to recruit workers whose skills and reputations are already known. For workers, social networks can provide rapid access to employment when alternative jobs are limited. Yet the same networks can constrain exit. A crew member whose employment is linked to relatives, neighbours, advances, or community obligations may have fewer practical options than a worker in a formal labour market. Comparative evidence from Indonesia and Myanmar shows similar dependence on local networks, whereas OECD systems rely more heavily on standardized recruitment, certification, and contracts (Henry and Olson, 2014; Belton et al., 2019). The gender dimension further complicates the definition of the fisheries workforce. Although offshore fishing is male dominated, women contribute substantially to processing, marketing, household finance, and other post-harvest activities. Their labour is often statistically and institutionally invisible, which limits access to formal recognition and social protection (Febri et al., 2017; Frangoudes and Gerrard, 2018; Torell et al., 2021). A labour-system perspective therefore requires attention to the full value chain rather than only the workers on board.

4.2. Contracts, remuneration, credit, and mobility

The defining feature of Vietnam's labour-market structure is the combination of share-based remuneration, informal or verbal employment arrangements, and informal credit. Under share systems, crew earnings vary with catch volume, market prices, and operating costs (Phuong and Pomeroy, 2025; Le et al., 2026). Such arrangements align incentives between owners and crews because both benefit from higher production, but they also transfer substantial income risk to workers. Estimates in the reviewed literature place monthly fishing earnings broadly around USD 250 – 600, compared with substantially higher earnings in many OECD fisheries (Hoang et al., 2020; OECD, 2025; Le et al., 2026) (Table 1). The income gap should not be interpreted as a simple productivity comparison because cost structures, purchasing power, taxation, social protection, and definitions of fishing income differ across countries.

Informal credit is an equally important component of the labour system (Table 1). Advances from vessel owners or intermediaries can help households finance consumption and fishing operations, but they may also generate dependence and reduce workers' freedom to leave. Ruddle (2011) describes informal credit as an established feature of Vietnamese fishing communities, while comparative evidence shows that debt-linked labour relationships can become more coercive in distant-water fisheries (Marschke and Vandergeest, 2016; Yea and Stringer, 2023). Informal credit should not, however, be equated automatically with exploitation. Rather, credit and employment become intertwined when workers lack alternative sources of finance and when debts are settled through continued labour. Labour mobility is consequently both a response to insecurity and a mechanism that can reproduce it. Workers may move between vessels when earnings or working conditions are poor, but high turnover can also weaken crew cohesion, complicate training, and increase safety risks. Recent research on Vietnam's labour shortage suggests that recruitment and retention are becoming increasingly important constraints on fishing operations (Phuong and Pomeroy, 2025). In this sense, labour scarcity may become a driver of formalization if vessel owners increasingly need to attract and retain workers through better conditions rather than relying on community recruitment alone.

4.3. Comparative interpretation

Table 1 shows that the major difference between Vietnam and OECD systems is not one labour practice in isolation but the degree to which several institutions are integrated. Informal recruitment becomes more consequential when contracts are weak; share-based remuneration becomes more risky when cost deductions are opaque; and informal credit becomes more restrictive when social protection and alternative finance are limited. In more formalized systems, these mechanisms are partially separated by contracts, financial institutions, insurance, inspection, and collective representation. Fig. 2 therefore depicts institutional differentiation as a continuum. Vietnam's labour system should be understood as partially formalized rather than simply informal: formal rules exist, but their reach and integration into everyday labour relations remain uneven.

5. Behavioural responses

5.1. Risk perception and occupational culture

Behavioural responses are the third component of the framework because fishers do not respond mechanically to institutional or economic conditions. They interpret risk through experience, occupational identity, social expectations, and immediate livelihood needs. In Vietnam, repeated exposure to storms, rough seas, equipment failures, vessel instability, and onboard injuries can normalize danger and make

Table 1
Comparative socio-economic characteristics of fisheries labour systems.

Indicator	Vietnam	Selected ASEAN evidence	OECD evidence	Interpretation	References
Labour structure	Predominantly informal	Mixed; transitional	More formalized	Institutional differences shape bargaining power and worker protection	(Johnsen and Vik, 2013; Henry and Olson, 2014; Le et al., 2026)
Monthly income	Approx. USD 250–600	Approx. USD 300–800 in reviewed cases	Often USD 2500–6000	Income levels are not directly comparable across currencies and protection systems	(Hoang et al., 2020; Pham and Saizen, 2023; OECD, 2025; Le et al., 2026)
Contracts	Verbal/informal dominant	Increasing formalization	Generally regulated	Contracts determine transparency, rights and access to protection	(ILO, 2007; Henry and Olson, 2014; Phuong and Pomeroy, 2025; Le et al., 2026)
Credit	Informal credit important	Mixed	Formal finance more prevalent	Employer-linked credit can increase dependency	(Béné, 2003; Phuong and Pomeroy, 2025; FAO, 2026)
Training	Limited/variable	Moderate and improving	High and institutionalized	Training interacts with safety culture and enforcement	(Håvold and Oltedal, 2018; Shan, 2022; Le et al., 2026)
Mobility	Relatively high	Moderate	Lower in more stable segments	Mobility can signal precarity but also worker bargaining power	(Johnsen and Vik, 2013; Alonso, 2022; Phuong and Pomeroy, 2025)

Fig. 2. Structural contrast between community-embedded fisheries labour systems of Vietnam and ASEAN vs. formalized OECD systems.

hazardous situations appear routine (Carruth et al., 2010; Nguyen and Tran, 2013; Cao, 2025). This should not be understood as evidence that fishers are unaware of danger. Rather, experience changes the threshold at which a hazard is considered unacceptable. Risk normalization is closely connected to the economic organization described above. When earnings depend on catch and fishing days, suspending operations during uncertain weather has an immediate financial cost. Decisions to continue fishing, postpone maintenance, or use protective equipment inconsistently may therefore be rational responses to livelihood constraints, even when workers recognize the underlying hazard (Pham and Saizen, 2023; Nguyen et al., 2024b). This interpretation is important because it avoids treating safety behaviour as a purely individual failure.

Occupational masculinity also shapes behavioural responses. Vietnamese fishing culture places strong value on endurance, independence, resilience, and practical competence, and these attributes can become associated with the ability to tolerate difficult conditions (Alonso, 2022; Le et al., 2026). Similar patterns occur in Norway, Australia, and distant-water fleets, where professional identity can sometimes favour experience and self-reliance over formal procedures (Johnsen and Vik, 2013; Yea and Stringer, 2023; Syddall and Fisher, 2026). The difference is institutional: stronger regulatory systems can counterbalance cultural norms through mandatory training, organizational safety management, and enforceable standards.

5.2. *Experience, personal protective equipment (PPE), communication, and adaptive decision-making*

Experience has an ambiguous relationship with safety. Less experienced workers may face higher injury risks because they have weaker hazard recognition and less familiarity with gear and vessel operations. At the same time, highly experienced fishers may become more confident and tolerant of risk, relying on intuition developed through years of successful fishing (Nguyen and Tran, 2013; Tatar, 2019; Nguyen et al., 2024a, 2024b). Experience therefore acts as both a protective resource and a potential source of overconfidence. Effective safety systems should preserve experiential knowledge while adding standardized procedures that prevent experience from becoming a substitute for risk assessment. Personal protective equipment illustrates the same interaction between structure and behaviour. Vietnamese fishers without appropriate protective equipment have been reported to face approximately 3.7 times the injury risk of those using appropriate protection (Nguyen et al., 2024b). Yet low PPE use cannot be explained by negligence alone. Cost, availability, discomfort, production pressure, and occupational norms all affect compliance. The behavioural component of the framework therefore directs attention to the conditions under which safe behaviour becomes feasible rather than merely instructing workers to behave differently. Communication and hierarchy are also important. Fishing operations require coordination during gear deployment, hauling, navigation, and emergencies. In hierarchical crews, junior workers may hesitate to challenge captains or report hazards, which can suppress learning from near misses (Nguyen and Tran, 2013; Phuong and Pomeroy, 2025). International evidence similarly shows that communication problems can undermine safety even in highly regulated fisheries (Thorvaldsen and Sønvisen, 2014). Safety culture, therefore, depends on formal procedures as well as the social relationships through which those procedures are accepted and used.

5.3. *Comparative behavioural evidence*

The comparative evidence indicates that behavioural risk is universal but shaped by institutional conditions. OECD fisheries have not eliminated fatigue, risk of misjudgment, human error, or reliance on practical judgement. Instead, organizational systems reduce the probability that these behaviours produce severe outcomes through training, inspections, emergency systems, and standardized risk management (Håvold, 2010; Håvold and Oltedal, 2018; Shan, 2022). In Vietnam and other more informal fisheries, the same behavioural tendencies operate with fewer institutional buffers. This suggests that safety interventions are unlikely to work well if they are separated from the labour-market and institutional conditions in which fishers work.

6. Labour outcomes

6.1. *Income security, social protection, and labour retention*

The labour-market structures identified above translate directly into labour outcomes. Share-based remuneration exposes crews to fluctuations in catch, prices, and operating costs, while informal contracts can limit access to social insurance, health coverage, and formal grievance mechanisms (Hoang et al., 2020; Phuong and Pomeroy, 2025; Le et al., 2026). Informal credit can smooth short-term consumption but may deepen dependence over longer periods. These mechanisms help explain why labour insecurity can persist even when fishing remains economically important. Labour shortages and turnover are increasingly visible as additional outcomes. Phuong and Pomeroy (2025) identify recruitment and retention difficulties as important constraints in Vietnamese capture fisheries. This creates a potential feedback loop within the framework: precarious employment can encourage workers to leave, while labour shortages can increase the bargaining power of some workers and encourage vessel owners to improve conditions. Whether that feedback produces sustained formalization depends on the availability of alternative employment, the strength of worker organization, and enforcement capacity.

The invisibility of women's labour is another important outcome. Women's contributions to processing, trading, household management, and value addition are often poorly represented in fisheries employment statistics and governance processes. This limits their access to recognition and social protection and can lead to an incomplete understanding of the labour system (Febri et al., 2017; Torell et al., 2021). A critical review of fisheries labour must therefore distinguish between offshore crew employment and the wider fisheries workforce.

6.2. *Occupational injuries, fatalities, and health*

Occupational risk is the most visible labour outcome in the reviewed literature, but the evidence also reveals a major measurement problem. Vietnam has limited systematic data on fisheries-specific fatality rates, and underreporting is likely substantial (Nguyen et al., 2024b; FAO, 2026). Consequently, comparisons of absolute fatality rates should be interpreted cautiously. Table 2 summarizes the available evidence and, importantly, identifies data limitations rather than presenting all country estimates as directly comparable.

The available Vietnamese evidence indicates that soft-tissue injuries,

Table 2
Comparative occupational safety evidence in selected fisheries.

Context	Evidence base	Main hazards/outcomes	Institutional interpretation	References
Vietnam	Limited national surveillance; empirical studies of offshore crews	Collisions, falls, gear/equipment injuries, fatigue; substantial non-fatal injuries	High exposure combined with weakly integrated labour and safety governance.	(Tuan, 2012; Nguyen et al., 2024b; FAO, 2026; Le et al., 2026)
Thailand/ Indonesia	Regional and reform literature	Vessel accidents, unsafe work, labour abuse in some segments	Transitional systems; formal reforms coexist with enforcement challenges.	(Yea and Stringer, 2023; Liliansa, 2024; Sunardi et al., 2025; ILO, 2026)
Myanmar/ high-risk frontier fisheries	Limited and fragmented data	Unsafe vessels, labour precarity and exploitation	Weak governance increases exposure and reduces accountability.	(Vandergeest et al., 2021; Belton et al., 2019)
United States	Longitudinal occupational surveillance	Vessel disasters, falls overboard and onboard injuries	Strong institutional capacity reduces but does not eliminate risk.	(Tatar, 2019; Wilson, 2022)
Canada	Occupational safety and enforcement literature	Falls overboard, vessel instability and human-factor risks	Regulated system with persistent small-vessel challenges.	(Shan, 2022; Wilson, 2022)
Norway	Long-term safety research	Man-overboard and equipment-related incidents	Highly regulated system with established safety culture.	(Håvold, 2010; Håvold and Oltedal, 2018)

lacerations, sprains, fractures, crush injuries, and falls are common, reflecting physically demanding work and frequent contact with hooks, ropes, nets, knives, and machinery (Nguyen et al., 2024b). Fishers without appropriate PPE have substantially higher injury risk (Nguyen and Tran, 2013). These findings are consistent with international evidence showing that gear handling, heavy machinery, overexertion, slips, trips, and falls are major sources of non-fatal injuries across fisheries (Jensen et al., 2006; Shan, 2022). The important difference is the capacity to prevent or contain these hazards. Fatal incidents show a similar pattern. Global syntheses identify vessel disasters, falls overboard, and onboard injuries as major categories of fishing fatalities (Remolà and Gudmundsson, 2018; Tatar, 2019). Table 3 summarizes these broad categories. In Vietnam, small vessel size, ageing infrastructure, uneven access to communication and emergency technologies, and severe weather can increase the consequences of otherwise survivable incidents (Vu and Nguyen, 2008; Tuan, 2012). OECD fisheries face the same environmental hazards but generally have stronger emergency response, inspection, and vessel-safety systems.

Health outcomes also extend beyond traumatic injuries. Repetitive lifting, awkward postures, vibration, engine noise, ultraviolet exposure, fatigue, and psychological stress can accumulate over time (Vandergeest et al., 2021; Vandergeest and Marschke, 2021; Nguyen et al., 2024b; Van et al., 2025). Fatigue is particularly important because it links labour-market organization to behaviour and injury: long hours, night fishing, irregular sleep, and pressure to maximize catch can reduce reaction time and situational awareness. Mental-health risks are less well documented in Vietnam but may be associated with income uncertainty, debt, family separation, and increasingly variable weather (Pham and Saizen, 2023).

6.3. Comparative interpretation

The comparison does not suggest that OECD fisheries are safe while Vietnamese fisheries are dangerous (Table 3). Fishing is hazardous in both settings. The more important difference is how institutional systems shape what happens when hazards are encountered. In OECD fisheries, stronger vessel standards, training, inspection, emergency response, and organizational safety cultures create multiple layers of protection. In Vietnam, the same hazards interact with labour informality and economic insecurity, leaving fewer institutional buffers. Thus, occupational injuries should be interpreted as labour-system outcomes rather than as evidence of poor individual decision-making alone.

7. Governance and sustainability outcomes

7.1. Formalization, compliance, and labour governance

The fifth component of the framework concerns what happens to the broader governance system as labour conditions interact with fisheries management (Table 4). Vietnam has made substantial progress in fisheries surveillance and IUU-related compliance, but labour governance remains less integrated. Vessel monitoring, traceability, catch documentation, and port controls strengthen accountability for fishing activity, yet they do not automatically establish written contracts, transparent remuneration, social protection, or systematic occupational safety management (Alonso and Marschke, 2023; Ho and Ngo, 2023). This creates a form of partial formalization. Formal laws and monitoring technologies coexist with informal recruitment, share-based remuneration, and community-based labour relations. Informality persists partly because it provides flexibility and reduces transaction costs under uncertain production conditions (Ruddle, 2011; Pham et al., 2013). It therefore cannot be eliminated simply by issuing additional regulations. Formalization must also alter the economic incentives that make informal arrangements functional. International market governance increasingly strengthens the case for integration. Labour due diligence and measures targeting forced labour can link worker protection with seafood trade and supply-chain accountability (Haas et al., 2023; Selig

Table 3
Global structure of fishing-related fatalities and contextual modifiers.

Primary fatality category	Approximate global pattern	Contextual modifiers	Key implication	References
Vessel disasters	~40–50% in broad syntheses	Small/older vessels and weak emergency systems increase consequences	Prevention depends on vessel standards, stability, weather decisions and emergency preparedness.	(Remolà and Gudmundsson, 2018; Tatar, 2019; Nguyen et al., 2024a, 2024b; FAO, 2026; Le et al., 2026)
Falls overboard	~20–30%	Deck design, PPE, fatigue, weather and work organization matter	Human and technological controls must operate together.	(Håvold, 2010; Håvold and Oltedal, 2018; Tatar, 2019; Shan, 2022)
Onboard injuries	~10–20%	Gear, machinery, overexertion and work pace	Training and equipment are most effective when embedded in organizational safety systems.	(ILO, 2007; Tatar, 2019; Vandergeest et al., 2021; Wilson, 2022; Yea and Stringer, 2023)
Other causes	Remainder	Diving, illness, conflict and context-specific hazards	Surveillance should capture chronic and acute outcomes.	(Remolà and Gudmundsson, 2018; Tatar, 2019; Wilson, 2022)

Table 4
Comparative fisheries labour governance frameworks.

Dimension	Vietnam	Thailand	Indonesia / Philippines	OECD	Distant-water fisheries	References
C188	Not ratified	Ratified (2019)	Partial/ transitioning	Ratified or equivalent standards in many systems	Variable	(ILO, 2007; Belton et al., 2019; Kadfak and Linke, 2021; FAO, 2026)
Labour contracts	Mostly informal	Mandatory in regulated segments	Increasing formalization	Generally formalized	Mixed	(Henry and Olson, 2014; Yea and Stringer, 2023; Nguyen et al., 2024a, 2024b; Phuong and Pomeroy, 2025; Le et al., 2026)
Labour inspection	Limited/ fragmented	Expanded substantially	Moderate/ transitioning	Strong institutional capacity	Fragmented across jurisdictions	(ILO, 2007; Henry and Olson, 2014; Håvold and Oltedal, 2018; Belton et al., 2019; Shan, 2022)
Migrant labour	Limited formal integration	Formalized registration systems	Increasing bilateral arrangements	More controlled	High vulnerability in some segments	(Marschke and Vandergeest, 2016; Vandergeest and Marschke, 2021; Yea and Stringer, 2023)
Enforcement capacity	Weak–moderate	Moderate and improving	Moderate/ variable	Strong	Fragmented	(Håvold, 2010; Shan, 2022 Nguyen et al., 2024b; FAO, 2026; Le et al., 2026)
Overall governance pattern	Partial formalization	Reform with enforcement gaps	Transitional	Integrated	Jurisdictionally complex	(Shan, 2022; Yea and Stringer, 2023)

et al., 2022; Honniball, 2026). This means labour governance is becoming part of fisheries sustainability rather than a separate social-policy issue. For Vietnam, the policy challenge is to connect existing fisheries surveillance infrastructure with labour standards without creating burdens that disproportionately exclude small-scale operators.

7.2. C188 and institutional alignment

ILO C188 provides a useful benchmark because it brings together minimum standards for work in fishing, including conditions of service, occupational safety and health, accommodation, food, and related worker protections (ILO, 2007). Vietnam has not ratified C188, while Thailand ratified it in 2019 as part of a broader reform process (MWG, 2021) (Table 4). The contrast is informative but should not be reduced to a simple ratification effect. Thailand's experience shows that formal commitments can improve institutional architecture while enforcement problems persist (Kadfak and Linke, 2021).

For Vietnam, the significance of C188 lies in its potential to provide a common reference across fisheries, labour, and maritime institutions. Ratification alone would not resolve informality. Implementation would require worker registration, standardized contracts, inspection procedures, safety training, accessible grievance mechanisms, and coordination across national and provincial authorities. In this review, C188 is best understood as a potential bridge between fisheries, labour, and maritime institutions, rather than as a policy solution on its own.

7.3. Comparative governance outcomes

Table 4 supports a continuum interpretation rather than a simple ranking. Vietnam occupies an intermediate position: it has substantial formal fisheries governance and increasingly sophisticated monitoring, but labour institutions remain less integrated. Thailand demonstrates that rapid formalization is possible, but also that implementation can lag behind legal reform. OECD systems show the benefits of long-term institutional capacity, while distant-water fisheries demonstrate how even formal rules can become fragmented when labour, flag-state, port-state, and supply-country jurisdictions overlap (Haas et al., 2023).

8. Discussion and conclusion

8.1. What the framework reveals about Vietnam

The framework brings together problems that are often discussed separately in the literature. Community-based recruitment, share-based remuneration, informal credit, risk normalization, occupational masculinity, injuries, labour turnover, and fragmented governance form a connected system. Institutional settings shape the labour market; the labour market shapes incentives and behaviour; behaviour and structural exposure shape labour outcomes; and those outcomes feed back into governance through labour shortages, safety concerns, compliance pressures, and international market scrutiny. Seen this way, informality has a different meaning. Informality should not be treated solely as a regulatory deficit. It functions partly as an institutional equilibrium because it offers flexibility, social trust, and low transaction costs in an uncertain production environment (Boonstra and Dang, 2010; Ruddle, 2011). However, the same equilibrium distributes risk toward workers and limits their access to social protection. The policy challenge is consequently more specific than simply eliminating informality. It is to retain arrangements that provide useful social support while reducing those that shift excessive risk onto workers or weaken basic labour rights.

The framework also clarifies why behavioural interventions alone are unlikely to be sufficient. Risk normalization is reinforced by economic incentives; economic incentives are shaped by remuneration and credit; remuneration and credit operate within institutional arrangements; and institutional arrangements determine the credibility of safety rules. A training program delivered to a crew that lacks protective equipment, faces unstable income, and fears losing earnings during bad weather is unlikely to produce durable change. Conversely, formal rules without attention to occupational identity and local social organization may also fail. The OECD comparison is most useful when it is read in terms of mechanisms rather than as a simple ranking of countries. OECD systems do not demonstrate that regulation can remove risk. They show that institutional capacity can create multiple protective layers around inherently hazardous work. Vietnam can draw on this lesson without simply copying OECD institutions. Reforms need to fit the social organization of Vietnamese fishing communities and should use community networks as channels for worker registration, safety education, recruitment standards, and grievance mechanisms rather than treating them solely as barriers.

8.2. A human-centred governance pathway

Four priorities emerge from the evidence. First, labour governance should be integrated into fisheries governance. Existing vessel registration, monitoring, and port-control systems provide an institutional platform for documenting crew members, checking basic employment conditions, and identifying safety risks. Second, labour formalization should focus on minimum viable protections: written contracts,

transparent share calculations and deductions, crew registration, access to social insurance, and clear responsibilities for safety equipment and emergency preparedness. Third, enforcement should be strengthened through coordination among fisheries, labour, and maritime authorities, particularly at provincial and local levels. Fourth, economic policies should reduce the incentives that sustain informality through access to formal credit, livelihood diversification, and better-targeted fisheries support (Pham et al., 2021; Le et al., 2025). These measures should be sequenced rather than implemented as isolated rules. Formal contracts without enforcement may become symbolic. Enforcement without alternative finance may push workers and owners toward more hidden arrangements. Safety training without improvements in work organization may not change behaviour. For this reason, labour formalization, economic resilience, occupational safety, and fisheries compliance should be pursued as complementary measures rather than separate policy streams. A human-centred approach also has implications for sustainability. Fisheries management often focuses on stock status, effort, capacity, and compliance. Yet labour conditions affect whether fishers comply, whether they remain in the sector, whether they can respond to closed seasons or weather restrictions, and whether households can absorb income shocks. Labour governance should therefore be treated as part of fisheries resilience. This is consistent with broader international efforts to connect decent work with sustainable fisheries and the Sustainable Development Goals (SDGs), particularly SDG 8 (create quality jobs, fair incomes, and safe working environments) and SDG 14 (protect marine and coastal ecosystems from pollution and address overfishing).

8.3. Research and data priorities

The literature points to an important empirical limitation. Vietnam lacks a consistently reported national series that isolates marine capture fish workers from broader agriculture, forestry, fisheries, and aquaculture employment. FAO's employment statistics provide a valuable international benchmark, while national statistics provide broader labour-sector indicators, but neither alone captures the full structure of fishing crews, migrant fish workers, women's post-harvest labour, or informal employment (National Statistics Office, 2024; FAO, 2026). Future national labour surveys should therefore record fishing occupation, fishing method, vessel type, employment status, contract type, remuneration, gender, age, migration status, social-insurance coverage, and occupational injury. Longitudinal research is also needed to test the feedback mechanisms proposed in Fig. 1. Cross-sectional surveys can identify associations between experience, PPE use, income, and injury, but they are less able to establish how reforms alter behaviour over time. Comparative ASEAN studies could further identify which elements of Vietnam's labour system are distinctive and which reflect wider regional conditions. Particular attention should be given to women's work, mental health, fatigue, migrant labour, labour shortages, and the effects of fisheries subsidies on labour incentives.

In conclusion, this critical review shows that Vietnamese fisheries labour is best understood as an integrated labour system embedded within a broader social-ecological and governance context. The proposed Fisheries Labour Systems Framework provides a coherent organizing structure linking institutional settings, labour-market structures, behavioural responses, labour outcomes, and governance and sustainability outcomes. Applying this structure reveals that informality, economic vulnerability, occupational risk, and fragmented governance are mutually reinforcing rather than separate problems. Vietnam's labour system retains important strengths, including community trust, occupational knowledge, flexible recruitment, and social networks that help sustain fishing livelihoods. However, these same institutions can reproduce unequal bargaining power, income instability, labour dependency, and weak access to protection. Behavioural responses such as risk normalization and reliance on experience should therefore be interpreted within these structural conditions. Evidence from ASEAN and OECD fisheries suggests that formalization can reduce vulnerability, but legal reform by itself is not enough. Enforcement, economic incentives, organizational learning, and worker participation determine whether formal rules become meaningful in practice. The evidence points to a practical conclusion: fisheries sustainability and labour protection need to be addressed together. Vietnam has already developed important fisheries-monitoring and IUU-compliance institutions; the next step is to connect these systems with labour registration, contracts, occupational safety, social protection, and international labour standards. C188 offers a useful benchmark, but durable reform will depend on implementation and on addressing the economic conditions that sustain informality. A human-centred fisheries governance model, one that treats fishers as workers as well as resource users, offers a more realistic pathway toward decent work, safer fishing, stronger compliance, and long-term fisheries sustainability.

CRediT authorship contribution statement

Khanh Q. Nguyen: Writing – review & editing, Writing – original draft, Visualization, Validation, Methodology, Investigation, Formal analysis, Conceptualization, Data curation, Project administration, Software. **Minh-Hoang Tran:** Conceptualization, Formal analysis, Investigation, Methodology, Validation, Visualization, Writing – original draft, Writing – review & editing. **Phuong Viet Le:** Conceptualization, Data curation, Investigation, Validation, Visualization, Writing – original draft, Writing – review & editing. **Luong T. Nguyen:** Conceptualization, Data curation, Formal analysis, Funding acquisition, Project administration, Writing – original draft, Writing – review & editing.

Declaration of Competing Interest

The authors declare that they have no known competing financial interests or personal relationships that could have appeared to influence the work reported in this paper.

Acknowledgement

This study received funding from Nha Trang University, Vietnam for Science and Technology under grant number 39/QĐ-ĐHNT, dated 05/01/2024. We acknowledge Nguyen Tat Thanh University (Ho Chi Minh City, Vietnam) for supporting this study. We also thank our colleagues in the Faculty of Fisheries Science of the School of Fisheries and Life Science and the Faculty of Social Sciences and Humanities for their helpful discussion, improvement, and review of feedback on early drafts. We are grateful to the editors and anonymous reviewers who had useful comments and improvements throughout the peer review process. This work contributes to the celebration of the 50th anniversary of Nha Trang University, located in Khanh Hoa Province, Vietnam.

Data availability

The data that has been used is confidential.

References

Alonso, G., 2022. Managing masculinities: dynamics of offshore fishing labour in Vietnam. Gend. Place. Cult. 29, 1677–1693. https://doi.org/10.1080/0966369X.2022.2134314.

Alonso, G., Marschke, M., 2023. Blue boats in deep waters: how aspects of IUU policy impact Vietnamese fish workers. Marit. Stud. 22, 1–10. https://doi.org/10.1007/s40152-023-00303-7.

Basurto, X., Gelcich, S., Ostrom, E., 2013. The social-ecological system framework as a knowledge classificatory system for benthic small-scale fisheries. Glob. Environ. Chang. 23, 1366–1380. https://doi.org/10.1016/j.gloenvcha.2013.08.001.

Belton, B., Marschke, M., Vandergeest, P., 2019. Fisheries development, labour and working conditions on Myanmar's marine resource frontier. J. Rural. Stud. 69, 204–213. https://doi.org/10.1016/j.jrurstud.2019.05.007.

Béné, C., 2003. When fishery rhymes with poverty: a first step beyond the old paradigm on poverty in small-scale fisheries. World Dev. 31, 949–975. https://doi.org/10.1016/S0305-750X(03)00045-7.
Bình, T.T., Cường, N.M., Hải, N.T., 2025. Current status and solutions for human resource training and development in Vietnam's fisheries sector. Vietnam. J. Sci. Technol. 67, 34–39. https://doi.org/10.31276/VJST.2024.0018.
Boonstra, W.J., Dang, N.B., 2010. A history of breaking laws — Social dynamics of non-compliance in Vietnamese marine fisheries. Mar. Policy 34, 1261–1267. https://doi.org/10.1016/j.marpol.2010.05.003.
Cao, N.T.H., 2025. Fishermen's perceptions of negative events affecting fishing activities. A case study of a Vietnamese purse seine fishery. Mar. Policy 175, 106628. https://doi.org/10.1016/j.marpol.2025.106628.
Carruth, A.K., Levin, J.L., Gilmore, K., Bui, T., Gallardo, G., Evert, W., Sealey, L., 2010. Cultural influences on safety and health education among Vietnamese fishermen. J. Agromedicine 15, 375–385. https://doi.org/10.1080/1059924X.2010.513647.
Cinner, J.E., MacNeil, M.A., Basurto, X., Gelcich, S., 2013. Looking beyond the fisheries crisis: Cumulative learning from small-scale fisheries through diagnostic approaches. Glob. Environ. Chang. 23, 1359–1365. https://doi.org/10.1016/j.gloenvcha.2013.11.001.
Cuong, D.V., Thi, N., Anh, L., Thi, N., Thuy, P., Cường, Đ.V., Thị, N., Anh, L., Thị, N., Thúy, P., 2025. Labour Law in fisheries and recommendations for Vietnam. VNU J. Sci. Leg. Stud. 41, 1–15. https://doi.org/10.25073/2588-1167/vnuls.4724.
Danial, Jaya, Aulia, B.P.M., Taufiqurrohman, A., Suryani, H.A., Bawono, I.R., 2024. Standardisation of work agreement between Indonesian fisheries crew and foreign companies. Trans. Marit. Sci. 13, 1–26. https://doi.org/10.7225/toms.v13.n02.w09.
FAO, 2026. Blue Transformation: turning vision into impact. Rome. The State of World Fisheries and Aquaculture 2026. https://doi.org/10.4060/cd8357en.
Febri, S.P., Wiyono, E.S., Wisudo, S.H., Haluan, J., Iskandar, B.H., 2017. The role of women in small-scale fisheries of Langsa City, Aceh, Indonesia. AACL Bioflux 10, 402–409.
Frangoudes, K., Gerrard, S., 2018. En)Gendering change in small-scale fisheries and fishing communities in a globalized world. Marit. Stud. 17, 117–124. https://doi.org/10.1007/s40152-018-0113-9.
Haas, B., Oh, S., Dalton, K., Chang, S., Fitzpatrick, J., Matsui, H., An, J., Azmi, K., Davis, R., Lin, H., Jung, M., Hanich, Q., 2023. Untangling jurisdictional complexities for crew labour regulations on fishing vessels in the Western and Central Pacific Ocean. Int. J. Mar. Coast. Law 38, 661–680. https://doi.org/10.1163/15718085-bja10120.
Håvold, J.I., 2010. Safety culture aboard fishing vessels. Saf. Sci. 48, 1054–1061. https://doi.org/10.1016/j.ssci.2009.11.004.
Håvold, J.I., Oltedal, H.A., 2018. Culture and maritime safety. Managing Maritime Safety. Routledge, pp. 53–70.
Henry, A.E., Olson, J.A., 2014. An overview of the survey on the socio-economic aspects of commercial fishing crew in the northeast. NOAA Tech. 48. https://doi.org/10.7289/V52J68S4.
Ho, A.N., Ngo, P.H., 2023. Combating illegal, unreported, and unregulated fishing: a vietnamese perspective. Int. J. Mar. Coast. Law 38, 1–35. https://doi.org/10.1163/15718085-bja10117.
Hoang, H.H., Vu, T.B., Ho, H.V., Vu, H.T., Nguyen, Q.D., 2020. Factors affecting offshore fishing households' income in southern central coast of Vietnam. Manag. Sci. Lett. 10, 1369–1376. https://doi.org/10.5267/j.msl.2019.11.020.
Honniball, A.N., 2026. Combating forced labour in fisheries through trade restrictions: first steps and their consistency with international law. Ocean. Dev. Int. Law 57, 190–227. https://doi.org/10.1080/00908320.2025.2609767.
Hung, P., Lee, H., Lin, C., Liu, W., 2022. Promoting human rights for Taiwan's fishermen: Collaboration with the primary source countries of Taiwan's DWF migrant fishermen. Front. Mar. Sci. 9, 1097378. https://doi.org/10.3389/fmars.2022.1097378.
ILO, 2007. Work in Fishing Convention. https://normlex.ilo.org/dyn/nrmlx_en/f?p=NORMLEXPUB:12100:0::NO::P12100_ILO_CODE:C188 (accessed 12.22.24).
ILO, 2026. Safe seas, fair work: Indonesia's push for ratification of ILO Convention No. 188 on Work in Fishing. https://www.ilo.org/resource/news/safe-seas-fair-work-indonesia's-push-ratification-ilo-convention-no-188#:~:text=Echoing this view%2C Qistina Satriavi, rights abuses and forced labour (accessed 4.6.26).
Jensen, O.C., Stage, S., Noer, P., 2006. Injury and time studies of working processes in fishing. Saf. Sci. 44, 349–358. https://doi.org/10.1016/j.ssci.2005.11.001.
Johnsen, J.P., Vik, J., 2013. Pushed or pulled? Understanding fishery exit in a welfare society context. Marit. Stud. 12, 1–20. https://doi.org/10.1186/2212-9790-12-4.
Kadfak, A., Linke, S., 2021. More than just a carding system: Labour implications of the EU's illegal, unreported and unregulated (IUU) fishing policy in Thailand. Mar. Policy 127, 104445. https://doi.org/10.1016/j.marpol.2021.104445.
Le, P.V., Nguyen, L.T., Nguyen, K.Q., 2025. An overview of financial subsidy programs in Vietnamese fisheries during the past 25 years: an evaluation and recommendations towards improved future mechanisms. World Dev. Perspect. 39, 100704. https://doi.org/10.1016/j.wdp.2025.100704.
Le, P.V., Tran, M.H., Nguyen, K.Q., Nguyen, L.T., Nguyen, H.V., Le, T.P.H., Vu, N.K., 2026. An overview of the socioeconomic and biodemographic aspects of the Vietnamese fishing crews. Societies 16, 133. https://doi.org/10.3390/soc16040133.
Liliansa, D., 2024. Regional Cooperation on Fishing Vessel Safety in Southeast Asia. In: Hong Thao, N., Dang, V.H. (Eds.), Asia and UNCLOS 30 Years' Implementation. International Law in Asia. Springer, Singapore. https://doi.org/10.1007/978-981-97-1556-5_3.
Marschke, M., Vandergeest, P., 2016. Slavery scandals: unpacking labour challenges and policy responses within the off-shore fisheries sector. Mar. Policy 68, 39–46. https://doi.org/10.1016/j.marpol.2016.02.009.
McGinnis, M.D., Ostrom, E., 2014. Social-ecological system framework: initial changes and continuing challenges. Ecol. Soc. 19, 30. https://doi.org/10.5751/ES-06387-190230.
MWG, 2021. The implementation of laws and policies relevant to the fisher rights' protection under the ILO working in fishing convention 2007 (No. 188). Thail. Report. Work. Fish. Conv. 2007 (188).
National Statistics Office, 2024. Statistical yearbook of Vietnam 2024. Statistical Publishing House, Ha Noi, Vietnam.
Nguyen, D.T., Ruddle, K., 2010. Vietnam: The van chai system of social organization and fisheries community management. In: Ruddle, K., Satria, A. (Eds.), Managing Coastal and Inland Waters. Springer, Dordrecht, pp. 129–160. https://doi.org/10.1007/978-90-481-9555-8_6.
Nguyen, K.Q., Tran, P.D., 2013. The accident status and solutions to improve the safety of purpleback flying-squid jigging in Quang Nam province, Vietnam. Fish. Sci. Technol. 1/2013 37–41.
Nguyen, K.Q., Tran, P.D., Le, P.V., Nguyen, L.T., To, P., Van, 2024a. Advancing fishing technology education and research: a 65-year legacy at Nha Trang University, Vietnam. J. Fish. 12, 123501. https://doi.org/10.17017/j.fish.787.
Nguyen, V.T., Nguyen, B.N., Nguyen, T.S., Tran, T.Q.C., Ho, V.H., Nguyen, T.H.H., 2024b. Prevalence of accidents and injuries and related factors of fishermen fishing offshore in the North of Vietnam. Int. J. Occup. Saf. Heal. 14, 228–236. https://doi.org/10.3126/ijosh.v14i2.56367.
OECD, 2025. OECD Review of Fisheries 2025. OECD Publishing, Paris. https://doi.org/10.1787/560cd8fc-en.
Ostrom, E., 2009. A general framework for analyzing sustainability of social-ecological systems. Science 325, 419–422. https://doi.org/10.1126/science.1172133.
Pham, T.L., Saizen, I., 2023. Coastal fishers' livelihood adaptations to extreme weather events: an analysis of household strategies in Quang Ngai Province, Vietnam. Humanit. Soc. Sci. Commun. 10, 1–12. https://doi.org/10.1057/s41599-023-02263-z.
Pham, T.T.T., Flaaten, O., Nguyen, L.T., Vu, N.K., 2021. Subsidies—help or hurt? A study from Vietnamese fisheries. Mar. Resour. Econ. 36, 369–387. https://doi.org/10.1086/715358.
Pham, T.T.T., Flaaten, O., Nguyen, T.K.A., 2013. Remuneration systems and economic performance: theory and Vietnamese small-scale purse seine fisheries. Mar. Resour. Econ. 28, 19–41. https://doi.org/10.5950/0738-1360-28.1.19.
Phuong, T.Van, Pomeroy, R.S., 2025. Vietnam's capture fisheries labor shortage explored: difficulties and responses. J. Fish. 13, 132205. https://doi.org/10.17017/j.fish.821.
Remolà, A.O., Gudmundsson, A., 2018. Global review of safety at sea in the fisheries sector. FAO Fisheries and Aquaculture Circular No. 1153. FAO, Rome.
Ruddle, K., 1998. Traditional community-based coastal marine fisheries management in Viet Nam. Ocean. Coast. Manag. 40, 1–22. https://doi.org/10.1016/S0964-5691(98)00072-6.
Ruddle, K., 2011. Informal" credit systems in fishing communities: issues and examples from Vietnam. Hum. Organ. 70, 224–232. https://doi.org/10.17730/humo.70.3.v4810k37717h9g01.
Selig, E.R., Nakayama, S., Wabnitz, C.C.C., Österblom, H., Spijkers, J., Miller, N.A., Bebbington, J., Decker Sparks, J.L., 2022. Revealing global risks of labor abuse and illegal, unreported, and unregulated fishing. Nat. Commun. 13, 1612. https://doi.org/10.1038/s41467-022-28916-2.
Shan, D., 2022. Enforcement of fishing occupational health and safety (OHS) standards: challenges in Atlantic Canada. Mar. Policy 145, 105282. https://doi.org/10.1016/j.marpol.2022.105282.
Sunardi, N., Aleik, S., Eko, S., Arief, S., Heri, K., Sapto, P., 2025. Safety risk evaluation by vessel type and accident category in an Archipelagic State: an empirical data analysis from Indonesia. Int. J. Saf. Secur. Eng. 15, 2103. https://doi.org/10.18280/ijsse.151013.
Syddall, V.M., Fisher, K.T., 2026. Exposing multiple masculinities across hierarchies and performance and experience of risk-taking on-board tuna longlining vessels in the Western and Central Pacific. Marit. Stud. 25. https://doi.org/10.1007/s40152-025-00462-9.
Tatar, V., 2019. Evaluation of occupational safety and health in the global fishing sector. Online J. Sci. Technol. 9, 156–170.
Thorvaldsen, T., Sønvisen, S.A., 2014. Multilingual crews on Norwegian fishing vessels: Implications for communication and safety on board. Mar. Policy 43, 301–306. https://doi.org/10.1016/j.marpol.2013.06.013.
Torell, E., Castro, J., Lazarte, A., Bilecki, D., 2021. Analysis of gender roles in Philippine fishing communities. J. Int. Dev. 33, 233–255. https://doi.org/10.1002/jid.3520.
Tuan, H.A., 2012. The tragedy of Vietnamese fishermen: the forgotten faces of territorial disputes in the South China Sea. Asia J. Glob. Stud. 5, 94–107.
Van, T.N., Nguyen, H., Truong, S.N., Bao, N.N., 2025. Occupational injury of Vietnamese seafarers on board merchant vessels. Int. Marit. Health 76, 193–199. https://doi.org/10.5603/imh.97662.
Vandergeest, P., Marschke, M., 2021. Beyond slavery scandals: explaining working conditions among fish workers in Taiwan and Thailand. Mar. Policy 132, 104685. https://doi.org/10.1016/j.marpol.2021.104685.
Vandergeest, P., Marschke, M., Macdonnell, M., 2021. Seafarers in fishing: a year into the COVID-19 pandemic. Mar. Policy 134, 104796. https://doi.org/10.1016/j.marpol.2021.104796.
Vu, V.Y., Nguyen, H.T., 2008. Research on communication and localization of small and medium fishing boats in Vietnam- Ad-hoc network associated to software defined

radio approach. 2008 s International Conference on Communications and Electronics. IEEE, Hoi An, Vietnam. https://doi.org/10.1109/CCE.2008.4578983.
Wilson, J., 2022. Profession is among the most dangerous occupations in Canada. Can. Occup. Saf. https://www.thesafetymag.com/ca/news/general/over-100000-fishing-related-deaths-recorded-globally-each-year-report/426349?utm_source=chatgpt.com (accessed 5.12.26).
Yea, S., Stringer, C., 2023. The informalisation of precarious work in fishing crew: experiences of Fijian fishers on distant water vessels. Mar. Policy 155, 105709. https://doi.org/10.1016/j.marpol.2023.105709.